UNIVERSITY OF CALIFORNIA, SAN DIEGO

Synthesis and Reactivity of Group 6 *m*–Terphenyl Isocyanides

A dissertation submitted in partial satisfaction of the
requirements for the degree of Doctor of Philosophy

in

Chemistry

by

Treffly Brian Ditri

Committee in charge:

Professor Joshua S. Figueroa, Chair
Professor Clifford P. Kubiak
Professor Joseph O'Connor
Professor Michael J. Tauber
Professor Kenneth S. Vecchio

2014

The dissertation of Treffly Brian Ditri is approved, and it is acceptable in quality and form for publication on microfilm and electronically:

_____

_____

_____

_____

_____

Chair

University of California, San Diego

2014

DEDICATION

This thesis is dedicated to my family,

to Mrs. Janice Ditri,

Mr. Brian Ditri,

Mr. Brent Ditri,

And Mr. Luke Ditri

EPIGRAPH

Get over it!

–Don Henley

TABLE OF CONTENTS

LIST OF ABBREVIATIONS

Å = Angstrom (10^{-10} m)

a = unit cell axis a

Anal. = combustion analysis (elemental)

Ar = aryl

α = unit cell angle α, orientation of magnetic nuclei aligned with an extern magnetic field

b = unit cell axis b

β = unit cell angle β, position two atoms removed, orientation of magnetic nuclei aligned against a external magnetic field

br = broad

C_{ipso} = arene ring carbon attached to substituent

C_{iso} = terminal isocyanide carbon

CNR = isocyanide

CO = carbon monoxide, carbonyl

COD = 1,5–cyclooctadiene (C_8H_{12})

Cp = cyclopentadienyl (C_5H_5)

Cy = cyclohexyl (*cyclo*–C_6H_{11})

c = unit cell axis c

calcd. = calculated

cm^{-1} = wavenumber

°C = degrees Celsium

d = doublet, days, deuterated

DFT = Density Functional Theory

Dipp = 2,6,–diisopropylphenyl (2,6–$^{i}Pr_2C_6H_3$)

δ = chemical shift

η^n = hapticity of a ligand with n contiguous atoms bound to a metal center

E = energy, main–group atom

EI = electron impact

equiv = equivalents

Et_2O = diethyl ether

eV = electron volts

FTIR = Fourier Transform Infrared Spectroscopy

GC–MS = Gas Chromatography – Mass Spectrometry

GoF = Goodness of Fit

g = grams

γ = unit cell angle γ

HOMO = Highest Occupied Molecular Orbital

HRMS = High Resolution Mass Spectrometry

Hz = Hertz (s^{-1})

h = hours

IR = Infared

^{i}Pr = isopropyl ($CH(CH_3)_2$)

J = NMR coupling constant, magnetic coupling constant

κ^n = hapticity of a ligand win n non–contiguous atoms bound to a metal center

K = degrees Kelvin

kcal = kilocalories

L = ligand (neutral), liters

LDA = lithium diisopropylamide

LUMO = Lowest Unoccupied Molecular Orbital

M = transition–metal, mega– (10^6), molar (mol/L)

Me = methyl (CH_3)

$(Me_3Si)_2O$ = bis–trimethylsilyl ether

MeCN = acetonitrile

Mes = mesityl, 2,4,6–trimethylphenyl (2,4,6–$Me_3C_6H_2$)

MO = Molecular Orbital

m = *meta* position

m = multiplet, mili– (10^{-3})

min = minutes

mol = moles

μ = bridging ligands, absorption coefficient (X–Ray crystallography), magnetic moment

NMR = Nuclear Magnetic Resonance

ν = infrared stretching frequency

OTf = triflate, trifluoromethylsulfonate ([OSO_2CF_3])

o = *ortho* position

Ph = phenyl (C_6H_5)

p = *para* position

ppm = parts per million

π = pi

q = quartet

R = organic group, alkyl group

R = residual value (X–ray crystallography)

RT = room temperature

S = single electronic state

S = electronic spin

SOF = Site Occupancy Factor

SOMO = Singly Occupied Molecular Orbital

SQUID = Superconducting Quantum Interference Device

s = singlet, seconds

σ = sigma

T = temperature, triplet electronic state

THF = tetrahydrofuran

t = triplet

Tol = toluene, tolyl (C_7H_8)

^{t}Bu = tertiary–butyl ($C(CH_3)_3$)

Tripp = triisopropylphenyl (2,4,6–$^{i}Pr_3C_6H_2$)

V = unit cell volume

VT = variable temperature

X = halide or pseudo halide

Xyl = xylyl

Z = number of molecules in unit cell

LIST OF FIGURES

LIST OF SCHEMES

LIST OF TABLES

ACKNOWLEDGEMENTS

The work presented here would not have been possible without the assistance and support of many gracious individuals. To all of those involved, I would like to express my deepest gratitude for their roles in my intellectual advancement and for their contributions to the work presented here.

Most importantly, the utmost thanks needs to be given to my graduate advisor, Professor Joshua Figueroa. Knowing I was struggling, he once told me that if I quit, I should at least show the decency of telling him in person, and that sliding a resignation letter under the door would be inappropriate and unacceptable. What I didn't realize then, was that by agreeing to show him that courtesy, I had made it impossible to quit, because although I could tell him anything I like, that didn't ensure he was going to listen. Through our many interactions (i.e. group meetings, one on one discussion in his office, beers) he taught me that most often the only thing worth listening to is the scientific data, not the scientist. With respect to the latter, I suppose given the data he had, he reasoned I could make it, but nevertheless, without his encouragement and support during the times I wanted to throw in the towel, I'm not sure I would have stuck with it, and for that I will be forever indebted to him. He has been an integral part of my maturation as a chemist. The level of intellect, creativity, thoroughness, and scrutiny displayed in the way he conducts science is something to really aspire towards. Furthermore, the amount of energy he spends in fostering the progression of his students from amateurs into seasoned scientist (i.e. assistance with papers, presentations, fellowships, resumes, job placement, etc.) is above and beyond what I would have ever expected from an advisor. Simply, because there is too much to list: Thank you, Josh, for everything. It's been a wild ride that I won't soon forget.

Additionally, I express my thanks to all the faculty and staff at UCSD who have shared their time and expertise with me. Professor Arnie Rheingold; I can only hope I live to see the day where I am half as old, wise, knowledgeable, and cantankerous as him. I greatly appreciate the countless hours he's spent trying to turn me into a competent crystallographer. Dr. Curtis Moore had patience and willingness to share his knowledge of X–ray crystallography, which was a boon for this novice crystallographer. Also, I greatly appreciate his many contributions to our joint publications. He creates order where there is disorder. I also need to thank Professor Charles Perrin and Professor Yitzhak Tor. Without our thoughtful discussions, the synthesis of at least two new isocyanide ligands may never have occurred. Great thanks to Dr. Anthony Mrse for taking the time to assist me with numerous NMR experiments and for sharing his knowledge of record players with me. I would like to thank my graduate committee, Professors Clifford Kubiak, Joseph O'Connor, David Hendrickson, Michael Tauber, and Kenneth Vecchio, who have given their time to make sure I reach the next phases of my educational career. I also thank Professors Seth Cohen, Akif Tezcan, William Trogler, and Nathan Gianneschi for their help and guidance over the years.

I especially thank the other two pioneering graduate students of the Figueroa group, Matt Millard and Liezel Labios. I could not have asked for two more uniquely gifted individuals to begin this endeavor with, and the friendship and support I received from the two of them is immeasurable. The early days of the group, when we consisted of solely Josh and his curious triplet of henchmen, were some of the most intense and rewarding days of my life. In total, the four of us made for a pretty special team and I am better for being a part of it.

Other group members have also had an integral role in this endeavor, and need to be thanked. Brian Fox and Queena Sun, both undergraduate students, essentially taught me both glove box and schlenk line chemistry. Ryan Holland, although not officially a Figueroa group member, made many significant contributions to our lab. Beyond his moral support, Steve George was a big help with DFT calculations for my various projects. Nils Weidemann, and his encyclopedic knowledge of inorganic transformations, was of huge help to me when I reached synthetic road blocks. Grant Margulieux, I don't quite know why I am thanking Grant, but there might be a reason. Donald Ripatti made significant contributions to my work with group 6 isocyanides. Alex Carpenter was a giant help in the development of synthetic strategies for isocyanide syntheses. More importantly, I also need to thank Alex for taking over my role as lab manager; your tireless dedication to the lab is greatly appreciated. I would also like to thank Brandon Barnett, Charles Mokhtarzadeh, and Douglas Agnew for renewing my faith in graduate students and also for their various contributions to my work.

There are several other graduate students at UCSD that I need thank for their time, expertise, and most importantly, their friendship. I would like to thank the artistically gifted Anthony Rush for his help in making cover art. Much thanks to Carrie James for her assistance with ESI–MS and HPLC. I would like to Thank Candace Seu for sharing job postings with me and for giving me tips on thesis formatting. I would like to acknowledge Dr. Mohamed Melaimi and Dr. Sergio Garibay for their aid in conducting cyclic voltammetry and thermogravimetric analysis experiments, respectively. Other graduate students I would like to recognize include: David Hitt, Stephen Cope, Marissa Aubrey, Arpita Agrawal, Matthieu Rouffet, Eric Benson, Jonathan Smieja, Starla Glover, Aaron Sathrum, Robert Radford, Andro Rios, Patrick Feng, Adrian Garcia Sega, Matthew Kinsella, and Jim Royer.

Finally, I need to thank my family. Your love and support over the years has been my greatest gift.

Chapter 2 is adapted from Ditri, T. B.; Fox. B.J.; Moore, C. E.; Rheingold, A. L.; Figueroa, J. S. “Effective Control of Ligation and Geometric Isomerism: Direct Comparison of Steric Properties Associated with Bis–mesityl and Bis–diisopropylphenyl *m*–Terphenyl Ioscyanides” *Inorg. Chem.* **2009,** *48*, 8362–8375. Copyright 2009 American Chemical Society. Permission to use copyrighted images and data in the manuscript was also obtained from Fox. B.J.; Moore, C. E.; Rheingold, A. L.; Figueroa, J. S. The dissertation author is the first author of this paper.

Chapter 3 is adapted from Ditri, T. B.; Moore, C. E.; Rheingold, A. L.; Figueroa, J. S. “Oxidative Decarbonylation of *m*–Terphenyl Isocyanide Complexes of Molybdenum and Tungsten: Precursors to Low–Coordinate Isocyanide Complexes.” *Inorg. Chem.* **2011,** *50*, 10448–10459. Copyright 2011 American Chemical Society. Permission to use copyrighted images and data in the manuscript was also obtained from Moore, C. E.; Rheingold, A. L.; Figueroa, J. S.

Chapter 4 is adapted from Ditri, T. B.; Carpenter, A. E.; Ripatti, D. S.; Moore, C. E.; Rheingold, A. L.; Figueroa, J. S. “Chloro– and Trifluoromethyl–Substituted Flanking–Ring *m*–Terphenyl Isocyanides: η^6–Arene Binding to Zerovalent Molybdenum Centers and Comparison to Alkyl–Substituted Derivatives.” *Inorg. Chem.* **2013,** *52*, 13216–13229. Copyright 2013 American Chemical Society. Permission to use copyrighted images and data in the manuscript was also obtained from Carpenter, A. E., Ripatti, D. S., Moore, C. E., Rheingold, A. L., and Figueroa, J. S. The dissertation author is the first author of this paper.

Chapter 5 is currently being prepared for publication by Ditri, T. B.; Ripatti, D. S.; Moore, C. E.; Rheingold, A. L.; Figueroa, J. S. The dissertation author is the primary author of this paper.

Chapter 6 is currently being prepared for publication by Ditri, T. B.; Moore, C. E.; Rheingold, A. L.; Figueroa, J. S. The dissertation author is the primary author of this paper.

VITA

2007	Bachelor of Science, Wayne State University
2009	Master of Science, University of California, San Diego
2014	Doctor of Philosophy, University of California, San Diego

PUBLICATIONS

Ditri, T. B.; Carpenter, A. E.; Ripatti, D. S.; Moore, C. E.; Rheingold, A. L.; Figueroa, J. S. *"Chloro– and Trifluoromethyl–Substituted Flanking Ring m–Terphenyl Isocyanides: η^6–Arene Binding to Zerovalent Molybdenum Centers and Comparison to Alkyl–Substituted Derivatives."* Inorg. Chem. **2013**, *52*(22), pp *13216–13229*.

Ditri, T. B.; Moore, C. E.; Rheingold, A. L.; Figueroa, J. S. *"Oxidative Decarbonylation of m–Terphenyl Isocyanide Complexes of Molybdenum and Tungsten: Precursors to Low–Coordinate Isocyanide Complexes."* Inorg. Chem. **2011**, *50*(20), pp 10448–10459.

Ditri, T. B.; Fox, B. J.; Moore, C. E.; Rheingold, A. L.; Figueroa, J. S. *"Effective Control of Ligation and Geometric Isomerism: Direct Comparison of Steric Properties Associated with Bis–mesityl and Bis–diisopropylphenyl m–Terphenyl Isocyanides."* Inorg. Chem. **2009**, *48*, 8362–8375.

Radford, R. J.; Nguyen, P. C.; **Ditri, T. B.**; Figueroa, J. S.; Tezcan, F. A. *"Controlled Protein Dimerization Through Hybrid Coordination Motifs."* Inorg. Chem. **2010**, *49* (9), pp 4362–4369.

Stewart, M. A.; Moore, C. E.; **Ditri; T. B.**; Labios, L. A.; Rheingold, A. L; Figueroa, J. S. *"Electrophilic Functionalization of Well–Behaved Manganese Monoanions Supported by m–Terphenyl Isocyanides."* Chem. Commun. **2011**, 406–408.

ABSTRACT OF THE DISSERTATION

Synthesis and Reactivity of Group 6 *m*–Terphenyl Isocyanides

by

Treffly B. Ditri

Doctor of Philosophy in Chemistry

University of California, San Diego, 2014

Professor Joshua S. Figueroa, Chair

A series of isocyanide ligands supported by *m*–terphenyls were synthesized and their utility for the isolation of isocyanide analogues to the unsaturated group 6 metal carbonyls was explored.

The *m*–terphenyl isocyanide $CNAr^{Dipp2}$ (Ar^{Dipp2} = 2,6–(2,6–(*i*–Pr)$_2C_6H_3$)$_2C_6H_3$) was prepared. The steric attributes of $CNAr^{Dipp2}$ and the less encumbering *m*–terphenyl isocyanide $CNAr^{Mes2}$ (Ar^{Mes2} = 2,6–(2,4,6–$Me_3C_6H_2$)$_2C_6H_3$) are compared through the extent of isocyanide ligation to Cu(I), Ag(I), and Mo(0) centers. Structural comparisons of the resulting complexes revealed that while the aforementioned metals could bind three equivalents of $CNAr^{Mes2}$, maximal ligation was limited to two isocyanides with $CNAr^{Dipp2}$.

Additionally, an oxidative decarbonylation/reduction synthetic strategy was used in efforts to generate coordinatively unsaturated group 6 isocyanides [$M(CNAr^{R2})_{2–3}$] from the mixed carbonyl/isocyanide precursors. Accordingly, the zerovalent, bisisocyanide (η^6–C_6H_6)$Mo(N_2)(CNAr^{Dipp2})_2$, and trisisocyanide $M(\eta^6$–(Mes)–κ^1–*C*–$CNAr^{Mes})(CNAr^{Mes2})_2$ (M = Cr and Mo) complexes were prepared. However, coordinative unsaturation in these species was precluded by η^6–binding of benzene or the mesityl ring of the *m*–terphenyl group to the metal center.

Further, in an effort to prevent or weaken the formation of flanking ring η^6–arene interactions observed with the trisisocyanide $Mo(\eta^6$–(R)–κ^1–*C*–$CNAr^{R})(CNAr^{R2})_2$ (Ar^{R2} = Ar^{Mes2} and Ar^{Dipp2}) complexes, the halo–substituted *m*–terphenyl isocyanide ligands $CNAr^{Clips2}$ (Ar^{Clips2} = 2,6–(2,6–Cl-$_2C_6H_3$)$_2$(4–*t*–Bu)C_6H_2) and $CNAr^{DArF2}$ (Ar^{DArF2} = 2,6–(3,5–$(CF_3)_2C_6H_3)_2C_6H_3$) were prepared. Although $Mo(\eta^6$–(R)–κ^1–*C*–$CNAr^{R})(CNAr^{R2})_2$ (Ar^{R2} = $CNAr^{Clips2}$ and $CNAr^{DArF2}$) complexes were obtained, in contrast to their alkyl–substituted counterparts, η^6–coordination of the tethered isocyanide ligand could be disrupted by addition of benzene or acetonitrile.

Following, the reactivity of the $M(\eta^6$–(Mes)–κ^1–*C*–$CNAr^{Mes})(CNAr^{Mes2})_2$ (M = Cr and Mo) complexes towards electrophilic substrates was investigated. Electrophilic addition of [H^+] and [CH_3^+] was shown to occur exclusively at the nitrogen atom of the geometrically

constrained, arene–tethered isocyanide ligands of the M(η^6–(Mes)–κ^1–*C*–$CNAr^{Mes}$)($CNAr^{Mes2}$)$_2$ (M = Cr and Mo) complexes.

Lastly, the four–coordinate tetrakisisocyanide complex [Mo($CNAr^{Mes2}$)$_4$] was targeted. However, reduction of the tetraisocyanide salt [MoI_2($CNAr^{Mes2}$)$_4$](OTf) proceeded wtih loss of $CNAr^{Mes2}$ and formation of Mo(η^6–(Mes)–κ^1–*C*–$CNAr^{Mes}$)($CNAr^{Mes2}$)$_2$.

Chapter 1

Isocyanide Analogues of the Unsaturated Metal Carbonyls

1.1 Introduction

To date, a comprehensive chemical survey of the unsaturated metal carbonyls has been complicated by their lack of kinetic stability. The inherent high reactivity of these species, as exemplified in the representative examples $Mo(CO)_4$, $Ni(CO)_3$, and $Pd(CO)_2$, is attributed to the electron richness of their zerovalent metal centers and their low coordination numbers. Consequently, their marginal stability has limited their study to gas phase or low temperature matrix isolation experiments.[1,2] Although the aforementioned studies have afforded a fundamental understanding of the unsaturated carbonyls, without corroboration by condensed phase studies there remains much ambiguity in the reactivity and preferred coordination geometries of many of these species. In an effort to further elucidate the chemical reactivity, and definitively characterize the molecular structures of the binary unsaturated metal carbonyls, our group has targeted low coordinate isocyanides as potential models for this elusive class of molecules.

1.2 Transition–Metal Carbonyls

The onset of transition–metal carbonyl chemistry can be attributed to Ludwig Mond's discovery of $Ni(CO)_4$ in 1890.[3] Following this seminal report, in 1891 Mond incorrectly reported the synthesis of $Fe(CO)_4$, arguably the first mention of an unsaturated metal carbonyl in the literature.[4] Amazingly, the first spectroscopic evidence for $Fe(CO)_4$ would not be obtained for another 72 years,[5] and complete spectroscopic characterization would require an additional twelve.[6] Nevertheless, in spite of the transient nature of unsaturated metal carbonyls like $Fe(CO)_4$, their presumed roles as active intermediates in various catalytic transformations has led to their continuous study over the last several decades.[7–9] For example, photolysis of $Fe(CO)_5$ has been shown to catalyze the isomerization, hydrogenation, and hydrosilation of alkenes, presumably through the generation of $Fe(CO)_3$ as the active species.[10–13] Similarly, $Co(CO)_4$ has been proposed as a reactive intermediate in industrial hydroformylation and carbonylation processes.[14–16] Other reports have purposed $Cr(CO)_4$ as the catalytically active species in the photochemical hydrogenation of dienes catalyzed by $Cr(CO)_6$.[9]

In addition to their role as catalytic intermediates, extensive attention has also been focused on the coordination behavior of the unsaturated carbonyls. Although the VSEPR and valence bond theories sufficiently account for coordination geometry of many main–group compounds, they are not reliable when extended to most transition–metal complexes. Consequently, the coordination geometries determined spectroscopically by gas phase and frozen matrix studies for the unsaturated carbonyls are in contrast to those predicted by these outdated bonding models. For example, whereas the VSPER model predicts $Ni(CO)_3$ and $Fe(CO)_4$ will adopt trigonal pyramidal (C_{3v}) and tetrahedral (T_d) geometries respectively, they were experimentally determined to possess trigonal planar (D_{3h})[17,18] and distorted tetrahedral

(C_{2v})[6,19] geometries, respectively. The preference for these geometries was elegantly explained by the molecular orbital theory and angular overlap arguments purposed by Burdett. [20,21] By accounting for the non–spherical charge density on the metal center and appropriately addressing the π^* orbitals of the carbonyl ligands, he reasoned that the preferred geometries are the result of maximizing the π–back donation from the metal to the ligands.

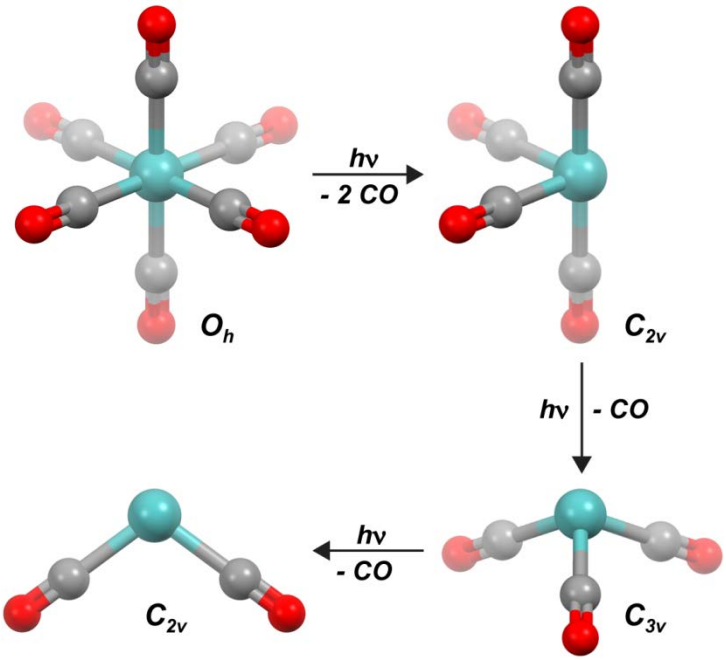

Figure 1.1. Predicted geometries for the unsaturated group 6 metal carbonyls generated from the photodecomposition of $M(CO)_6$.

The most extensively studied unsaturated carbonyls are those generated from the photodecomposition of the group 6 hexacarbonyl $M(CO)_6$ (M = Cr, Mo, and W) complexes (Figure 1.1).[22–35] Beginning in 1975, molecular orbital calculations conducted by Burdett[20,21] and Hoffmann,[36] theorized that contrary to the geometries predicted by the VESPR model, $M(CO)_4$, $M(CO)_3$, and $M(CO)_2$ would possess *cis*–divacant octahedron (C_{2v}), trigonal pyramidal (C_{3v}), and bent (C_{2v}) geometries respectively. Over the following two decades,

matrix isolation[24–26] and gas phase[27–33] IR studies would substantiate these claims. More recently, density functional calculations would also be found to be consistent with these early molecular orbital reports.[34,35] Nevertheless, to date, corroboration of the spectroscopically determined structures with definitive atomic–level structural studies has been precluded by the instability of the unsaturated carbonyls in the condensed phase. For example, reports indicate that $Cr(CO)_5$ binds cyclohexane 2.5 picoseconds after its formation by the photolysis of $Cr(CO)_6$ in cyclohexane solution.[37] Moreover, low temperature mixed matrix studies reveal that the ν_{CO} stretches in the $M(CO)_5$ species are sensitive to the identity of the matrix (Ne, SF_6, CF_4, Ar, Kr, Xe, and CH_4 were surveyed), suggesting that even the noble gases can form appreciable interactions with the coordinatively unsaturated metal centers at low temperatures.[26] In total, the latter reports contextualize the limits of condense phase study of these highly reactive species.

In order to further the study of unsaturated carbonyls, stable and isolable analogues that can be handled and observed in the condensed phase are necessitated. We envisioned that isocyanide analogues of unsaturated carbonyls would provide such models.

1.3 Transition–Metal Isocyanides

The isolobal relationship between CO and organoisocyanides (CNR) make them suitable organic surrogates to CO because they provide a largely similar ligand field (Figure 1.2).[38–41] The resulting isocyanide analogues are particularly appealing models because they have convenient spectroscopic handles. For example, the strong ν_{CN} stretching frequencies in the IR spectroscopy of transition–metal isocyanides provide a wealth of information about the metal complex. Whereas the energy of the ν_{CN} stretches is a strong indicator of the electronics of the metal center, their pattern and intensity provide insight to the coordination geometry the complex. Additionally, similar to CO, the ^{13}C NMR chemical shift of the terminal

isocyanide carbon (C_{iso}) is telling of the magnitude of metal→ligand π–backbonding.[42–44] Moreover, isocyanides have the added benefit of being detectable by ^{1}H NMR spectroscopy. Also, the difficulty encountered in probing the structure and reactivity of the unsaturated metal carbonyls in the condensed phase is alleviated with their isocyanide analogues because both their solubility and crystallinity is tunable through modification of their R–group.

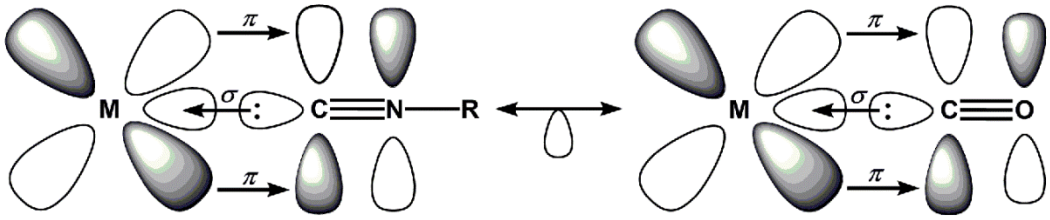

Figure 1.2. Molecular Orbital representations of the isolobal M(CO) and M(CNR) fragments.

Isocyanide analogues of the mononuclear, zerovalent carbonyls have been isolated for several transition–metals.[45] Many of these examples belong to group 6 metals, akin to the $M(CO)_6$ series of compounds.[46–51] Additionally, although less common, representatives featuring early–row and late–row transition–metals have been obtained.[41,45,52] Furthermore, recent reports have established stable, mononuclear, zerovalent, homoleptic isocyanides featuring odd–number transition–metals, a previously elusive target.[53,54] Still, despite their wide application as models for the binary carbonyls, isocyanides have demonstrated very limited success at stabilizing electronically and coordinatively unsaturated metal centers. As illustrated in the $Mo(CNXylyl)_6$[55] and $[Mo(CNPh)_7](PF_6)_2$[56] complexes (Figure 1.3), coordination numbers of isocyanide complexes are often equal to or exceed those of their CO congeners ($Mo(CO)_6$ and $[Mo(CO)_6]^{2+}$, respectively). In light of the previous reports and many others like them, we rationalized that the stabilization of coordinatively and electronically unsaturated isocyanides would require a new class of isocyanide ligand.

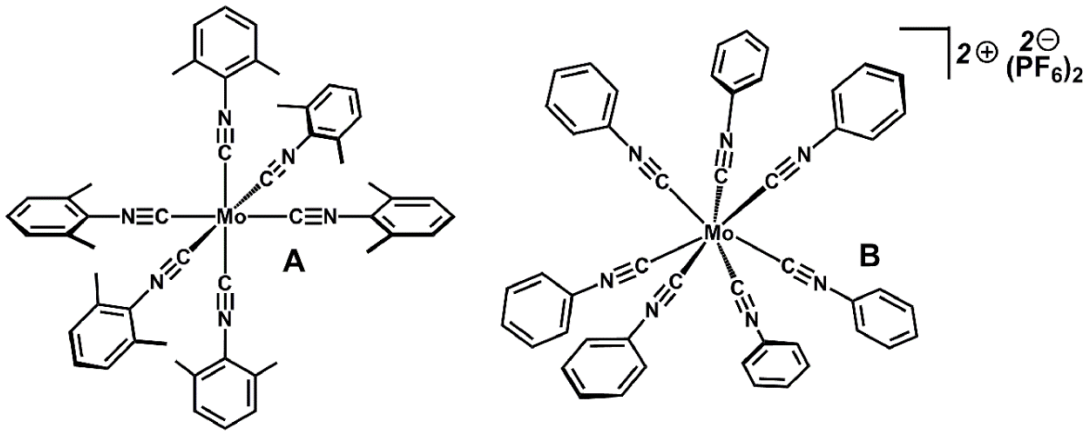

Figure 1.3. Homoleptic molybdenum isocyanide complexes. A) $Mo(CNXylyl)_6$. B) $[Mo(CNPh)_7](PF_6)_2$. Adapted from references 55 and 56.

1.4 Transition–Metal Complexes Supported by *m*–terphenyl Isocyanides

In our efforts to generate isolable analogues of the unsaturated transition–metal carbonyls, our group has employed isocyanides featuring the sterically encumbering *m*–terphenyl group. The proven ability of the *m*–terphenyl to stabilize low–coordinate main–group and transition–metal species made it an obvious choice for our goals. Another appealing feature of the *m*–terphenyl group is the ease with which the steric properties of the ligand framework can be altered. Importantly, subtle changes in the ligand framework have been shown to significantly affect the structure and reactivity of both main–group and transition–metal atoms supported by *m*–terphenyl groups. The earliest examples of the latter were observed in comparative studies between different alkyl–substituted *m*–terphenyl variants.

For example, equilibrium studies of chlorine atom transfer processes revealed that the steric properties of the *m*–terphenyl group control the thermodynamics of the reaction.[57] In this report, phosphorus atoms were shown to more readily foster higher coordination number with

the *m*–terphenyl Ar^{Mes2} (Mes = 2,4,6–$Me_3C_6H_2$) than the more sterically encumbering Ar^{Tripp2} (Tripp = 2,4,6,–(*i*–Pr)$_3C_6H_2$, Scheme 1.1). Similarly, Power and co–workers have demonstrated that the products obtained in the reduction of the Cr(II) dimer {Ar^{Dipp2}Cr(μ–Cl)}$_2$ (Dipp = 2,6–(*i*–Pr)$_2C_6H_3$) and the Cr(II) monomer CrCl(3,5–(*i*–Pr)$_2$–Ar^{Tripp2}) is highly dependent of the identity of the *m*–terphenyl group. Remarkably, whereas the more sterically encumbering *m*–terphenyl 3,5–(*i*–Pr)$_2$–Ar^{Tripp2} stabilized Cr(I) monomers, the less encumbering Ar^{Dipp2} facilitated the formation of chromium dimers featuring 5–fold bonding between the two chromium centers (Figure 1.4).[58,59] Importantly, when a series of unsaturated isocyanides of varying coordination number for a single metal center is desired, as is the case with the M(CO)$_{6–n}$ (n =2 – 4) complexes, a sterically tunable ligand framework is a desirable feature.

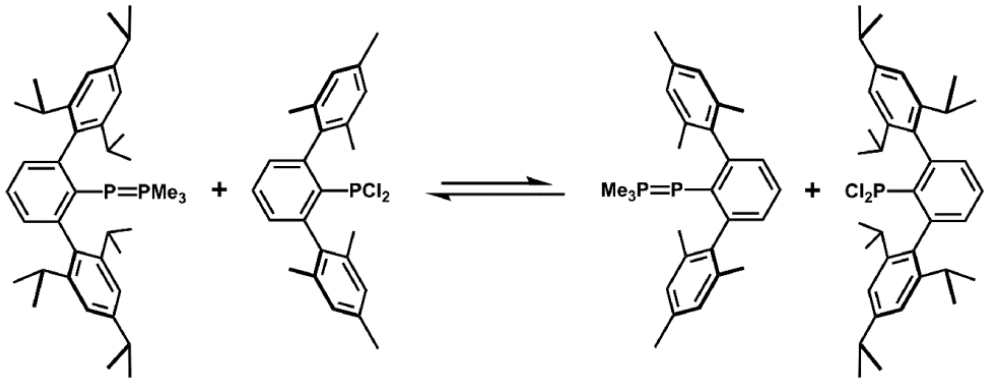

Scheme 1.1. Equilibrium chlorine atom transfer reaction. Adapted from reference 57.

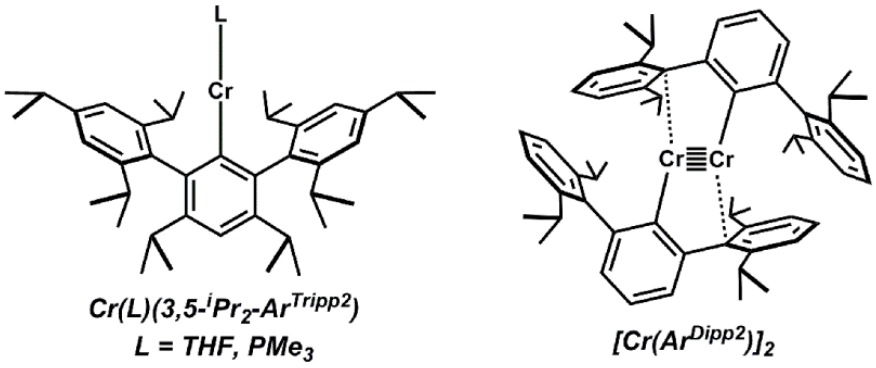

Figure 1.4. Chromium complexes supported by the *m*–terphenyl ligands Ar^{Dipp2} and 3,5–(*i*–$Pr)_2$–Ar^{Tripp2}. Adapted from references 58 and 59.

The *m*–terphenyl group has been utilized as a supporting ancillary for a variety of ligand types including aryls,[58–82] thiolates,[83–87] amidos,[88–95] imidos,[96,97] aryloxides,[98–102] and carboxylates.[103–109] However, in contrast to the aforementioned ligand types, *m*–terphenyl isocyanides have received substantially less attention, and prior to our endeavors, only two reports of their use as supporting ligands for transition–metal complexes had been made. Nagashima and co–workers surveyed the catalytic activity of a series of Ni(II) halide bisisocyanides complexes for the polymerization of ethylene, two of which were supported by *m*–terphenyl isocyanides.[110] Also, Ito and Sawarmura have explored their use in Rh–catalyzed hydrosilylation of ketones.[111,112]

Over the past 6 years our group has successfully utilized *m*–terphenyl isocyanides to generate a host of novel transition–metal complexes of unprecedented structure and reactivity.[54,113–123] The majority of our pursuits have focused on transition–metal complexes supported by the *bis*–mesityl $CNAr^{Mes2}$ and the more sterically encumbering *bis*–diisopropylphenyl $CNAr^{Dipp2}$ *m*–terphenyl isocyanides.[122,123] Not only have $CNAr^{Mes2}$ and $CNAr^{Dipp2}$ been successfully employed for the isolation of isocyanide analogues of the unsaturated binary carbonyls,[54,118,121,124] they have additionally been used to model other key intermediates of metal carbonyl catalyzed reactions.[115,117,118,121,125] Furthermore, transition–

metal *m*–terphenyl isocyanides isolated by our group have displayed reactivity patterns distinct from their CO congeners,[54,115,125] and have been proven to be competent catalyst for chemical transformations.[121]

Low–coordinate *m*–terphenyl isocyanide analogues of the unsaturated binary carbonyls were first isolated by our group for zerovalent group 10 metals.[118,121,124] One of our first targets, an isocyanide analogue of $Ni(CO)_3$ was of interest because of its presumed role as the active intermediate in reactions catalyzed by $Ni(CO)_4$. Through application of a thallium(I) triflate (TlOTf) coordination–site protection strategy, $Ni(CNAr^{Mes2})_3$ was isolated and characterized, and shown to have structural and electronic properties similar to $Ni(CO)_3$ (Scheme 1.2).[124] Interestingly, where $Ni(CNAr^{Mes2})_3$ was shown to readily accommodate a forth equivalent of ligand $CNAr^{Mes2}$, the isocyanide analogue of $Ni(CO)_3$ featuring the more sterically encumbering $CNAr^{Dipp2}$ was resistant to ligation of a forth isocyanide.[118]

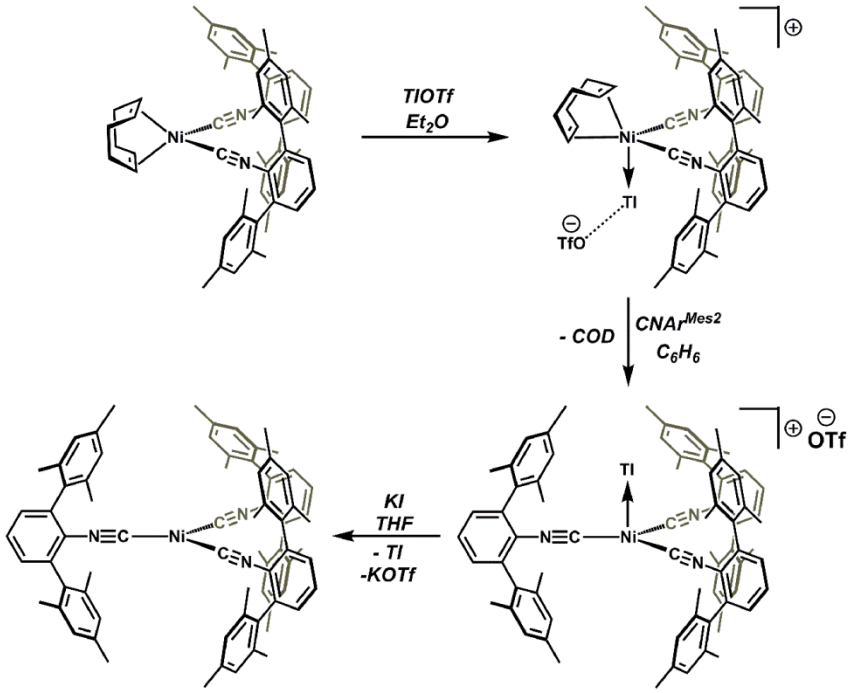

Scheme 1.2. Synthesis of $Ni(CNAr^{Mes2})_2$ by thallium (I) triflate (TlOTf) coordination–site protection strategy.

The added steric protection provided by $CNAr^{Dipp2}$ to zerovalent metals would prove useful in the isolation of an isocyanide analogue to $Pd(CO)_2$. Accordingly, reduction of the dichloride $PdCl_2(CNAr^{Dipp2})_2$ in a 4:1 Et_2O/THF mixture afforded the zerovalent bisisocyanide $Pd(CNAr^{Dipp2})_2$ (Scheme 1.3).[121] Although palladium bisisocyanides had previously been reported, spectroscopic evidence suggested a trimeric $[Pd_3(CNR)_6]$ formulation for these species.[126–130] Therefore, $Pd(CNAr^{Dipp2})_2$ was the first example of a palladium *bis*–isocyanide complex that both solution and condense phase data supported a monomeric constitution. Remarkably, $Pd(CNAr^{Dipp2})_2$ was shown to be catalytically competent for Suzuki–Miyaura cross–coupling reactions.[121]

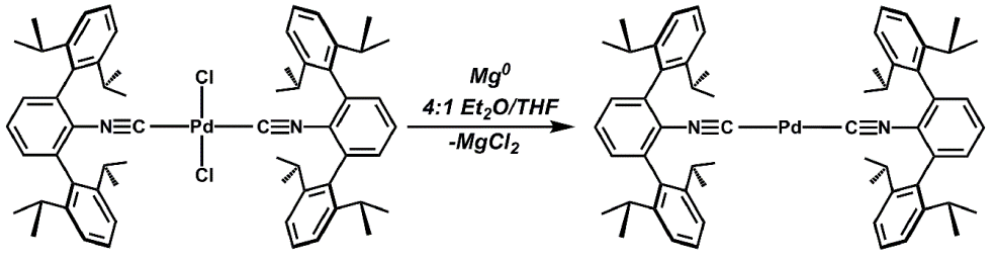

Scheme 1.3. Synthesis of $Pd(CNAr^{Dipp2})_2$.

In addition to our study of *m*–terphenyl isocyanides in conjunction with group 10 metals, extensive efforts have been directed towards their application as supporting ligands for cobalt systems. We were particularly interested in isocyanide analogues of $Co(CO)_4$[14–16] and $[Co(CO)_4]^+$[131–134] because of their presumed role as reactive intermediates in industrial hydroformylation and carbonylation processes. Accordingly, the *m*–terphenyl isocyanide $CNAr^{Mes2}$ was used for the isolation of a full series of mononuclear $[Co(CNAr^{Mes2})_4]^n$ complexes (n = 1+, 0, 1–, Scheme 1.4).[54] Interestingly, while the isocyanide complexes in this series appropriately modeled some of the geometric and structural properties their carbonyl analogues, in other aspects they failed to do so, thus indicating certain limits to the

validity of isolobal substitution of CO for CNR in model systems.[54] For example, in contrast to the $[Co(CNAr^{Mes2})_4]^+$ cation which is diamagnetic and square planer in geometry, gas–phase studies of $[Co(CO)_4]^+$ strongly suggest a "saw–horse" C_{2v}–symmetric geometry and a S =1 ground state.[135–137] In ensuing studies, the ability of $CNAr^{Mes2}$ to support three–coordinate cobalt metallates was demonstrated by the isolation of the trisisocyanide salt (η^2–PPN)$[Co(CNAr^{Mes2})_3]$ (PPN = $[Ph_3PNPPh_3]^+$).[115] Importantly, treatment of (η^2–PPN)$[Co(CNAr^{Mes2})_3]$ with pivaloyl chloride (tBuC(O)Cl) resulted in acyl–group decarbonylation and formation of the monohydride $HCo(CO)(CNAr^{Mes2})_3$.[115] Notably, $HCo(CO)(CNAr^{Mes2})_3$ provides an isolable mixed carbonyl/isocyanide analogue of yet another intermediate in the hydroformylation catalytic cycle, $HCo(CO)_4$.[138] Also noteworthy, a m–terphenyl isocyanide analogue of $HCo(CO)_4$ has recently been obtained.[125]

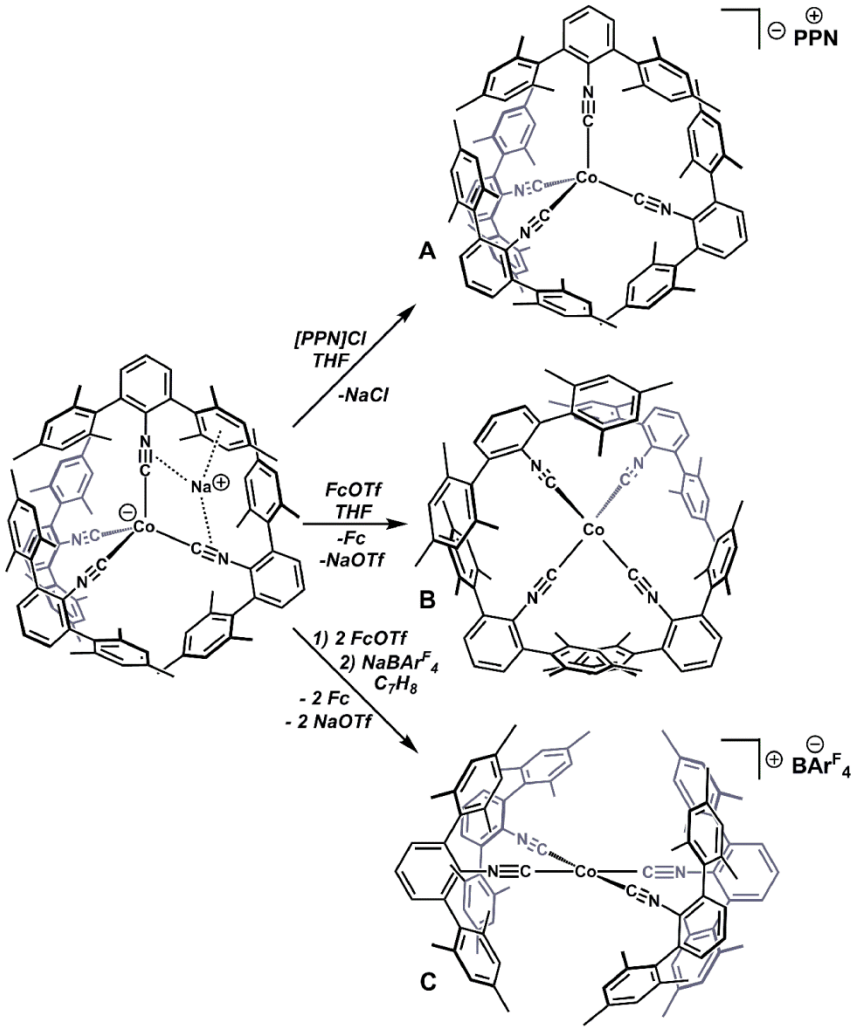

Scheme 1.4. Synthesis of a full series of mononuclear $[Co(CNAr^{Mes2})_4]^n$ complexes (n = 1+, 0, 1–). A) $[Co(CNAr^{Mes2})_4](PPN)$. B) $Co(CNAr^{Mes2})_4$. C) $[Co(CNAr^{Mes2})_4](BAr^F{}_4)$.

Given the proven ability of $CNAr^{Mes2}$ and $CNAr^{Dipp2}$ to effectively stabilize isocyanide analogues of $Co(CO)_4$, $Ni(CO)_3$, and $Pd(CO)_2$, we reasoned that these encumbering ligands could provide a route to the unsaturated group 6 species $[Mo(CNR)_4]$, $[Mo(CNR)_3]$, and $[Mo(CNR)_2]$. In particular, we were interested to determine if $[Mo(CNR)_4]$, $[Mo(CNR)_3]$, and $[Mo(CNR)_2]$ would adopt similar geometries to those determined for their carbonyl analogues or have distinct electronic and structural properties. Moreover, without any definitive examples of structurally characterized, coordinatively–unsaturated, zerovalent

group 6 complexes, we were curious to explore whether or not *m*–terphenyl isocyanides could provide entry into this unknown class of compounds. Accordingly, the chemistry and reactivity of group 6 complexes supported by *m*–terphenyl isocyanides is described in the following chapters.

1.5 References

(1) Zhou, M.; Andrews, L.; Bauschlicher, C. W. *Chem. Rev.* **2001**, *101*, 1931–1962.

(2) Ozin, G. A.; Voet, A. V. In *Prog. Inorg. Chem.*; John Wiley & Sons, Inc.: 2007, p 105–172.

(3) Mond, L.; Langer, C.; Quincke, F. *Journal of the Chemical Society, Transactions* **1890**, *57*, 749–753.

(4) Mond, L.; Quincke, F. *Journal of the Chemical Society, Transactions* **1891**, *59*, 604–607.

(5) Stolz, I. W.; Dobson, G. R.; Sheline, R. K. *J. Am. Chem. Soc.* **1962**, *84*, 3589–3590.

(6) Poliakoff, M.; Turner, J. J. *J. Chem. Soc., Dalton Trans.* **1974**, 2276–2285.

(7) Bailey, D. C.; Langer, S. H. *Chem. Rev.* **1981**, *81*, 109–148.

(8) Wrighton, M. S.; Graff, J. L.; Kazlauskas, R. J.; Mitchener, J. C.; Reichel, C. L. *Pure Appl. Chem.* **1982**, *54*, 161–176.

(9) Moggi, L.; Juris, A.; Sandrini, D.; Manfrin, M. F. *Reviews of Chemical Intermediates* **1981**, *4*, 171–223.

(10) Schroeder, M. A.; Wrighton, M. S. *J. Am. Chem. Soc.* **1976**, *98*, 551–558.

(11) A. Schroeder, M.; S. Wrighton, M. *J. Organomet. Chem.* **1977**, *128*, 345–358.

(12) Mitchener, J. C.; Wrighton, M. S. *J. Am. Chem. Soc.* **1981**, *103*, 975–977.

(13) Whetten, R. L.; Fu, K. J.; Grant, E. R. *J. Am. Chem. Soc.* **1982**, *104*, 4270–4272.

(14) Nalesnik, T. E.; Orchin, M. *Organometallics* **1982**, *1*, 222–223.

(15) Klingler, R. J.; Rathke, J. W. *J. Am. Chem. Soc.* **1994**, *116*, 4772–4785.

(16) Wegman, R. W.; Brown, T. L. *J. Am. Chem. Soc.* **1980**, *102*, 2494–2495.

(17) DeKock, R. L. *Inorg. Chem.* **1971**, *10*, 1205–1211.

(18) Rest, A. J.; Turner, J. J. *J. Chem. Soc. D: Chem. Commun.* **1969**, 1026–1026.

(19) Poliakoff, M.; Weitz, E. *Acc. Chem. Res.* **1987**, *20*, 408–414.

(20) Burdett, J. K. *J.Chem. Soc., Faraday Trans. 2* **1974**, *70*, 1599–1613.

(21) Burdett, J. K. *Inorg. Chem.* **1975**, *14*, 375–382.

(22) Graham, M. A.; Poliakoff, M.; Turner, J. J. *J. Phys. Chem. A* **1971**, 2939–2948.

(23) Burdett, J. K.; Graham, M. A.; Perutz, R. N.; Poliakoff, M.; Rest, A. J.; Turner, J. J.; Turner, R. F. *J. Am. Chem. Soc.* **1975**, *97*, 4805–4808.

(24) Perutz, R. N.; Turner, J. J. *J. Am. Chem. Soc.* **1975**, *97*, 4800–4804.

(25) Perutz, R. N.; Turner, J. J. *Inorg. Chem.* **1975**, *14*, 262–270.

(26) Perutz, R. N.; Turner, J. J. *J. Am. Chem. Soc.* **1975**, *97*, 4791–4800.

(27) Fletcher, T. R.; Rosenfeld, R. N. *J. Am. Chem. Soc.* **1985**, *107*, 2203–2212.

(28) Seder, T. A.; Church, S. P.; Weitz, E. *J. Am. Chem. Soc.* **1986**, *108*, 4721–4728.

(29) Ishikawa, Y.; Hackett, P. A.; Rayner, D. M. *J. Phys. Chem.* **1988**, *92*, 3863–3869.

(30) Ganske, J. A.; Rosenfeld, R. N. *J. Phys. Chem.* **1989**, *93*, 1959–1963.

(31) Ishikawa, Y.; Brown, C. E.; Hackett, P. A.; Rayner, D. M. *J. Phys. Chem.* **1990**, *94*, 2404–2413.

(32) Andrews, L.; Zhou, M.; Gutsev, G. L. *J. Phys. Chem. A* **2003**, *107*, 990–999.

(33) Andrews, L.; Zhou, M.; Gutsev, G. L.; Wang, X. *J. Phys. Chem. A* **2003**, *107*, 561–569.

(34) Ishikawa, Y.; Kawakami, K. *J. Phys. Chem. A* **2007**, *111*, 9940–9944.

(35) Ehlers, A. W.; Frenking, G. *J. Am. Chem. Soc.* **1994**, *116*, 1514–1520.

(36) Elian, M.; Hoffmann, R. *Inorg. Chem.* **1975**, *14*, 1058–1076.

(37) Simon, J. D.; Xie, X. *J. Phys. Chem.* **1986**, *90*, 6751–6753.

(38) Malatesta, L.; Bonati, F. *Isocyanide complexes of metals*; Wiley, 1969.

(39) Bonati, F.; Minghetti, G. *Inorg. Chim. Acta* **1974**, *9*, 95–112.

(40) Sarapu, A. C.; Fenske, R. F. *Inorg. Chem.* **1974**, *14*, 247–253.

(41) Yamamoto, Y. *Coord. Chem. Rev.* **1980**, *32*, 193–233.

(42) Guy, M. P.; Coffer, J. L.; Rommel, J. S.; Bennett, D. W. *Inorg. Chem.* **1988**, *27*, 2942–2945.

(43) Minelli, M.; Maley, W. J. *Inorg. Chem.* **1989**, *28*, 2954–2958.

(44) Rommel, J. S.; Weinrach, J. B.; Grubisha, D. S.; Bennett, D. W. *Inorg. Chem.* **1988**, *27*, 2945–2949.

(45) Barybin, M. V.; Meyers, J. J.; Neal, B. M. In *Isocyanide Chemistry*; Wiley–VCH Verlag GmbH & Co. KGaA: 2012, p 493–529.

(46) Mann, K. R.; Cimolino, M.; Geoffroy, G. L.; Hammond, G. S.; Orio, A. A.; Albertin, G.; Gray, H. B. *Inorg. Chim. Acta* **1976**, *16*, 97–101.

(47) Treichel, P. M.; Essenmacher, G. J. *Inorg. Chem.* **1976**, *15*, 146–150.

(48) Yamamoto, Y.; Yamazaki, H. *J. Organomet. Chem.* **1985**, *282*, 191–200.

(49) Filippou, A. C.; Grünleitner, W. *J. Organomet. Chem.* **1990**, *398*, 99–115.

(50) Barybin, M. V.; Holovics, T. C.; Deplazes, S. F.; Lushington, G. H.; Powell, D. R.; Toriyama, M. *J. Am. Chem. Soc.* **2002**, *124*, 13668–13669.

(51) Robinson, R. E.; Holovics, T. C.; Deplazes, S. F.; Lushington, G. H.; Powell, D. R.; Barybin, M. V. *J. Am. Chem. Soc.* **2003**, *125*, 4432–4433.

(52) Singleton, E.; Oosthuizen, H. E. In *Adv. Organomet. Chem.*; Stone, F. G. A., Robert, W., Eds.; Academic Press: 1983; Vol. Volume 22, p 209–310.

(53) Barybin, M. V.; Young, V. G.; Ellis, J. E. *J. Am. Chem. Soc.* **2000**, *122*, 4678–4691.

(54) Margulieux, G. W.; Weidemann, N.; Lacy, D. C.; Moore, C. E.; Rheingold, A. L.; Figueroa, J. S. *J. Am. Chem. Soc.* **2010**, *132*, 5033–5035.

(55) Yamamoto, Y.; Yamazaki, H. *J. Organomet. Chem.* **1985**, *282*, 191–200.

(56) Dewan, J. C.; Lippard, S. J. *Inorg. Chem.* **1982**, *21*, 1682–1684.

(57) Smith, R. C.; Shah, S.; Urnezius, E.; Protasiewicz, J. D. *J. Am. Chem. Soc.* **2002**, *125*, 40–41.

(58) Nguyen, T.; Sutton, A. D.; Brynda, M.; Fettinger, J. C.; Long, G. J.; Power, P. P. *Science* **2005**, *310*, 844–847.

(59) Wolf, R.; Brynda, M.; Ni, C.; Long, G. J.; Power, P. P. *J. Am. Chem. Soc.* **2007**, *129*, 6076–6077.

(60) Peng, Y.; Fischer, R. C.; Merrill, W. A.; Fischer, J.; Pu, L.; Ellis, B. D.; Fettinger, J. C.; Herber, R. H.; Power, P. P. *Chem. Sci.* **2010**, *1*, 461–468.

(61) Zhu, Z.; Fischer, R. C.; Ellis, B. D.; Rivard, E.; Merrill, W. A.; Olmstead, M. M.; Power, P. P.; Guo, J. D.; Nagase, S.; Pu, L. *Chem.—Eur. J.* **2009**, *15*, 5263–5272.

(62) Ni, C.; Long, G. J.; Power, P. P. *Organometallics* **2009**, *28*, 5012–5016.

(63) Nguyen, T.; Merrill, W. A.; Ni, C.; Lei, H.; Fettinger, J. C.; Ellis, B. D.; Long, G. J.; Brynda, M.; Power, P. P. *Angew. Chem., Int. Ed.* **2008**, *47*, 9115–9117.

(64) Lei, H.; Ellis, B. D.; Ni, C.; Grandjean, F.; Long, G. J.; Power, P. P. *Inorg. Chem.* **2008**, *47*, 10205–10207.

(65) La Macchia, G.; Gagliardi, L.; Power, P. P.; Brynda, M. *J. Am. Chem. Soc.* **2008**, *130*, 5104–5114.

(66) Wolf, R.; Ni, C.; Nguyen, T.; Brynda, M.; Long, G. J.; Sutton, A. D.; Fischer, R. C.; Fettinger, J. C.; Hellman, M.; Pu, L.; Power, P. P. *Inorg. Chem.* **2007**, *46*, 11277–11290.

(67) Wang, Y.; Quillian, B.; Wannere, C. S.; Wei, P.; Schleyer, P. v. R.; Robinson, G. H. *Organometallics* **2007**, *26*, 3054–3056.

(68) Rivard, E.; Power, P. P. *Inorg. Chem.* **2007**, *46*, 10047–10064.

(69) Power, P. P. *Organometallics* **2007**, *26*, 4362–4372.

(70) Yang, X.–J.; Wang, Y.; Quillian, B.; Wei, P.; Chen, Z.; Schleyer, P. v. R.; Robinson, G. H. *Organometallics* **2006**, *25*, 925–929.

(71) Wang, Y.; Quillian, B.; Yang, X.–J.; Wei, P.; Chen, Z.; Wannere, C. S.; Schleyer, P. v. R.; Robinson, G. H. *J. Am. Chem. Soc.* **2005**, *127*, 7672–7673.

(72) Power, P. P. *Chem. Commun.* **2003**, 2091–2101.

(73) Stender, M.; Phillips, A. D.; Wright, R. J.; Power, P. P. *Angew. Chem., Int. Ed.* **2002**, *41*, 1785–1787.

(74) Phillips, A. D.; Wright, R. J.; Olmstead, M. M.; Power, P. P. *J. Am. Chem. Soc.* **2002**, *124*, 5930–5931.

(75) Eichler, B. E.; Power, P. P. *Angew. Chem., Int. Ed.* **2001**, *40*, 796–797.

(76) Robinson, G. H. *Chem. Commun.* **2000**, 2175–2181.

(77) Robinson, G. H. *Acc. Chem. Res.* **1999**, *32*, 773–782.

(78) Su, J.; Li, X.–W.; Crittendon, R. C.; Campana, C. F.; Robinson, G. H. *Organometallics* **1997**, *16*, 4511–4513.

(79) Olmstead, M. M.; Simons, R. S.; Power, P. P. *J. Am. Chem. Soc.* **1997**, *119*, 11705–11706.

(80) Wehmschulte, R. J.; Grigsby, W. J.; Schiemenz, B.; Bartlett, R. A.; Power, P. P. *Inorg. Chem.* **1996**, *35*, 6694–6702.

(81) Schiemenz, B.; Power, P. P. *Angew. Chem., Int. Ed. Engl.* **1996**, *35*, 2150–2152.

(82) Protasiewicz, J. D. *J. Chem. Soc., Chem. Commun.* **1995**, 1115–1116.

(83) Bryan, A. M.; Merrill, W. A.; Reiff, W. M.; Fettinger, J. C.; Power, P. P. *Inorg. Chem.* **2012**, *51*, 3366–3373.

(84) Ellison, J. J.; Ruhlandt–Senge, K.; Power, P. P. *Angew. Chem., Int. Ed. Engl.* **1994**, *33*, 1178–1180.

(85) Rekken, B. D.; Brown, T. M.; Fettinger, J. C.; Lips, F.; Tuononen, H. M.; Herber, R. H.; Power, P. P. *J. Am. Chem. Soc.* **2013**, *135*, 10134–10148.

(86) Rekken, B. D.; Brown, T. M.; Olmstead, M. M.; Fettinger, J. C.; Power, P. P. *Inorg. Chem.* **2013**, *52*, 3054–3062.

(87) S. Buyuktas, B.; P. Power, P. *Chem. Commun.* **1998**, 1689–1690.

(88) Alexander Merrill, W.; Stich, T. A.; Brynda, M.; Yeagle, G. J.; Fettinger, J. C.; Hont, R. D.; Reiff, W. M.; Schulz, C. E.; Britt, R. D.; Power, P. P. *J. Am. Chem. Soc.* **2009**, *131*, 12693–12702.

(89) Boynton, J. N.; Guo, J.–D.; Fettinger, J. C.; Melton, C. E.; Nagase, S.; Power, P. P. *J. Am. Chem. Soc.* **2013**, *135*, 10720–10728.

(90) Boynton, J. N.; Merrill, W. A.; Reiff, W. M.; Fettinger, J. C.; Power, P. P. *Inorg. Chem.* **2012**, *51*, 3212–3219.

(91) Li, J.; Song, H.; Cui, C.; Cheng, J.–P. *Inorg. Chem.* **2008**, *47*, 3468–3470.

(92) Merrill, W. A.; Steiner, J.; Betzer, A.; Nowik, I.; Herber, R.; Power, P. P. *Dalton Trans.* **2008**, 5905–5910.

(93) Merrill, W. A.; Wright, R. J.; Stanciu, C. S.; Olmstead, M. M.; Fettinger, J. C.; Power, P. P. *Inorg. Chem.* **2010**, *49*, 7097–7105.

(94) Ni, C.; Fettinger, J. C.; Long, G. J.; Power, P. P. *Inorg. Chem.* **2009**, *48*, 2443–2448.

(95) Ni, C.; Rekken, B.; Fettinger, J. C.; Long, G. J.; Power, P. P. *Dalton Trans.* **2009**, 8349–8355.

(96) Gavenonis, J.; Tilley, T. D. *Organometallics* **2002**, *21*, 5549–5563.

(97) Gavenonis, J.; Tilley, T. D. *J. Am. Chem. Soc.* **2002**, *124*, 8536–8537.

(98) Hill, J. E.; Balaich, G. J.; Fanwick, P. E.; Rothwell, I. P. *Organometallics* **1991**, *10*, 3428–3430.

(99) Hill, J. E.; Fanwick, P. E.; Rothwell, I. P. *Organometallics* **1990**, *9*, 2211–2213.

(100) Hill, J. E.; Fanwick, P. E.; Rothwell, I. P. *Organometallics* **1991**, *10*, 15–16.

(101) Ni, C.; Power, P. P. *Chem. Commun.* **2009**, 5543–5545.

(102) Stanciu, C.; Olmstead, Marilyn M.; Phillips, Andrew D.; Stender, M.; Power, Philip P. *Eur. J. Inorg. Chem.* **2003**, *2003*, 3495–3500.

(103) Carson, E. C.; Lippard, S. J. *J. Am. Chem. Soc.* **2004**, *126*, 3412–3413.

(104) Carson, E. C.; Lippard, S. J. *Inorg. Chem.* **2005**, *45*, 828–836.

(105) Carson, E. C.; Lippard, S. J. *Inorg. Chem.* **2005**, *45*, 837–848.

(106) Hagadorn, J. R.; Que, L.; Tolman, W. B. *Inorg. Chem.* **2000**, *39*, 6086–6090.

(107) Hagadorn, J. R.; Que, L.; Tolman, W. B.; Prisecaru, I.; Münck, E. *J. Am. Chem. Soc.* **1999**, *121*, 9760–9761.

(108) Klein, D. P.; Young, V. G.; Tolman, W. B.; Que, L. *Inorg. Chem.* **2006**, *45*, 8006–8008.

(109) Yoon, S.; Lippard, S. J. *J. Am. Chem. Soc.* **2005**, *127*, 8386–8397.

(110) Tanabiki, M.; Tsuchiya, K.; Kumanomido, Y.; Matsubara, K.; Motoyama, Y.; Nagashima, H. *Organometallics* **2004**, *23*, 3976–3981.

(111) Ito, H.; Kato, T.; Sawamura, M. *Chem. Lett.* **2006**, *35*, 1038–1039.

(112) Ito, H.; Kato, T.; Sawamura, M. *Chem.—Asian J.* **2007**, *2*, 1436–1446.

(113) Ditri, T. B.; Carpenter, A. E.; Ripatti, D. S.; Moore, C. E.; Rheingold, A. L.; Figueroa, J. S. *Inorg. Chem.* **2013**, *52*, 13216–13229.

(114) Carpenter, A. E.; Wen, I.; Moore, C. E.; Rheingold, A. L.; Figueroa, J. S. *Chem. Eur. J.* **2013**, *19*, 10452–10457.

(115) Carpenter, A. E.; Margulieux, G. W.; Millard, M. D.; Moore, C. E.; Weidemann, N.; Rheingold, A. L.; Figueroa, J. S. *Angew. Chem., Int. Ed.* **2012**, *51*, 9412–9416.

(116) Tomson, N. C.; Labios, L. A.; Weyhermüller, T.; Figueroa, J. S.; Wieghardt, K. *Inorg. Chem.* **2011**, *50*, 5763–5776.

(117) Stewart, M. A.; Moore, C. E.; Ditri, T. B.; Labios, L. A.; Rheingold, A. L.; Figueroa, J. S. *Chem. Commun.* **2011**, *47*, 406–408.

(118) Emerich, B. M.; Moore, C. E.; Fox, B. J.; Rheingold, A. L.; Figueroa, J. S. *Organometallics* **2011**, *30*, 2598–2608.

(119) Ditri, T. B.; Moore, C. E.; Rheingold, A. L.; Figueroa, J. S. *Inorg. Chem.* **2011**, *50*, 10448–10459.

(120) Weidemann, N.; Margulieux, G. W.; Moore, C. E.; Rheingold, A. L.; Figueroa, J. S. *Inorg. Chim. Acta* **2010**, *364*, 238–245.

(121) Labios, L. A.; Millard, M. D.; Rheingold, A. L.; Figueroa, J. S. *J. Am. Chem. Soc.* **2009**, *131*, 11318–11319.

(122) Ditri, T. B.; Fox, B. J.; Moore, C. E.; Rheingold, A. L.; Figueroa, J. S. *Inorg. Chem.* **2009**, *48*, 8362–8375.

(123) Fox, B. J.; Sun, Q. Y.; DiPasquale, A. G.; Fox, A. R.; Rheingold, A. L.; Figueroa, J. S. *Inorg. Chem.* **2008**, *47*, 9010–9020.

(124) Fox, B. J.; Millard, M. D.; DiPasquale, A. G.; Rheingold, A. L.; Figueroa, J. S. *Angew. Chem., Int. Ed.* **2009**, *48*, 3473–3477.

(125) Carpenter, A. E.; Moore, C. E.; Rheingold, A. L.; Figueroa, J. S.; Critical Assessment of the Isocyanide for Carbonyl Isolobal Substitution I: Synthesis, Decomposition Pathways, and Reactivity of a Well–Defined *m*–Terphenyl Isocyanide Analogue of $HCo(CO)_4$. *Inorg.*, In Preperation.

(126) Yamamoto, Y.; Yamazaki, H. *J. Chem. Soc., Dalton Trans.* **1989**, 2161–2166.

(127) Francis, C. G.; Khan, S. I.; Morton, P. R. *Inorg. Chem.* **1984**, *23*, 3680–3681.

(128) Christofides, A. *J. Organomet. Chem.* **1983**, *259*, 355–365.

(129) Thomas, M. G.; Pretzer, W. R.; Beier, B. F.; Hirsekorn, F. J.; Muetterties, E. L. *J. Am. Chem. Soc.* **1977**, *99*, 743–748.

(130) Day, V. W.; Day, R. O.; Kristoff, J. S.; Hirsekorn, F. J.; Muetterties, E. L. *J. Am. Chem. Soc.* **1975**, *97*, 2571–2573.

(131) Zhou, M.; Andrews, L. *J. Phys. Chem. A* **1999**, *103*, 7773–7784.

(132) Goebel, S.; Haynes, C. L.; Khan, F. A.; Armentrout, P. B. *J. Am. Chem. Soc.* **1995**, *117*, 6994–7002.

(133) Bidinosti, D. R.; McIntyre, N. S. *Chemical Communications (London)* **1967**, 1–2.

(134) Winters, R. E.; Kiser, R. W. *J. Phys. Chem.* **1965**, *69*, 1618–1622.

(135) Huo, C.–F.; Li, Y.–W.; Wu, G.–S.; Beller, M.; Jiao, H. *J. Phys. Chem. A* **2002**, *106*, 12161–12169.

(136) Ricks, A. M.; Bakker, J. M.; Douberly, G. E.; Duncan, M. A. *J. Phys. Chem. A* **2009**, *113*, 4701–4708.

(137) Ryeng, H.; Gropen, O.; Swang, O. *J. Phys. Chem. A* **1997**, *101*, 8956–8958.

(138) Wender, I.; Sternberg, H. W.; Orchin, M. *J. Am. Chem. Soc.* **1953**, *75*, 3041–3042.

Chapter 2

Direct Comparison of Steric Properties Associated with Bis–mesityl and Bis–diisopropylphenyl *m*–Terphenyl Isocyanides

2.1 Introduction

Isocyanides (C≡NR) have long been recognized as effective ligands for transition–metals because of their standing as isolobal fragments to carbon monoxide (CO).[1–3] Accordingly, this electronic structure attribute has enabled the use of isocyanides as tunable organic surrogates to CO within a host of low–valent metal complexes. For example, 18–electron homoleptic isocyanometallates[4–6] of Fe and Co have been prepared (e.g., $[Fe(CNXyl)_4]^{2-}$ and $[Co(CNXyl)_4]^{-}$, Xyl = 2,6–$Me_2C_6H_3$), which are clear analogues of the well–known carbonylmetallates $[Fe(CO)_4]^{2-}$ and $[Co(CO)_4]^{-}$. In addition, homoleptic isocyanide complexes of Group 6 metals, akin to the classic $Mo(CO)_6$ series of compounds, have been reported.[7–14] Most interestingly however, metal isocyanides and isocyanometallates often display reactivity patterns distinct from their carbonyl congeners owing to the attenuated π–acidity and increased σ–basicity of the C≡NR functionality relative to CO.[1–3,15]

Seeking to further enhance the reactivity of isocyanide complexes by enforcing low metal coordination numbers, we have recently introduced the sterically encumbering bis–mesityl substituted *m*–terphenyl isocyanide ligand $CNAr^{Mes2}$ (Mes = 2,4,6–$Me_3C_6H_2$).[16] It was demonstrated that the $CNAr^{Mes2}$ ligand affords trisisocyanide Cu(I) species under conditions where *tetrakis*–isocyanide Cu(I) complexes are normally obtained. Thus, in comparison to less sterically protective C≡NR ligands, the spatial properties of $CNAr^{Mes2}$ can effectively prevent maximal isocyanide ligation with respect to a given metal center. The ability of the *m*–terphenyl framework[17,18] to significantly affect the structure and reactivity of transition–metal and main–group atoms is well established.[17–35] For example, Power has recently demonstrated that certain hindered *m*–terphenyl ligands can kinetically stabilize remarkably low–coordinate Cr monomers,[36,37] whereas less encumbering *m*–terphenyls give rise to Cr–Cr dimers with 5–fold bonding interactions.[36,38] Furthermore, Protasiewicz has reported an elegant intermolecular chlorine atom transfer reaction, which is thermodynamically controlled by the steric properties of the *m*–terphenyl group.[39] In this latter work, it was shown that phosphorus atoms bearing the Ar^{Mes2} *m*–terphenyl group more readily accommodate a higher coordination number than those featuring the larger bis–triisopropylphenyl derivative Ar^{Tripp2} (Tripp = 2,4,6,–(*i*–Pr)$_3C_6H_2$, see Figure 2.1).

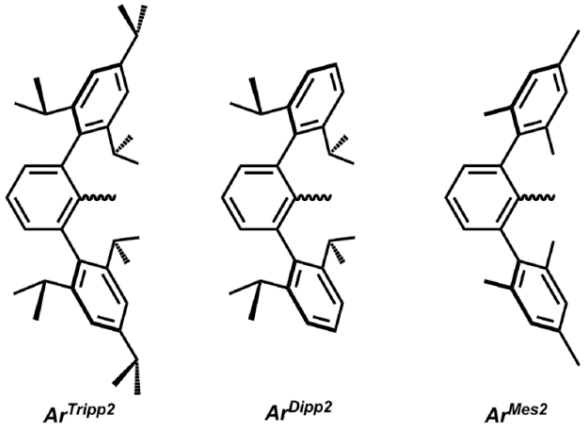

Figure 2.1. Common substituted *m*–terphenyl frameworks.

Inspired by these studies, we sought to generate additional encumbering *m*–terphenyl isocyanides to compare the effect of the Ar^{R2} group on the relative coordination behavior of the isocyanide functionality and structural properties of ensuing complexes. We hoped that by increasing the steric demand of the *m*–terphenyl framework, lower–coordinate metal complexes may be prepared which are otherwise inaccessible with our prototype $CNAr^{Mes2}$ system. Furthermore, we were particularly curious if the spacing provided by the two–atom, isocyanide linkage would serve to negate any added steric influence of the *m*–terphenyl group. Such long metal–to–balk distances could potentially render the steric properties of various flanking substituents of an *m*–terphenyl unit identical. Accordingly, herein we present a new *m*–terphenyl isocyanide variant, namely, the bis–diisopropylphenyl derivative[17,18,40] $CNAr^{Dipp2}$ (Dipp = 2,6,–(*i*–Pr)$_2$C$_6$H$_3$), and show that relative to $CNAr^{Mes2}$, its increased steric demand is indeed significant, and further controls the extent of isocyanide ligation for Group 11 metal centers. In addition, we have investigated the relative coordination behavior of both $CNAr^{Mes}$ and $CNAr^{Dipp}$ toward zerovalent molybdenum–carbonyl fragments ([Mo(CO)$_n$], *n* = 3,4). As with the Group 11 metals surveyed, $CNAr^{Mes2}$ and $CNAr^{Dipp2}$ differ in the extent of their ligation to these reduced molybdenum centers. However, both *m*–terphenyl isocyanides dramatically affect the coordination geometry of the resulting molybdenum complexes and are shown to provide geometric isomers that are exceptionally rare in context of mixed isocyanide/carbonyl Group 6 species.

2.2 Preparation of the *m*–Terphenyl Isocyanide $CNAr^{Dipp2}$

A synthetic route to $CNAr^{Dipp2}$ is outlined in Scheme 2.1. Unlike the synthesis of $CNAr^{Mes2}$, the steric properties of the Ar^{Dipp2} framework prevent a smooth condensation reaction between the aniline[41] H_2NAr^{Dipp2} and formic acid (HC(O)OH). We thus turned to the potent electrophile acetic formic anhydride ($H_3CC(O)OC(O)H$),[42,43] which successfully

effected the formylation of H_2Nar^{Dipp2} in high yield over the course of 36 h. Dehydration of the corresponding formaniline $HC(O)HNAr^{Dipp2}$ with $OPCl_3$ in the presence of $HN(i\text{–}Pr)_2$ preceded readily to afford the isocyanide $CNAr^{Dipp2}$ in 90% yield. Crystallographic characterization of $CNAr^{Dipp2}$ confirmed the presence of the isocyano group (d(C1–N1) = 1.1557(18) Å, Figure 2.2), as did FTIR spectroscopy, which revealed solid–state (KBr) and solution (C_6D_6) ν_{CN} stretches of 2124 and 2118 cm^{-1}, respectively.

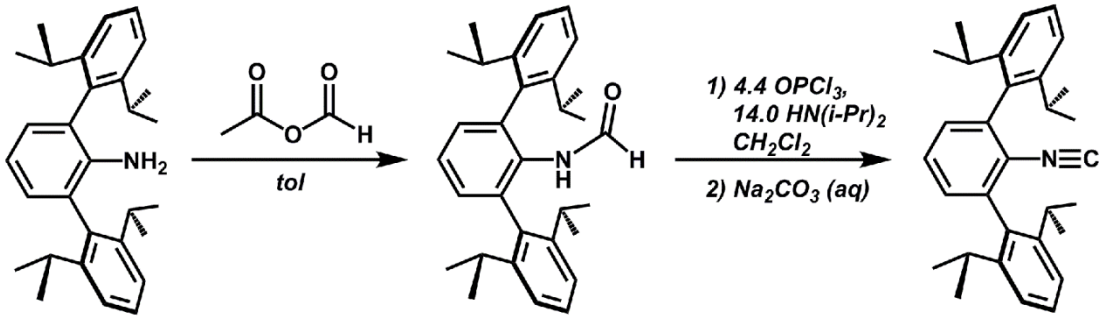

Scheme 2.1. Synthesis or $CNAr^{Dipp2}$.

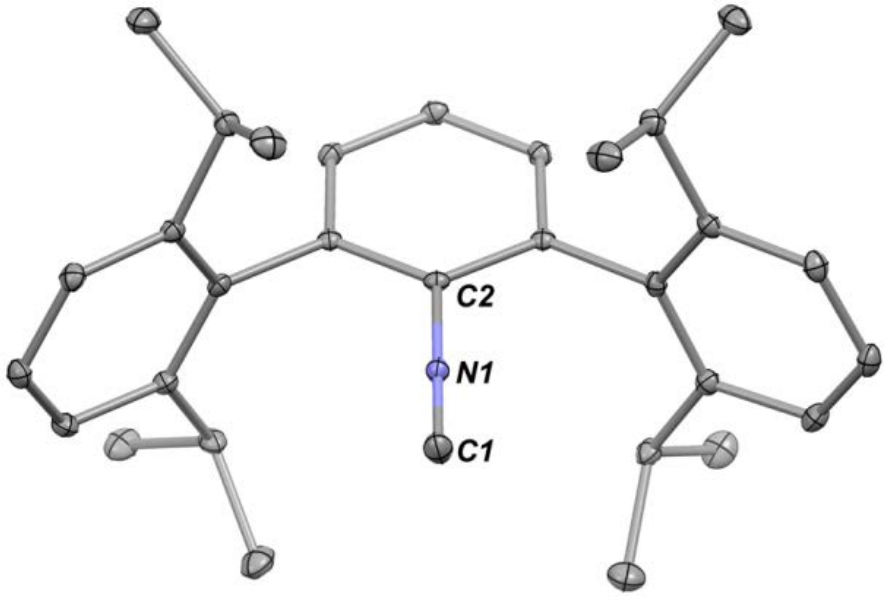

Figure 2.2. Molecular structure of $CNAr^{Dipp2}$. Selected bond distances (Å) and angles (deg): C1−N1 = 1.1577(18); N1−C2 = 1.4009(16); C1−N1−C2 = 176.72(13).

2.3 Coordination Platforms Lacking Significant π–Basicity: Monovalent Cu and Ag Centers

The steric differences between $CNAr^{Dipp2}$ and $CNAr^{Mes2}$ are immediately evidenced by their coordination behavior toward the Cu(I) triflate fragment. In the case of $CNAr^{Mes2}$, the trisisocyanide salt $[(THF)Cu(CNAr^{Mes2}{}_{)3}]OTf$ (OTf = $[OS_2OCF_3]^-$) was readily obtained upon its combination with $(C_6H_6)[Cu(OTf)]_2$ in THF solution.[16] Contrastingly, the sterically expanded $CNAr^{Dipp2}$ ligand permits only isolation of bisisocyanide Cu(I) monomers. As depicted in Scheme 2.2, addition of 4.0 equiv of $CNAr^{Dipp2}$ to $(C_6H_6)[Cu(OTf)]_2$ in THF results in the formation of the salt, $[(THF)_2Cu(CNAr^{Dipp2}{}_{)2}]OTf$ (**1**), as a colorless crystalline solid in 62% isolated yield. Structural characterization of $[(THF)_2Cu(CNAr^{Dipp2}{}_{)2}]OTf$ (**1**) by X–ray diffraction (Figure 2.3) confirmed the non–coordinating nature of OTf^- counterion when two THF ligands are present in the Cu primary coordination sphere. Most importantly, however, treatment of pure $[(THF)_2Cu(CNAr^{Dipp2}{}_{)2}]OTf$ (**1**) with an additional equivalent of $CNAr^{Dipp2}$ does not lead to a trisisocyanide complex. Instead, analysis of 1:1 $[(THF)_2Cu(CNAr^{Dipp2}{}_{)2}]OTf/CNAr^{Dipp2}$ mixtures by ^1H NMR spectroscopy (C_6D_6) revealed slightly broadened resonances for the two reactants indicative of a slow isocyanide exchange process on the ^1H NMR time scale (Figures 2.4 and 2.5). Solution FTIR spectroscopic studies (C_6D_6) on these mixtures revealed ν_{CN} stretches corresponding only to $[(THF)_2Cu(CNAr^{Dipp2}{}_{)2}]OTf$ (**1)** and free $CNAr^{Dipp2}$, thereby corroborating the notion that a tris–$CNAr^{Dipp2}$ species is not formed to an appreciable extent.

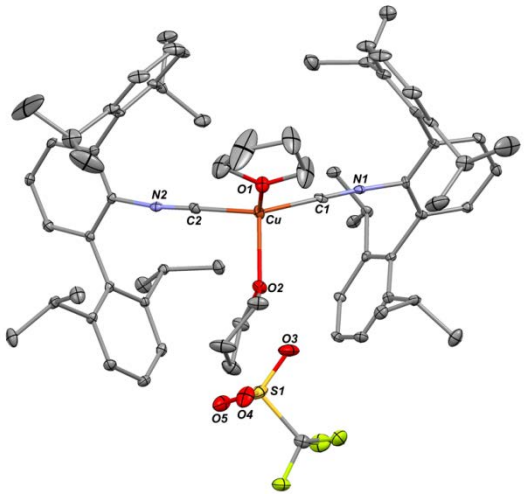

Figure 2.3. Molecular structure of $[(THF)_2Cu(CNAr^{Dipp2})_2]OTf$ (**1**). Selected bond distances (Å) and angles (deg): Cu3−C1 = 1.902(5); Cu1−C2 = 1.903(5); Cu1−O1 = 2.125(3); Cu1−O2 = 2.187(3); C1−Cu1−C2 = 135.16(19); C1−Cu1−O1 = 103.57(16); C2−Cu1−O1 = 109.62(16); C1−Cu1−O2 = 107.95(16); C2−Cu1−O2 = 99.69(16); O1−Cu1−O2 = 92.92(12). C1−N2−C11(ipso) = 175.9(4); C2−N1−C42(ipso) = 171.2(4).

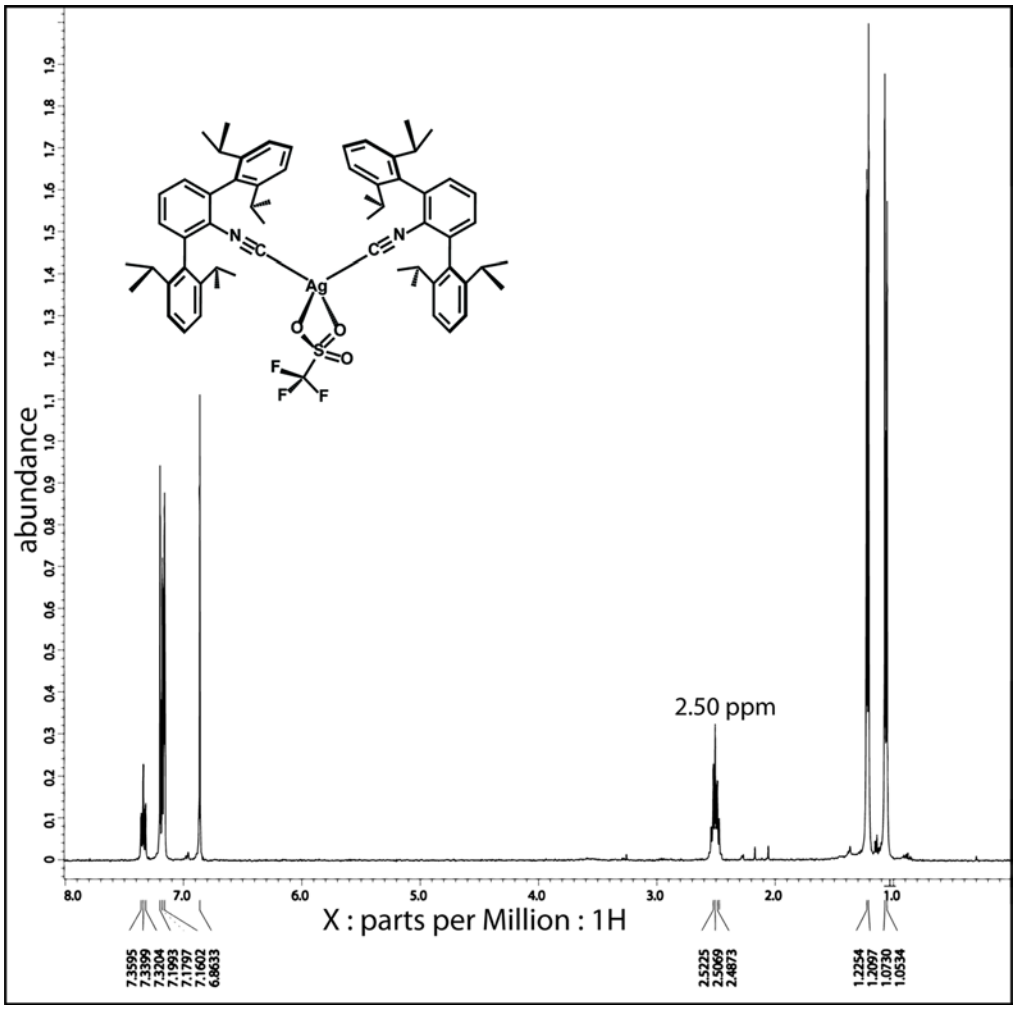

Figure 2.4. ^{1}H NMR (400 MHz) spectrum of (TfO)Cu(CNAr^{Dipp2})$_2$ (**1**) in C_6D_6.

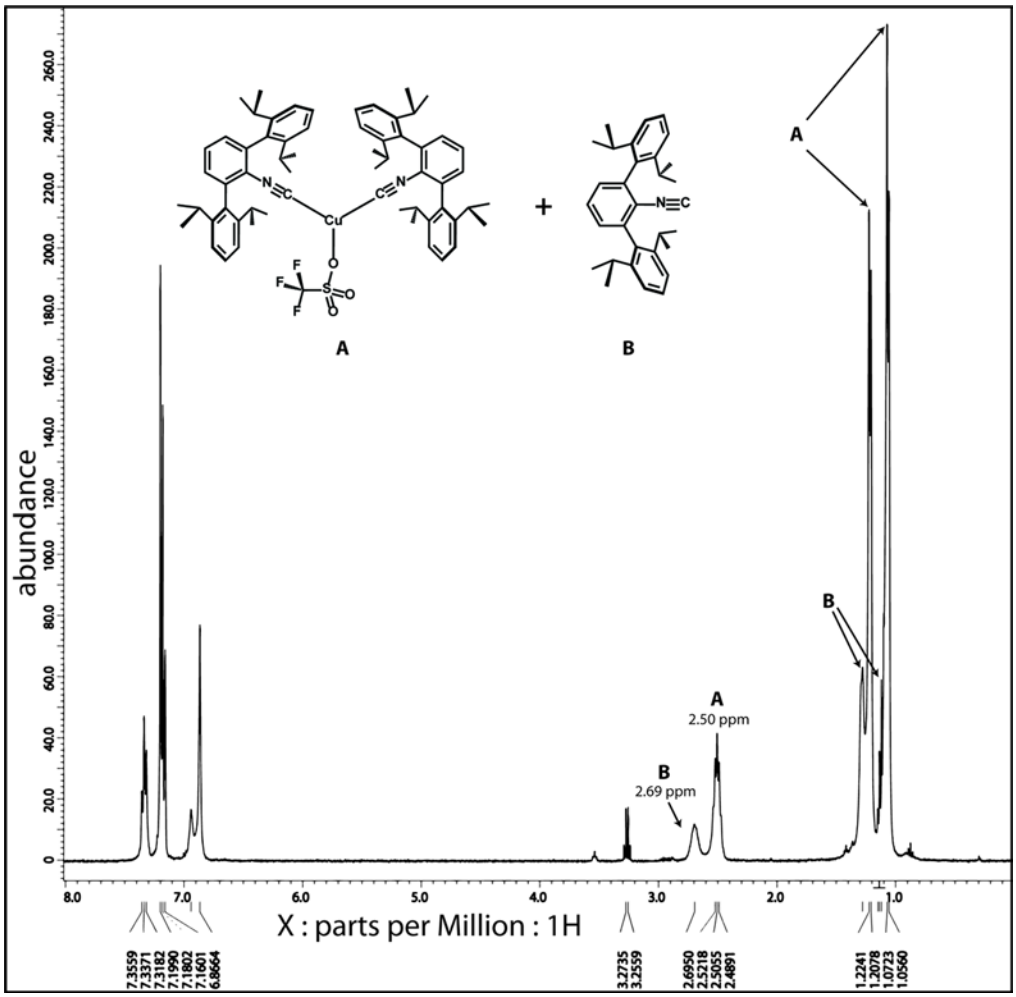

Figure 2.5. ^{1}H NMR (400 MHz) spectrum of (TfO)Cu(CNAr^{Dipp2})$_2$/CNAr^{Dipp2} mixture in C_6D_6. Slow exchange is suggested by the broadening of resonances for the components relative to their pure spectra.

The resistance of [(THF)$_2$Cu(CNAr^{Dipp2})$_2$]OTf (**1)** toward binding a third CNAr^{Dipp2} ligand can be readily traced to the encumbering nature of the flanking Dipp units.[19] As revealed by the molecular structure of [(THF)$_2$Cu(CNAr^{Dipp2})$_2$]OTf (**1)** (Figure 2.3), the steric congestion posed by these fragments forces a markedly expanded C(1)–Cu–C(2) angle of 135.16(19)° in the nominally four–coordinate d^{10} Cu(I) center. In comparison, the largest angle found for [(THF)Cu(CNAr^{Mes2})$_3$]OTf, which possesses three less encumbering ligands, is 119.14(13)°. Notably for [(THF)$_2$Cu(CNAr^{Dipp2})$_2$]OTf, (**1)** the C_{iso}–Cu–C_{aryl} angles in each

$CNAr^{Dipp2}$ ligand retain a near linear disposition. This observation is consistent with the absence of significant π–back bonding from the Cu(I) center,[44–46] and thus reflects the fact that electronic factors (i.e., isocyanide bending as induced by π back–bonding) do not aid in maximizing the distance between the two Ar^{Dipp2} substituents. Thus we contend that the C_{iso}–Cu–C_{aryl} angle simply expands to minimize steric interferences between the large $CNAr^{Dipp2}$ units. Accordingly, the inability of $[(THF)_2Cu(CNAr^{Dipp2})_2]OTf$ (**1**) to bind a third $CNAr^{Dipp2}$ unit can be rationalized by the impossibility of accommodating three 120° or greater C_{iso}–Cu–C_{aryl} bond angles within a trigonal or pseudotetrahedral coordination geometry. Contrastingly, three C_{iso}–Cu–C_{aryl} bond angles of 120° or less are readily accommodated with the $CNAr^{Mes2}$ system, resulting in stable trisisocyanide complexes. In addition, the steric influences attendant within the $[Cu(CNAr^{Dipp2})_2]$ fragment are consistent irrespective of the coordination number at Cu or the nature of the other ligands present. This fact is demonstrated by the structural characterization of the solvent–free triflate complex, $(\kappa^1$–TfO)$Cu(CNAr^{Dipp2})_2$ (**2**), which possesses a significantly expanded C(1)–Cu–C(2) angle of 138.5(2)° for a nominally three–coordinate, Cu(I) complex featuring only monodentate ligands (Figure 2.6, Scheme 2.2).[47–52]

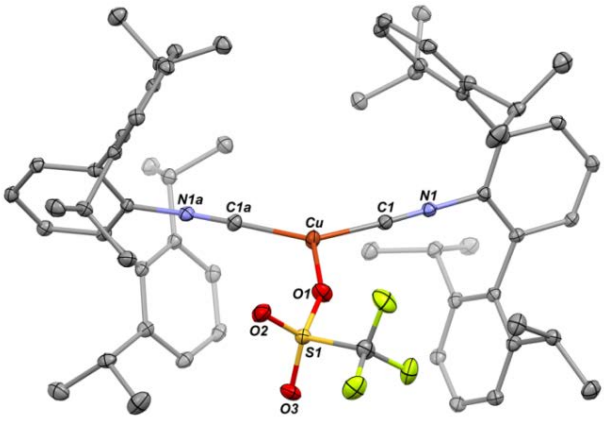

Figure 2.6. Molecular structure of $(\kappa^1$–TfO)$Cu(CNAr^{Dipp2})_2$ (**2**). Selected bond distances (Å) and angles (deg): C1−Cu1 = 1.884(4); Cu1−O1 = 2.082(4); C1−Cu1−C1a = 138.5(2); C1−Cu1−O1 = 110.77(12); S1−O1−Cu1 = 152.91(11); C1−N1−C2(ipso) = 177.1(4).

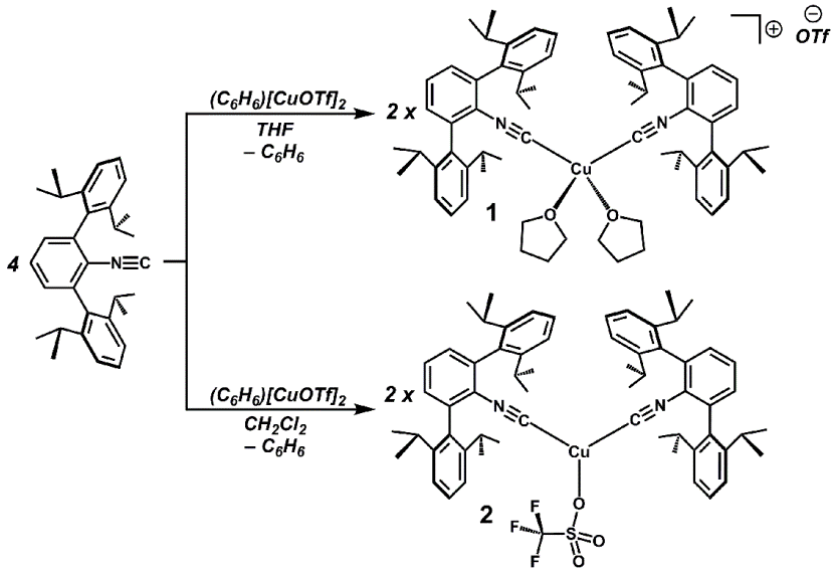

Scheme 2.2. Synthesis of $[(THF)_2Cu(CNAr^{Dipp2})_2]OTf$ (**1**) and $(OTf)Cu(CNAr^{Dipp2})_2$ (**2**).

The steric interference posed by the $CNAr^{Dipp2}$ framework is also not overcome by moderate changes in M–C_{iso} bond lengths. Accordingly, in an attempt to increase the likelihood of obtaining a tris–$CNAr^{Dipp2}$ Group 11 complex, we postulated that a Ag(I) center, with its larger covalent radius relative to that of Cu(I),[53] may possibly allow the ligation of three encumbering isocyanide units. As with the [CuOTf] fragment, three of the relatively smaller $CNAr^{Mes2}$ ligands are easily accommodated within the primary coordination sphere of Ag(I). Thus, treatment of AgOTf with 3 equiv of $CNAr^{Mes2}$ in THF solution affords the trisisocyanide salt $[(THF)Ag(CNAr^{Mes2})_3]OTf$ (**3**) as assayed by ^1H NMR spectroscopy (C_6D_6, Scheme 2.3). Dissolution of $[(THF)Ag(CNAr^{Mes2})_3]OTf$ (**3**) in Et_2O results in solvent exchange, affording the salt $[(Et_2O–Ag(CNAr^{Mes2})_3]OTf$, which was subjected to structural characterization (Figure 2.7). In contrast to $CNAr^{Mes2}$, however, ligation of three $CNAr^{Dipp2}$ ligands is in fact resisted by Ag(I) centers. For example, treatment of AgOTf with 2.0 equiv of $CNAr^{Dipp2}$ in THF, followed by crystallization of the resultant solids from an Et_2O/*n*–hexane mixture, provides the solvent–free complex (κ^2–OTf)$Ag(CNAr^{Dipp2})_2$ (**4**) (Scheme 2.3). The molecular structure of (κ^2–OTf)$Ag(CNAr^{Dipp2})_2$ (**4**) has been determined by X–ray

diffraction and is shown in Figure 2.8. In contrast to its Cu(I) analogue, a bidentate κ^2 binding mode is observed for the triflate unit in (κ^2–OTf)Ag(CNAr^{Dipp2})$_2$ (**4**), but and expanded C_{iso}–Cu–C_{aryl} angle of 142.2(2)° is still observed. As determined by both ^{1}H NMR and FTIR spectroscopy, however, treatment of (κ^2–OTf)Ag(CNAr^{Dipp2})$_2$ (**4**) with an additional equivalent of CNAr^{Dipp2} in C_6D_6 results in fast exchange between free and coordinated isocyanide but does not lead to an isolable trisisocyanide (Figures 2.9, 2.10, 2.11., and 2.12).

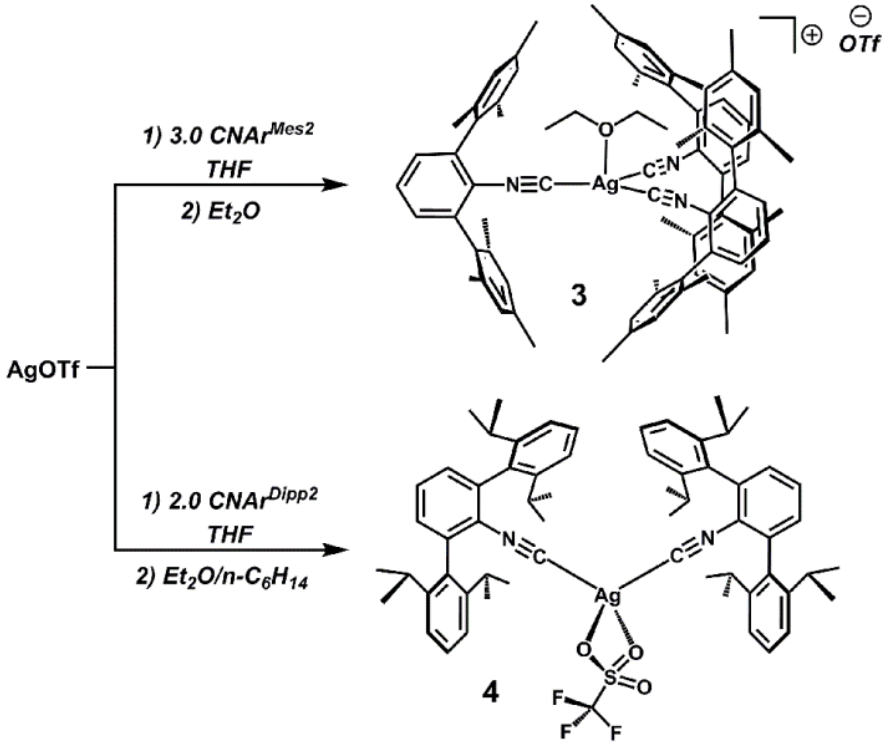

Scheme 2.3. Synthesis of [(Et$_2$O)Ag(CNAr^{Mes2})$_3$]OTf (**3**) and (κ^2–TfO)Ag(CNAr^{Dipp2})$_2$ (**4**).

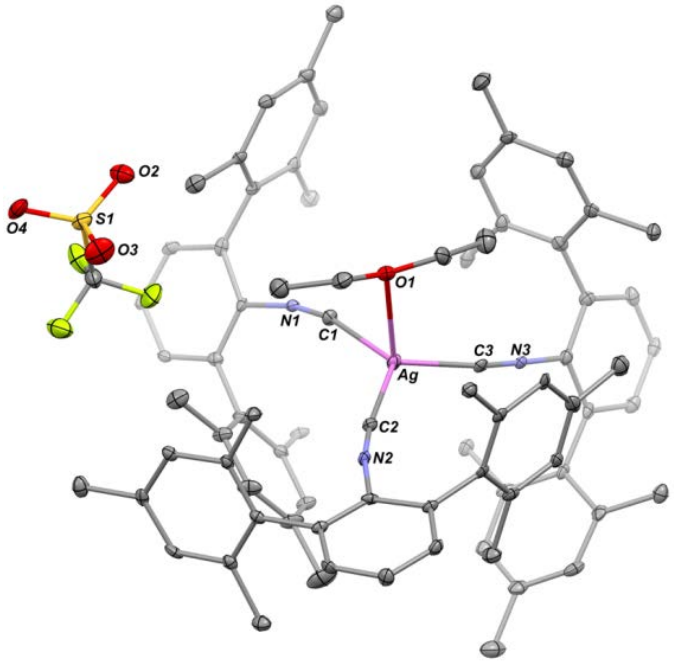

Figure 2.7. Molecular structure of [(Et_2O)Ag($CNAr^{Mes2}$)$_3$]OTf. Selected bond distances (Å) and angles (deg): C1−Ag1 = 2.188(7); C2−Ag1 = 2.134(8); C3−Ag1 = 2.167(7); O1−Ag1 = 2.673(10); C3−Ag−C1 = 107.0(2); C2−Ag1−C1 = 125.0(3); C2−Ag1−C3 = 122.3(2); O1−Ag1−C1 = 93.2(3); O1−Ag1−C2 = 88.1(2); O1−Ag1−C3 = 114.2(3).

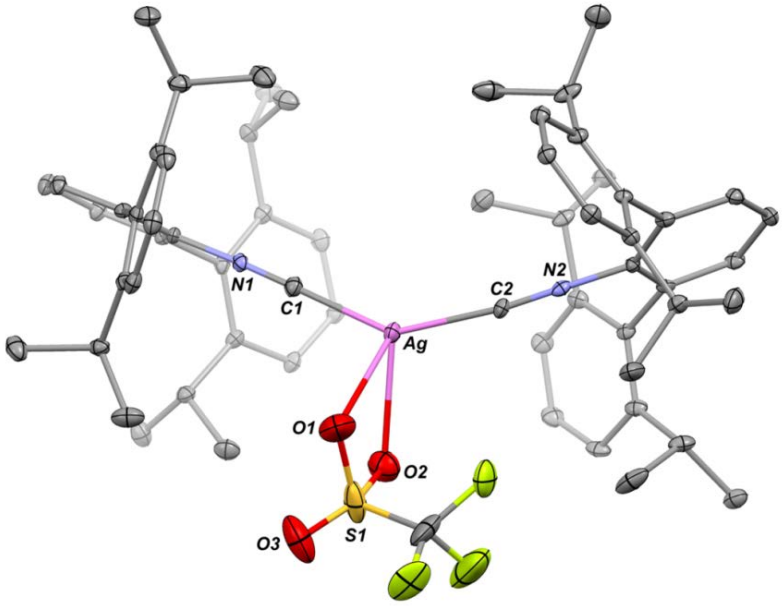

Figure 2.8. Molecular structure of (κ^2–TfO)Ag($CNAr^{Dipp2}$)$_2$ (**4**). Selected bond distances (Å) and angles (deg): Ag1−C1 = 2.083(5); Ag1−C2 = 2.097(6); Ag1−O1 = 2.486(6); Ag1−O2 = 2.568(9); C1)−Ag1−C2 = 142.2(2); C1−Ag1−O1 = 107.1(2); C2−Ag1−O1 = 108.4(2); C1−Ag1−O2 = 116.5(2); C2−Ag1−O2 = 95.9(2).

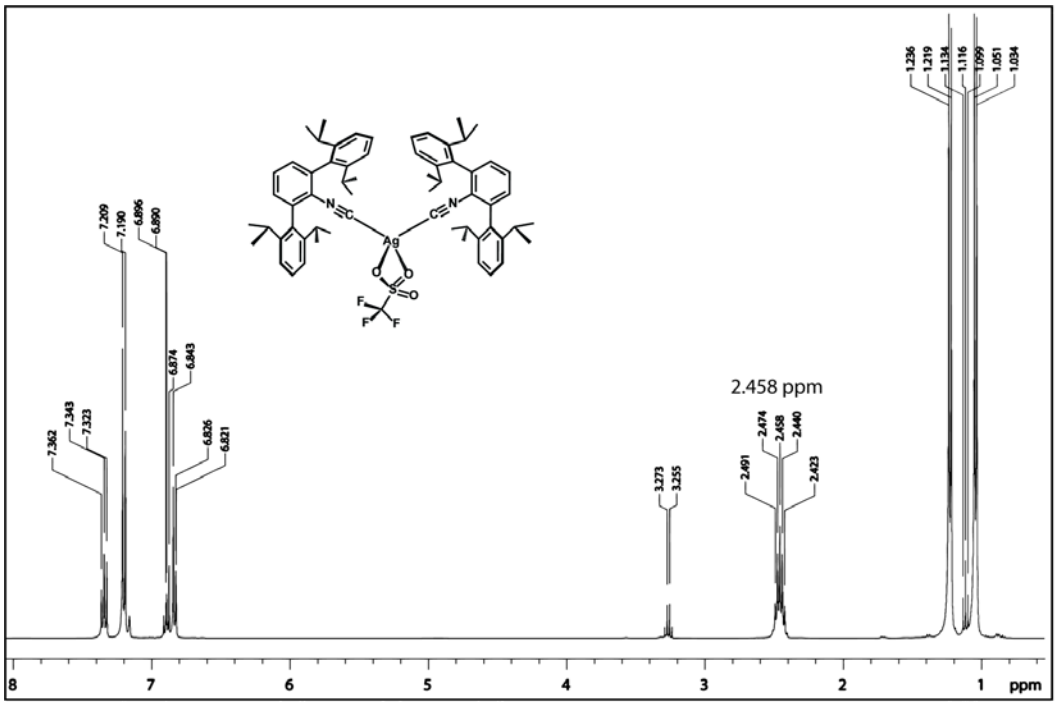

Figure 2.9. ^{1}H NMR (400 MHz) spectrum of (κ^2–TfO)Ag(CNAr^{Dipp2})$_2$ (**4**) in C_6D_6.

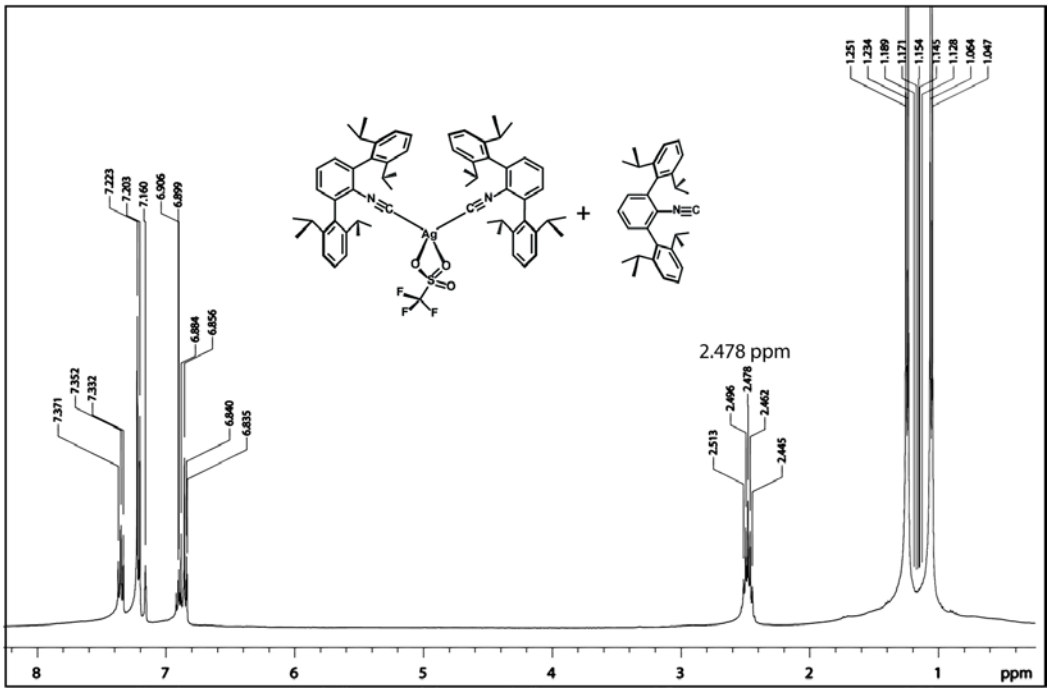

Figure 2.10. ^{1}H NMR (400 MHz) spectrum of a 1:1 (κ^2–TfO)Ag(CNAr^{Dipp2})$_2$/CNAr^{Dipp2} mixture in C_6D_6. Fast exchange is indicated by the presence of a seemingly new set of resonances located at the weighted average for the two components.

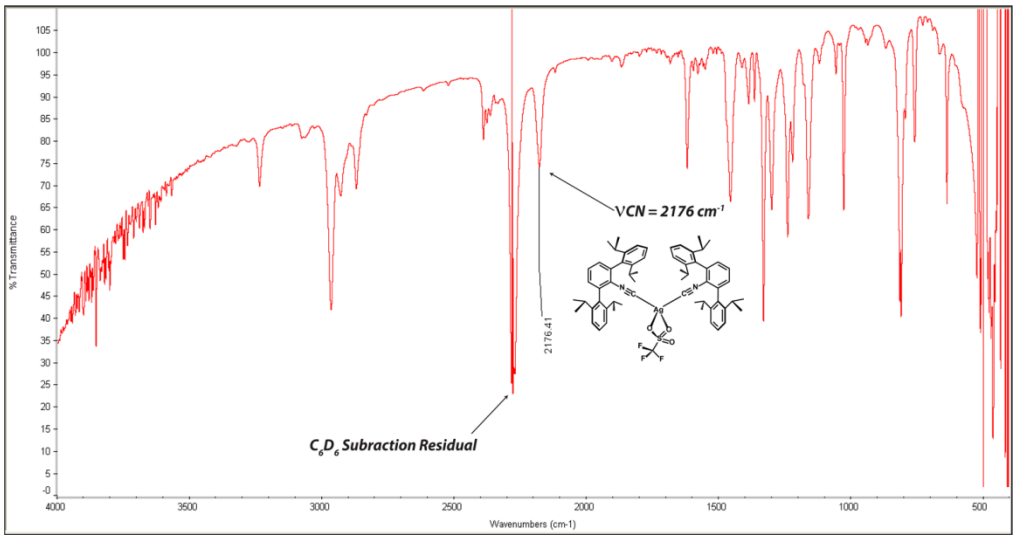

Figure 2.11. FTIR spectrum of (κ^2–TfO)Ag(CNAr^{Dipp2})$_2$ (**4**) in C_6D_6 (NaCl windows).

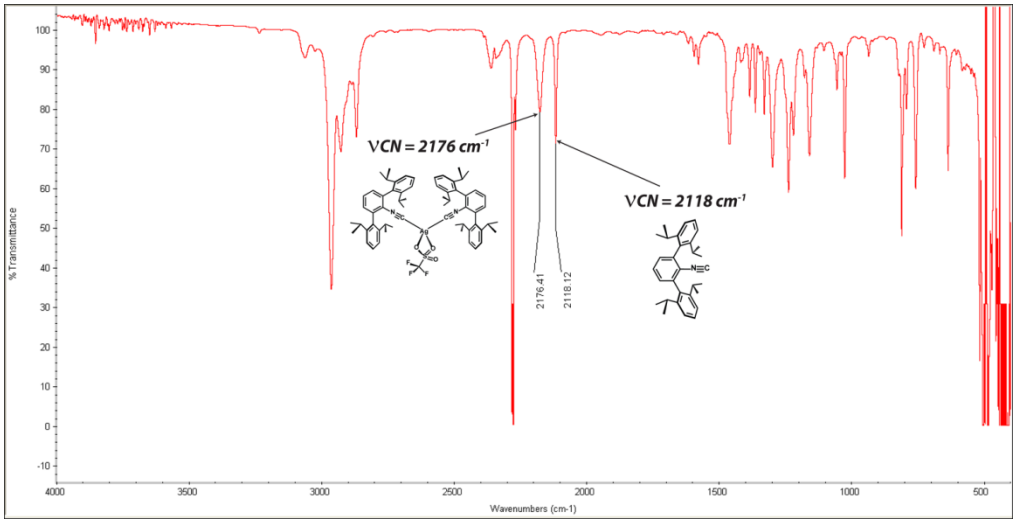

Figure 2.12. FTIR spectrum of a 1:1 (κ^2–TfO)Ag(CNAr^{Dipp2})$_2$/CNAr^{Dipp2} mixture in C_6D_6 (NaCl windows). The spectrum exclusively shows ν_{CN} stretches for the starting materials and does not reveal a ν_{CN} stretch for a new complex.

2.4 Mixed Isocyanide/Carbonyl Complexes of Zerovalent Molybdenum

Whereas the differences in steric properties between $CNAr^{Mes2}$ and $CNAr^{Dipp2}$ are illustrated by their coordination behavior toward monovalent Group 11 centers, it was of interest to additionally compare their behavior toward a π–basic metal fragment.[54] Therefore, we next focused on the ability of both $CNAr^{Mes2}$ and $CNAr^{Dipp2}$ to form mixed carbonyl/isocyanide complexes of zerovalent molybdenum. The choice for zerovalent Mo centers as a suitable coordination platform stems from a number of factors. First, there are several examples of isolated $Mo(CO)_n(CNR)_m$ ($m = 6 - n$) complexes representing all possible n permutations.[7–14,55–67] Moreover, the strong *trans* directing nature of the CO ligands reliably controls the geometric isomerism of these octahedral complexes. This latter feature of the $Mo(CO)_n(CNR)_m$ system is important since deviations from the preferred isocyanide or carbonyl orientations (i.e., *mer* vs *fac* or *cis* vs *trans*) can be readily traced to the steric or electronic influences of the bound isocyanide ligands. Further, the presence of the strong CO and CNR oscillators allow the geometrical isomerism in $Mo(CO)_n(CNR)_m$ complexes to be conveniently probed by infrared spectroscopy. Because of the geometrical and compositional richness offered by the $Mo(CO)_n(CNR)_m$ platform, we were curios to compare not only the differing extent of ligation between $CNAr^{Mes2}$ and $CNAr^{Dipp2}$, but also the effect of the encumbering *m*–terphenyl group on isocyanide orientation. Indeed, all $Mo(CO)_n(CNR)_m$ complexes reported to date have contained isocyanide ligands that are significantly less encumbering than either $CNAr^{Mes2}$ and $CNAr^{Dipp2}$.

2.5 Isomeric Modulation of $Mo(CO)_3(CNR)_3$ Complexes Utilizing $CNAr^{Mes2}$

Treatment of *fac*–$Mo(CO)_3(NCMe)_3$ with 3 equiv of $CNAr^{Mes2}$ in toluene leads to complete consumption of the isocyanide and exclusive formation of the yellow complex *fac*–$Mo(CO)_3(CNAr^{Mes2})_3$ (**5**) (Scheme 2.4). The latter was characterized by X–ray diffraction and several views of its molecular structure are displayed in Figure 2.13. ^1H NMR spectra of *fac*–$Mo(CO)_3(CNAr^{Mes2})_3$ (**5**) in C_6D_6 reveal a single set of Ar^{Mes2} resonances, thereby providing a geometrical consistency between the solid state and solution. In addition, the solution phase (C_6D_6) FTIR spectrum of *fac*–$Mo(CO)_3(CNAr^{Mes2})_3$ gives rise to two ν_{CO} and two ν_{CN} frequencies expected for a *fac* conformation.[68] The structure of *fac*–$Mo(CO)_3(CNAr^{Mes2})_3$ is remarkable because of the congestion posed by the facial arrangement of the $CNAr^{Mes2}$ ligands. Figure 2.13 shows *fac*–$Mo(CO)_3(CNAr^{Mes2})_3$ (**5**) viewed down the trigonal faces defined by both the CO and $CNAr^{Mes2}$ ligands (a and b, respectively), as well as the corresponding space filing models (c and d). The views down the $CNAr^{Mes2}$ trigonal face clearly show a crowded, interdigitated environment for the Mes substituents. Such congestion suggested that a *fac–mer* isomerization process may be possible to relieve excessive steric pressures. Accordingly, *fac*–$Mo(CO)_3(CNAr^{Mes2})_3$ (**5**) slowly, but irreversibly, converts to *mer*–$Mo(CO)_3(CNAr^{Mes2})_3$ (**6**) when heated in solution (C_6D_6, 90°C, 3 days, Scheme 2.4). Both ^1H NMR and FTIR analysis of *mer*–$Mo(CO)_3(CNAr^{Mes2})_3$ (**6**) showed the expected spectroscopic signatures for a distinct meridional conformation (Table 2.1). Crystallographic structure determination (Figure 2.14) revealed, qualitatively, a significantly less congested coordination environment for *mer*–$Mo(CO)_3(CNAr^{Mes2})_3$ (**6**) that is found for its *fac* isomer. Notably, extended heating of *mer*–$Mo(CO)_3(CNAr^{Mes2})_3$ (**6**) in C_6D_6 (100 °C, 2 day) does not lead to degradation or any additional isomerization processes, thus indication that the *mer*

isomer is robust and thermodynamically preferred to the *fac* isomer under the conditions probed.

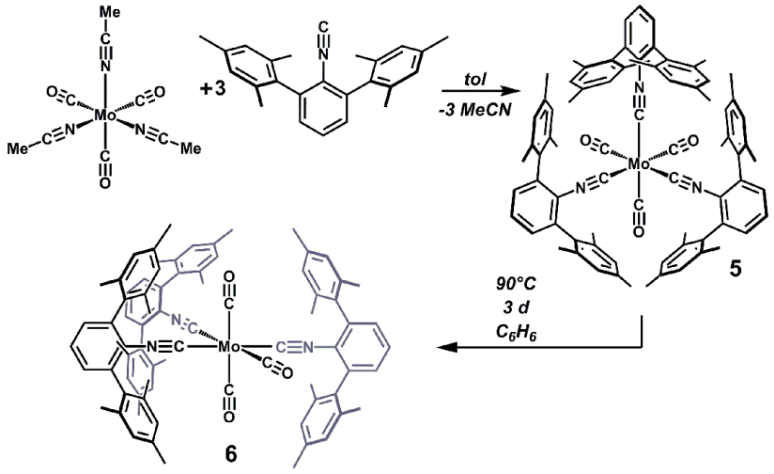

Scheme 2.4. Synthesis of *fac*–Mo(CO)$_3$(CNAr^{Mes2})$_3$ (**5**) and *mer*–Mo(CO)$_3$(CNAr^{Mes2})$_3$ (**6**).

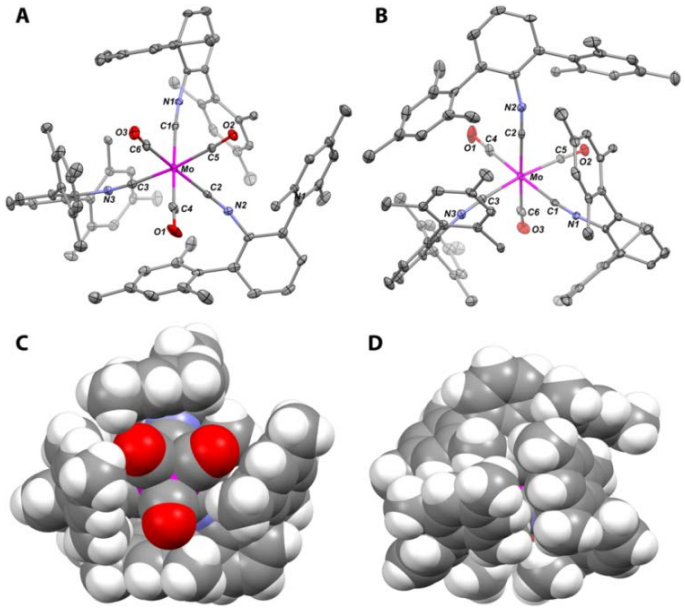

Figure 2.13. Molecular structure of *fac*–Mo(CO)$_3$(CNAr^{Mes2})$_3$ (**5**). (A) View down the trigonal face defined by the three carbonyl ligands. (B) View down the trigonal face defined by the three CNAr^{Mes} ligands. (C) Space filling model corresponding to view A. (D) Space filling model corresponding to view B. Selected bond distances (Å) and angles (deg): Mo1−C1 = 2.106(6); Mo1−C2 = 2.093(6); Mo1−C3 = 2.114(7); Mo1−C4 = 2.015(7); Mo1−C5 = 2.015(7); Mo1−C6 = 2.037(6); C1−Mo1−C2 = 95.1(2); C1−Mo1−C3 = 89.4(2); C1−Mo1−C4 = 178.4(2); C2−Mo1−C3 = 95.6(2); C2−Mo1−C6 = 169.2(2); C3−Mo1−C5 = 173.9(2).

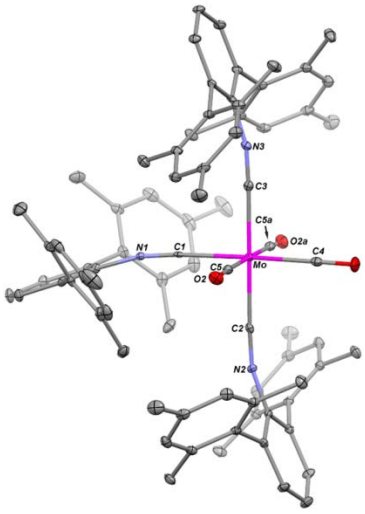

Figure 2.14. Molecular structure of *mer*–Mo(CO)$_3$(CNAr^{Mes2})$_3$ (**6**). Selected bond distances (Å) and angles (deg): Mo1−C1 = 2.118(5); Mo1−C2 = 2.077(5); Mo1−C3 = 2.077(5); Mo1−C4 = 2.025(5); Mo1−C5 = 2.038(4); C1−Mo1−C2 = 89.34(16); C1−Mo1−C3 = 90.41(17); C2−Mo1−C3 = 179.75(17); C1−Mo1−C4 = 178.2(2); C5−Mo1−C5a = 178.4(2).

Table 2.1. Solution ν_{CN} and ν_{CO} Stretching Frequencies for Mixed Isocyanide/Carbonyl Molybdenum Complexes of CNAr^{Mes2} and CNAr^{Dipp2} (C_6D_6)

Complex	ν_{CN} (cm^{-1})	ν_{CO} (cm^{-1})
fac–Mo(CO)$_3$(CNAr^{Mes2})$_3$ (**5**)	2046(s)	1942(s)
	2000(m)	1910(s)
mer–Mo(CO)$_3$(CNAr^{Mes2})$_3$ (**6**)	2046(m)	1926(vs)
	2024(s)	1902(s)
	1993(s)	
trans–Mo(CO)$_4$(CNAr^{Dipp2})$_2$ (**7**)	2054(vs)	1934(vs)
	2007(w)	
trans–Mo(NCMe)(CO)$_3$(CNAr^{Dipp2})$_2$ (**8**)	2021(s)	1932(w)
	1993(s)	1901(s)
		1873(m)
fac,*cis*–Mo(py)(CO)$_3$(CNAr^{Dipp2})$_2$ (**9**)	2018(s)	1888(s)
	1992(s)	1862(s)
trans–Mo(THF)(CO)$_3$(CNAr^{Dipp2})$_2$ (**10**)	2041(vw)	1924(w)
	2017(m)	1888(s)
	1987(s)	1859(m)

The preference of Mo(CO)$_3$(CNAr^{Mes2})$_3$ to adopt its meridional isomeric form is particularly noteworthy given that a facial disposition of isocyanide ligands is the preferred coordination geometry in the overwhelming majority of Group 6 Mo(CO)$_3$(CNR)$_3$ complexes.[55–67] However, as testament to the small energetic difference that can exist

between these geometric isomers, reversible *fac–mer* interconversions have been observed for some $Mo(CO)_3(CNR)_3$ complexes on the ^1H NMR time scale.[69] Furthermore, *mer*–$Mo(CO)_3(CNR)_3$ isomers have been isolated in low yield from *fac*/*mer* mixtures in which the *fac* isomer is the predominant species.[68] We are unaware of any example in which simple thermolysis of *fac*–$Mo(CO)_3(CNR)_3$ complex provides its *mer*–isomer quantitatively, as is the case for $Mo(CO)_3(CNAr^{Mes2})_3$.

In the absence of significant steric pressures, the preference for *fac* over *mer* configurations in Group 6 $Mo(CO)_3(CNR)_3$ complexes may be attributed to an interplay of two electronic factors: (i) the preference for each CNR ligand to be *trans* to the relatively weaker σ–donating CO ligands and (ii) maximization of the π–acceptor ability of the CO units in the *fac*–geometry.[70,71] Indeed, the *fac* orientation ensures a triply degenerate configuration wherein each doubly occupied, nonbonding t_{2g}–type orbital interacts via π back–bonding with two CO ligands. Such orbital degeneracy is removed in the alternative *mer* orientation, which renders it the preferred geometry for Jahn–Teller susceptible 17–electron $M(CO)_3(L)_3$ complexes.[55–67] However, in only two prior reports has the *mer* isomer of a neutral, 18–electron Group 6 $M(CO)_3(CNR)_3$ complex been reported to form preferentially to its *fac*–isomer.[72,73] In these cases the perfluorinated isocyanides[74] $CNCF_3$ and CNC_6F_5 were employed. Accordingly, such strongly π–acidic isocyanides may be reasonably expected to withdraw a fair degree of additional electron density from a metal center relative to non–fluorinated alkyl or aryl isocyanides. Thus it is interesting to speculate that the strongly π–accepting nature of fluorinated isocyanides enables them to destabilize the *fac*–conformation. In contrast, we suggest that for $CNAr^{Mes2}$, steric pressures, rather than electronic factors, attendant in placing three encumbering *m*–terphenyl isocyanide units at the face of an octahedron significantly destabilize the *fac*–conformation. Such steric

destabilization of octahedral *fac* isomers is known for complexes featuring three phosphine (PR_3) ligands of large cone angle.[69]

2.6 Ligation Control and Isomeric Enforcement by $CNAr^{Dipp2}$ in $Mo(CO)_4(CNR)_2$ and $Mo(solvento)(CO)_3(CNR)_2$ Complexes

Unlike $CNAr^{Mes2}$, treatment of *fac*–$Mo(CO)_3(NCMe)_3$ with 3 equiv of the larger $CNAr^{Dipp2}$ lends to a mixture of products and incomplete consumption of the isocyanide. However, when 2 equiv of $CNAr^{Dipp2}$ are employed, a mixture of *trans*–$Mo(CO)_4(CNAr^{Dipp2})_2$ (**7**) and *trans*–$Mo(NCMe)(CO)_3(CNAr^{Dipp2})_2$ (**8**) is obtained (Scheme 2.5). Treatment of this mixture with an excess of CO in THF solution generates *trans*–$Mo(CO)_4(CNAr^{Dipp2})_2$ (**7**) in pure form. Correspondingly, photolysis (Hg lamp, 254 nm) of the mixture under and argon purge in acetonitrile/Et_2O (1:1) leads to *trans*–$Mo(NCMe)(CO)_3(CNAr^{Dipp2})_2$ (**8**) as the exclusive product (Scheme 2.5). The *trans* configuration of the $CNAr^{Dipp2}$ ligands in both *trans*–$Mo(CO)_4(CNAr^{Dipp2})_2$ (**7**) and *trans*–$Mo(NCMe)(CO)_3(CNAr^{Dipp2})_2$ (**8**) was established by X–ray diffraction (Figures 2.15 and 2.16, respectively). In addition, the solution phase (C_6D_6) FTIR spectrum of *trans*–$Mo(CO)_4(CNAr^{Dipp2})_2$ (**7**) exhibits two ν_{CN} stretches and only a single ν_{CO} stretch, thereby confirming that the *trans* disposition of the isocyanide ligands can be spectroscopically identified. Notably, however, *trans*–$Mo(NCMe)(CO)_3(CNAr^{Dipp2})_2$ (**8**) crystallized with severe positional disorder between the equatorial CO and NCMe ligands, but the *trans*–disposition of the $CNAr^{Dipp2}$ units is not in question (one component of the disorder model is shown in Figure 2.16). Furthermore, it is important that *trans*–$Mo(NCMe)(CO)_3(CNAr^{Dipp2})_2$ (**8**) exhibits two ν_{CN} and three ν_{CO} FTIR stretches (C_6D_6), which is consistent with *trans*–disposed isocyanides and a meridional arrangement of carbonyl ligands.[75]

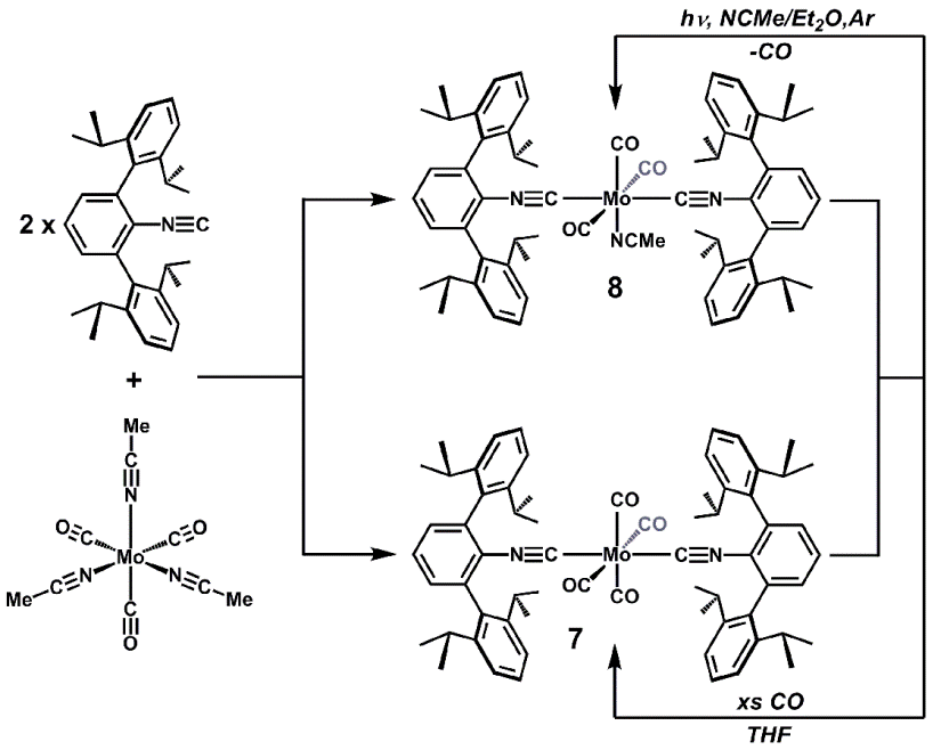

Scheme 2.5. Synthesis of *trans*–$Mo(CO)_4(CNAr^{Dipp2})_2$ (**7**) and *trans*–$Mo(NCMe)(CO)_3(CNAr^{Dipp2})_2$ (**8**).

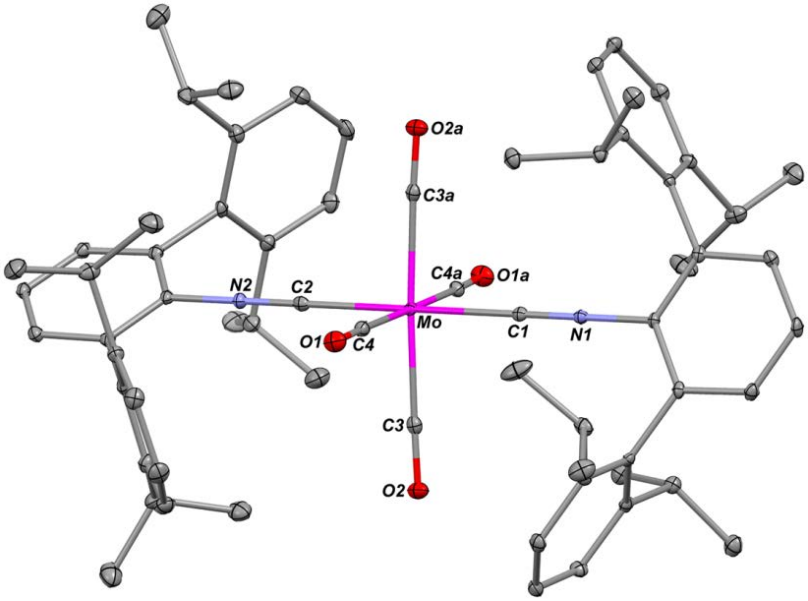

Figure 2.15. Molecular structure of one crystallographically independent molecule of *trans*–$Mo(CO)_4(CNAr^{Dipp2})_2$ (**7**). Selected bond distances (Å) and angles (deg): Mo1−C1 = 2.087(3); Mo1−C2 2.092(4); Mo1−C3 = 2.043(3); C1−Mo1−C1a = 180.000(2); C1−Mo1−C2 = 91.66(7); C1−Mo1−C3 = 90.61(7); C2−Mo1−C3 = 89.39(7).

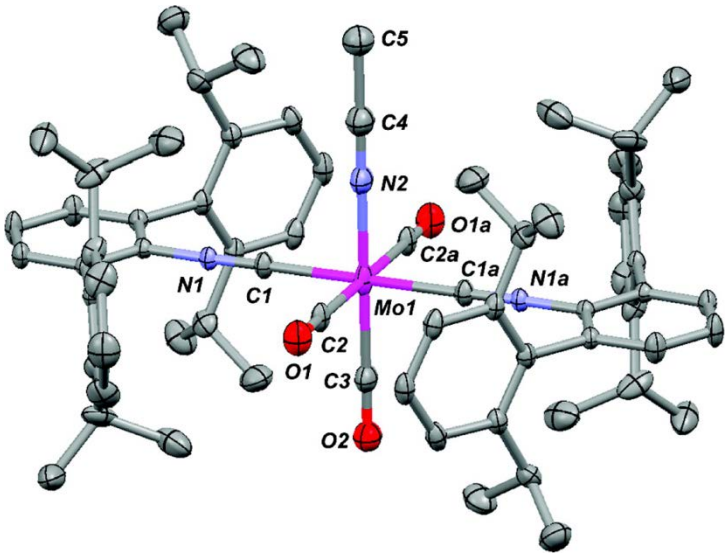

Figure 2.16. One disorder component of the molecular structure of *trans*–$Mo(NCMe)(CO)_3(CNAr^{Dipp2})_2$ (**8**). d(Mo1−C1) = 2.083(5) Å. ∠(C1−Mo1−C1a) = 180.000(2)°.

The *trans*–isocyanide configuration in *trans*–$Mo(CO)_4(CNAr^{Dipp2})_2$ (**7**) is remarkable given that the *cis*–isomer is observed in the vast majority of Group 6 $M(CO)_4(CNR)_2$ complexes.[55–62,76–80] We are aware of only two instances of Group 6 $M(CO)_4(CNR)_2$ complexes containing *trans*–isocyanides, namely, *trans*–$Cr(CNCH_3)(CNC_6F_5)(CO)_4$ and *trans*–$Cr(CNCH_3)(CNCF_3)(CO)_4$ both prepared by Lentz et al.[81] Interestingly, whereas the CNC_6F_5 derivative is obtained in pure form, *trans*–$Cr(CNCH_3)(CNCF_3)(CO)_4$ is formed in a 10:1 ratio with its *cis*–isomer. In similar fashion to the trisisocyanide isomeric form can be rationalized on the basis of placing the isocyanide units *trans* to the weakly σ–donating CO ligands. Furthermore, it has been proposed that fluorination significantly attenuates the σ–donor strength of the isocyanide unit, while concomitantly strengthening its π–acceptor character.[74] Thus, the non–fluorinated $CNCH_3$ ligand may prefer a *trans* orientation with respect to either $CNCF_3$ or CNC_6F_5. Such arguments, in conjunction with the unique behavior of fluorinated isocyanides mentioned above, may therefore account for the observed *trans*–geometry in *trans*–$Cr(CNCH_3)(CNC_6F_5)(CO)_4$ and *trans*–$Cr(CNCH_3)(CNCF_3)(CO)_4$. For

trans–$Mo(CO)_4(CNAr^{Dipp2})_2$ (**7**), however, we suggest that steric pressures between the Ar^{Dipp2} units are large enough to overcome the electronic penalty of placing the two stronger *σ*–donating ligands in a *trans* configuration. To this end it is notable that *trans*–$Mo(CO)_2(CNAr^{Dipp2})_2$ (**7**) retains its conformation purity when heated for extended periods, as assayed by solution ^1H NMR spectroscopy (C_6H_6, 90 °C, 24h). Tricarbonyl *trans*–$Mo(NCMe)(CO)_3(CNAr^{Dipp2})_2$ (**8**) is noteworthy in that it represents a rare example of a structurally characterized Group 6 nitrile–adduct featuring five strongly *π*–acidic ligands.[82–88] Incidentally, *trans*–$Mo(NCMe)(CO)_3(CNAr^{Dipp2})_2$ (**8**) is the first such Mo complex to be structurally characterized. Despite the presence of positional disorder, the solid–state structure of *trans*–$Mo(NCMe)(CO)_3(CNAr^{Dipp2})_2$ (**8**) possesses overall feature similar to its tetracarbonyl counterpart, *trans*–$Mo(CO)_4(CNAr^{Dipp2})_2$ (**7**). Most importantly however, the presence of the labile NCMe ligand in *trans*–$Mo(NCMe)(CO)_3(CNAr^{Dipp2})_2$ (**8**) allows the opportunity to assess the effect of the encumbering Ar^{Dipp2} units on the substitution chemistry of the $[Mo(CO)_3(CNR)_2]$ core.[89,90]

As is the case for Group 11 complexes described above, three $CNAr^{Dipp2}$ ligands are not accommodated by the $[Mo(CO)_3]$ fragment. Thus treatment of *trans*–$Mo(NCMe)(CO)_3(CNAr^{Dipp2})_2$ (**8**) with an additional equivalent of $CNAr^{Dipp2}$ in C_6D_6 solution does not result in the formation of a new species when assayed by ^1H NMR spectroscopy (Figure 2.17). Rather, ^1H NMR spectra (20 °C) of 1:1 $CNAr^{Dipp2}$/*trans*–$Mo(NCMe)(CO)_3(CNAr^{Dipp2})_2$ mixtures reveal static resonances for both species, thereby indicating that rapid isocyanide exchange does not take place on the NMR time scale. In addition, two–dimensional EXSY ^1H NMR experiments did not reveal a slow exchange processes between free and coordinated $CNAr^{Dipp2}$ when mixing times ranging from 50–500 ms were employed (Figures 2.18 and 2.19). Accordingly, we tentatively suggest that the resistance of *trans*–$Mo(NCMe)(CO)_3(CNAr^{Dipp2})_2$ (**8**) toward degenerate isocyanide exchange

manifests from steric inhibition by the Ar^{Dipp2} substituents of a seemingly associative substitution process. Such a postulate is qualitatively consistent with strong binding of the isocyanide and carbonyl ligands to the π–basic Mo(0) center.

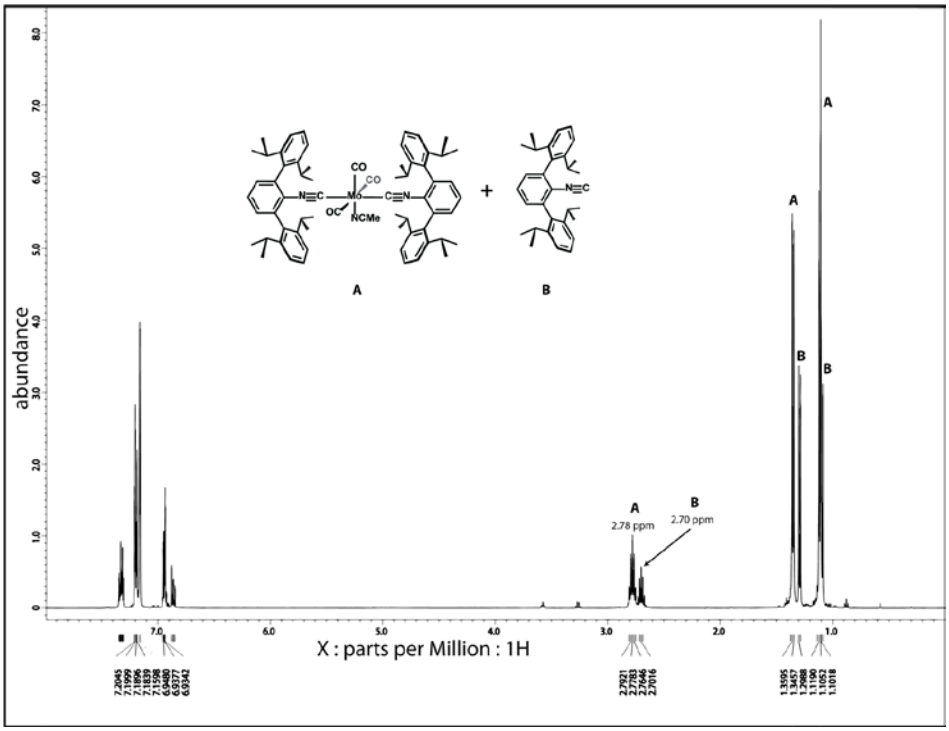

Figure 2.17. ^{1}H NMR (400 MHz) spectrum of a 1:1 *trans*–$Mo(NCMe)(CO)_3(CNAr^{Dipp2})_2/CNAr^{Dipp2}$ mixture in C_6D_6 showing static resonances for both species.

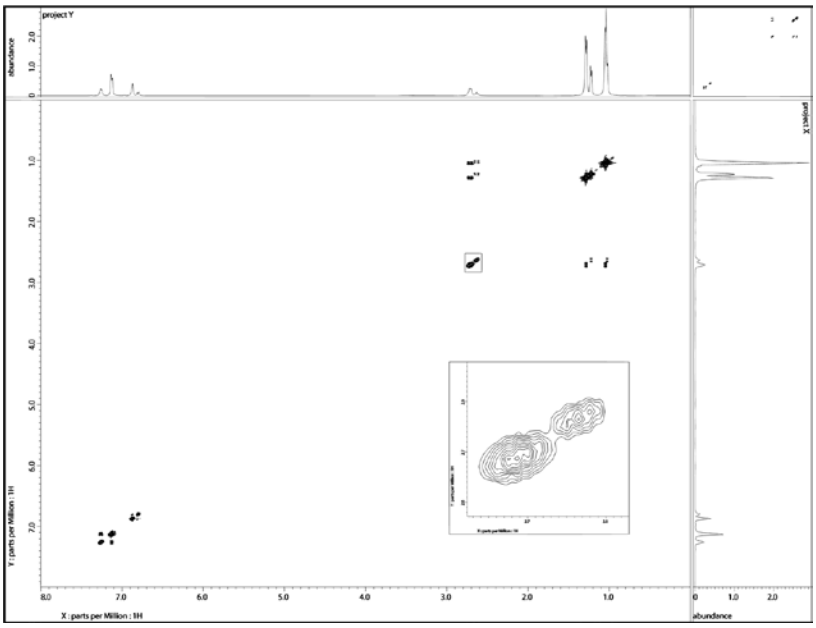

Figure 2.18. 2D ^{1}H EXSY NMR spectrum (500 MHz, C_6D_6) of a 1:1 *trans*–$Mo(NCMe)(CO)_3(CNAr^{Dipp2})_2$/$CNAr^{Dipp2}$ mixture with a 50 ms mixing time. Inset highlights the isopropyl methine region, which does not show off–diagonal elements indicative of magnetization transfer.

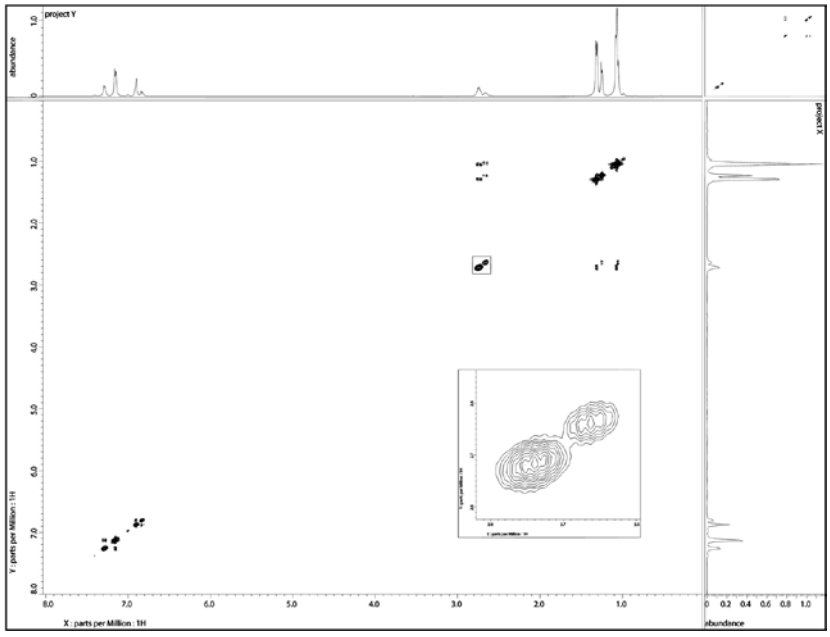

Figure 2.19. 2D ^{1}H EXSY NMR spectrum (500 MHz, C_6D_6) of a 1:1 *trans*–$Mo(NCMe)(CO)_3(CNAr^{Dipp2})_2$/$CNAr^{Dipp2}$ mixture with a 300 ms mixing time. Inset highlights the isopropyl methine region, which does not show off–diagonal elements indicative of magnetization transfer.

While resistant to substitution by additional $CNAr^{Dipp2}$, *trans*–$Mo(NCMe)(CO)_3(CNAr^{Dipp2})_2$ (**8**) is found to readily react with smaller Lewis bases. Thus treatment of *trans*–$Mo(NCMe)(CO)_3(CNAr^{Dipp2})_2$ (**8**) with an excess of pyridine (py) in C_6H_6 solution replaces only the coordinated NCMe ligand en route to the complex $Mo(py)(CO)_3(CNAr^{Dipp2})_2$ (**9**) (Scheme 2.6). Most remarkably, crystallographic analysis revealed that coordination of py induces a *trans*→*cis* isomerization of the $CNAr^{Dipp2}$ ligands within the $[Mo(CO)_3(CNAr^{Dipp2})_2]$ core (Figure 2.20). The *cis*,*fac* configuration in *cis*,*fac*–$Mo(py)(CO)_3(CNAr^{Dipp2})_2$ (**9**) is also indicated from its solution FTIR spectrum (C_6D_6), which contains two ν_{CN} and two ν_{CO} stretches. Similar to the Cu(I) and Ag(I) $CNAr^{Dipp2}$ complexes discussed above, steric interferences between the encumbering Ar^{Dipp2} units are clearly evident when the isocyanides are *cis*–disposed. As shown in Figure 2.20, *cis*,*fac*–$Mo(py)(CO)_3(CNAr^{Dipp2})_2$ (**9**) features a C_{iso}–Mo–C_{iso} angle of 99.7(3)°, which is fairly obtuse for a nominally octahedral Mo(0) complex featuring six monodentate ligands. Furthermore, that a *cis* orientation can indeed be accommodated by two $CNAr^{Dipp2}$ ligands in an octahedral complex further highlights the preference of $Mo(CO)_4(CNAr^{Dipp2})_2$ (**7**) and $Mo(NCMe)(CO)_3(CNAr^{Dipp2})_2$ (**8**) to adopt a *trans*–isocyanide configuration. We suggest that the $[Mo(CO)_3(CNAr^{Dipp2})_2]$ core converts from *trans* to *cis* isocyanide configuration to accommodate an increase in electron density at the metal center brought on by the more strongly σ–donating py ligand. Such an interconversion allows both the isocyanide and py groups to be situated *trans* to carbonyl ligands, while also maximizing the π–acceptor ability of the tricarbonyl construct in its facial, rather than meridional, configuration.[70] Lending further credence to this notion is the finding that replacement of the NCMe ligand in *trans*–$Mo(NCMe)(CO)_3(CNAr^{Dipp2})_2$ (**8**) with the weakly σ–donating THF molecule preserves the *trans*–isocyanide configuration as determined by X–ray crystallography and FTIR spectroscopy (Figure 2.21, Scheme 2.6). Accordingly, the ability to modulate the geometric

isomerism of the [Mo(CNAr^{Dipp2})$_n$] unit by varying ligand donor strength may be potentially beneficial in small molecule activation applications. It is also noteworthy that *trans*–Mo(THF)(CO)$_3$(CNAr^{Dipp2})$_2$ (**10**) is only the second structurally characterized Group 6 metal THF–adduct featuring five π–acidic ligands.[91] This fact thus highlights the ability of the CNAr^{Dipp2} unit to stabilize potentially reactive transition–metal species.[92]

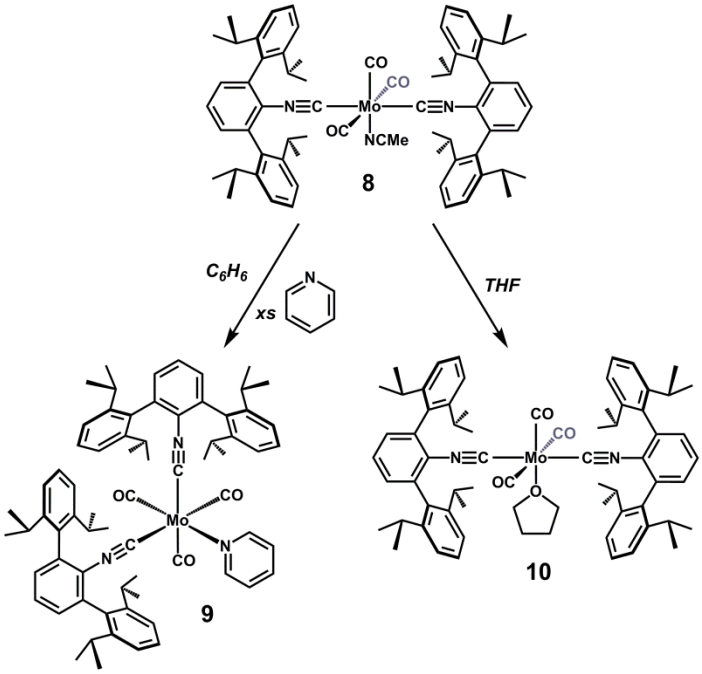

Scheme 2.6. Synthesis *cis,fac*–Mo(py)(CO)$_3$(CNAr^{Dipp2})$_2$ (**9**) and *trans*–Mo(THF)(CO)$_3$(CNAr^{Dipp2})$_2$ (**10**).

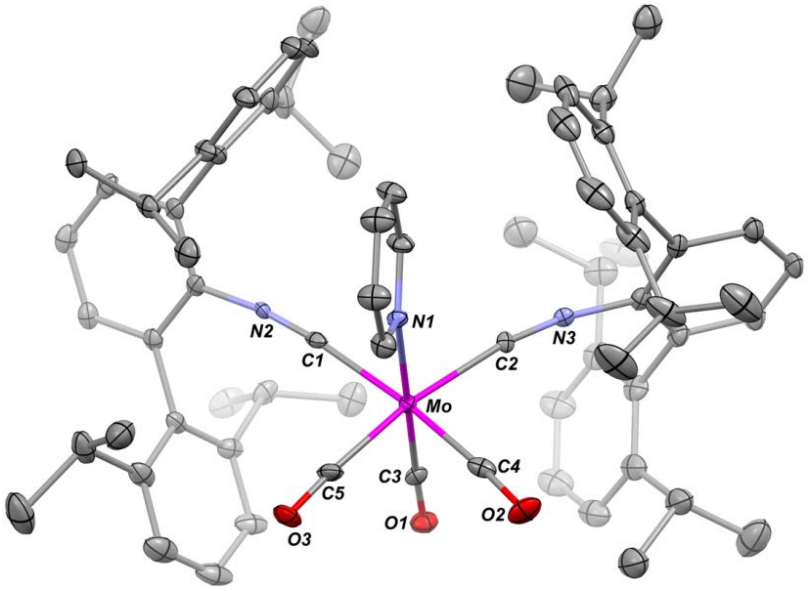

Figure 2.20. Molecular structure of *cis*,*fac*–Mo(py)$(CO)_3(CNAr^{Dipp2})_2$ (**9**). Selected bond distances (Å) and angles (deg): Mo1−C1 = 2.160(10); Mo1−C2 = 2.147(8); Mo1−C3 = 1.945(10); Mo1−C4 = 1.949(11); Mo1−C5 = 1.980(11); Mo1−N1 = 2.275(7); C1−Mo1−C2 = 99.7(3); C1−Mo1−N1 = 86.6(3); C2−Mo1−N1 = 90.1(3); C1−Mo1−C5 = 89.7(4); C2−Mo1−C4 = 86.3(4); C4−Mo1−C5 = 84.3(5); C1−Mo1−C4 = 174.0(4); C2−Mo1−C5 = 170.6(4); C3−Mo1−N1 = 179.3(3).

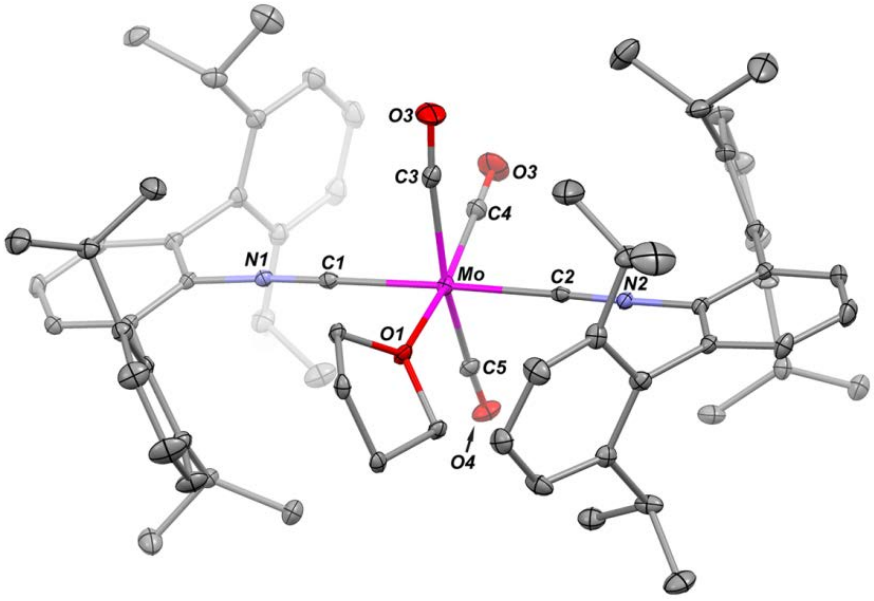

Figure 2.21. One disorder component of the molecular structure of *trans*–Mo(THF)$(CO)_3(CNAr^{Dipp2})_2$ (**10**). Selected bond distances (Å) and angles (deg): Mo1−C1 = 2.099(3); Mo1−C2 = 2.087(3); Mo1−C3 = 1.980(4); Mo1−C4 = 1.979(4); C1−Mo1−C2 = 177.03(12); C1−Mo1−C3 = 90.14(13); C1−Mo1−C4 = 93.27(13); C2−Mo1−C3 = 89.69(13); C2−Mo1−C4 = 90.38(13); C3−Mo1−C4 = 84.71(15).

2.7 Concluding Remarks

In conclusion, when compared to Ar^{Mes2} substituent, the steric properties of the Ar^{Dipp2} group significantly alter the structural and coordination chemistry of complexes supported by *m*–terphenyl isocyanide ligands. Notably, monovalent Cu and Ag centers and the zerovalent [$Mo(CO)_3$] fragment are seemingly capable of ligating only two $CNAr^{Dipp2}$ units, whereas three less encumbering $CNAr^{Mes2}$ ligands can be readily accommodated. As an added benefit, there steric properties of both $CNAr^{Mes2}$ and $CNAr^{Dipp2}$ can foster unusual coordination environments. This latter feature is exemplified by *mer*–$Mo(CO)_3(CNAr^{Mes2})_3$ (**6**) and *trans*–$Mo(CO)_4(CNAr^{Dipp2})_2$ (**7**), respectively, which represent unique geometrical isomers for mixed isocyanide/carbonyl complexes of zerovalent Mo.

2.8 Synthetic Procedures

General Considerations. All manipulations were carried out under an atmosphere of dry dinitrogen using standard Schlenk and glovebox techniques. Solvents were dried and deoxygenated according to standard procedures.[93] Unless otherwise stated, reagent–grade starting materials were purchased from commercial sources and either used as received or purified by standard procedures.[94] The isocyanide ligand $CNAr^{Mes2}$,[16] $LiAr^{Dipp2}$,[40] acetic formic anhydride (HC(O)OC(O)Me),[42,43] $TosN_3$,[95] and $(C_6H_6)[Cu(OTf)]_2$ were prepared according to literature procedures.[96] Benzene–d_6 and chloroform–d_1 (Cambridge Isotope Laboratories) were degassed and stored over 4 Å molecular sieves under N_2 for 2 d prior to use. Chloroform–*d* (Cambridge Isotope Laboratories) was vacuum distilled from NaH and then stored over 3 and 4 Å molecular sieves under N_2 for 2 d prior to use. Celite 405 (Fisher Scientific) was dried under vacuum (24 h) at a temperature above 250 ˚C and stored in the glovebox prior to use. Solution ^1H, $^{13}C\{^1H\}$ and ^{19}F spectra were recorded on Varian Mercury

300 and 400 spectrometers, a Varian X–Sens500 spectrometer, or a JEOL ECA–500 spectrometer. ^{1}H and ^{13}C{^{1}H} chemical shifts are reported in ppm relative to $SiMe_4$ (^{1}H and ^{13}C δ = 0.0 ppm) with reference to residual solvent resonances of 7.16 ppm (^{1}H) and 128.06 pm (^{13}C) for benzene–d_6 and 7.26 ppm (^{1}H) and 77.1 ppm (^{13}C) for chloroform–*d*. ^{19}F{^{1}H} NMR chemical shifts were referenced externally to neat trifluoroacetic acid $F_3CC(O)OH$ (δ = –78.5 ppm vs. $CFCl_3$ = 0.0 ppm). FTIR spectra were recorded on a Thermo–Nicolet iS10 FTIR spectrometer. Samples were prepared as C_6D_6 and $CDCl_3$ solutions injected into a ThermoFisher solution cell equipped with NaCl windows or as KBr pellets. For solution FTIR spectra, solvent peaks were digitally subtracted from all spectra by comparison with an authentic spectrum obtained immediately prior to that of the sample. The following abbreviations were used for the intensities and characteristics of important IR absorption bands: vs = very strong, s = strong, m = medium, w = weak, vw = very weak; b = broad, vb = very broad, sh = shoulder. Combustion analyses were performed by Robertson Microlit Laboratories of Madison, NJ (USA).

Synthesis of N_3Ar^{Dipp2}. To an Et_2O solution of $LiAr^{Dipp2}$ (14.72 g, 36.41 mmol, 250 mL) was added an Et_2O solution of $TosN_3$ (7.25 g, 36.71 mmol, 1.01 equiv, 75 mL) dropwise via an addition funnel over 2 h. The resulting pale yellow solution was allowed to stir at room temperature for 48 h, after which 100 mL of H_2O was added. The organic and aqueous layers were separated, and the latter was washed with Et_2O (3 × 200 mL). The combined Et_2O extracts were stirred over $MgSO_4$, filtered, and dried *in vacuo*, affording N_3Ar^{Dipp2} as a yellow solid. Yield: 14.94 g, 34.00 mmol, 93%. ^{1}H NMR (400.1 MHz, $CDCl_3$, 20 °C): δ = 7.40 (t, 2H, *J* = 8 Hz, *p*–Dipp), 7.24 (t, 1H, *J* = 7 Hz, *p*–Ph), 7.22 (d, 4H, *J* = 8 Hz, *m*–Dipp), 7.12 (d, 2H, *J* = 8 Hz, *m*–Ph), 2.67 (sept, 4H, *J* = 7 Hz, C*H*$(CH_3)_2$), 1.15 (d, 12H, *J* = 7 Hz, CH(C*H*$_3)_2$), 1.14 (d, 12H, *J* = 7 Hz, CH(C*H*$_3)_2$) ppm. ^{13}C{^{1}H} NMR (100.6 MHz, $CDCl_3$, 20

°C): δ = 146.7, 130.8, 129.4, 124.6, 123.9, 30.9 (*C*H(CH_3)$_2$), 25.0 (CH(*C*H_3)$_2$), 23.3 (CH(*C*H_3)$_2$) ppm. FTIR (KBr pellet): (ν_{N3}) 2154, 2118, and 2090 cm^{-1} also 3064, 3020, 2959, 2929, 2870, 1580, 1460, 1413, 1382, 1363, 1307, 1279, 1249, 1180, 1052, 935, 841, 805, 794, 760, 685, 669, 608, 585, 553 cm^{-1}. Anal. Calcd For $C_{30}H_{37}N_3$: C, 81.96; H, 8.48; N, 9.56. Found: C, 81.68; H, 8.43; N, 9.33.

Synthesis of NH_2Ar^{Dipp2}. A THF slurry of $LiAlH_4$ (7.61 g, 201 mmol, 5 equiv, 400 mL) was cooled to 0 °C under an N_2 atmosphere. To this slurry was added a THF solution of N_3Ar^{Dipp2} (17.64 g, 40.20 mmol, 1 equiv, 200 mL) dropwise via cannula over 3 h. Following the addition, the resulting gray/green mixture was refluxed for 12 h. After this period, the reaction mixture was cooled to 0 °C and added dropwise via cannula to 500 mL of an equally cold H_2O. The resulting slurry was filtered through a medium porosity frit to remove insoluble material. The filter cake was then washed with Et_2O (3 × 200 mL) and added to the filtrate. The aqueous and organic layers of the filtrate were separated, and the latter was stirred over $MgSO_4$, filtered and dried *in vacuo* to afford NH_2Ar^{Dipp2} as a colorless solid. Yield: 6.78 g, 164 mmol, 82%. ^{1}H NMR (400.1 MHz, $CDCl_3$, 20 °C): δ = 7.37 (t, 2H, *J* = 8 Hz, *p*–Dipp), 7.25 (d, 4H, *J* = 8 Hz, *m*–Dipp), 7.97 (d, 2H,*J* = 8 Hz, *m*–Ph), 6.85 (d, 1H, *J* = 7 Hz, *p*–Ph), 3.13 (s, 2H, N*H*$_2$), 2.77 (sept, 4H, *J* = 7 Hz, C*H*(CH_3)$_2$), 1.13 (d, 12H, *J* = 7 Hz, CH(C*H*$_3$)$_2$), 1.11 (d, 12H, *J* = 7 Hz, CH(C*H*$_3$)$_2$) ppm. ^{13}C{^{1}H} NMR (100.6 MHz, $CDCl_3$, 20 °C): δ = 148.1 (*C*–NH_2), 129.2, 129.4, 125.0, 123.3, 30.6 (*C*H(CH_3)$_2$), 24.6 (CH(*C*H_3)$_2$), 24.1 (CH(*C*H_3)$_2$) ppm. FTIR (KBr pellet): (ν_{NH}) 3472 and 3376 cm^{-1} also 2957, 2926, 2866, 1599, 1460, 1436, 1382, 1367, 1058, 1028, 808, 786, 761, 738 cm^{-1}. Anal. Calcd For $C_{30}H_{39}N$: C, 87.10; H, 9.51; N, 3.39. Found: C, 87.39; H, 9.32; N, 3.27.

Synthesis of HC(O)NHAr^{Dipp2}. Neat acetic anhydride (15.86 g, 153 mmol, 8.13 equiv) was cooled to 0 °C under an N_2 atmosphere and formic acid (8.79 g, 191.2 mmol, 10 equiv) was added via syringe over 20 min. The resulting colorless solution was heated at 60 °C for 3 h and then allowed to cool to room temperature. To this mixture was added a THF solution of NH_2Ar^{Dipp2} (7.86 g, 19.1 mmol, 1 equiv) via cannula over 1 h. The reaction mixture was allowed to stir for 36 h after which, 50 mL of H_2O was added. The organic and aqueous layers were then separated, and the latter was washed with Et_2O (3 × 200 mL). The combined Et_2O extracts were stirred over $MgSO_4$, filtered, and dried *in vacuo*. The resulting residue was then slurried in cold hexanes (100 mL, 0 °C), filtered, and dried *in vacuo* to afford HC(O)NHAr^{Dipp2} as a colorless solid. Yield: 7.50 g, 16.70 mmol, 87.3%. ^{1}H NMR (400.1 MHz, $CDCl_3$, 20 °C): δ = 7.64 (d, 1H, *J* = 11 Hz, *H*C(O)), 7.40 (t, 2H, *J*= 8 Hz, *p*–Dipp), 7.29 (t, 2H, *J* = 7 Hz, *p*–Ph), 7.50 (d, 4H, *J* = 8 Hz, *m*–dipp), 7.19 (d, 2H, *J* = 8 Hz, *m*–Ph), 6.59 (d, 1H, *J* = 11 Hz, *H*–N), 2.62 (sept, 4H, *J* = 7 Hz, C*H*(CH_3)$_2$) 1.12 (d, 24H, *J* = 7 Hz, CH(C*H*$_3$)$_2$) ppm. ^{13}C{^{1}H} NMR (100.6 MHz, $CDCl_3$, 20 °C): δ = 162.6 (H*C*(O)N), 146.7, 134.9, 133.4, 131.8, 130.8, 129.4, 124.6, 123.9, 30.9 (*C*H(CH_3)$_2$), 25.0 (CH(*C*H$_3$)$_2$), 23.3 (CH(*C*H$_3$)$_2$) ppm. FTIR (KBr pellet): (ν_{NH}) 3448 cm^{-1}, (ν_{CO}) 1699 cm^{-1} also 3057, 2959, 2882, 2862, 1462, 1424, 1383, 1361, 1324, 1299, 1057, 800, 791, 763, 747 cm^{-1}. Anal. Calcd For $C_{31}H_{39}NO$: C, 84.30; H, 8.91; N, 3.17. Found: C, 83.40; H, 8.88; N, 3.08.

Synthesis of CNAr^{Dipp2}. To a $CHCl_3$ solution of HC(O)NHAr^{Dipp2} (21.23 g, 48.11 mmol, 1 equiv, 150 mL) was added diisopropylamine (34.31 g, 336.8 mmol, 7 equiv). The solution was cooled to 0 °C under an N_2 atmosphere and $POCl_3$ (11 mL, 18.44 g, 120.3 mmol, 2.5 equiv) was added dropwise via syringe. The resulting mixture was allowed to stir for 48 h, after which 150 mL of aqueous 1.5 M Na_2CO_3 was transferred via cannula. After an additional 2 h of stirring, the organic and aqueous layers were separated, and the latter was

washed with CH_2Cl_2 (3 x 200 mL). The combined organic extracts wee stirred over $MgSO_4$ filtered, and dried *in vacuo* to afford the isocyanide $CNAr^{Dipp2}$ as a colorless solid. Yield: 18.25 g, 430.7 mmol, 90%. ^{1}H NMR (400.1 MHz, $CDCl_3$, 20 °C): δ = 7.51 (t, 1H, J = 8 Hz, *p*–Ph), 7.41 (t, 2H, J = 8 Hz, *p*–Dipp), 7.28 (d, 2H, J = 8 Hz, *m*–Ph), 6.26 (d, 4H, J = 8 Hz, *m*–Dipp), 2.54 (sept, 4H, J = 7 Hz, C*H*$(CH_3)_2$), 1.18 (d, 12H, J = 7 Hz, CH(C*H*$_3)_2$), 1.14 (d, 12H, J = 7 Hz, CH(C*H*$_3)_2$) ppm. ^{13}C{^{1}H} NMR (100.6 MHz, C_6D_6, 20 °C): δ = 171.9 (C≡N), 146.7, 139.4, 135.0, 129.7, 129.6, 128.6, 123.4, 31.5 (*C*H$(CH_3)_2$), 24.5 (CH(*C*H$_3)_2$), 24.2 (CH(*C*H$_3)_2$) ppm. FTIR (KBr pellet): (ν_{CN}) 2124 cm^{-1} also 3061, 3025, 2959, 2925, 2867, 1578, 1458, 1417, 1382, 1363, 1328, 1252, 1177, 1055, 1039, 824, 806, 792, 758 cm^{-1}. FTIR (C_6D_6, NaCl windows): (ν_{CN}) 2118 cm^{-1} also 3062, 3023, 2962, 2929, 2868, 2118, 1616, 1594, 1580, 1460, 1419, 1385, 1363, 1324, 1180, 1052, 811, 794, 760 cm^{-1}. Anal. Calcd For $C_{31}H_{37}N$: C, 87.89; H, 8.80; N, 3.31. Found: C, 88.03; H, 8.61; N, 3.12.

Synthesis of $[(THF)_2Cu(CNAr^{Dipp2})_2]OTf$ (1). To a THF solution of $(C_6H_6)[CuOTf]_2$ (0.074 g, 0.147 mmol, 3 mL) was added a THF solution of $CNAr^{Dipp2}$ (0.250 g, 0.509 mmol, 4 equiv, 10 mL). The reaction mixture was allowed to stir for 3 h, after which time all volatile materials were removed under reduced pressure. Dissolution of the resulting colorless residue in THF (5 mL) followed by filtration and storage at –35 °C for 36 h resulted in colorless crystals, which were collected and dried *in vacuo*. Yield: 0.110 g, 0.091 mmol, 62%. ^{1}H NMR (400.1 MHz, C_6D_6, 20 °C): δ = 7.34 (t, 4H, J = 8 Hz, *p*–Dipp), 7.18 (d, 8H, J = 8 Hz, *m*–Dipp), 6.86 (s, 6H, J = 8 Hz, *p*–Ph + *m*–Ph), 3.48 (bs, 8H, THF), 2.51 (sept, 8H, J = 7 Hz, C*H*$(CH_3)_2$), 1.40 (bs, 8H, THF), 1.22 (d, 24H, J = 7 Hz, CH(C*H*$_3)_2$), 1.06 (d, 24H, J = 7 Hz, CH(C*H*$_3)_2$) ppm. ^{13}C{^{1}H} NMR (100.6 MHz, C_6D_6, 20 °C): δ = 166.5 (C≡N), 146.3, 140.3, 133.5, 133.3, 130.2, 130.0, 129.9, 123.7, 31.5 (*C*H$(CH_3)_2$), 24.6 (CH(*C*H$_3)_2$), 24.2 (CH(*C*H$_3)_2$) ppm. ^{19}F{^{1}H} NMR (282.3 MHz, C_6D_6, 20 °C) δ = –78.3 ppm. FTIR (KBr

pellet): (ν_{CN}) 2167 cm^{-1} also 3063, 2964, 2928, 2569, 1578, 1460 1363, 1315, 1236, 12101, 1027, 757, 636 cm^{-1}. FTIR (C_6D_6, NaCl windows): (ν_{CN}) 2165 cm^{-1}. Anal. Calcd For $C_{71}H_{90}F_3N_2O_5SCu$: C, 70.82; H, 7.53; N, 2.33. Found: C, 71.32; H, 7.34; N, 2.27.

Synthesis of (OTf)Cu(CNArDipp$_2$)$_2$ (2). To a CH_2Cl_2 solution of $(C_6H_6)[CuOTf]_2$ (0.050 g, 0.099 mmol, 3 mL) was added a CH_2Cl_2 solution of $CNAr^{Dipp2}$ (0.170 g, 0.401 mmol, 4.04 equiv, 5 mL). The reaction mixture was allowed to stir for 3 h, after which all volatile materials were removed under reduced pressure. Dissolution of the resulting colorless residue in CH_2Cl_2 (3 mL) followed by filtration and storage at −35 °C for 12 h resulted in colorless crystals, which were collected and dried in vacuo. Yield: 0.124 g, 0.117 mmol, 59%. ^{1}H NMR (400.1 MHz, C_6D_6, 20 °C): δ = 7.34 (t, 4H, J = 8 Hz, *p*–Dipp), 7.19 (d, 8H, J = 8 Hz, *m*–Dipp), 6.86 (s, 6H, *p*–Ph + *m*–Ph), 2.50 (sept, 8H, J = 6 Hz, C*H*(CH_3)$_2$), 1.21 (d, 24H, J = 6 Hz, CH(C*H*$_3$)$_2$), 1.06 (d, 24H, J = 6 Hz, CH(C*H*$_3$)$_2$) ppm. ^{13}C{^{1}H} NMR (100.6 MHz, C_6D_6, 20 °C): δ = 166.5 (*C*≡N), 146.2, 140.3, 133.5, 133.3, 130.2, 130.0, 129.9, 123.7, 31.5 (*C*H(CH_3)$_2$), 24.6 (CH(*C*H$_3$)$_2$), 24.2 (CH(*C*H$_3$)$_2$) ppm. ^{19}F{^{1}H}NMR (282.3 MHz, C_6D_6, 20 °C): δ = −78.0 ppm. FTIR (KBr pellet): (ν_{CN}) 2167 cm^{-1} also 3063, 2962, 2928, 2869, 1596, 1579, 1460, 1412, 1385, 1364, 1316, 1235, 1209, 1165, 1056, 1020, 806, 757, 636 cm^{-1}. FTIR (C_6D_6, NaCl windows): (ν_{CN}) 2165 cm^{-1}. Anal. Calcd for $C_{63}H_{74}F_3N_2O_3SCu$: C, 71.39; H, 7.04; N, 2.64. Found: C, 71.23; H, 7.12; N, 2.59.

Synthesis of [(Et$_2$O)Ag(CNAr^{Mes2})$_3$]OTf (3). To a THF solution of AgOTf (0.050 g, 0.196 mmol, 3 mL) was added a THF solution of $CNAr^{Mes2}$ (0.200 g, 0.589 mmol, 3 equiv, 5 mL). The reaction mixture was allowed to stir for 3 h, after which all volatile materials were removed under reduced pressure. Dissolution of the resulting colorless residue in a 15:1 Et_2O/THF mixture (4 mL total) followed by filtration and storage at −35 °C for 24 h resulted

in colorless crystals, which were collected and dried *in vacuo*. Yield: 0.162 g, 0.120 mmol, 61%. ^{1}H NMR (400.1 MHz, C_6D_6, 20 °C): δ = 6.93 (t, 3H, J = 8 Hz, *p*–Ph), 6.89 (s, 12H, *m*–Mes), 6.75(d, 6H, J = 8 Hz, *m*–Ph), 3.27 (q, 4H, J = 7 Hz, H_3CCH_2O), 2.20 (s, 18H, *p*–CH_3), 2.01 (s, 36H, *o*–CH_3), 1.12 (t, 6H, J = 7 Hz, H_3CCH_2O) ppm. ^{13}C{^{1}H} NMR (100.6 MHz, C_6D_6, 20 °C): δ = 140.8, 138.6, 136.0, 134.1, 130.7, 129.9, 129.4, 21.5 (*p*–CH_3–Mes), 20.5 (*o*–CH_3–Mes) ppm (the C≡N resonance was not conclusively identified after prolonged scanning). ^{19}F{^{1}H} NMR (282.3 MHz, C_6D_6, 20 °C): δ = −77.9 ppm. FTIR (KBr pellet): (ν_{CN}) 2166 cm^{-1}, also 2977, 2947, 2919, 2858, 2613, 1577, 1457, 1379, 1279 cm^{-1}. Anal. Calcd for $C_{80}H_{85}F_3N_3O_4SAg$: C, 71.20; H, 6.35; N, 3.11. Found: C, 71.29; H, 6.12; N, 3.19.

Synthesis of (κ^2–OTf)Ag(CNAr^{Dipp2})$_2$. (4) To a THF solution of AgOTf (0.030 g, 0.118 mmol, 5 mL) was added a THF solution of CNAr^{Dipp2} (0.100 g, 0.236 mmol, 5 mL). The reaction mixture was allowed to stir for 3 h, after which all volatile materials were removed under reduced pressure. Dissolution of the resulting colorless residue in an Et_2O/*n*–hexane mixture (1:1, 2 mL total) followed by filtration and storage at −35 °C for 12 h resulted in colorless crystals, which were collected and dried *in vacuo*. Yield: 0.070 g, 0.063 mmol, 54%. ^{1}H NMR (400.1 MHz, $CDCl_3$, 20 °C): δ = 7.34 (t, 4H, J = 8 Hz, *p*–Dipp), 7.20 (d, 8H, J = 8 Hz, *m*–Dipp), 6.89 (t, 2H, J = 9 Hz, *p*–Ph), 6.80 (t, 4H, J = 9 Hz, *m*–Ph), 2.43 (sept, 8H, J = 7 Hz, C*H*(CH_3)$_2$), 1.20 (d, 24H, J = 7 Hz, CH(C*H*$_3$)$_2$), 1.03 (d, 24H, J = 7 Hz, CH(C*H*$_3$)$_2$) ppm. ^{13}C{^{1}H} NMR (100.6 MHz, $CDCl_3$, 20 °C): δ = 169.6 (*C*≡N), 146.5, 140.4, 133.4, 130.6, 130.3, 130.0, 127.3, 127.1, 123.8, 67.9 (*C*F_3), 31.5 (*C*H(CH_3)$_2$), 24.5 (CH(*C*H$_3$)$_2$), 24.2 (CH(*C*H$_3$)$_2$) ppm. ^{19}F{^{1}H} NMR (282.3 MHz, C_6D_6, 20 °C) δ = −77.7 ppm. FTIR (C_6D_6, NaCl windows): (ν_{CN}) 2176 cm^{-1} also 3231, 3061, 2962, 2926, 2862, 2390, 2376, 2362, 2174, 1616, 1460, 1333, 1299, 1235, 1221, 1158, 1027, 755, 639 cm^{-1}. Anal. Calcd for $C_{63}H_{74}AgF_3N_2O_3S$: C, 68.53; H, 6.76; N, 2.54. Found: C, 70.91; H, 7.26; N, 2.31.

Synthesis of *fac*–Mo(CO)$_3$(CNAr^{Mes2})$_3$ (5). To a toluene solution of Mo(CO)$_3$(NCMe)$_3$ (0.060 g, 0.197 mmol, 4 mL) was added a toluene solution of CNAr^{Mes2} (0.200 g, 0.590 mmol, 4 mL). The reaction mixture was allowed to stir for 6 h, after which all volatile materials were removed under reduced pressure. Dissolution of the resulting orange residue in a CH_2Cl_2/*n*–pentane mixture (1:5, 12 mL total) followed by filtration and storage at −35 °C for 24 h resulted in yellow crystals, which were collected and dried *in vacuo*. Yield: 0.130 g, 0.108 mmol, 50%. ^{1}H NMR (400.1 MHz, C_6D_6, 20 °C): δ = 6.92 (s, 12H, *m*–Mes), 6.89 (t, 3H, J = 7 Hz, *p*–Ph), 6.85 (d, 6H, J = 7 Hz, *m*–Ph), 2.25 (s, 18H, *p*–C*H*$_3$), 2.08 (s, 36H,*o*–C*H*$_3$) ppm. ^{13}C{^{1}H} NMR (100.6 MHz, C_6D_6, 20 °C): δ = 209.4 (*C*≡O), 175.7 (*C*≡N), 139.0, 137.2, 135.8, 135.0, 130.2, 129.1, 128.4, 127.1, 21.5 (*p*–*C*H$_3$–Mes), 20.7 (*o*–*C*H$_3$–Mes). FTIR (C_6D_6, NaCl windows): (ν_{CN}) 2046 and 2000 cm^{-1}, (ν_{CO}) 1942 and 1910 cm^{-1} also 3234, 2920, 2853, 1614, 1579, 1454, 1413, 1375, 1164, 1033, 812, 582 cm^{-1}. Anal. Calcd for $C_{78}H_{75}N_3O_3Mo$: C, 78.17; H, 6.31; N, 3.51. Found: C, 77.48; H, 6.01; N, 3.48.

Synthesis of *mer*–Mo(CO)$_3$(CNAr^{Mes2})$_3$ (6). A benzene solution of *fac*–Mo(CO)$_3$(CNAr^{Mes2})$_3$ (**5**, 0.100 g, 0.083 mmol, 20 mL) was stirred at 90 °C for 72 h, after which all volatile materials were removed under reduced pressure. Dissolution of the resulting orange residue in a toluene/*n*–pentane mixture (1:3, 4 mL total) followed by filtration and storage at −35 °C for 24 h resulted in orange crystals, which were collected and dried *in vacuo*. Yield: 0.060 g, 0.050 mmol, 60%. ^{1}H NMR (400.1 MHz, C_6D_6, 20 °C): δ = 6.98 (s, 4H, *m*–Mes), 6.94 (s, 8H, *m*–Mes), 6.92 (t, 2H, J = 8 Hz, *p*–Ph), 6.88 (d, 2H, J = 8 Hz, *m*–Ph), 6.87 (t, 1H, J = 8 Hz, *p*–Ph), 6.84 (d, 4H, J = 8 Hz, *m*–Ph), 2.51 (s, 6H, *p*–CH$_3$), 2.44 (s, 12H, *p*–CH$_3$), 2.01 (s, 24H, *o*–CH$_3$), 2.01 (s, 12H, *o*–CH$_3$) ppm. ^{13}C{^{1}H} NMR (100.6 MHz, C_6D_6, 20 °C): δ = 211.2 (*C*≡O), 205.1 (*C*≡O), 177.3 (*C*≡N), 175.1 (*C*≡N),

138.8, 138.7, 137.2, 137.1, 135.7, 135.7, 135.2, 134.7, 129.7, 129.5, 129.0, 129.1, 127.2, 126.8, 21.9, and 21.7 (*p*–*C*H$_3$–Mes), 20.5 and 20.4 (*o*–*C*H$_3$–Mes). FTIR (C_6D_6, NaCl windows): (ν_{CN}) 2046, 2024, and 1993 cm^{-1}, (ν_{CO}) 1926 and 1902 cm^{-1} also 2970, 2948, 2920, 2856, 2359, 2340, 1615, 1576, 1418, 852, 811, 755, 625 cm^{-1}. Anal. Calcd for $C_{78}H_{75}N_3O_3Mo$: C, 78.17; H, 6.31; N, 3.51. Found: C, 77.50; H, 6.27; N, 4.18.

Formation of Mixtures Containing *trans*–Mo(CO)$_4$(CNAr^{Dipp2})$_2$ (7) and *trans*–Mo(NCMe)(CO)$_3$(CNAr^{Dipp2})$_2$ (8). To an Et_2O solution of *fac*–Mo(CO)$_3$(NCMe)$_3$ (0.358 g, 1.180 mmol, 50 mL) was added an Et_2O solution of CNAr^{Dipp2} (1.000 g, 2.360 mmol, 2 equiv, 50 mL) and stirred. Over a 24 h period the reaction mixture turned from green to orange resulting in an approximate 1:1 mixture of *trans*–Mo(CO)$_4$(CNAr^{Dipp2})$_2$ (**7**) and *trans*–Mo(NCMe)(CO)$_3$(CNAr^{Dipp2})$_2$ (**8**) as determined by ^{1}H NMR analysis.

Synthesis of *trans*–Mo(CO)$_4$(CNAr^{Dipp2})$_2$. (7) Method A. To a Et_2O solution of *fac*–Mo(CO)$_3$(NCMe)$_3$ (0.072 g, 0.236 mmol, 7 mL) was added an Et_2O solution of CNAr^{Dipp2} (0.200 g, 0.472 mmol, 2 equiv, 7 mL). The reaction mixture was allowed to stir for 24 h, after which all volatile materials were removed under reduced pressure. The resulting orange residue was dissolved in 30 mL of THF and CO gas (0.070 mL, 2.909 mmol, 12 equiv) was added. The reaction mixture was stirred for 24 h, after which all the volatile materials were removed under reduced pressure. Dissolution of the resulting yellow residue in a THF/*n*–pentane mixture (3:1, 60 mL total) followed by filtration and storage at −35 °C for 24 h resulted in pale green crystals, which were collected and dried *in vacuo*. Yield: 0.140 g, 0.133 mmol, 56%.

Method B. To a THF solution of *trans*–Mo(NCMe)(CO)$_3$CNAr^{Dipp2})$_2$ (**8**, 0.100 g, 0.093 mmol, 20 mL) was added CO gas (0.080 mL, 3.326 mmol, 36 equiv) and was then

stirred for 24 h. All volatile materials were then removed under reduced pressure. Dissolution of the resulting yellow residue in a THF/*n*–pentane mixture (3:1, 20 mL total) followed by filtration and storage at −35 °C for 24 h resulted in pale green crystals, which were collected and dried in vacuo. Yield: 0.042 g, 0.040 mmol, 42%. ^{1}H NMR (400.1 MHz, C_6D_6, 20 °C): δ = 7.36 (t, 4H, *J* = 8 Hz, *p*–Dipp), 7.19 (d, 8H, *J* = 8 Hz, *m*–Dipp), 6.91 (d, 4H, *J* = 7 Hz, *m*–Ph), 6.85 (t, 2H, *J* = 6 Hz, *p*–Ph), 2.68 (sept, 8H, *J* = 6 Hz, C*H*$(CH_3)_2$), 1.33 (d, 24H, *J* = 7 Hz, CH(C*H*$_3)_2$), 1.06 (d, 24H, *J* = 7 Hz, CH(C*H*$_3)_2$) ppm. ^{13}C{^{1}H} NMR (100.6 MHz, C_6D_6, 20 °C): δ = 205.4 (*C*≡O), 172.4 (*C*≡N), 146.7, 139.4, 135.1, 129.8, 129.7, 128.8, 127.4, 123.6, 31.6 (*CH*$(CH_3)_2$), 24.7 (CH(*C*H$_3)_2$), 24.5 (CH(*C*H$_3)_2$) ppm. FTIR (C_6D_6, NaCl windows): (ν_{CN}) 2054, 2007 cm^{-1}, (ν_{CO}) 1934 cm^{-1} also 3234, 2961, 2925, 2861, 2387, 2360, 1618, 1454, 1330, 1163, 808 cm^{-1}. Anal. Calcd for $C_{66}H_{74}N_2O_4Mo$: C, 75.12; H, 7.07; N, 2.66 Found: C, 74.74; H, 7.14; N, 2.63.

Synthesis of *trans*–Mo(NCMe)(CO)$_3$(CNAr^{Dipp2})$_2$. (8) To an Et_2O solution of *fac*–$Mo(CO)_3(NCMe)_3$ (0.358 g, 1.180 mmol, 50 mL) was added an Et_2O solution of CNAr^{Dipp2} (1.000 g, 2.360 mmol, 2 equiv, 50 mL). The reaction mixture was allowed to stir for 24 h while gradually changing in color from green to orange. Acetonitrile (NCMe, 50 mL) was then added and the reaction mixture was irradiated with a 254 nm Hg lamp under an Ar purge for 24 h. The total volume of the mixture was reduced by half *in vacuo* resulting in the precipitation of a yellow solid, which was collected by filtration. The yellow precipitate was then slurried in cold acetonitrile (20 mL, 0 °C), filtered, and dried *in vacuo* to afford *trans*–Mo(NCMe)(CO)$_3$(CNAr^{Dipp2})$_2$ (**8**). Yield: 0.703 g, 0.658 mmol, 56%. ^{1}H NMR (400.1 MHz, C_6D_6, 20 °C): δ = 7.33 (t, 4H, *J* = 7 Hz, *p*–Dipp), 7.19 (d, 8H, *J* = 8 Hz, *m*–Dipp), 6.95 (d, 4H, *J* = 7 Hz, *m*–Ph), 6.87 (t, 2H, *J* = 7 Hz, *p*–Ph), 2.78 (sept, 8H, *J* = 6 Hz, C*H*$(CH_3)_2$), 1.36 (d, 24H, *J* = 7 Hz, CH(C*H*$_3)_2$), 1.12 (d, 24H, *J* = 7 Hz, CH(C*H*$_3)_2$), 1.11 (s, 3H, NCC*H*$_3$)

ppm. $^{13}C\{^{1}H\}$ NMR (100.6 MHz, C_6D_6, 20 °C): δ = 216.1 (*C*≡O), 206.7 (*C*≡O), 178.7 (*C*≡N), 146.7, 138.7, 135.6, 129.5, 129.2, 126.1, 123.2, 119.9 (N*C*CH_3), 31.5 (*CH*$(CH_3)_2$), 24.5 (CH(*C*$H_3)_2$), 24.4 (CH(*C*$H_3)_2$), 2.61 (NC*C*H_3) ppm. FTIR (C_6D_6, NaCl windows): (ν_{CN}) 2021 and 1993 cm^{-1}, (ν_{CO}) 1932, 1901, and 1873 cm^{-1} also 2956, 2920, 2861, 2362, 2337, 1579, 1457, 1413, 808, 755 cm^{-1}. Anal. Calcd for $C_{67}H_{77}N_3O_3Mo$: C, 75.32; H, 7.27; N, 3.93. Found: C, 76.00; H, 7.20; N, 3.80.

Synthesis of *cis,fac*–Mo(py)$(CO)_3(CNAr^{Dipp2})_2$. (9) Pyridine (2.000 g, 25.284 mmol, 272 equiv) was added to a benzene solution of *trans*–Mo(NCMe)$(CO)_3(CNAr^{Dipp2})$ (**8**, 0.100 g, 0.093 mmol, 2 mL). The reaction mixture was allowed to stir for 4 h, after which all volatile materials were removed under reduced pressure. Dissolution of the resulting red residue in an Et_2O/*n*–pentane mixture (1:4, 5 mL total) followed by filtration and storage at −35 °C for 24 h resulted in fine orange crystals, which were collected and dried *in vacuo*. Yield: 0.071 g, 0.064 mmol, 71%. A very large excess of pyridine is required for the reaction to proceed to completion in a timely fashion. Reaction times of several days are required when employing lesser amounts (e.g., 10 equiv). ^{1}H NMR (400.1 MHz, C_6D_6, 20 °C): δ = 7.83 (m, 2H, py), 7.34 (t, 4H, *J* = 8 Hz, *p*–Dipp), 7.18 (d, 8H, *J* = 8 Hz, *m*–Dipp), 6.93 (d, 4H, *J* = 7 Hz, *m*–Ph), 6.84 (t, 2H, *J* = 4 Hz, *p*–Ph), 6.81 (m, 1H, p–py), 6.40 (m, 2H, py), 2.71 (sept, 8H, *J* = 7 Hz, C*H*$(CH_3)_2$), 1.22 (d, 24H, *J* = 7 Hz, CH(C*H*$_3)_2$), 1.08 (d, 24H, *J* = 7 Hz, CH(C*H*$_3)_2$) ppm. $^{13}C\{^{1}H\}$ NMR (100.6 MHz, C_6D_6, 20 °C): δ = 219.6 (*C*≡O), 207.6 (*C*≡O), 180.2 (*C*≡N), 154.3, 146.4, 138.7, 135.6, 134.2, 129.6, 129.5, 129.2, 126.1, 123.8, 123.4, 31.4 (*CH*$(CH_3)_2$), 24.6 (CH(*C*$H_3)_2$), 24.3 (CH(*C*$H_3)_2$) ppm. FTIR (C_6D_6, NaCl windows): (ν_{CN}) 2018 and 1992 cm^{-1}, (ν_{CO}) 1888 and 1862 cm^{-1} also 3064, 2962, 2928, 2868, 1580, 1459, 1440, 1411, 1380, 1357, 802, 158, 691, 603 cm^{-1}. Anal. Calcd for $C_{70}H_{79}N_3O_3Mo$: C, 75.99; H, 7.20; N, 2.34. Found: C, 75.98; H, 7.43; N, 2.79.

Synthesis of *trans*–Mo(THF)(CO)$_3$(CNAr^{Dipp2})$_2$ (10). A THF solution of *trans*–Mo(NCMe)(CO)$_3$(CNAr^{Dipp2})$_2$ (**8**, 0.200 g, 0.182 mmol, 10 mL) was allowed to stir for 12 h and then dried under reduced pressure. This process was then repeated for five iterations. Dissolution of the resulting orange residue in a toluene/*n*–pentane mixture (1:3, 4 mL total) followed by filtration and storage at −35 °C for 24 h resulted in orange crystals, which were collected and dried *in vacuo*. Yield: 0.075 g, 0.068 mmol, 53%. ^{1}H NMR (400.1 MHz, C_6D_6, 20 °C): δ = 7.33 (t, 4H, *J* = 8 Hz, *p*–Dipp), 7.19 (d, 8H, *J* = 8 Hz, *m*–Dipp), 6.92 (d, 4H, *J* = 7 Hz, *m*–Ph), 6.85 (t, 2H, *J* = 7 Hz, *p*–Ph), 2.78 (sept, 8H, *J* = 7 Hz, C*H*(CH$_3$)$_2$), 2.66 (bs, 4H, THF), 1.39 (d, 24H, *J* = 7 Hz, CH(C*H*$_3$)$_2$), 1.29 (bs, 4H, THF), 1.10 (d, 24H, *J* = 7 Hz, CH(C*H*$_3$)$_2$) ppm. ^{13}C{^{1}H} NMR (100.6 MHz, C_6D_6, 20 °C): δ = 220.5 (*C*≡O), 207.5 (*C*≡O), 179.6 (*C*≡N), 146.6, 138.7, 135.7, 129.7, 129.2, 126.3, 123.4, 76.5 (THF), 31.4 (*C*H(CH$_3$)$_2$), 26.6 (THF), 24.5 (CH(*C*H$_3$)$_2$), 24.4 (CH(*C*H$_3$)$_2$) ppm. FTIR (C_6D_6, NaCl windows): (ν_{CN}) 2041, 2018, and 1987 cm^{-1}, (ν_{CO}) 1924, 1888, and 1859 cm^{-1} also 2964, 2925, 2867, 1582, 1463, 1413, 1383, 1363, 752 cm^{-1}. Prolonged exposure to vacuum partially removes the coordinated THF ligand. Accordingly, repeated combustion analyses gave inconsistent results.

2.9 Crystallographic Structure Determinations

General Considerations. Single crystal X–ray structure determinations were carried out at low temperature on a Bruker Platform or Kappa Diffractometers equipped with a Bruker APEX, APEX II, and Photon 100 area detectors. All structures were solved via direct methods with SIR 2004[92] and refined by full–matrix least–squares procedures utilizing SHELXL–2013.[97] Crystallographic data collection and refinement information are listed in Table 2.2 through 2.5. Crystals of *fac,cis*–Mo(py)(CO)$_3$(CNAr^{Dipp2})$_2$ (**9**) repeatedly gave rise to poor quality data sets because of the formation of weakly diffracting crystals. The highest

quality data set, which is reported here, gave rise to a final R_1 value of 0.1094. However, connectivity is clearly established and a stable anisotropic refinement was achieved for all non–hydrogen atoms. Cambridge Structural Database (CSD) version 5.30 (Nov. 2008) was used for all searches.[98]

Table 2.2. Crystallographic Data Collection and Refinement Information for $CNAr^{Dipp2}$, $[(THF)_2Cu(CNAr^{Dipp2})_2]OTf$, and $(OTf)Cu(CNAr^{Dipp2})_2 \cdot CH_2Cl_2$

	$CNAr^{Dipp2}$	$[(THF)_2Cu(CNAr^{Dipp2})_2]OTf$ (**1**)	$(OTf)Cu(CNAr^{Dipp2})_2 \cdot CH_2Cl_2$ (**2**$\cdot CH_2Cl_2$)
Formula	$C_{31}H_{37}N$	$C_{71}H_{90}CuF_3N_2O_5S$	$C_{67}H_{82}Cl_8CuF_3N_2O_3S$
Crystal System	Monoclinic	Monoclinic	Monoclinic
Space Group	$P2_1/n$	$P2_1/c$	$C2/c$
a, Å	12.0083(11)	12.002(5)	22.0775(17)
b, Å	17.2200(16)	34.000(5)	13.8153(12)
c, Å	12.7738(12)	18.363(5)	23.525(2)
α, deg	90	90	90
β, deg	99.3020(10)	107.463(5)	100.020(5)
γ, deg	90	90	90
V, Å^3	2606.7(4)	7148(4)	7065.9(10)
Z	4	4	4
Radiation (λ, Å)	Mo–Kα, 0.71073	Mo–Kα, 0.71073	Cu–Kα, 1.54178
ρ (calcd.), g/cm^3	1.079	1.119	1.316
μ, mm^{-1}	0.061	0.388	3.917
Temp, K	100(2)	100(2)	100(2)
θ max, deg	25.43	23.25	68.13
data/parameters	4812/297	10043/764	6078/425
R_1	0.0404	0.0656	0.0658
wR_2	0.0987	0.1306	0.1729
GOF	1.043	1.030	1.035

Table 2.3. Crystallographic Data Collection and Refinement Information for $[(Et_2O)Ag(CNAr^{Mes2})_3]OTf$, $(\kappa^2\text{–}OTf)Ag(CNAr^{Dipp2})_2$, and *fac*–$Mo(CO)_3(CNAr^{Mes2})_3$

	$[(Et_2O)Ag(CNAr^{Mes2})_3]OTf$ (**3**)	$(\kappa^2\text{–}OTf)Ag(CNAr^{Dipp2})_2$ (**4**)	*fac*–$Mo(CO)_3(CNAr^{Mes2})_3$ (**5**)
Formula	$C_{80}H_{83}AgF_3N_3O_4S$	$C_{63}H_{74}AgF_3N_2O_3S$	$C_{78}H_{75}MoN_3O_3$
Crystal System	Orthorhombic	Orthorhombic	Monoclinic
Space Group	$P2_12_12_1$	*Pbca*	$P2_1/c$
a, Å	14.480(14)	24.7376(14)	28.853(19)
b, Å	19.449(11)	19.1647(11)	12.336(9)
c, Å	25.316(19)	27.0246(16)	24.925(19)
α, deg	90	90	90
β, deg	90	90	103.458(10)
γ, deg	90	90	90
V, Å^3	7129.5	12812.1(13)	7133(9)
Z	4	8	4
Radiation (λ, Å)	Mo–Kα, 0.71073	Mo–Kα, 0.71073	Mo–Kα, 0.71073
ρ (calcd.), g/cm^3	1.255	1.145	1.116
μ, mm^{-1}	0.371	0.397	0.230
Temp, K	100(2)	100(2)	100(2)
θ max, deg	23.25	23.82	23.53
data/parameters	9918/849	9838/683	10578/784
R_1	0.0583	0.0686	0.0798
wR_2	0.0996	0.1829	0.1645
GOF	1.004	1.062	1.032

Table 2.4. Crystallographic Data Collection and Refinement Information for *mer*–$Mo(CO)_3(CNAr^{Mes2})_3$, *trans*–$Mo(CO)_4(CNAr^{Mes2})_2$, and *trans*–$Mo(NCMe)(CO)_3(CNAr^{Mes2})_2$

	mer–$Mo(CO)_3(CNAr^{Mes2})_3$ (**6**)	*trans*–$Mo(CO)_4(CNAr^{Mes2})_2$ (**7**)	*trans*–$Mo(NCMe)(CO)_3(CNAr^{Mes2})_2$ (**8**)
Formula	$MoC_{78}H_{75}N_3O_3$	$MoC_{66}H_{74}N_2O_4$	$MoC_{66}H_{77}N_3O_3$
Crystal System	Monoclinic	Monoclinic	Tetragonal
Space Group	$P2_1/m$	$C2/c$	$I4/m$
a, Å	12.3865(11)	24.0662(17)	20.7048(5)
b, Å	16.6448(14)	23.9799(17)	20.7048(5)
c, Å	16.2852(14)	21.1907(15)	19.9285(6)
α, deg	90	90	90
β, deg	99.2460(10)	108.3150(10)	90
γ, deg	90	90	90
V, Å^3	3313.9(5)	11609.8(14)	8543.1(4)
Z	2	8	4
Radiation (λ, Å)	Mo–Kα, 0.71073	Mo–Kα, 0.71073	Cu–Kα, 1.54178
ρ (calcd.), g/cm^3	1.201	1.207	0.806
μ, mm^{-1}	0.247	0.274	1.491
Temp, K	100(2)	100(2)	100(2)
θ max, deg	28.36	27.88	65.97
data/parameters	6054/415	13455/679	3739/232
R_1	0.0516	0.0415	0.0699
wR_2	0.0943	0.0821	0.2205
GOF	1.013	1.009	1.098

Table 2.5. Crystallographic Data Collection and Refinement Information for *cis,fac*–$Mo(py)(CO)_3(CNAr^{Dipp2})_2 \cdot 1.5Et_2O$, and *trans*–$Mo(NCMe)(CO)_3(CNAr^{Dipp2})_2 \cdot 2THF$

	cis,fac–$Mo(py)(CO)_3(CNAr^{Dipp2})_2 \cdot 1.5Et_2O$ (**9**·$1.5Et_2O$)	*trans*–$Mo(NCMe)(CO)_3(CNAr^{Dipp2})_2 \cdot 2THF$ (**10**·2THF)
Formula	$MoC_{76}H_{94}N_3O_{4.50}$	$MoC_{77}H_{98}N_2O_6$
Crystal System	Orthorhombic	Orthorhombic
Space Group	$P2_12_12_1$	$P2_1/n$
a, Å	16.5415(11)	16.950(9)
b, Å	17.4785(12)	17.551(9)
c, Å	24.6126(17)	25.085(13)
α, deg	90	90
β, deg	90	107.81(8)
γ, deg	90	90
V, $Å^3$	7159.0(8)	7104.9(11)
Z	4	4
Radiation (λ, Å)	Mo–Kα, 0.71073	Mo–Kα, 0.71073
ρ (calcd.), g/cm^3	1.135	1.163
μ, mm^{-1}	0.231	0.235
Temp, K	150(2)	100(2)
θ max, deg	27.92	25.57
data/parameters	15976/805	13107/1101
R_1	0.1094	0.0590
wR_2	0.2237	0.1000
GOF	1.095	1.109

2.10 Acknowledgements

Chapter 2 is adapted from Ditri, T. B.; Fox. B.J.; Moore, C. E.; Rheingold, A. L.; Figueroa, J. S. "Effective Control of Ligation and Geometric Isomerism: Direct Comparison of Steric Properties Associated with Bis–mesityl and Bis–diisopropylphenyl *m*–Terphenyl Isocyanides." *Inorg. Chem.* **2009,** *48*, 8362–8375. Copyright 2009 American Chemical

Society. Permission to use copyrighted images and data in the manuscript was also obtained from Fox. B.J.; Moore, C. E.; Rheingold, A. L.; Figueroa, J. S. The dissertation author is the first author of this paper.

2.11 References

(1) Yamamoto, Y. *Coord. Chem. Rev.* **1980**, *32*, 193–233.

(2) Sarapu, A. C.; Fenske, R. F. *Inorg. Chem.* **1974**, *14*, 247–253.

(3) Bonati, F.; Minghetti, G. *Inorg. Chim. Acta* **1974**, *9*, 95–112.

(4) Brennessel, W. W.; Ellis, J. E. *Angew. Chem., Int. Ed.* **2007**, *46*, 598–600.

(5) Warnock, G. F.; Cooper, N. J. *Organometallics* **1989**, *8*, 1826–1827.

(6) Leach, P. A.; Geib, S. J.; Corella, J. A.; Warnock, G. F.; Cooper, N. J. *J. Am. Chem. Soc.* **1994**, *116*, 8566–8574.

(7) Yamamoto, Y.; Yamazaki, H. *J. Organomet. Chem.* **1985**, *282*, 191–200.

(8) Treichel, P. M.; Essenmacher, G. J. *Inorg. Chem.* **1976**, *15*, 146–150.

(9) Robinson, R. E.; Holovics, T. C.; Deplazes, S. F.; Lushington, G. H.; Powell, D. R.; Barybin, M. V. *J. Am. Chem. Soc.* **2003**, *125*, 4432–4433.

(10) Mann, K. R.; Cimolino, M.; Geoffroy, G. L.; Hammond, G. S.; Orio, A. A.; Albertin, G.; Gray, H. B. *Inorg. Chim. Acta* **1976**, *16*, 97–101.

(11) Chiu, K. W.; Jones, R. A.; Wilkinson, G.; Galas, A. M. R.; Hursthouse, M. B. *J. Chem. Soc., Dalton Trans.* **1981**, 2088–2097.

(12) Carnahan, E. M.; Lippard, S. J. *J. Chem. Soc., Dalton Trans.* **1991**, 699–706.

(13) Barybin, M. V.; Holovics, T. C.; Deplazes, S. F.; Lushington, G. H.; Powell, D. R.; Toriyama, M. *J. Am. Chem. Soc.* **2002**, *124*, 13668–13669.

(14) Acho, J. A.; Lippard, S. J. *Organometallics* **1994**, *13*, 1294–1299.

(15) Weber, L. *Angew. Chem., Int. Ed.* **1998**, *37*, 1515–1517.

(16) Fox, B. J.; Sun, Q. Y.; DiPasquale, A. G.; Fox, A. R.; Rheingold, A. L.; Figueroa, J. S. *Inorg. Chem.* **2008**, *47*, 9010–9020.

(17) Twamley, B.; Haubrich, S. T.; Power, P. P. *Adv. Organomet. Chem.* **1999**, *44*, 1–65.

(18) Clyburne, J. A. C.; McMullen, N. *Coord. Chem. Rev.* **2000**, *210*, 73–99.

(19) Wehmschulte, R. J.; Grigsby, W. J.; Schiemenz, B.; Bartlett, R. A.; Power, P. P. *Inorg. Chem.* **1996**, *35*, 6694–6702.

(20) Su, J.; Li, X. W.; Crittendon, C.; Robinson, G. H. *J. Am. Chem. Soc.* **1997**, *119*, 5471–5472.

(21) Phillips, A. D.; Wright, R. J.; Olmstead, M. M.; Power, P. P. *J. Am. Chem. Soc.* **2002**, *124*, 5930–5931.

(22) Li, X. W.; Pennington, W. T.; Robinson, G. H. *J. Am. Chem. Soc.* **1995**, *117*, 7578–7579.

(23) Robinson, G. H. *Chem. Commun.* **2000**, 2175–2181.

(24) Robinson, G. H. *Acc. Chem. Res.* **1999**, *32*, 773–782.

(25) Rivard, E.; Power, P. P. *Inorg. Chem.* **2007**, *46*, 10047–10064.

(26) Power, P. P. *Organometallics* **2007**, *26*, 4362–4372.

(27) Power, P. P. *Chem. Commun.* **2003**, 2091–2101.

(28) Power, P. P. *Chem. Rev.* **1999**, *99*, 3463–3504.

(29) Waterman, R.; Hillhouse, G. L. *Organometallics* **2003**, *22*, 5182–5184.

(30) Shah, S.; Simpson, M. C.; Smith, R. C.; Protasiewicz, J. D. *J. Am. Chem. Soc.* **2001**, *123*, 6925–6926.

(31) Klein, D. P.; Young, V. G.; Tolman, W. B.; Que, L. *Inorg. Chem.* **2006**, *45*, 8006–8008.

(32) Gavenonis, J.; Tilley, T. D. *Organometallics* **2004**, *23*, 31–43.

(33) Gavenonis, J.; Tilley, T. D. *Organometallics* **2002**, *21*, 5549–5563.

(34) Filippou, A. C.; Weidemann, N.; Philippopoulos, A. I.; Schnakenburg, G. *Angew. Chem., Int. Ed. Engl.* **2006**, *45*, 5987–5991.

(35) Carson, E. C.; Lippard, S. J. *Inorg. Chem.* **2006**, *45*, 828–836.

(36) Wolf, R.; Ni, C.; Nguyen, T.; Brynda, M.; Long, G. J.; Sutton, A. D.; Fischer, R. C.; Fettinger, J. C.; Hellman, M.; Pu, L.; Power, P. P. *Inorg. Chem.* **2007**, *46*, 11277–11290.

(37) Wolf, R.; Brynda, M.; Ni, C.; Long, G. J.; Power, P. P. *J. Am. Chem. Soc.* **2007**, *129*, 6076–6077.

(38) Nguyen, T.; Sutton, A. D.; Brynda, M.; Fettinger, J. C.; Long, G. J.; Power, P. P. *Science* **2005**, *310*, 844–847.

(39) Smith, R. C.; Shah, S.; Urnezius, E.; Protasiewicz, J. D. *J. Am. Chem. Soc.* **2002**, *125*, 40–41.

(40) Schiemenz, B.; Power, P. P. *Angew. Chem., Int. Ed. Engl.* **1996**, *35*, 2150–2152.

(41) Li, J.; Song, H.; Cui, C.; Cheng, J.–P. *Inorg. Chem.* **2008**, *47*, 3468–3470.

(42) Krimen, L. I. *Org. Synth.* **1970**, *50*, 1–3.

(43) Huffman, C. W. *J. Org. Chem.* **1958**, *23*, 727–729.

(44) Shih, K.–C.; Angelici, R. J. *Langmuir* **1995**, *11*, 2539–2546.

(45) Robertson, M. J.; Angelici, R. J. *Langmuir* **1994**, *10*, 1488–1492.

(46) Henderson, J. I.; Feng, S.; Bein, T.; Kubiak, C. P. *Langmuir* **2000**, *16*, 6183–6187.

(47) Tolman, C. A. *Chem. Rev.* **1977**, *77*, 313–348.

(48) Restivo, R. J.; Costin, A.; Ferguson, G.; Carty, A. J. *Can. J. Chem.* **1975**, *53*, 1949–1957.

(49) Lobbia, G. G.; Pellei, M.; Pettinari, C.; Santini, C.; Somers, N.; White, A. H. *Inorg. Chim. Acta* **2002**, *333*, 100–108.

(50) Green, J.; Sinn, E.; Woodward, S.; Butcher, R. *Polyhedron* **1993**, *12*, 991–1001.

(51) Darensbourg, D. J.; Holtcamp, M. W.; Longridge, E. M.; Khandelwal, B.; Klausmeyer, K. K.; Reibenspies, J. H. *J. Am. Chem. Soc.* **1995**, *117*, 318–328.

(52) Ainscough, E. W.; Brodie, A. M.; Burrell, A. K.; Freeman, G. H.; Jameson, G. B.; Bowmaker, G. A.; Hanna, J. V.; Healy, P. C. *J. Chem. Soc., Dalton Trans.* **2001**, 144–151.

(53) Lyapkalo, I. M.; Ioffe, S. L.; Strelenko, Y. A.; Tartakovsky, V. A. *Russ. Chem. Bull.* **1996**, *45*, 2245–2247.

(54) Cotton, F. A.; Zingales, F. *J. Am. Chem. Soc.* **1961**, *83*, 351–355.

(55) Treichel, P. M.; Shaw, D. B. *Inorg. Chim. Acta* **1976**, *16*, 199–202.

(56) Minelli, M.; Maley, W. J. *Inorg. Chem.* **1989**, *28*, 2954–2958.

(57) Lyons, L. J.; Pitz, S. L.; Boyd, D. C. *Inorg. Chem.* **1995**, *34*, 316–322.

(58) Li, H.; Butler, I. S.; Uhm, H. L. *J. Raman Spectrosc.* **1992**, *23*, 457–464.

(59) Li, H.; Butler, I. S. *Appl. Spectrosc.* **1993**, *47*, 218–221.

(60) Hershberger, J. W.; Klingler, R. J.; Kochi, J. K. *J. Am. Chem. Soc.* **1982**, *104*, 3034–3043.

(61) Connor, J. A.; Jones, E. M.; McEwen, G. K.; Lloyd, M. K.; McCleverty, J. A. *J. Chem. Soc., Dalton Trans.* **1972**, 1246–1253.

(62) Albers, M. O.; Coville, N. J.; Ashworth, T. V.; Singleton, E.; Swanepoel, H. E. *J. Organomet. Chem.* **1980**, *199*, 55–62.

(63) Imhof, W.; Halbauer, K.; Dönnecke, D.; Görls, H. *Acta Crystallographica Section E* **2006**, *62*, m462–m464.

(64) Filippou, A. C.; Grünleitner, W. *J. Organomet. Chem.* **1990**, *398*, 99–115.

(65) Hahn, F. E.; Tamm, M. *Organometallics* **1994**, *13*, 3002–3008.

(66) Hahn, F. E.; Tamm, M. *Organometallics* **1992**, *11*, 84–90.

(67) Hahn, E. E.; Tamm, M. *Angew. Chem., Int. Ed. Engl.* **1991**, *30*, 203–205.

(68) King, R. B.; Saran, M. S. *Inorg. Chem.* **1974**, *13*, 74–78.

(69) Howell, J. A. S.; Yates, P. C.; Ashford, N. F.; Dixon, D. T.; Warren, R. *J. Chem. Soc., Dalton Trans.* **1996**, 3959–3966.

(70) Burdett, J. K. *Inorg. Chem.* **1975**, *14*, 375–382.

(71) Mingos, D. M. P. *J. Organomet. Chem.* **1979**, *179*, C29–C33.

(72) Lentz, D. *J. Organomet. Chem.* **1990**, *381*, 205–212.

(73) Lentz, D.; Anibarro, M.; Preugschat, D.; Bertrand, G. *J. Fluorine Chem.* **1998**, *89*, 73–81.

(74) Lentz, D. *Angew. Chem., Int. Ed. Engl.* **1994**, *33*, 1315–1331.

(75) Timney, J. A. In *Encyclopedia of Inorganic Chemistry*; John Wiley & Sons, Ltd: 2006.

(76) Drummond , H. M.; Henzi, R. *J. Organomet. Chem.* **1966**, *5*, 166–175.

(77) Treichel, P. M.; Firsich, D. W.; Essenmacher, G. P. *Inorg. Chem.* **1979**, *18*, 2405–2409.

(78) King, R. B.; Borodinsky, L. *Tetrahedron* **1985**, *41*, 3235–3240.

(79) Yang, L.; Cheung, K.–K.; Mayr, A. *J. Organomet. Chem.* **1999**, *585*, 26–34.

(80) Coville, N. J.; Albers, M. O. *Inorg. Chim. Acta* **1982**, *65*, L7–L8.

(81) Lentz, D.; Pötter, B.; Marschall, R.; Brügam, I.; Fuchs, J. *Chem. Ber.* **1990**, *123*, 257–260.

(82) Tang, Y.; Sun, J.; Chen, J. *Organometallics* **1999**, *18*, 2459–2465.

(83) Duclos, S.; Conan, F.; Triki, S.; Le Mest, Y.; Liu Gonzalez, M.; Sala Pala, J. *Polyhedron* **1999**, *18*, 1935–1939.

(84) Trylus, K.–H.; Kernbach, U.; Brüdgam, I.; Fehlhammer, W. P. *Inorg. Chim. Acta* **1999**, *291*, 266–278.

(85) Jefford, V. J.; Schriver, M. J.; Zaworotko, M. J. *Can. J. Chem.* **1996**, *74*, 107–113.

(86) Darensbourg, D. J.; Atnip, E. V.; Reibenspies, J. H. *Inorg. Chem.* **1992**, *31*, 4475–4480.

(87) Denise, B.; Massoud, A.; Parlier, A.; Rudler, H.; Daran, J. C.; Vaissermann, J.; Alvarez, C.; Patino, R.; Toscano, R. A. *J. Organomet. Chem.* **1990**, *386*, 51–62.

(88) Bachman, R. E.; Whitmire, K. H. *Inorg. Chem.* **1995**, *34*, 1542–1551.

(89) Dickson, C.–A.; McFarlane, A. W.; Coville, N. J. *Inorg. Chim. Acta* **1989**, *158*, 205–209.

(90) Wieland, S.; Van Eldik, R. *Organometallics* **1991**, *10*, 3110–3114.

(91) Schubert, U.; Friedrich, P.; Orama, O. *J. Organomet. Chem.* **1978**, *144*, 175–179.

(92) Burla, M. C.; Caliandro, R.; Camalli, M.; Carrozzini, B.; Cascarano, G. L.; De Caro, L.; Giacovazzo, C.; Polidori, G.; Spagna, R. *J. Appl. Crystallogr.* **2005**, *38*, 381–388.

(93) Pangborn, A. B.; Giardello, M. A.; Grubbs, R. H.; Rosen, R. K.; Timmers, F. J. *Organometallics* **1996**, *15*, 1518–1520.

(94) Arnarego, W. L. F.; Chai, C. L. L. *Purification of Laboratory Chemicals*; 5th ed.; Elsevier, 2003.

(95) McElwee–White, L.; Dougherty, D. A. *J. Am. Chem. Soc.* **1984**, *106*, 3466–3474.

(96) Salomon, R. G.; Kochi, J. K. *J. Am. Chem. Soc.* **1973**, *95*, 3300–3310.

(97) Sheldrick, G. M. *Acta. Crystallogr.* **2008**, *64*, 112–122.

(98) Allen, F. *Acta Crystallographica Section B* **2002**, *58*, 380–388.

Chapter 3

Oxidative Decarbonylation of *m*–Terphenyl Isocyanide Complexes of Molybdenum and Tungsten

3.1 Introduction

The unsaturated group 6 metal carbonyls, as exemplified by [$Mo(CO)_4$], [$Mo(CO)_{3,}$], and [$Mo(CO)_2$],[1–11] serve as the conceptual hallmark for metal–defined coordination geometry.[12–14] Paradoxically, the properties that render these species so intriguing have also prevented systematic surveys of their reactivity patterns. Thus, the high inherent reactivity of the unsaturated group 6 carbonyls, as derived from the juxtaposition of unencumbering ligands, low–coordination numbers, electron–rich metal centers, and a strongly π–acidic ligand field, has required that they be generated and observed by gas phase or matrix isolation techniques. Accordingly, definitive atomic–level detail of their structures and information regarding their reactivity toward substrates is limited.

In an effort to construct isolable analogues of the unsaturated transition–metal carbonyls, we have recently introduced the *m*–terphenyl isocyanide ligands $CNAr^{Mes2}$ and

$CNAr^{Dipp2}$ (Ar^{Mes2} = 2,6–(2,4,6–$Me_3C_6H_2$)C_6H_3; Ar^{Dipp2} = 2,6–(2,6–(*i*–Pr)$_2C_6H_3$)$_2C_6H_3$.[15,16] These ancillaries were targeted because of (i) the isolobal relationship between organoisocyanides and CO[17–20] and (ii) the established ability of the *m*–terphenyl framework[21,22] to stabilize low–coordinate transition–metal and main–group complexes.[23–41] Indeed, when studied in conjunction with zerovalent group 10 metals, $CNAr^{Mes2}$ and $CNAr^{Dipp2}$ have been shown to effectively stabilize analogues of binary carbonyls, $[Ni(CO)_3]$[42,43] and $[Pd(CO)_2]$.[44] In addition, the $CNAr^{Mes2}$ ligand has been used to provide a stable, homoleptic isocyanide analogue of $Co(CO)_4$,[45] which has been proposed as a reactive intermediate[46–48] in cobalt carbonyl–catalyzed hydroformylation.[49–51] Accordingly, we reasoned that these encumbering isocyanides could similarly provide a protective shield for group 6 species of the type $[M(CNR)_4]$, $[M(CNR)_3]$, or $[M(CNR)_2]$, without significantly affecting their preferred coordination geometries (i.e., *cis*–divacant octahedral–C_{2v}, trigonal pyramidal–C_{3v}, and bent–C_{2v}).[12–14]

Our approach toward the synthesis of these low–coordinate, group 6 species has focused on the reduction of suitable mid– to high–valent isocyanide precursor complexes. Herein we present synthetic studies leading to such iodo– and carboxylate–containing precursors supported by the isocyanides $CNAr^{Dipp2}$ and $CNAr^{Mes2}$. Furthermore, we provide evidence that chemical reduction of molybdenum–iodo species, in particular, lead to low–coordinate Mo–$CNAr^{Dipp2}$ complexes that can be trapped by arene–solvent molecules.

We initially hoped that chemical reduction of commercially available group 6 metal halides in the presence of $CNAr^{Dipp2}$ would provide a straightforward route to low–valent, low–coordinate $[M(CNAr^{Dipp2})_n]$ complexes. Such methods have been successful for the synthesis of homoleptic $M(CNR)_6$ complexes of the low–valent group 6 metals,[52,53] in addition to low–valent isocyanides of other metals such as Fe[54] and Co.[45] In our hands, however, such reduction experiments using $CNAr^{Dipp2}$ have led to intractable mixtures. We

have also found that addition of $CNAr^{Dipp2}$ to common molybdenum starting materials[55] such as $MoCl_3(THF)_3$ or $MoCl_4(NCMe)_2$ does not result in productive isocyanide binding. Presumably, the presence of chloride ligands renders these Mo centers insufficiently Lewis acidic to tightly bind the encumbering $CNAr^{Dipp2}$ isocyanide.[56,57] Accordingly, we have pursued an alternate synthetic strategy to access precursor compounds. On the basis of our previous findings that $CNAr^{Dipp2}$ readily binds to the zerovalent $[Mo(CO)_3(sol)]$ (sol = solvento) fragment,[16] we focused on an approach involving oxidative decarbonylation of preformed group 6 $M(sol)(CO)_3(CNAr^{Dipp2})_2$ complexes in a manner that preserves metal–isocyanide ligation. This approach was inspired in part from Colton's classic oxidative–decarbonylation studies of the homoleptic group 6 carbonyls with elemental halogens.[58–64]

3.2 Synthesis of $W(sol)_n(CO)_{4-n}(CNAr^{Dipp2})_2$ Complexes

Previously, we reported that treatment of 2.0 equiv of $CNAr^{Dipp2}$ with $Mo(CO)_3(NCR)_3$ (R = Me or Et) produced a mixture of the tricarbonyl and tetracarbonyl molybdenum complexes *trans*–$Mo(CO)_4(CNAr^{Dipp2})_2$ (**8**) and *trans*–$Mo(NCMe)(CO)_3(CNAr^{Dipp2})_2$ (**7**).[16] As shown in Scheme 3.1, a similar mixture of tungsten complexes is available by combination of $CNAr^{Dipp2}$ and $W(CO)_3(NCEt)_3$ in a 2:1 ratio. Extended photolysis of this mixture in 1:1 Et_2O/MeCN solution with a low–pressure Hg lamp (254 nm) provides *trans*–$W(NCMe)(CO)_3(CNAr^{Dipp2})_2$ (**11**) as the exclusive product. Correspondingly, addition of an excess of CO to the mixture is sufficient to fully generate *trans*–$W(CO)_4(CNAr^{Dipp2})_2$ (**12**). As expected, single–crystal X–ray diffraction revealed that both *trans*–$W(NCMe)(CO)_3(CNAr^{Dipp2})_2$ (**11**) and *trans*–$W(CO)_4(CNAr^{Dipp2})_2$ (**12**) are isostructural with their Mo counterparts (Figures 3.1 and 3.2). In addition, the IR spectra of *trans*–$W(NCMe)(CO)_3(CNAr^{Dipp2})_2$ (**11**) and *trans*–$W(CO)_4(CNAr^{Dipp2})_2$ (**12**) are identical in pattern to their Mo congeners and feature the expected slight shift of the ν_{CO} bands to lower

energy (Table 3.1).[65–67] This shift is consistent with the increased π–basicity of W relative to Mo. Despite the presence of a labile NCMe ligand, *trans*–W(NCMe)(CO)$_3$(CNAr^{Dipp2})$_2$ (**11**), like its MO counterpart, resist ligation of another equivalent of CNAr^{Dipp2} and does not engage in isocyanide exchange as assayed by ^{1}H NMR and IR spectroscopy (C_6D_6, 20 °C).

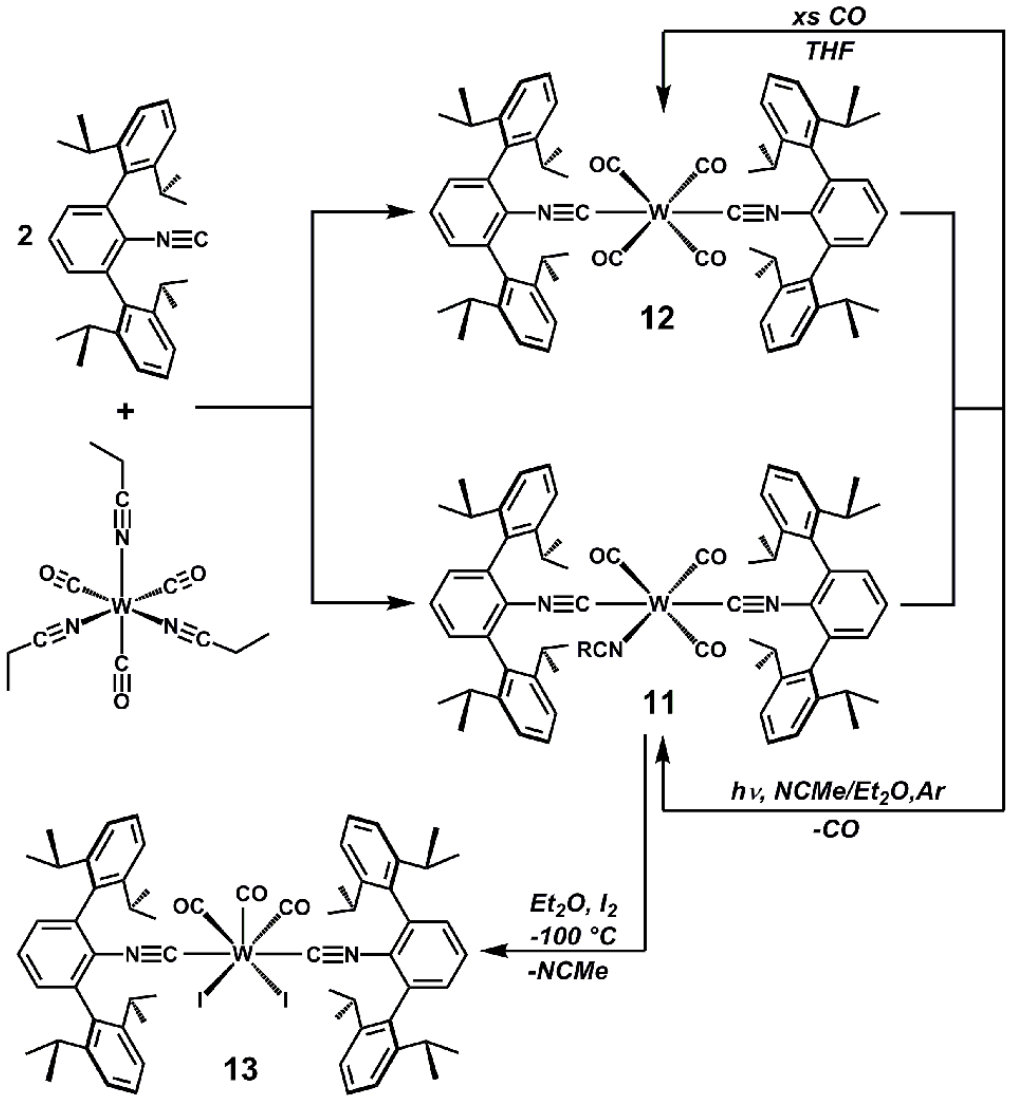

Scheme 3.1. Synthesis of *trans*–W(NCMe)(CO)$_3$(CNAr^{Dipp2})$_2$ (**11**), *trans*–W(CO)$_4$(CNAr^{Dipp2})$_2$ (**12**), and WI$_2$(CO)$_3$(CNAr^{Dipp2})$_2$ (**13**).

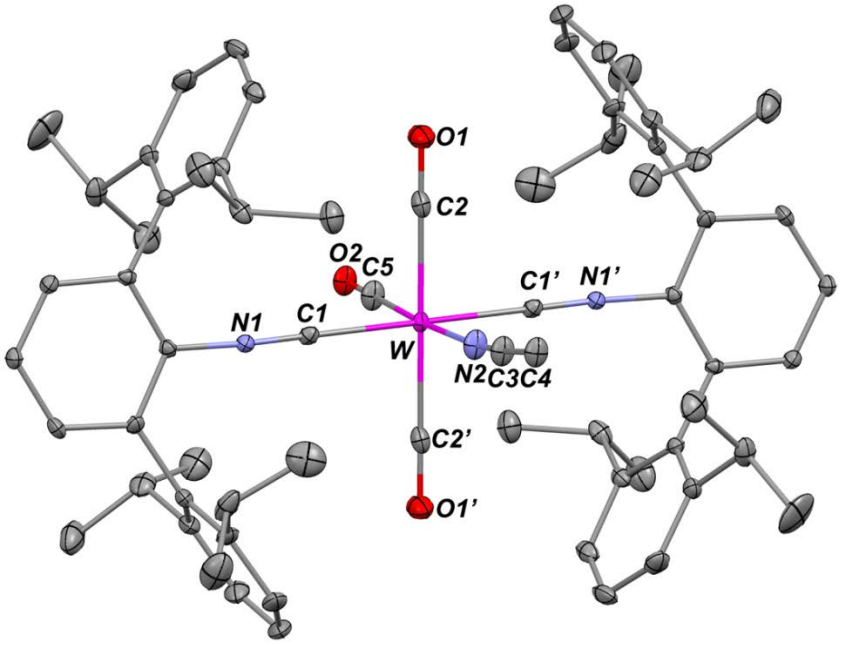

Figure 3.1. Molecular structure of *trans*–W(NCMe)(CO)$_3$(CNAr^{Dipp2})$_2$ (**11**). Selected bond distances (Å) and angles (deg): W1–C1 = 2.067(4); W1–C2 = 2.029(6); W1–N2 = 2.262(10); C1–W1–C1′ = 180.0(3); C2–W1–C2′ = 179.998(1); C5–W1–N2 = 176.5(13); C1–W1–C5 = 90.9(7); C1–W1–N2 = 91.5(4); C1–W1–C2 = 90.5(2).

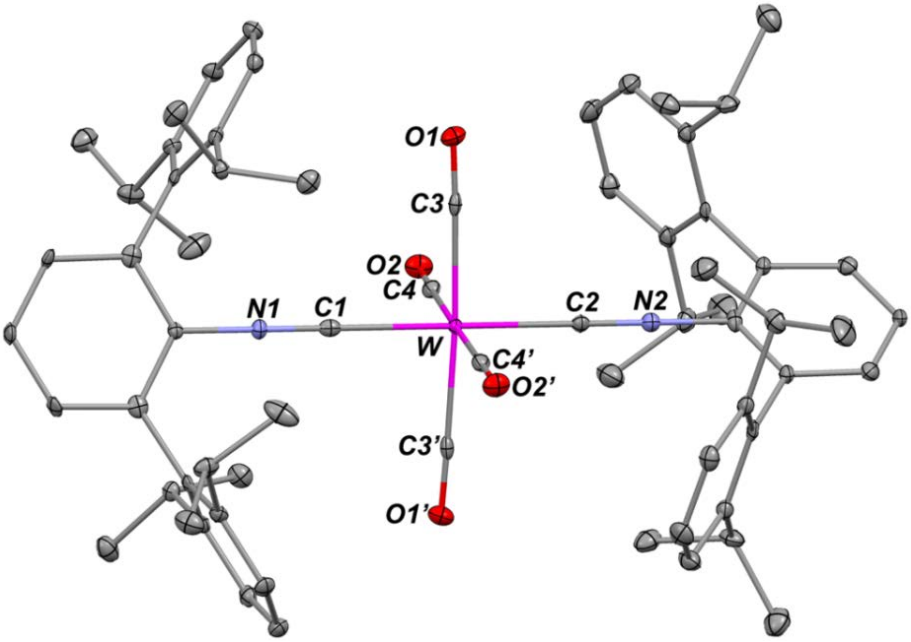

Figure 3.2. Molecular structure of *trans*–W(CO)$_4$(CNAr^{Dipp2})$_2$ (**12**). Selected bond distances (Å) and angles (deg): W1–C1 = 2.081(10); W1–C2 = 2.084(9); W1–C3 = 2.049(7); W1–C4 = 2.041(7); C1–W1–C2 = 180.000(2); C1–W1–C3 = 91.82(17); C1–W1–C4 = 90.43(18); C2–W1–C3 = 91.82(17); C2–W1–C4 = 89.57(18); C3–W1–C4 = 93.1(2).

3.3 Chemical Oxidation of $M(NCMe)(CO)_3(CNAr^{Dipp2})_2$ Complexes with I_2

To promote isocyanide retention in higher valent complexes, we targeted group 6 metal centers featuring multiple iodide ligands. This choice stemmed from the successful isolation of stable *m*–terphenyl–isocyanide–ligated Cu and Co iodo complexes in a range of formal oxidation states.[15,68] Notably, direct treatment of $CNAr^{Dipp2}$ with the trivalent molybdenum complex, $MoI_3(THF)_3$,[69] resulted in an array of products and insoluble materials. We believe that aggregation and disproportionation processes of incipiently formed $[MoI_3(CNAr^{Dipp2})(sol)_n]$ complexes may kinetically compete with the binding of a second isocyanide, ultimately leading to undesired products.[70] We reasoned that preligation of two $CNAr^{Dipp2}$ units to the metal center may succeed in controlling reaction outcomes by (i) sterically inhibiting multinuclear aggregation and (ii) disfavoring electron transfer reactions by furnishing strong π–back–bonding interactions. Importantly, a cursory survey showed that the tetracarbonyl complexes *trans*–$M(CO)_4(CNAr^{Dipp2})_2$ (M = Mo, W) did not react with elemental iodine under ambient conditions (THF, 20°C). We therefore focused on the reactivity of the acetonitrile adducts *trans*–$M(NCMe)(CO)_3(CNAr^{Dipp2})_2$ (M = Mo, W) toward I_2, in anticipation that dissociation of the labile NCMe ligand would promote inner–sphere oxidation events.

Importantly, this isocyanide retention strategy was successful, but the extent of decarbonylation between the Mo and W congeners differed. Accordingly, treatment of the tungsten derivative *trans*–$W(NCMe)(CO)_3(CNAr^{Dipp2})_2$ (**11**) with 1.0 equiv of I_2 in Et_2O readily afforded the seven coordinate complex, $WI_2(CO)_3(CNAr^{Dipp2})_2$ (**13**), as determined by X–ray diffraction (Scheme 3.1, Figure 3.3). The solid–state geometry of $WI_2(CO)_3(CNAr^{Dipp2})_2$ (**13**) is readily described as capped–octahedral[71] and is similar to other

structurally characterized $MX_2(CO)n(L)m$ ($m = 5 - n$) group 6 complexes.[72] In the solid state, $WI_2(CO)_3(CNAr^{Dipp2})_2$ (**13**) possesses mirror symmetry and two inequivalent CO sites. However, its $^{13}C\{H\}$ NMR spectrum in C_6D_6 at 20 °C shows only one carbonyl resonance, thus indicating that the encumbering $CNAr^{Dipp2}$ ligands do not impede CO–ligand site exchange in solution at this temperature.

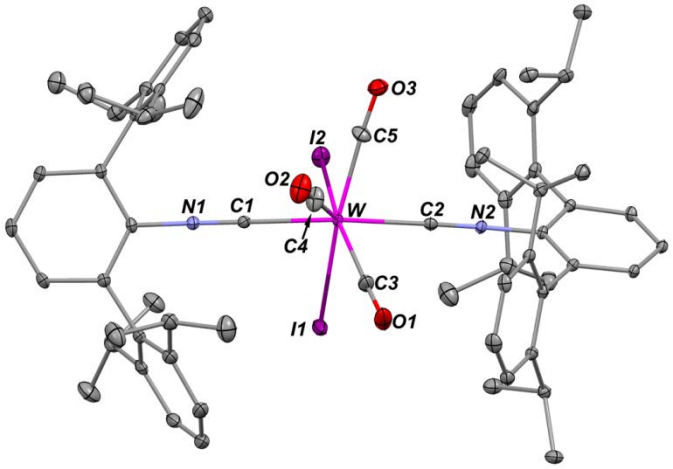

Figure 3.3. Molecular structure of $WI_2(CO)_3(CNAr^{Dipp2})_2$ (**13**). Selected bond distances (Å) and angles (deg): W1–C1 = 2.113(6); W1–C2 = 2.134(6); W1–C3 = 2.032(7); W1–C4 = 1.980(7); W1–C5 = 2.039(6); W1–I1 = 2.8401(5); W1–I2 = 2.8174(5); C1–W1–C2 = 168.7(2); I1–W1–C5 = 159.5(2); I2–W1–C3 = 159.3(2); C1–W1–I1 = 80.20(15); C1–W1–I2 = 82.08(15); C1–W1–C3 = 108.2(2); C1–W1–C4 = 76.2(3); C1–W1–C5 = 107.2(3); C2–W1–I1 = 90.97(15); C2–W1–I2 = 90.79(15); C2–W1–C3 = 76.0(3); C2–W1–C4 = 115.1(3); C2–W1–C5 = 78.9(3); C2–W1–I1 = 90.97(15); C2–W1–I2 = 90.79(15); I1–W1–I2 = 89.452(18); I1–W1–C3 =; C3–W1–C4 = 75.1(2); C4–W1–C5 = 71.7(3); C5–W1–I2 = 73.1(2).

In contrast to its W counterpart, treatment of *trans*–$Mo(NCMe)(CO)_3(CNAr^{Dipp2})_2$ (**8**) with 1.0 equiv of I_2 in Et_2O solution leads to CO loss and formation of the paramagnetic dicarbonyl complex, $MoI_2(CO)_2(CNAr^{Dipp2})_2$ (**14**, Scheme 3.2). Evans method magnetic moment determination (C_6D_6/$(Me_3Si)_2O$, 20 °C) resulted in a μ_{eff} value of 2.71(3) μ_B, consistent with a S = 1 ground state in solution for the d^4 Mo center in $MoI_2(CO)_2(CNAr^{Dipp2})_2$ (**14**). Importantly, the ^1H NMR spectrum of $MoI_2(CO)_2(CNAr^{Dipp2})_2$ (**14**) in C_6D_6 solution at 20 °C indicates the presence of a single species with resonance

ranging from +16.18 to –6.33 ppm (Figure 3.4). This species is persistent at room temperature for at least 24 h as assayed by ^{1}H NMR spectroscopy, and no additional resonances appear in the spectra recorded over this time. However, while structural determination on red crystals grown from toluene at –35 °C revealed a six–coordinate complex with *trans*–disposed isocyanides, refinement indicated a 50/50 mixture of the *cis*– and *trans*–carbonyl orientations in the solid state (Figure 3.5). In C_6D_6 solution and before crystallization from toluene, $MoI_2(CO)_2(CNAr^{Dipp2})_2$ (**14**) features a single ν_{CN} band (2109 cm^{-1}) and two strong, closely separated, ν_{CO} bands(2004 and 1994 cm^{-1}) in its IR spectrum (Table 3.1, Figure 3.6). We attribute the close separation of the ν_{CO} bands to splitting of a single band from coupling with other vibronic modes and therefore assign this species as the *trans*–dicarbonyl isomer of $MoI_2(CO)_2(CNAr^{Dipp2})_2$ (**14**). A solid–state IR spectrum (KBr) on the toluene–grown crystals, however, features an additional set of well–separated ν_{CO} bands of unequal intensity (1982 and 1940 cm^{-1}), which we believe indicates the presence of the *cis*–carbonyl complex in the solid state (Table 3.1, Figure 3.7). Dissolution of these crystals is C_6D_6 followed by analysis with both ^{1}H NMR and IR spectroscopy within 20 min revealed near–complete regeneration of the spectroscopic signatures for the *trans*–dicarbonyl configuration in solution at room temperature (Figure 3.8).

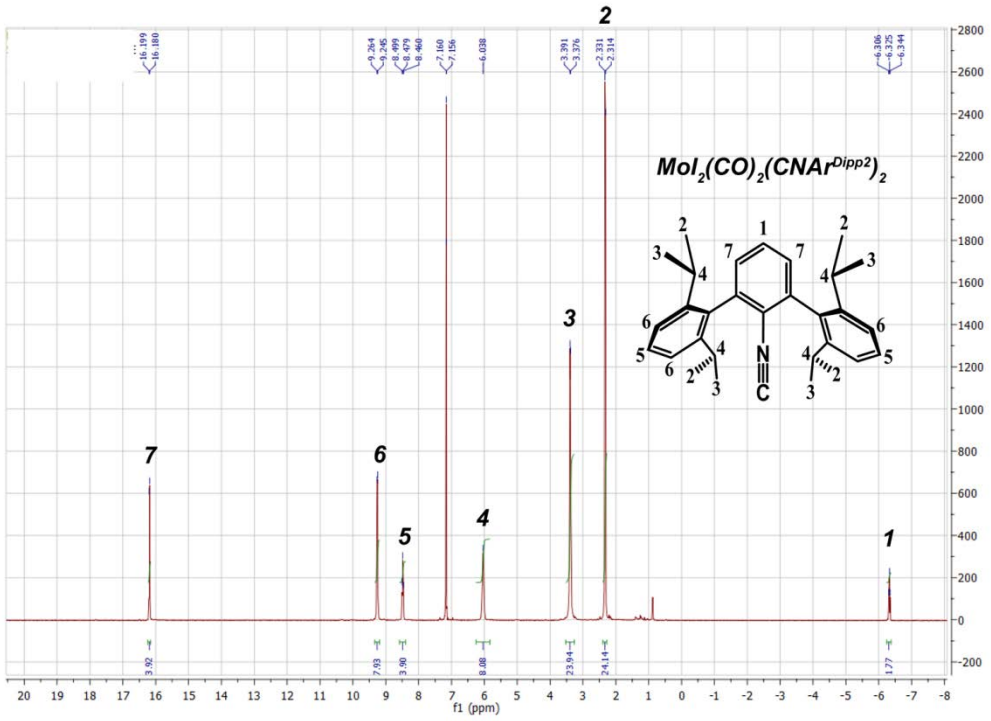

Figure 3.4. ^{1}H NMR spectrum (400 MHz, 20 °C) of freshly prepared $MoI_2(CO)_2(CNAr^{Dipp2})_2$ (**14**).

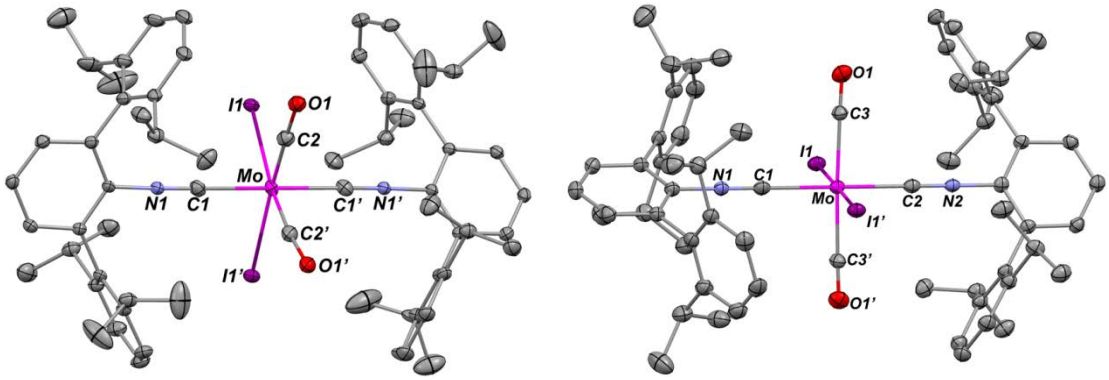

Figure 3.5. Disorder models for the molecular structure of $MoI_2(CO)_2(CNAr^{Dipp2})_2$ (**14**). Top: disorder model for *trans*,*trans*,*trans*–$MoI_2(CO)_2(CNAr^{Dipp2})_2$. Bottom: disorder model for *cis*,*cis*,*trans*– $MoI_2(CO)_2(CNAr^{Dipp2})_2$. Both isomers are present in crystals of $MoI_2(CO)_2(CNAr^{Dipp2})_2$ (**14**) grown from toluene at −35 °C.

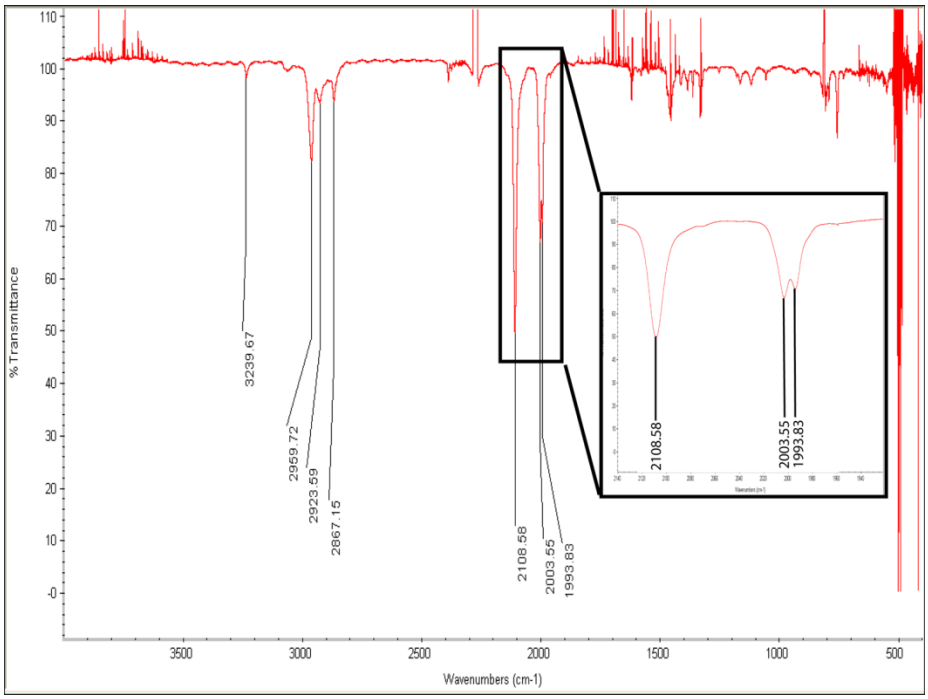

Figure 3.6. Solution FTIR spectrum (C_6D_6) of freshly prepared $MoI_2(CO)_2(CNAr^{Dipp2})_2$ (**14**). The presence of the *trans*–isomer is indicated from the ν_{CN} stretches (the splitting of this peak is due to vibronic coupling with other modes).

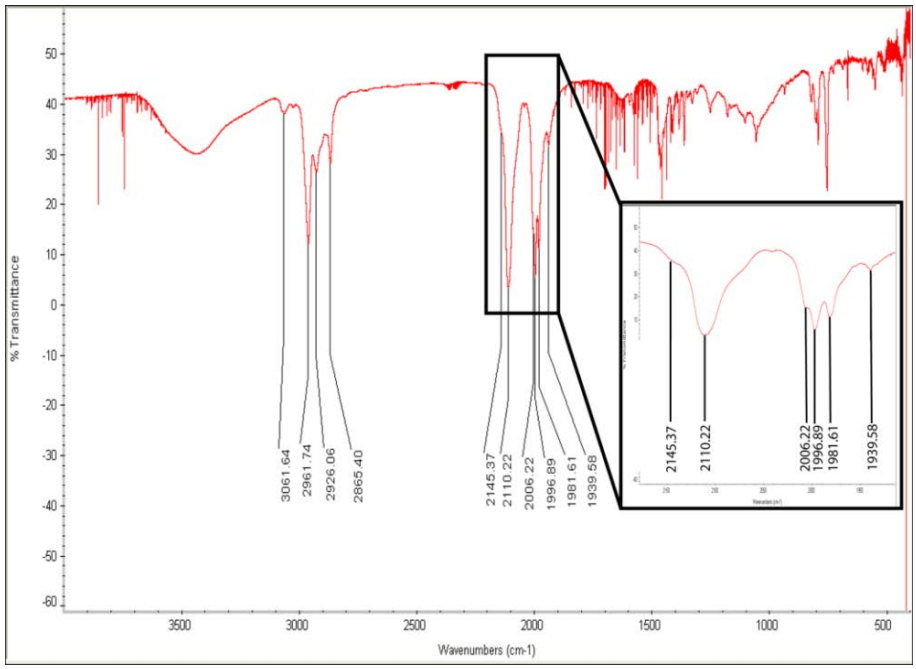

Figure 3.7. Solid–state FTIR spectrum (KBr) of $MoI_2(CO)_2(CNAr^{Dipp2})_2$ (**14**) crystals grown from toluene at –35 °C. Both *cis*–dicarbonyl and *trans*–dicarbonyl isomers are indicated from the ν_{CO} stretches.

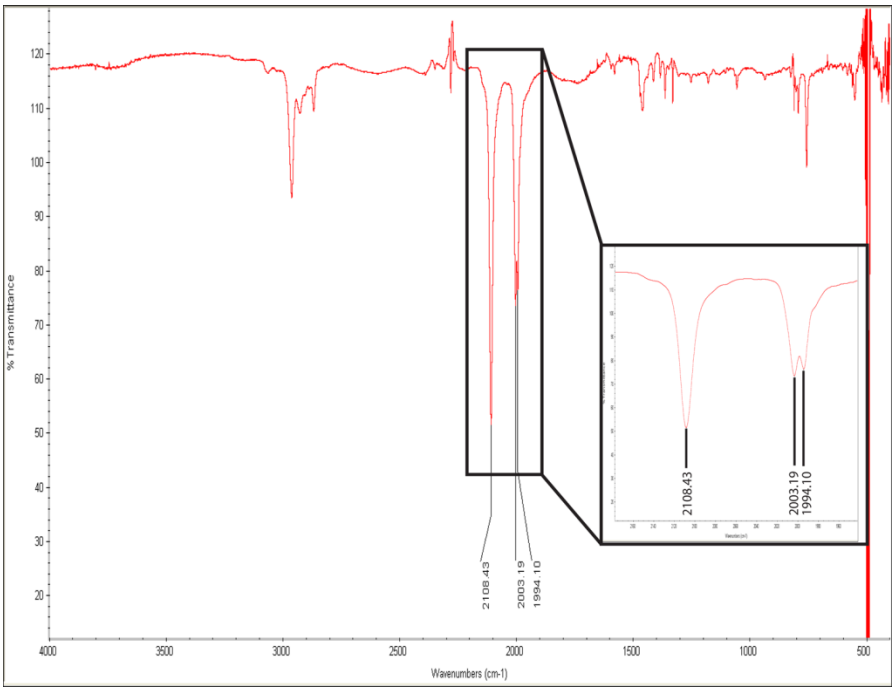

Figure 3.8. Solution FTIR spectrum (C_6D_6) of $MoI_2(CO)_2(CNAr^{Dipp2})_2$ (**14**) crystals grou from toluene at –35 °C taken 20 min after dissolution. Near–complete regeneration of the *trans*–dicarbonyl isomer is indicated from the ν_{CO} stretches.

Most interestingly, the room–temperature dominant isomer of $MoI_2(CO)_2(CNAr^{Dipp2})_2$ (**14**) represents a very rare paramagnetic group 6 complex with the general formula $MX_2(CO)_2L_2$ (*cis*– or *trans*–$(CO)_2$).[61,73,74] Indeed, the stability of $16e^-$, d^4 $MX_2(CO)_2L_2$ complexes (M = Mo, W) is well–known to arise from a pronounced $O_h \rightarrow C_{2v}$ electronic distortion that promotes a large HOMO–LUMO gap and, consequently, spin–pairing.[75,76] However, it has been proposed that strong π–acceptor L ligands, *trans*–oriented as found in *trans*–$MoI_2(CO)_2(CNAr^{Dipp2})_2$, can stabilize an octahedral S = 1 $MX_2(CO)_2L_2$ complex.[75,76] In this context $MoI_2(CO)_2(CNAr^{Dipp2})_2$ is notable, as the complexes $[MX_2(CO)_4]$ (M = Mo, W; X = Cl, Br, I), which are the prototypical $MX_2(CO)_2L_2$ examples containing only π–acidic ligands, have been well established as bridging–halide dimers featuring seven–coordinate, diamagnetic metal centers.[58,63,77–79] As shown in Figure 3.5, the isomers of $MoI_2(CO)_2(CNAr^{Dipp2})_2$ (**14**) possess fairly regular octahedral coordination geometries, with

C–Mo–C angles of 178(3)° and 180.0(3)° between the two *trans*–$CNAr^{Dipp2}$ ligands in the crystallographically independent molecules.

As expected for its electronically unsaturated nature, $MoI_2(CO)_2(CNAr^{Dipp2})_2$ (**14**) can bind additional Lewis basic ligands. Thus, dissolution in THF, followed by crystallization, provides the seven–coordinate, pentagonal bipyramidal complex $MoI_2(THF)(CO)_2(CNAr^{Dipp2})_2$ (**15**) as determined by X–Ray diffraction (Scheme 3.2, Figure 3.9). The THF ligand in $MoI_2(THF)(CO)_2(CNAr^{Dipp2})_2$ (**15**) is labile, and readily dissociates when the complex is dissolved in C_6D_6 solution. Furthermore, placement of $MoI_2(CO)_2(CNAr^{Dipp2})_2$ (**14**) under a CO atmosphere (1 atm) results in an equilibrium mixture between it and a diamagnetic species (Scheme 3.2). We presume that this species is the tricarbonyl complex, $MoI_2(CO)_3(CNAr^{Dipp2})_2$, on the basis of its ^1H NMR spectroscopic similarities to $WI_2(CO)_3(CNAr^{Dipp2})_2$ (**13**). However, removal of the CO atmosphere from the reaction mixture readily regenerates $MoI_2(CO)_2(CNAr^{Dipp2})_2$ (**14**). This behavior is similar to the reported for other d^4 $MoX_2(CO)_2L_2$ complexes.[63,80] Notably, the tungsten complex $WI_2(CO)_3(CNAr^{Dipp2})_2$ (**13**) shows no tendency to release CO at temperatures up to 80 °C (C_6D_6).

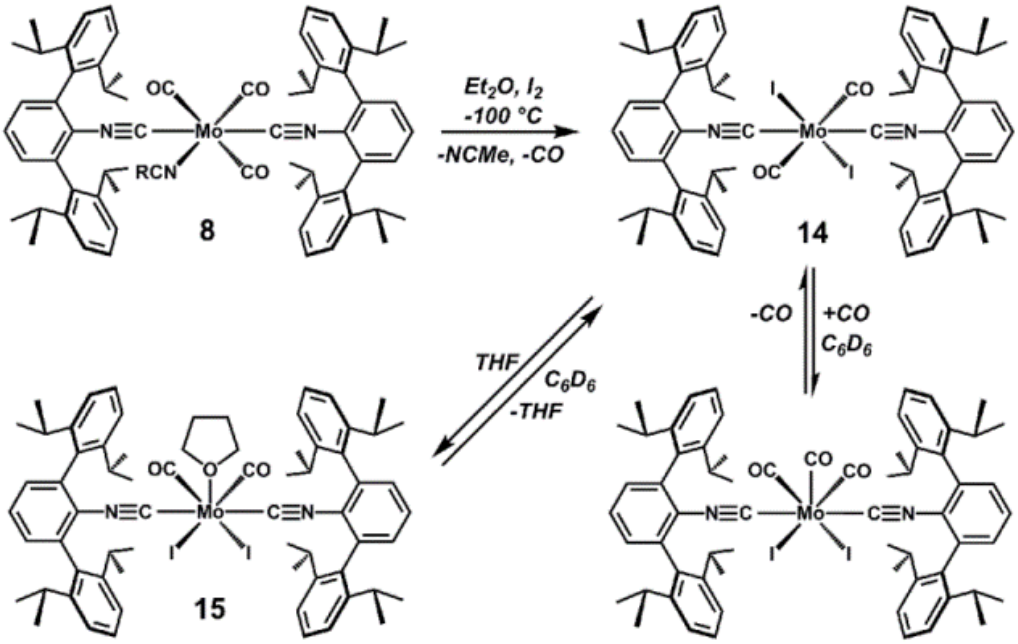

Scheme 3.2. Synthesis of *trans*–$Mo(CO)_4(CNAr^{Dipp2})_2$ (**14**) and $MoI_2(THF)(CO)_2(CNAr^{Dipp2})_2$ (**15**).

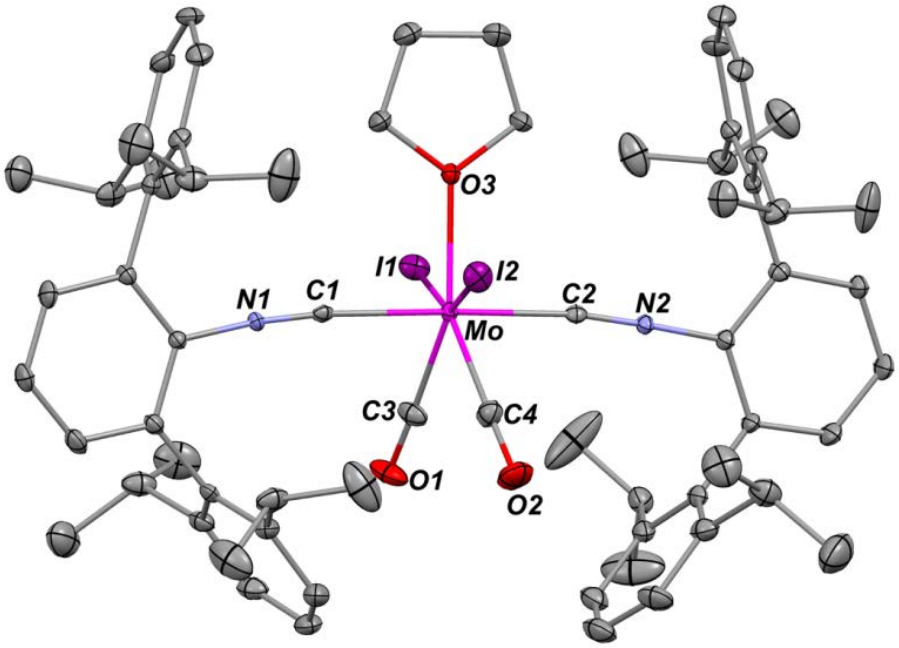

Figure 3.9. Molecular structure of $MoI_2(THF)(CO)_2(CNAr^{Dipp2})_2$ (**15**). Selected bond distances (Å) and angles (deg): Mo1–C1 = 2.121(6); Mo1–C2 = 2.114(6); Mo1–C3 = 1.977(7); Mo1–C4 = 1.960(8); Mo1–I1 = 2.8531(6); Mo1–I2 = 2.8523(6); Mo1–O3 = 2.199(4); C1–Mo1–C2 = 178.0(2); C3–Mo1–I1 = 72.0(2); C3–Mo1–C4 = 68.2(3); C4–Mo1–I2 = 70.8(2); I1–Mo1–I2 = 154.32(2); I1–Mo1–O3 = 77.34(10); I2–Mo1–O3 = 77.09(10).

Another contrast between these d^4 Mo– and W–$CNAr^{Dipp2}$ systems is that only the Mo complex is reactive toward additional I_2. Thus, treatment of $WI_2(CO)_3(CNAr^{Dipp2})_2$ (**13**) with another equivalent of I_2 results in no reaction, whereas $MoI_2(CO)_2(CNAr^{Dipp2})_2$ (**14**) reacts readily in fluorobenzene (C_6H_5F) to form the tetraiodo–complex *trans*–$MoI_4(CNAr^{Dipp2})_2$ (**16**, Scheme 3.3, Figure 3.10). As expected, *trans*–$MoI_4(CNAr^{Dipp2})_2$ (**16**) is paramagnetic and gives rise to a solution magnetic moment of μ_{eff} = 2.71(3) μ_B, consistent with an S = 1, d^2 metal center. The IR spectrum of *trans*–$MoI_4(CNAr^{Dipp2})_2$ (**16**) in C_6D_6 solution is also consistent with its formulation and exhibits ν_{CN} bands ca. 30–60 cm^{-1} higher in energy that the corresponding band in d^4 $MoI_2(CO)_2(CNAr^{Dipp2})_2$ (**14**). Thus, complete oxidative decarbonylation of *trans*–$Mo(NCMe)(CO)_3(CNAr^{Dipp2})_2$ (**8**) with isocyanide retention can be achieved for molybdenum in two synthetic steps. Unfortunately, we have found that much lower yields of *trans*–$MoI_4(CNAr^{Dipp2})_2$ (**16**) result from direct treatment of *trans*–$Mo(NCMe)(CO)_3(CNAr^{Dipp2})_2$ (**8**) with 2.0 equiv of I_2 (ca. 20%), that are obtained when $MoI_2(CO)_2(CNAr^{Dipp2})_2$ (**14**) is isolated and treated with I_2 in a subsequent step (ca. 40–45% overall). Notably, *trans*–$MoI_4(CNAr^{Dipp2})_2$ (**16**) represents, to our knowledge, the first example of a structurally characterized, neutral d^2 MoI_4L_2 complex.

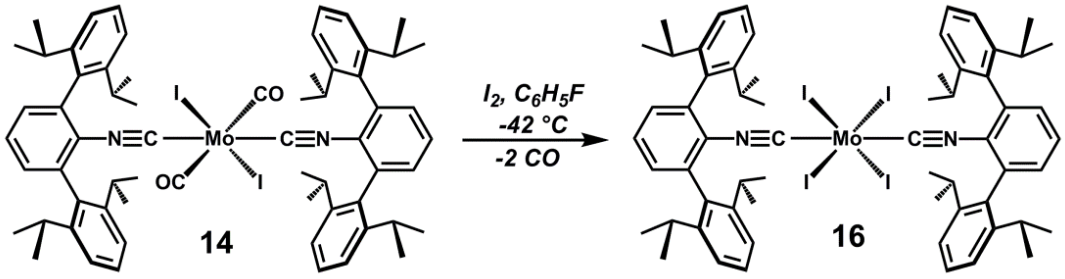

Scheme 3.3. Synthesis of *trans*–$MoI_4(CNAr^{Dipp2})_2$ (**16**).

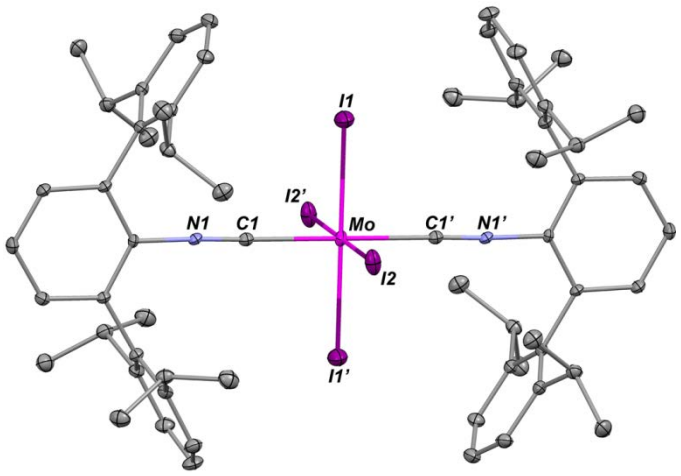

Figure 3.10. Molecular structure of *trans*–$MoI_4(CNAr^{Dipp2})_2$ (**16**). Selected bond distances (Å) and angles (deg): Mo1–C1 = 2.148(5); Mo1–I1 = 2.6508(8); Mo1–I2 = 2.7380(7); C1–Mo–I1′ = 89.26(13); C1′–Mo–I1′ = 90.74(13); I1–Mo1–I2 = 90.0.

3.4 Acyl Peroxide Oxidation and Coordinatively Induced Decarbonylation

In addition to iodine, it was of interest to survey if other chemical oxidants could similarly decarbonylate these $M(sol)(CO)_3(CNAr^{Dipp2})_2$ complexes while retaining isocyanide ligation. Particularly appealing were reagents that could deliver oxidizing equivalents while promoting additional decarbonylation events via secondary coordination. In this respect acyl peroxides were intriguing prospects. It was anticipated that the ability of acyl peroxides to affect $2e^-$ oxidations, coupled with the propensity for κ^2–coordination of the resultant carboxylate ligands could potentially induce the dissociation of several monodentate CO ligands. Furthermore, carboxylate complexes of medium– and high–valent Mo and W are known,[81–84] and could serve as useful precursors for subsequent reactions.

Addition of benzoyl peroxide to *trans*–$W(NCMe)(CO)_3(CNAr^{Dipp2})_2$ (**11**) in THF solution cleanly provided the orange, bis–benzoate dicarbonyl complex, $W(O_2CPh)_2(CO)_2(CNAr^{Dipp2})_2$ (**18**, Scheme 3.4). Crystallographic structure determination

revealed both κ^2– and κ^1–coordinated benzoate groups and an overall seven–coordinate geometry best described as a 4:3 piano stool (Figure 3.11).[85] The ^{1}H NMR spectrum of $W(O_2CPh)_2(CO)_2(CNAr^{Dipp2})_2$ (**18**) at room temperature (C_6D_6) exhibits only one benzoate environment, thus indicating interconversion of the κ^2– and κ^1–coordinated ligands. Such coordination behavior has been observed previously for group 6 dicarboxylate complexes[84,86] and, in this system, undoubtedly aids the loss of CO from the W center relative to the diiodie complex $WI_2(CO)_3(CNAr^{Dipp2})_2$ (**13**). To this end, CO loss from $WI_2(CO)_3(CNAr^{Dipp2})_2$ (**13**) can be induced by addition of external carboxylate ligands. As shown in Scheme 3.4, treatment of $WI_2(CO)_3(CNAr^{Dipp2})_2$ (**13**) with 2 equiv of silver acetate (AgOAc) results in the diacetate complex $W(O_2CMe)_2(CO)_2(CNAr^{Dipp2})_2$ (**19**). Crystallographic characterization of $W(O_2CMe)_2(CO)_2(CNAr^{Dipp2})_2$ (**19**) revealed overall structural features similar to the bis–benzoate derivative $W(O_2CPh)_2(CO)_2(CNAr^{Dipp2})_2$ (**18**) including both κ^2– and κ^1–coordinated carboxylate groups (Figure 3.12).

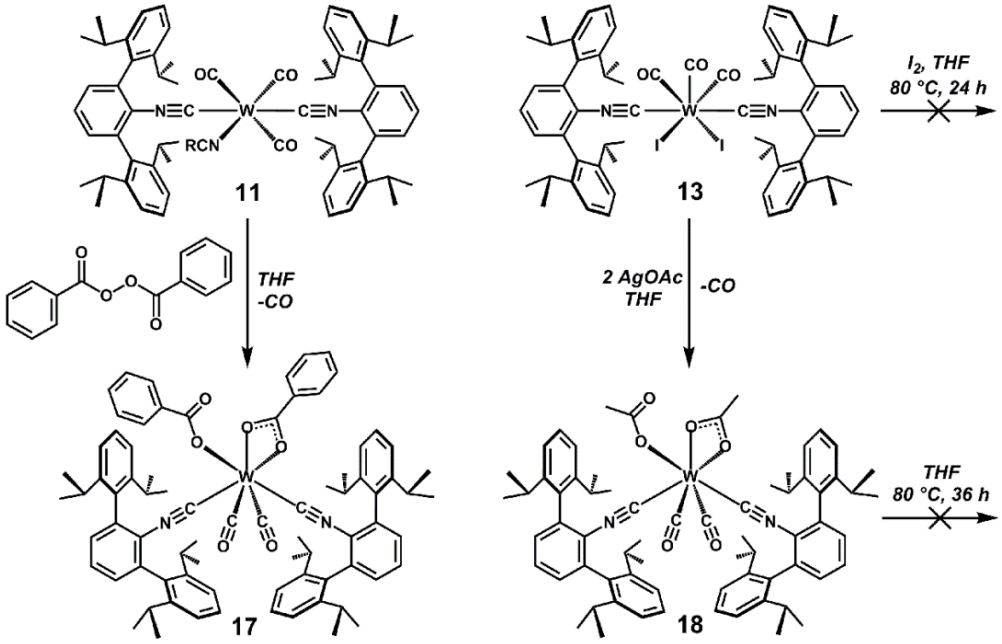

Scheme 3.4. Synthesis of $W(O_2CPh)_2(CO)_2(CNAr^{Dipp2})_2$ (**17**) and $W(O_2CMe)_2(CO)_2(CNAr^{Dipp2})_2$ (**18**).

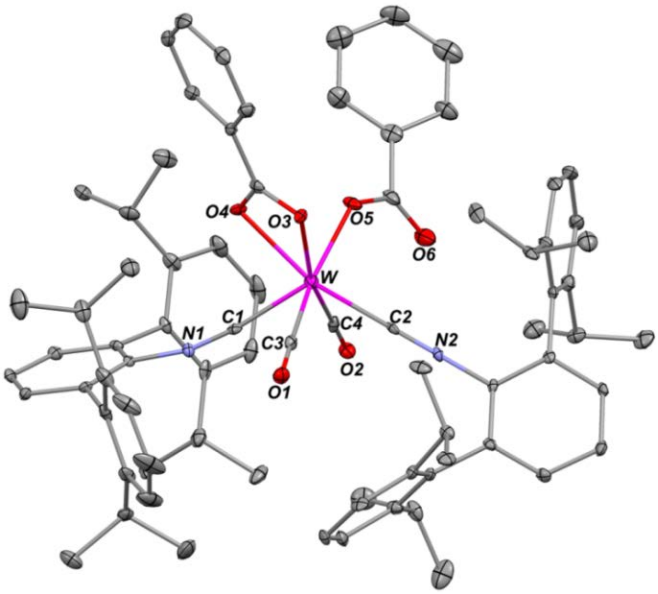

Figure 3.11. Molecular structure of $W(O_2CPh)_2(CO)_2(CNAr^{Dipp2})_2$ (**17**). Selected bond distances (Å) and angles (deg): W1–C1 = 2.038(6); W1–C2 = 2.065(6); W1–C3 = 2.018(7); W–C4 = 2.012(7); W1–O3 = 2.204(4); W1–O4 = 2.222(4); W1–O5 = 2.058(4); C1–W1–C2 = 120.1(2); C1–W1–C3 = 72.4(2); C1–W1–C4 = 73.9(2); C2–W1–C3 = 74.2(2); C2–W1–C4 = 74.2(2); C1–W1–O3 = 117.00(19); C1–W1–O4 = 76.7(2); C2–W1–O5 = 95.9(2); O3–W1–O4 = 58.90(15); O3–W1–O5 = 78.46(17); O4–W1–O5 = 74.19(17).

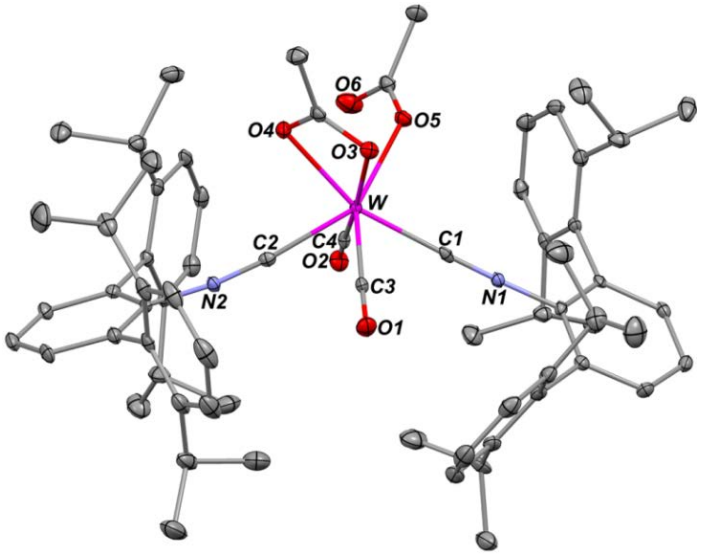

Figure 3.12. Molecular structure of $W(O_2CMe)_2(CO)_2(CNAr^{Dipp2})_2$ (**18**). Selected bond distances (Å) and angles (deg): W1–C1 = 2.077(4); W1–C2 = 2.037(4); W1–C3 = 1.999(4); W1–C4 = 2.022(4); W1–O3 = 2.213(2); W1–O4 = 2.191(3); W1–O5 = 2.083(2); C1–W1–C2 = 121.23(14); C1–W1–C3 = 75.43(14); C1–W1–C4 = 75.04(14); C2–W1–C3 = 70.98(13); C2–W1–C4 = 74.40(14); C1–W1–O3 = 108.77(12); C1–W1–O5 = 85.69(12); C2–W1–O4 = 77.90(12); O3–W1–O4 = 59.01(9); O3–W1–O5 = 75.60(10); O4–W1–O5 = 77.14(10).

The molybdenum complex *trans*–Mo(NCMe)(CO)$_3$(CNAr^{Dipp2})$_2$ (**8**) did not react cleanly with benzoyl peroxide under a variety of conditions. However, carboxylate ligands can be readily introduced by treatment of the diiodide complex MoI$_2$(CO)$_2$(CNAr^{Dipp2})$_2$ (**14**) with silver acetate (Scheme 3.5). Interestingly, ^{1}H NMR analysis of the reaction mixture after 24 h indicated complete consumption of the starting material and the presence of two new acetate–containing species. After an additional 24 h of stirring only a single product was present, which was identified as the monocarbonyl, diacetate complex Mo(κ^2–O$_2$CMe)$_2$(CO)(CNAr^{Dipp2})$_2$ (**19**) by X–ray diffraction (Figure 13.3). While not isolated, we strongly believe that the intermediate in this reaction is the dicarbonyl complex Mo(O$_2$CMe)$_2$(CO)$_2$(CNAr^{Dipp2})$_2$, as it possesses near–identical ^{1}H NMR signatures to the tungsten congener W(O$_2$CMe)$_2$(CO)$_2$(CNAr^{Dipp2})$_2$ (**18**). Notably, despite the presence of two acetate ligands, W(O$_2$CMe)$_2$(CO)$_2$(CNAr^{Dipp2})$_2$ (**18**) does not release an additional CO ligand in solution at temperatures up to 80 °C. Thus, like the Mo and W diiodide complexes discussed above, CO appears to be significantly more labile in the Mo dicarboxylate species relative to its W congener.

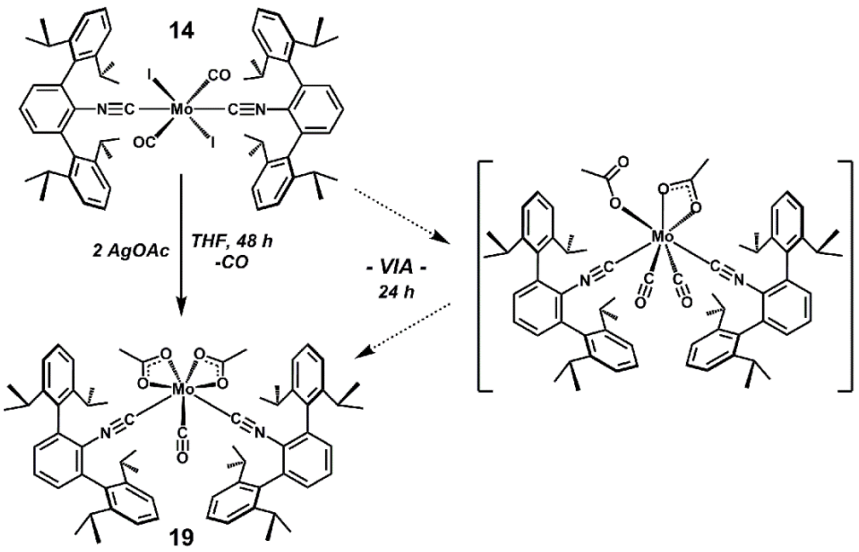

Scheme 3.5. Synthesis of Mo(κ^2–O$_2$CMe)$_2$(CO)(CNAr^{Dipp2})$_2$ (**19**).

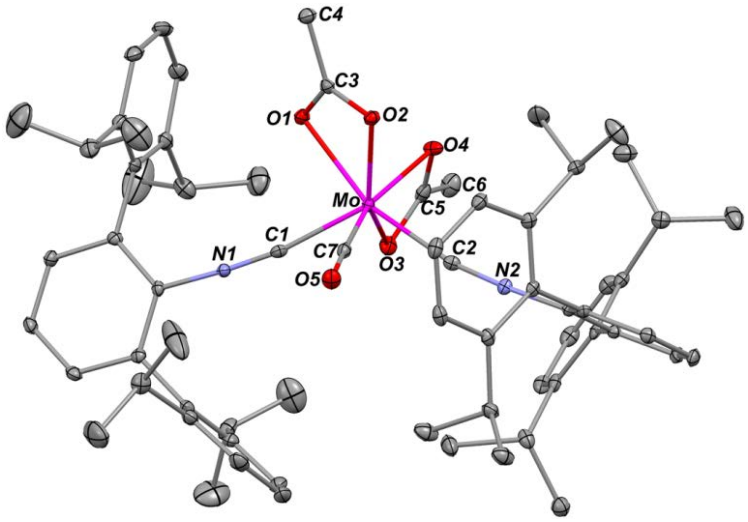

Figure 3.13. Molecular structure of Mo(κ^2–O_2CMe)$_2$(CO)(CNAr^{Dipp2})$_2$ (**19**). Selected bond distances (Å) and angles (deg): Mo1–C1 = 2.017(3); Mo1–C2 = 2.051(2); Mo1–C7 = 1.967(3); Mo1–O1 = 2.2175(16); Mo1–O2 = 2.1435(17); Mo1–O3 = 2.2085(18); Mo1–O4 = 2.2285(17); C1–Mo1–C2 = 118.69(9); C1–Mo1–C7 = 73.20(10); C1–Mo1–O3 = 81.11(8); C1–Mo1–O1 = 79.12(8); C2–Mo1–C7 = 76.58(9); C2–Mo1–O3 = 80.44(8); C2–Mo1–O2 = 107.77(8); C2–Mo1–O4 = 86.96(8); O1–Mo1–O2 = 59.77(6); O1–Mo1–O4 = 80.21(6); O2–Mo1–O4 = 88.02(7).

Monocarbonyl Mo(κ^2–O_2CMe)$_2$(CO)(CNAr^{Dipp2})$_2$ also potentially offers access to unique low–coordinate complexes upon reduction or further elaboration. In this reagard it is notable that attempts to convert Mo(κ^2–O_2CMe)$_2$(CO)(CNAr^{Dipp2})$_2$ to the five–coordinate diiodide via carboxylate esterification[87] with Me_3Si were unsuccessful. Instead, these reactions resulted in mixtures of the dicarbonyl complex $MoI_2(CO)_2$(CNAr^{Dipp2})$_2$ (**14**) along with several other unidentified products (^{1}H NMR), thereby further punctuating the liability of the Mo–CO unit in this isocyanide–supported system.

3.5 Chemical Reduction of Iodo–Molybdenum Complexes and Arene–Trapping of Low–Coordinate, Low–Valent Intermediates

Synthetic access to the di– and tetravalent iodo–molybdenum complexes $MoI_2(CO)_2(CNAr^{Dipp2})_2$ (**14**) and *trans*–$MoI_4(CNAr^{Dipp2})_2$ (**16**), allowed us to probe their utility as precursors to low–valent, low–coordinate molybdenum isocyanides. It was hoped that reduction of $MoI_2(CO)_2(CNAr^{Dipp2})_2$ (**14**) bye $2e^-$ with concomitant iodide loss would generate the four–coordinate complex $[Mo(CO)_2(CNAr^{Dipp2})_2]$. The latter represents a mixed isocyanide/carbonyl analogue of $[Mo(CO)_4]$ and should similarly adopt a C_{2v}, *cis*–divacant octahedral coordination geometry.[1–14] Correspondingly, full reduction of the tetraiodide *trans*–$MoI_4(CNAr^{Dipp2})_2$ (**16**), to the zerovalent state could potentially provide a two–coordinate molybdenum isocyanide complex sharing the bent–C_{2v} geometry of $[Mo(CO)_2]$.[1–11,13] Disappointingly, however, treatment of $MoI_2(CO)_2(CNAr^{Dipp2})_2$ (**14**) with a range of reducing agents resulted in complex and intractable mixtures. The tetracarbonyl complex *trans*–$Mo(CO)_4(CNAr^{Dipp2})_2$ (**7**) was generated in various quantities in these experiments, which we believe again reflects the lability of the Mo–CO linkage in these isocyanide systems. Accordingly, zerovalent, four–coordinate, isocyanide or mixed carbonyl/isocyanide MoL_4 complexes remain desired targets.

Despite our difficulties controlling the reduction chemistry of $MoI_2(CO)_2(CNAr^{Dipp2})_2$ (**14**), fully decarbonylated *trans*–$MoI_4(CNAr^{Dipp2})_2$ (**16**) displayed much cleaner reactivity toward chemical reductants and allowed for a more systematic survey of its reduction behavior. As shown in Scheme 3.6, treatment of *trans*–$MoI_4(CNAr^{Dipp2})_2$ (**16**) with an excess of Mg metal in THF solution afforded the triiodide complex *trans*–$MoI_3(THF)(CNAr^{Dipp2})_2$ (**20**) as determined by X–ray diffraction (Figure 3.14). Evans method magnetic moment

determination resulted in a μ_{eff} value of 3.95(1) μ_B, which is consistent with an S = 3/2 ground state for *trans*–$MoI_3(THF)(CNAr^{Dipp2})_2$ (**20**). In addition, *trans*–$MoI_3(THF)(CNAr^{Dipp2})_2$ (**20**) gives rise to a sharp ν_{CN} band at 2142 cm^{-1}, which is lower in energy that the corresponding band in the tetra–iodide *trans*–$MoI_4(CNAr^{Dipp2})_2$ (**16**) and reflects additional electron density of the Mo center (Table 3.1). Most notably, however, the isolation of *trans*–$MoI_3(THF)(CNAr^{Dipp2})_2$ (**20**) via $1e^-$ reduction of *trans*–$MoI_4(CNAr^{Dipp2})_2$ (**16**) highlights the success of isocyanide preligation as a synthetic strategy for this system, whereas direct treatment of $MoI_3(THF)_3$ with $CNAr^{Dipp2}$ failed to cleanly generate the desired bisisocyanide complex.

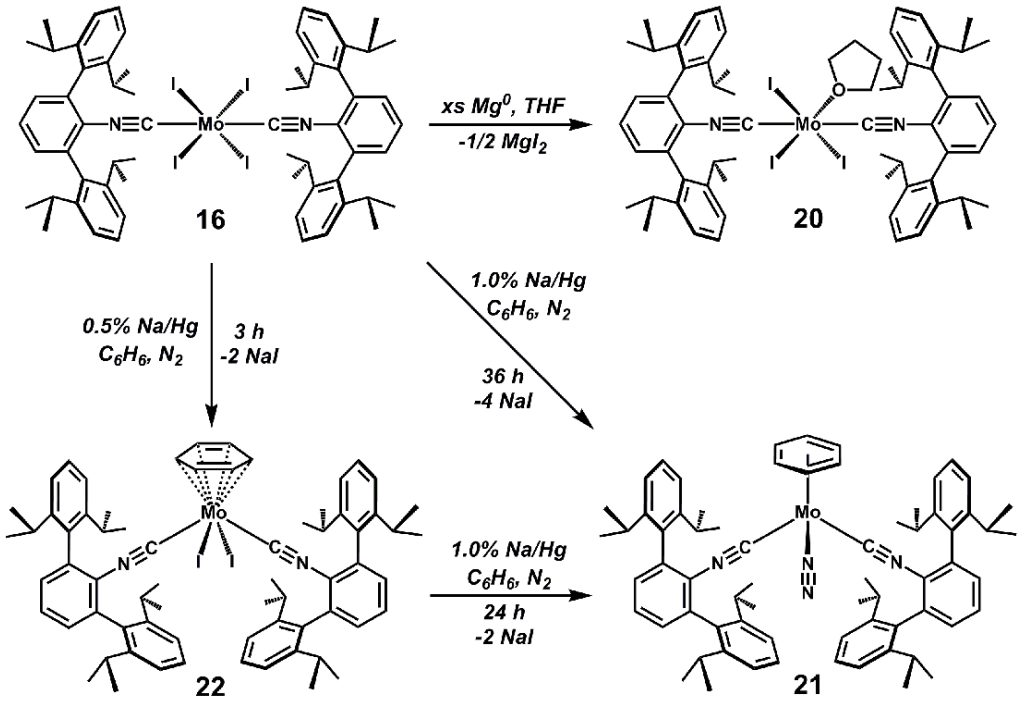

Scheme 3.6. Synthesis of *trans*–$MoI_3(THF)(CNAr^{Dipp2})_2$ (**20**), $(\eta^6$–$C_6H_6)Mo(N_2)(CNAr^{Dipp2})_2$ (**21**), and $(\eta^6$–$C_6H_6)MoI_2$ $(CNAr^{Dipp2})_2$ (**22**).

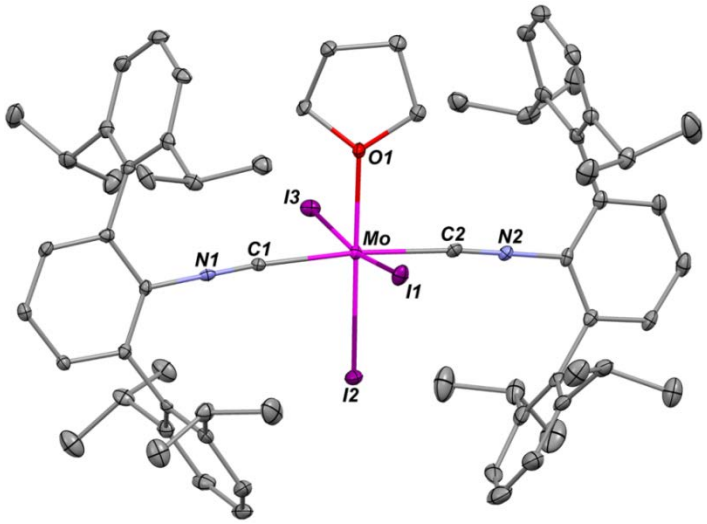

Figure 3.14. Molecular structure of *trans*–$MoI_3(THF)(CNAr^{Dipp2})_2$ (**20**). Selected bond distances (Å) and angles (deg): Mo1–C1 = 2.170(8); Mo1–C2 = 2.173(8); Mo1–I1 = 2.6925(14); Mo1–I2 = 2.7507(12); Mo1–I3 = 2.7497(12); Mo1–O1 = 2.188(5); C1–Mo1–C2 = 175.4(3); C1–Mo1–I1 = 88.77(18); C1–Mo1–I2 = 93.5(2); C1–Mo1–I3 = 88.3(2); C2–Mo1–I1 = 87.09(19); C2–Mo1–I2 = 88.8(2); C2–Mo1–I3 = 90.0(2); I2–Mo1–I1 = 95.34(4); I2–Mo1–I3 = 171.27(3).

Table 3.1. ν_{CN} and ν_{CO} Stretching Frequencies

complex	ν_{CN} (cm^{-1})	ν_{CO} (cm^{-1})
trans–$W(NCMe)(CO)_3(CNAr^{Dipp2})_2$ (**11**)[a]	2026(s)	1886(s)
	1996(s)	1873(s)
		1863(m)
trans–$Mo(NCMe)(CO)_3(CNAr^{Dipp2})_2$ (**8**)[a]	2027(s)	1895(s)
	1998(s)	1873(s)
		1864(m)
trans–$W(CO)_4(CNAr^{Dipp2})_2$ (**12**)[a]	2061(s)	1926(vs)
	2009(w)	
trans–$Mo(CO)_4(CNAr^{Dipp2})_2$ (**7**)[a]	2061(s)	1932(vs)
	2005(w)	
$WI_2(CO)_3(CNAr^{Dipp2})_2$ (**13**)[b]	2150(s)	2037(s)
	2099(m)	1982(vs)
		1944(s)
trans,trans,trans–$MoI_2(CO)_2(CNAr^{Dipp2})_2$ (**14**)[b]	2109(vs)	2004(s)
		1994(s)
cis,cis,trans–$MoI_2(CO)_2(CNAr^{Dipp2})_2$ (**14**)[a,c]	2110(vs)	1982(s)
		1940(s)
trans,trans,trans–$MoI_2(CO)_2(CNAr^{Dipp2})_2$ (**14**)[a,c]	2110(vs)	2006(s)
		1997(w)
$MoI_2(THF)(CO)_2(CNAr^{Dipp2})_2$ (**15**)[d]	2079(vs)	1969(s)
		1947(w)
trans–$MoI_4(CNAr^{Dipp2})_2$ (**16**)[b]	2163(s)	
	2135(w)	
$W(O_2CPh)_2(CO)_2(CNAr^{Dipp2})_2$ (**17**)[b]	2135(w)	2002(w)
	2071(vs)	1949(vs)
$W(O_2CMe)_2(CO)_2(CNAr^{Dipp2})_2$ (**18**)[b]	2131(w)	2002(w)
	2068(vs)	1943(vs)
$Mo(O_2CMe)_2(CO)(CNAr^{Dipp2})_2$ (**19**)[b]	2107(w)	2007(s)
	2032(vs)	1921(m)
trans–$MoI_3(THF)(CNAr^{Dipp2})_2$ (**20**)[b]	2142(vs)	
(η^6–C_6H_6)$Mo(N_2)(CNAr^{Dipp2})_2$ (**21**)[b]	1979(m)	
	1927(vs)	
(η^6–C_6H_6)MoI_2 $(CNAr^{Dipp2})_2$ (**22**)[b]	2086(m)	
	2040(vs)	
	2007(w)	

[a]KBr peller. [b]C_6D_6 solution. [c]Crystalline mixture of *trans,trans,trans*–$MoI_2(CO)_2(CNAr^{Dipp2})_2$ and *cis,cis,trans*–$MoI_2(CO)_2(CNAr^{Dipp2})_2$. [d]THF solution.

Tetraiodide *trans*–$MoI_4(CNAr^{Dipp2})_2$ (**16**) can also be reduced past the trivalent state when stronger reductants are employed. For example, treatment of *trans*–$MoI_4(CNAr^{Dipp2})_2$ (**16**) with 1% Na/Hg in C_6H_6 solution under an N_2 atmosphere generates the zerovalent, (η^6–C_6H_6)$Mo(N_2)(CNAr^{Dipp2})_2$ (**21**), which contains dinitrogen bound in an end–on fashion (Scheme 6, Figure 3.15). The molecular structure of (η^6–C_6H_6)$Mo(N_2)(CNAr^{Dipp2})_2$ (**21**) exhibits the three–legged piano stool motif of classical group 6, (η^6–C_6H_6)ML_3 (L =

monodentate, $2e^-$ donor ligand). However, it is noteworthy that dinitrogen–containing variants of this class are relatively rare.[88–91]

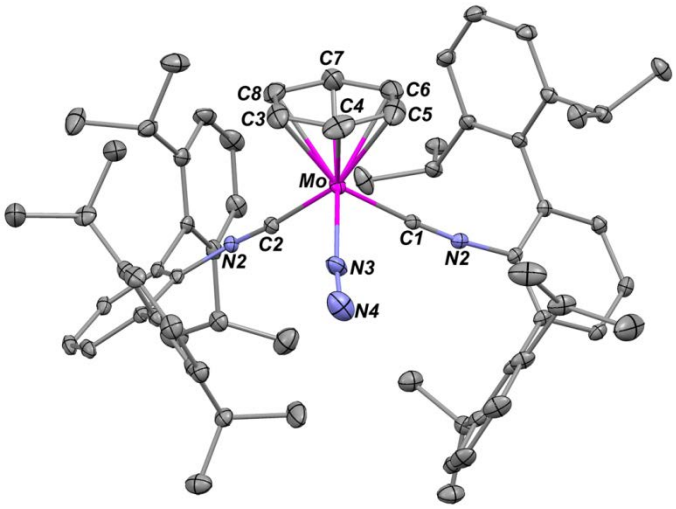

Figure 3.15. Molecular structure of $(\eta^6\text{–}C_6H_6)Mo(N_2)(CNAr^{Dipp2})_2$ (**21**). Selected bond distances (Å) and angles (deg): Mo1–C1 = 2.020(3); Mo1–C2 = 2.038(3); Mo1–N3 = 2.075(4); N3–N4 = 1.041(6); Mo1–C3 = 2.264(5); Mo1–C4 = 2.291(5); Mo1–C5 = 2.312(5); Mo1–C6 = 2.265(5); Mo1–C7 = 2.309(5); Mo1–C8 = 2.322(5); C1–Mo1–C2 = 92.63(13); C1–Mo1–N3 = 90.50(15); C2–Mo1–N3 = 91.74(14).

The most intriguing aspect of $(\eta^6\text{–}C_6H_6)Mo(N_2)(CNAr^{Dipp2})_2$ (**21**) concerns its formation upon reduction of *trans*–$MoI_4(CNAr^{Dipp2})_2$ (**16**). While it is interesting to speculate that a zerovalent molybdenum complex of the formulation $[Mo(N_2)_n(CNAr^{Dipp2})_2]$ ($n \leq 4$) is present fleetingly is solution, aliquots of the reaction mixture taken before complete formation of $(\eta^6\text{–}C_6H_6)Mo(N_2)(CNAr^{Dipp2})_2$ (**21**) revealed the presence of a diamagnetic intermediate (^{1}H NMR spectroscopy). This intermediate was amenable to isolation by quenching the reduction reaction after 3 h, and X–ray diffraction revealed it to be the η^6–benzene, diiodide complex $(\eta^6\text{–}C_6H_6)MoI_2(CNAr^{Dipp2})_2$ (**22**, Scheme 3.6, Figure 3.16). In contrast to zerovalent $(\eta^6\text{–}C_6H_6)Mo(N_2)(CNAr^{Dipp2})_2$ (**21**), $(\eta^6\text{–}C_6H_6)MoI_2(CNAr^{Dipp2})_2$ (**22**) possesses an asymmetrically bound benzene ring as indicated by short Mo–C3 and Mo–C6 bond distances (2.255(4) and 2.275(4) Å, respectively) relative to the remaining Mo–C_{ring}

contacts ($2.35(3)_{av}$). This "folded" or "boat" conformation of the bound benzene is accompanied by a fair degree of dearomatization and is consistent with a 1,4–dienediyl formulation as observed in other η^6–arene complexes (Figure 3.16).[92–97] Most importantly, however, addition of 1% Na/Hg to isolated (η^6–C_6H_6)$MoI_2(CNAr^{Dipp2})_2$ (**22**) in benzene solution under N_2 generates (η^6–C_6H_6)$Mo(N_2)(CNAr^{Dipp2})_2$ (**21**), thereby showing that the former is indeed a plausible intermediate en route to the zerovalent state.

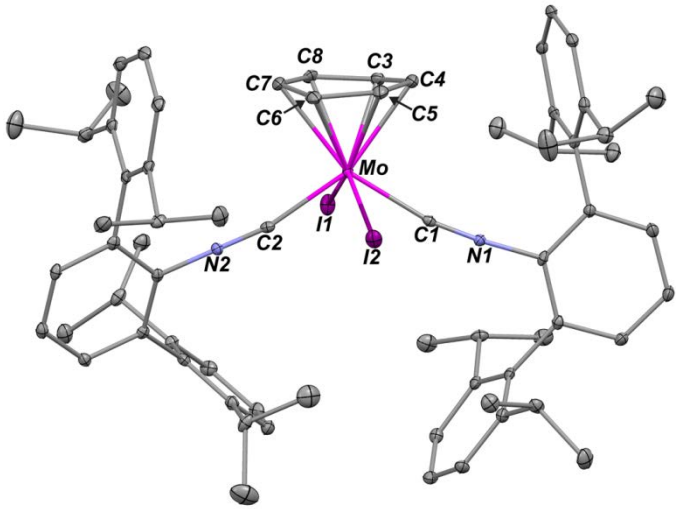

Figure 3.16. Molecular structure of (η^6–C_6H_6)$MoI_2(CNAr^{Dipp2})_2$ (**22**). Selected bond distances (Å) and angles (deg): Mo1–C1 = 2.067(3); Mo1–C2 = 2.068(3); Mo1–I1 = 2.8492(12); Mo1–I2 = 2.8481(19); Mo1–C3 = 2.255(4); Mo1–C4 = 2.361(4); Mo1–C5 = 2.329(4); Mo1–C6 = 2.275(4); Mo1–C7 = 2.385(3); Mo1–C8 = 2.330(4); C3–C4 = 1.404(5); C4–C5 = 1.380(5); C5–C6 = 1.425(5); C6–C7 = 1.402(6); C7–C8 = 1.382(5); C1–Mo1–C2 = 113.98(13); C1–Mo1–I1 = 78.60(9); C1–Mo1–I2 = 75.92(9); C2–Mo1–I1 = 76.88(9); C2–Mo1–I2 = 80.93(9).

Several elements of this reduction scheme are noteworthy in the context of generation low–coordinate group 6 isocyanide complexes. At present, we hypothesize that $2e^-$ reduction of *trans*–$MoI_4(CNAr^{Dipp2})_2$ (**16**) in benzene generates the four–coordinate, divalent complex [$MoI_2(CNAr^{Dipp2})_2$], which is the rapidly intercepted by solvent. Unfortunately, efforts to selectively generate [$MoI_2(CNAr^{Dipp2})_2$] in nonaromatic solvents have been unsuccessful thus far, with attempted reductions of *trans*–$MoI_4(CNAr^{Dipp2})_2$ (**16**) in

Et_2O, THF, or *n*–pentane in particular leading to intractable mixtures. Importantly, four–coordinate molybdenum ML_2X_2 complexes are extremely uncommon, as is expected for a heavier group 6 complex with a formal $12e^-$ configuration. However, Wolczanski has recently shown that the Mo complex, $Mo(silox)_2(PMe_3)_2$ (silox = $OSi(t\text{–}Bu)_3$), can in fact be isolated and that is possesses a pseudo–octahedral C_{2v} geometry owing to the combined effects of minimizing Mo–O σ^* interactions and maximizing $Mo\rightarrow PMe_3$ π–backbonding interactions within the d–orbital manifold.[98] While the coordination spheres of $Mo(silox)_2(PMe_3)_2$ and putative $[MoI_2(CNAr^{Dipp2})_2]$ are clearly different, they are related in both possess a $(\pi\text{–donor})_2(\pi\text{–acceptor})_2$ ligand set. However, the π–donor ability of iodide is clearly marginal relative to silox, and the π–acceptor of the isocyanide is much greater than that of PMe_3. How these differences ultimately affect the chemistry available to the $[MoI_2(CNAr^{Dipp2})_2]$ fragment is intriguing. To this end, isolation of $Mo(silox)_2(PMe_3)_2$ also reveals that such low–coordinate divalent Mo complexes can be stabilized when the proper steric protection is employed. Accordingly, we speculate that the two–atom linker between the metal center and the *m*–terphenyl unit in $[MoI_2(CNAr^{Dipp2})_2]$ is insufficient in this regard and evidently does not preclude arene binding.

3.6 Synthetic Procedures

General Considerations. All manipulations were carried out under an atmosphere of dry dinitrogen using standard Schlenk and glovebox techniques. Solvents were dried and deoxygenated according to standard procedures.[99] Unless otherwise stated, reagent–grade starting materials were purchased from commercial sources and either used as received or purified by standard procedures.[100] $CNAr^{Dipp2}$,[16] $CNAr^{Mes2}$,[15] $W(CO)_3(EtCN)_3$, $Mo(CO)_3(MeCN)_3$,[101] and *trans*–$Mo(NCMe)(CO)_3(CNAr^{Dipp2})_2$ were prepared according to literature procedures.[16] Benzene–d_6 (Cambridge Isotope Laboratories) was degassed and

stored over 4 Å molecular sieves under N_2 for 2 d prior to use. THF–d_8 (Cambridge Isotope Laboratories) was vacuum distilled from Na metal and then stored over 4 Å molecular sieves under N_2 for 2 d prior to use. Celite 405 (Fisher Scientific) was dried under vacuum (24 h) at a temperature above 250 ˚C and stored in the glovebox prior to use. Solution ^{1}H, and ^{13}C{^{1}H} spectra were recorded on Varian Mercury 300 and 400 spectrometers, a Varian X–Sens500 spectrometer, or a JEOL ECA–500 spectrometer. ^{1}H and ^{13}C{^{1}H} chemical shifts are reported in ppm relative to $SiMe_4$ (^{1}H and ^{13}C δ = 0.0 ppm) with reference to residual solvent resonances of 7.16 ppm (^{1}H) and 128.06 ppm (^{13}C) for benzene–d_6 and 1.72 ppm (^{1}H) for THF–d_8, 1.38 ppm (^{1}H). FTIR spectra were recorded on a Thermo–Nicolet iS10 FTIR spectrometer. Samples were prepared as C_6D_6 solutions injected into a ThermoFisher solution cell equipped with KBr windows or as KBr pellets. For solution FTIR spectra, solvent peaks were digitally subtracted from all spectra by comparison with an authentic spectrum obtained immediately prior to that of the sample. The following abbreviations were used for the intensities and characteristics of important IR absorption bands: vs = very strong, s = strong, m = medium, w = weak, vw = very weak; b = broad, vb = very broad, sh = shoulder. Combustion analyses were performed by Robertson Microlit Laboratories of Madison, NJ (USA).

Synthesis of *trans*–W(NCMe)(CO)$_3$(CNAr^{Dipp2})$_2$ (11). To a Et_2O slurry of $W(CO)_3(NCEt)_3$ (1.000 g, 2.257 mmol, 1 equiv, 30 mL) was added a Et_2O solution of $CNAr^{Dipp2}$ (1.912 g, 4.12 mmol, 2 equiv, 100 mL). The solution was stirred for 2 h, after which 70 mL of acetonitrile was added. The reaction mixture was irradiated with a 254 nm Hg lamp while under an Ar purge for 24h. The reaction mixture was the concentrated to ca. ½ its initial volume under reduced pressure, resulting in the precipitation of an orange solid. This solid was collected via filtration, slurried in cold acetonitrile (20 mL, –35 °C), and the

filtered again. Thorough drying of the resulting solid *in vacuo* afforded *trans*–W(NCMe)(CO)$_3$(CNAr^{Dipp2})$_2$. (**11**) Yield: 1.853 g, 0.160 mmol, 71%. ^{1}H NMR (400.1 MHz, C_6D_6, 20 °C): δ = 7.33 (t, 4H, J = 8 Hz, *p*–Dipp), 7.19 (d, 8H, J = 8 Hz, *m*–Dipp), 6.95 (d, 4H, J = 7 Hz, *m*–Ph), 6.86 (t, 2H, J = 7 Hz, *p*–Ph), 2.78 (sept, 8H, J = 7 Hz, C*H*(CH$_3$)$_2$), 1.34 (d, 24H, J = 7 Hz, CH(C*H*$_3$)$_2$), 1.18 (s, 3H, NCC*H*$_3$), 1.11 (d, 24H, J = 7 Hz, CH(C*H*$_3$)$_2$) ppm. ^{13}C{^{1}H} NMR (100.6 MHz, C_6D_6, 20 °C): δ = 205.0 (*C*≡O), 199.8 (*C*≡O), 170.9 (*C*≡N), 146.7, 138.8, 135.6, 129.9, 129.5, 129.2, 128.6, 125.9, 123.2, 119.0 (N*C*CH$_3$), 31.4 (*C*H(CH$_3$)$_2$), 24.5 (CH(*C*H$_3$)$_2$), 24.4 (CH(*C*H$_3$)$_2$), 2.8 (NC*C*H$_3$) ppm. FTIR (KBr pellet): (ν_{CN}) 2026(s) and 1996(s) cm^{-1}, (ν_{CO}) 1886(s), 1873(s) and 1863(m) cm^{-1} also 2960, 2925, 2866, 1459, 1415, 1382, 1362, 1046, 803, 755, 584, 521 cm^{-1}. Anal. Calcd for $C_{67}H_{77}N_3O_3W$: C, 69.60; H, 6.71; N, 3.63. Found: C, 69.05; H, 6.75; N, 3.51.

Synthesis of *trans*–W(CO)$_4$(CNAr^{Dipp2})$_2$ (12). CO gas (0.043 mL, 1.730 mmol, 10 equiv) was added to a THF solution of *trans*–W(NCMe)(CO)$_3$(CNAr^{Dipp2})$_2$ (**11**, 0.200 g, 0.173 mmol, 20 mL) and stirred for 24 h, resulting in the precipitation of a red solid. The reaction mixture was then filtered through a medium porosity frit, and the resulting red powder was washed with THF (2 x 5 mL), collected, and dried *in vacuo* to afford *Trans*–W(CO)$_4$(CNAr^{Dipp2})$_2$ (**12**). Yield: 0.137 g, 0.119 mmol, 68%. ^{1}H NMR (400.1 MHz, C_6D_6, 20 °C): δ = 7.36 (t, 4H, J = 8 Hz, *p*–Dipp), 7.18 (d, 8H, J = 8 Hz, *m*–Dipp), 6.92 (d, 4H, J = 8 Hz, *m*–Ph), 6.85 (t, 2H, J = 7 Hz, *p*–Ph), 2.68 (sept, 8H, J = 7 Hz, C*H*(CH$_3$)$_2$), 1.32 (d, 24H, J = 7 Hz, CH(C*H*$_3$)$_2$), 1.06 (d, 24H, J = 7 Hz, CH(C*H*$_3$)$_2$) ppm. ^{13}C{^{1}H} NMR (100.6 MHz, C_6D_6, 20 °C): δ = 195.5 (*C*≡O), 160.8 (*C*≡N), 146.5, 139.2, 134.9, 129.6, 129.5, 129.2, 127.2, 123.4, 31.4 (*C*H(CH$_3$)$_2$), 24.5 (CH(*C*H$_3$)$_2$), 24.3 (CH(*C*H$_3$)$_2$) ppm. FTIR (KBr pellet): (ν_{CN}) 2061(s) and 2009(w) cm^{-1}, (ν_{CO}) 1926(vs) cm^{-1} also 2961, 2927, 2868, 1459, 1415, 1363,

1055, 803, 755, 596, 570 cm^{-1}. Anal. Calcd for $C_{66}H_{74}N_2O_4W$: C, 69.34; H, 6.53; N, 2.45. Found: C, 67.95; H, 6.64; N, 2.46.

Synthesis of $WI_2(CO)_3(CNAr^{Dipp2})_2$ (13). To a thawing Et_2O solution of *trans*–$W(NCMe)(CO)_3(CNAr^{Dipp2})_2$ (**11**, 1.000 g, 0.864 mmol, 1.00 equiv, 50 mL) was added a thawing Et_2O solution of I_2 (0.230 g, 0.908 mmol, 1.05 equiv, 20 mL). The resulting solution was stirred for 1 h resulting in the precipitation of a yellow solid. The reaction mixture was then filtered, and the resulting yellow precipitate was washed with 10 mL of Et_2O, collected, and dried *in vacuo* to afford *Trans*–$WI_2(CO)_3(CNAr^{Dipp2})_2$ (**13**). Yield: 0.564 g, 0.412 mmol, 48%. ^1H NMR (300.1 MHz, C_6D_6, 20 °C): δ = 7.34 (t, 4H, J = 8 Hz, *p*–Dipp), 7.20 (d, 8H, J = 8 Hz, *m*–Dipp), 6.89 (d, 4H, J = 8 Hz, *m*–Ph), 6.78 (t, 2H, J = 7 Hz, *p*–Ph), 2.61 (sept, 8H, J = 7 Hz, C*H*$(CH_3)_2$), 1.39 (d, 24H, J = 7 Hz, CH(C*H*$_3)_2$), 1.00 (d, 24H, J = 7 Hz, CH(C*H*$_3)_2$) ppm. $^{13}C\{^1H\}$ NMR (100.6 MHz, C_6D_6, 20 °C): δ = 192.5 (*C*≡O), 188.5 (*C*≡N), 146.4, 140.4, 134.0, 130.7, 130.1, 129.3, 128.6, 126.9, 123.9, 31.4 (*C*H$(CH_3)_2$), 24.8 (CH(*C*H$_3)_2$), 24.4 (CH(*C*H$_3)_2$) ppm. FTIR (C_6D_6, KBr windows): (ν_{CN}) 2150(s) and 2099(m) cm^{-1}, (ν_{CO}) 2037(s), 1982(vs) and 1944(s) cm^{-1} also 2961, 2927, 2868, 1459, 1411, 1384, 1362, 1057, 794, 754 cm^{-1}. Anal. Calcd for $C_{65}H_{74}N_2O_3I_2W$: C, 57.03; H, 5.45; N, 2.05. Found: C, 57.12; H, 5.41; N, 1.93.

Synthesis of $MoI_2(CO)_2(CNAr^{Dipp2})_2$ (14). To a thawing Et_2O solution of *trans*–$Mo(NCMe)(CO)_3(CNAr^{Dipp2})_2$ (**8**, 0.100g, 0.0936 mmol, 1.00 equiv, 40 mL) was added a thawing Et_2O solution of I_2 (0.024 g, 0.0955 mmol, 1.02 equiv, 20 mL). The reaction mixture was allowed to stir for 6 h, after which the solution was filtered and all volatile materials were removed under reduced pressure. Dissolution of the resulting red residue in a 5:1 toluene/*n*–pentane mixture (6 mL total) followed by filtration and storage at –35 ˚C for 24 h

resulted in red crystals which were collected and dried *in vacuo*. Yield: 0.085 g, 0.0678 mmol, 77%. ^{1}H NMR (400.1 MHz, C_6D_6, 20 °C): δ = 16.18 (d, 4H, *J* = 7 Hz, *m*–Ph), 9.25 (d, 8H, *J* = 8 Hz, *m*–Dipp), 8.48 (t, 4H, *J* = 8 Hz, *p*–Dipp), 6.04 (s, 8H, C*H*$(CH_3)_2$), 3.38 (d, 24H, *J* = 6 Hz, CH(C*H*$_3)_2$), 2.32 (d, 24H, *J* = 7 Hz, CH(C*H*$_3)_2$), –6.33 (t, 2H, *J* = 8Hz, *p*–Ph) ppm. μ_{eff} (Evans Method, C_6D_6 with O(SiMe3)2, 400.1 MHz, 20 °C) = 2.71(±0.03) μB (average of 5 independent measurements). FTIR (C_6D_6, KBr window, *trans,trans,trans*–$MoI_2(CO)_2(CNAr^{Dipp2})_2$): ($\nu_{CN}$) 2109(vs) cm^{-1}, ($\nu_{CO}$) 2004(s) and 1994(s) cm^{-1} also 3061, 3020, 2925, 2868, 1577, 1462, 1415, 1386, 1357, 1333, 1252, 1180, 1060, 809, 755 cm^{-1}. FTIR (C_6D_6, KBr windows; *trans,trans,trans*–$MoI_2(CO)_2(CNAr^{Dipp2})_2$ and *cis,cis,trans*–$MoI_2(CO)_2(CNAr^{Dipp2})_2$): ($\nu_{CN}$) 2110(vs) cm^{-1}, ($\nu_{CO}$) 2006(s) and 1997(s) cm^{-1} (*trans*–Mo$((CO)_2)$), (ν_{CO}) 1982(s) and 1940(s) cm^{-1} (*cis*–Mo$((CO)_2)$). Anal. Calcd for $C_{64}H_{74}N_2O_2I_2Mo$: C, 61.35; H, 5.95; N, 2.24. Found: C, 61.16; H, 5.95; N, 2.23.

Alternative synthesis of $MoI_2(CO)_2(CNAr^{Dipp2})_2$ (14). To a thawing acetonitrile solution of $Mo(CO)_3(MeCN)_3$ (0.773 g, 2.552 mmol, 1 equiv, 25 mL) was added I_2 (0.648 g, 2.552 mmol, 1 equiv). The reaction mixture was stirred for 1 h, after which all volatile materials were removed under reduced pressure to afford $MoI_2(CO)_3(NCMe)_2$ as a burgundy solid. A 10:1 Et_2O/THF (75 mL/7.5 mL) solution was added to $MoI_2(CO)_3(NCMe)_2$ and the reaction mixture was frozen. To the thawing Et_2O/THF solution of $MoI_2(CO)_3(NCMe)_2$ was added a thawing Et_2O solution of $CNAr^{Dipp2}$ (2.000 g, 4.721 mmol, 1.85 equiv, 75 mL). The reaction mixture was allowed to stir for 2 h, after which all volatile materials were removed under reduced pressure. Dissolution of the resulting red residue in a toluene/*n*–pentane mixture (5:1, 100 mL total) followed by filtration and storage at –35 °C for 24 h resulted in red crystals, which were collected and dried *in vacuo*.

Synthesis of $MoI_2(THF)(CO)_2(CNAr^{Dipp2})_2$ (15). Solid $MoI_2(CO)_2(CNAr^{Dipp2})_2$ (**14**, 0.100g, 0.0798 mmol) was dissolved in 1 mL of THF and stirred for 10 min, gradually changing in color from red to brown. Addition of 0.5 mL of *n*–pentane to the resulting solution followed by filtration and storage at –35 °C for 24 h resulted in brown crystals, which were collected and dried *in vacuo*. Yield: 0.080g, 0.0604 mmol, 80%. ^{1}H NMR (400.1 MHz, THF–d_8, 20 °C): δ = 7.45 (t, 2H, *J* = 8 Hz, *m*–Dipp), 7.28 (t, 4H, *J* = 8 Hz, *m*–Ph), 7.24 (d, 4H, *J* = 8 Hz, *p*–Dipp), 7.18 (d, 8H, *J* = 8 Hz, *m*–Dipp), 7.2.54 (sept, 8H, *J* = 7 Hz, C*H*$(CH_3)_2$), 1.26 (d, 24H, *J* = 7 Hz, CH(C*H*$_3)_2$), 1.02 (d, 24H, *J* = 7 Hz, CH(C*H*$_3)_2$) ppm. FTIR (THF, KBr windows): (ν_{CN}) 2079(vs) cm^{-1}, (ν_{CO}) 1969(s) and 1947(s) cm^{-1} also 1594, 1559, 1472, 1465, 1414, 1386, 1364, 872, 823, 793, 158 cm^{-1}. Satisfactory combustion analysis was not obtained due to repeated and substoichiometric loss of THF. Dissolution of *trans*–$MoI_2(THF)(CO)_2(CNAr^{Dipp2})_2$ (**15**) in C_6D_6 retruned ^{1}HNMR resonances for $MoI_2(CO)_2(CNAr^{Dipp2})_2$ (**14**) and free THF.

Synthesis of *trans*–$MoI_4(CNAr^{Dipp2})_2$ (16). To a thawing fluorobenzene (C_6H_5F) solution of $MoI_2(CO)_2(CNAr^{Dipp2})_2$ (**14**, 0.200 g, 0.160 mmol, 1.00 equiv, 20 mL) was added a thawing fluorobenzene solution of I_2 (0.043 g, 0.168 mmol, 1.05 equiv, 10 mL). The reaction mixture was allowed to stir for 4 h, after which all volatile materials were removed under reduced pressure. Dissolution of the resulting royal–blue residue in a 2:1 toluene/*n*–pentane mixture (6 mL, total) followed by filtration and storage at –35 ˚C for 48 h resulted in royal–blue crystals which were collected and dried *in vacuo*. Yield: 0.125 g, 0.086 mmol, 53%. ^{1}H NMR (400.1 MHz, C_6D_6, 20 °C): δ = 14.79 (d, 4H, *J* = 8 Hz, *m*–Ph), 8.26 (d, 8H, *J* = 8 Hz, *m*–Dipp), 6.95 (t, 4H, *J* = 8 Hz, *p*–Dipp), 3.38 (d, 24H, J = 7Hz,(CH(C*H*$_3)_2$), 1.24 (sept, 8H, *J* = 7 Hz), 1.01(d, 24H, *J* = 7 Hz, CH(C*H*$_3)_2$) –10.69 (t, 2H, *J* = 8 Hz, *p*–Ph) ppm. μ_{eff} (Evans Method, C_6D_6 with O(SiMe3)2, 400.1 MHz, 20 °C) = 2.86(±0.03) μB (average of

3 independent measurements). FTIR (C_6D_6, KBr windows): (ν_{CN}) 2163(s) and 2135(w) cm^{-1} also 2956, 2926, 2867, 1615, 1587, 1579, 1460, 1407, 1385, 1363, 808, 758, 677 cm^{-1}. Anal. Calcd for $C_{62}H_{74}N_2I_4Mo$: C, 51.33; H, 5.14; N, 1.93. Found: C, 52.17; H, 5.38; N, 1.82.

Synthesis of $W(CO)_2(O_2CPh)_2(CNAr^{Dipp2})_2$ (17). To a THF solution of *trans*–$W(NCMe)(CO)_3(CNAr^{Dipp2})_2$ (**11**, 0.200 g, 0.173 mmol, 1 equiv, 5 mL) was added a THF solution of benzoyl peroxide (0.084 g, 0.346 mmol, 2 equiv, 5 mL). The reaction mixture was allowed to stir for 24 h, after which all volatile materials were removed under reduced pressure. Dissolution of the resulting orange residue in Et_2O (3 mL) followed by filtration and storage at –35 ˚C for 5 days resulted in orange crystals which were collected and dried *in vacuo*. Yield: 0.050 g, 0.038 mmol, 22%. ^1H NMR (400.1 MHz, C_6D_6, 20 °C): δ = 8.04 (m, 4H), 7.34 (t, 4H, *J* = 8 Hz, *p*–Dipp), 7.21 (d, 8H, *J* = 8 Hz, *m*–Dipp), 7.06 (t, 4H), 7.04 (d, 2H), 6.99 (d, 4H, *J* = 8 Hz, *m*–Ph), 6.86 (t, 2H, J = 8 Hz, *p*–Ph), 2.71 (sept, 8H, *J* = 7 Hz, C*H*$(CH_3)_2$), 1.27 (d, 24H, *J* = 7 Hz, CH(C*H*$_3)_2$), 1.08 (d, 24H, *J* = 7 Hz, CH(C*H*$_3)_2$) ppm. $^{13}C\{^1H\}$ NMR (100.6 MHz, C_6D_6, 20 °C): δ = 223.1 (*C*≡O), 177.3 (*C*≡N), 175.1 (*C*=O), 146.3, 139.1, 135.6, 134.2, 131.4, 130.3, 129.9, 128.6, 127.7, 123.63, 31.4 (*C*H$(CH_3)_2$), 24.9 (CH(*C*H$_3)_2$), 24.1 (CH(*C*H$_3)_2$) ppm. FTIR (C_6D_6, KBr windows): (ν_{CN}) 2135(w) and 2071(vs) cm^{-1}, (ν_{CO}) 2002(w) and 1949(vs) cm^{-1} also 2962, 2926, 2868, 1619 ($\nu_{C=O}$), 1505, 1449, 1161, 869, 755, 714 cm^{-1}. Anal. Calcd for $C_{78}H_{84}N_2O_6W$: C, 70.47; H, 6.37; N, 2.11. Found: C, 70.27; H, 6.40; N, 2.05.

Synthesis of $W(CO)_2(MeCO_2)_2(CNAr^{Dipp2})_2$ (18). To a THF solution of $WI_2(CO)_3(CNAr^{Dipp2})_2$ (**13**, 0.100 g, 0.073 mmol, 1 equiv, 3 mL) was added a THF slurry of AgOAc (0.037 g, 0.183 mmol, 3 equiv, 5 mL). The reaction mixture was allowed to stir for 12 h, after which the solution was filtered and all volatile materials were removed under

reduced pressure. Dissolution of the resulting red residue in a 4:1 Et_2O/acetonitrile mixture (5 mL total) followed by filtration and storage at –35 ˚C for 24 h resulted in orange crystals, which were collected and dried *in vacuo*. Yield: 0.083 g, 0.069 mmol, 38%. ^{1}H NMR (400.1 MHz, C_6D_6, 20 °C): δ = 7.36 (t, 4H, *J* = 8 Hz, *p*–Dipp), 7.24 (d, 8H, *J* = 8 Hz, *m*–Dipp), 6.99 (d, 4H, *J* = 7 Hz, *m*–Ph), 6.86 (t, 2H, *J* = 8 Hz, *p*–Ph), 2.69 (sept, 8H, *J* = 6 Hz, C*H*$(CH_3)_2$), 1.72 (s, 6H, C*H*$_3CO_2$), 1.28 (d, 24H, *J* = 6 Hz, CH(C*H*$_3)_2$), 1.09 (d, 24H, *J* = 6 Hz, CH(C*H*$_3)_2$) ppm. ^{13}C{^{1}H} NMR (100.6 MHz, C_6D_6, 20 °C): δ = 224.5 (*C*≡O), 182.0 (*C*≡N), 175.6 (*C*=O), 146.3, 139.0, 134.0, 130.3, 129.8, 128.2, 123.6, 123.4, 31.4 (*C*H$(CH_3)_2$), 25.0 (CO_2*C*H$_3$), 24.9 (CH(*C*H$_3)_2$), 24.0 (CH(*C*H$_3)_2$) ppm. FTIR (C_6D_6, KBr windows): (ν_{CN}) 2131(w) and 2068(vs) cm^{-1}, (ν_{CO}) 2002(w) and 1943(vs) cm^{-1} also 2963, 2925, 2868, 1476, 1413, 1386, 1360, 1302, 761, 691, 664 cm^{-1} (acetate $\nu_{C=O}$ not conclusively identified). Anal. Calcd for $C_{68}H_{80}N_2O_6W$: C, 67.77; H, 6.69; N, 2.32. Found: C, 67.69; H, 6.81; N, 2.32.

Synthesis of Mo(CO)(MeCO$_2$)$_2$(CNAr^{Dipp2})$_2$ (19). To a THF solution of $MoI_2(CO)_2(CNAr^{Dipp2})_2$ (**14**, 1.000 g, 0.779 mmol, 1 equiv, 30 mL) was added a THF slurry of AgOAc (0.280 g, 1.677 mmol, 2.05 equiv, 30 mL). The reaction mixture was allowed to stir for 6 h, filtered, and stirred for another 48 h. All volatile materials were removed under reduced pressure, and dissolution of the resulting red residue in a 4:1 Et_2O/acetonitrile mixture (20 mL total) followed by filtration and storage at –35 ˚C for 24 h resulted in orange crystals which were collected and dried *in vacuo*. Yield: 0.350 g, 0.321 mmol, 41%. ^{1}H NMR (400.1 MHz, C_6D_6, 20 °C): δ = 7.38 (t, 4H, *J* = 8 Hz, *p*–Dipp), 7.25 (d, 8H, *J* = 8 Hz, *m*–Dipp), 6.97 (d, 4H, *J* = 8 Hz, *m*–Ph), 6.85 (t, 2H, *J* = 7 Hz, *p*–Ph), 2.72 (sept, 7H, *J* = 7 Hz, C*H*$(CH_3)_2$), 1.53 (s, 6H, C*H*$_3CO_2$), 1.24 (d, 24H, *J* = 6 Hz, CH(C*H*$_3)_2$), 1.14 (d, 24H, *J* = 7 Hz, CH(C*H*$_3)_2$) ppm. ^{13}C{^{1}H} NMR (100.6 MHz, C_6D_6, 20 °C): δ = 265.2 (*C*≡O), 204.2 (*C*≡N), 186.3 (C=O), 146.5, 137.2, 135.0, 130.1, 129.4, 128.7, 127.4, 123.4, 31.5

($CH(CH_3)_2$), 24.7 (CO_2CH_3), 24.2 ($CH(CH_3)_2$), 23.9 ($CH(CH_3)_2$) ppm. FTIR (C_6D_6, KBr windows): (ν_{CN}) 2107(w) and 2032(vs) cm^{-1}, (ν_{CO}) 2007(s) and 1921(m) cm^{-1} also 2965, 1580, 1466, 1416, 1363, 755 cm^{-1} (acetate $\nu_{C=O}$ not conclusively identified). Anal. Calcd for $C_{67}H_{80}N_2O_5Mo$: C, 73.87; H, 7.40; N, 2.57. Found: C, 73.75; H, 7.59; N, 2.61.

Synthesis of *trans*–$MoI_3(THF)(CNAr^{Dipp2})_2$ (20). To a THF solution of *trans*–$MoI_4(CNAr^{Dipp2})_2$ (**16**, 0.200 g, 0.137 mmol, 50 mL total) was added I_2–activated magnesium turnings (0.083 g, 3.446 mmol, 25 equiv). The reaction mixture was allowed to stir for 12 h and gradually changed in color from pale–brown to pale–orange. The resulting solution was decanted off the residual magnesium turnings and then dried under reduced pressure. The residue was then slurried in Et_2O (15 mL), stirred for 20 min and then dried *in vacuo*. The resulting tan solid was then was slurried in Et_2O (20 mL) and filtered through Celite. The solid remaining on the Celite pad was dissolved in THF (5 mL), filtered, layered with *n*–pentane (5 mL) and stored at –35 °C for 1 day, whereupon tan crystals were obtained. Yield: 0.070 g, 0.050 mmol, 36%. ^{1}H NMR (400.1 MHz, C_6D_6, 20 °C): δ = 69.65 (s, 2H, *p*–Ph), 27.2 (s, 4H, *p*–Dipp), 8.35 (s, 8H, *m*–Dipp), 6.26 (s, 4H, THF), 6.04 (s, 4H, THF). 3.55 (s, 24H, $CH(CH_3)_2$), 2.48 (s, 24H, $CH(CH_3)_2$), 1.37 (s, 8H, $CH(CH_3)_2$), –17.71 (s, 4H, *m*–Ph) ppm. μ_{eff} (Evans Method, C_6D_6 with O(SiMe3)2, 400.1 MHz, 20 °C) = 3.95(±0.10) μB (average of 3 independent measurements). FTIR (C_6D_6, KBr windows): (ν_{CN}) 2142(vs) cm^{-1} also 2962, 2927, 2869, 1461, 1412, 1387, 1364, 1328 cm^{-1}. Anal. Calcd for $C_{66}H_{82}N_2OI_3Mo$: C, 56.14; H, 5.85; N, 1.89. Found: C, 56.21; H, 6.13; N, 1.94.

Synthesis of $MoN_2(C_6H_6)(CNAr^{Dipp2})_2$ (21). To a stirred mixture of 1.0% Na/Hg (Na: 0.633 g, 27.57 mmol; Hg: 63.4 g; 100 equiv Na per Mo) and C_6H_6 (50 mL) was added a C_6H_6 solution of $MoI_4(CNAr^{Dipp2})_2$ (**16**, 0.400 g, 0.276 mmol, 75 mL). The resulting mixture

was allowed to stir for 36 h and then filtered through Celite. All volatile materials were then removed under reduced pressure. The resulting red residue was then was suspended in Et_2O (10 mL) and filtered through Celite. The filtrate was evaporated to dryness *in vacuo*, and the remaining solid was dissolved in Et_2O (2 mL), filtered, and layered with $O(SiMe_3)_2$ (3 mL) and stored at –35 °C for 2 days, whereupon red crystals were obtained. Yield: 0.150 g, 0.143 mmol, 52%. ^{1}H NMR (400.1 MHz, C_6D_6, 20 °C): δ = 7.35 (t, 4H, *J* = 8 Hz, *p*–Dipp), 7.21 (dd, 8H, *J* = 8 Hz, *m*–Dipp), 6.96 (d, 4H, *J* = 8 Hz, *m*–Ph), 6.87 (t, 2H, *J* = 6 Hz, *p*–Ph), 3.57 (s, 6H, η^6–C_6H_6), 2.88 (m, 8H, *J* = 7 Hz, C*H*$(CH_3)_2$), 1.30 (d, 12H, *J* = 7 Hz, CH(C*H*$_3)_2$), 1.18 (d, 12H, *J* = 7 Hz, CH(C*H*$_3)_2$), 1.16 (d, 12H, *J* = 7 Hz, CH(C*H*$_3)_2$), 1.13 (d, 12H, *J* = 7 Hz, CH(C*H*$_3)_2$) ppm. ^{13}C{^{1}H} NMR (100.6 MHz, C_6D_6, 20 °C): δ = 196.1 (*C*≡N), 147.1, 146.6, 137.3, 137.1, 131.0, 130.5, 128.9, 124.3, 123.4, 123.2, 84.6 (*C*$_6H_6$), 31.2 (*C*H$(CH_3)_2$), 25.0 (CH(*C*H$_3)_2$), 24.6 (CH(*C*H$_3)_2$), 24.1 (CH(*C*H$_3)_2$), 24.0 (CH(*C*H$_3)_2$) ppm. FTIR (C_6D_6, KBr windows): (ν_{NN}) 2101(s) cm^{-1}, (ν_{CN}) 1979(m) and 1926(vs) cm^{-1} also 2965, 2923, 2870, 1618, 1455, 1410, 1155, 758 cm^{-1}. Anal. Calcd for $C_{68}H_{80}N_4Mo$: C, 77.86; H, 7.69; N, 5.34. Found: C, 75.56; H, 7.48; N, 4.27.

Synthesis of $MoI_2(C_6H_6)(CNAr^{Dipp2})_2$ (22). To a stirred mixture of 0.50% Na/Hg (Na: 0.023 g, 3.43 mmol; Hg: 15.8 g; 25 equiv Na per Mo) and C_6H_6 (50 mL), was added an C_6H_6 solution of $MoI_4(CNAr^{Dipp2})_2$ (**16**, 0.200 g, 0.137 mmol, 50 mL). The resulting mixture was allowed to stir for 3 h, and gradually changed from royal–blue to red. The reaction mixture was filtered through Celite and all volatile materials were removed under reduced pressure. The residue was then slurried in *n*–pentane (5 mL), filtered, and washed with *n*–pentane (2 x 5 mL). The remaining solid was dissolved in Et_2O (3 mL), filtered, and layered with $O(SiMe_3)_2$ (3 mL) and stored at –35 °C for 1 day, whereupon brown crystals were obtained. Yield: 0.040 g, 0.031 mmol, 23%. ^{1}H NMR (400.1 MHz, C_6D_6, 20 °C): δ = 7.36 (t,

4H, *J* = 8 Hz, *p*–Dipp), 7.23 (d, 8H, *J* = 8 Hz, *m*–Dipp), 6.95 (d, 4H, *J* = 7 Hz, *m*–Ph), 6.82 (t, 2H, *J* = 8 Hz, *p*–Ph), 4.35 (s, 6H, η^6–C_6H_6), 2.85 (sept, 8H, *J* = 7 Hz, C*H*$(CH_3)_2$), 1.43 (d, 24H, *J* = 7 Hz, CH(C*H*$_3)_2$), 1.09 (d, 24H, *J* = 7 Hz, CH(C*H*$_3)_2$) ppm. $^{13}C\{^1H\}$ NMR (100.6 MHz, C_6D_6, 20 °C): δ = 172.4 (*C*≡N), 147.2, 139.1, 136.6, 131.5, 129.5, 129.1, 128.6, 126.9, 123.5, 98.3 (C_6H_6), 31.3 (*C*H$(CH_3)_2$), 25.1 (CH(*C*H$_3)_2$), 24.9 (CH(*C*H$_3)_2$) ppm. FTIR (C_6D_6, KBr windows): (ν_{CN}) 2086(m), 2040(vs) and 2007(w) cm^{-1} also 2959, 2927, 2867, 1614, 1461, 1453, 1416, 1384, 1363, 807, 758 cm^{-1}. Anal. Calcd for $C_{68}H_{80}N_2I_2Mo$: C, 64.05; H, 6.32; N, 2.20. Found: C, 62.87; H, 6.13; N, 2.22.

3.7 Crystallographic Structure Determinations

General considerations. Single crystal Xray structure determinations were carried out at low temperature on a Bruker P4, Platform or Kappa Diffractometer equipped with a Bruker APEX detector. All structures were solved by direct methods with SIR 2004[102] and refined by full–matrix least–squares procedures utilizing SHELXL–97.[103] Crystallographic data–collection and refinement information are listed in Tables 3.2 through 3.5. The crystal structure of *trans*–W(NCMe)$(CO)_3(CNAr^{Dipp2})_2$ (**11**) contained positional disorder between one of CO ligands and the coordinated acetonitrile molecule. The disorder was modeled such that both the CO and acetonitrile molecules are represented at 50% occupancy at each of the two sites. The crystal structure of $MoI_2(CO)_2(CNAr^{Dipp2})_2$ (**14**) reveals cocrystalization of a 50/50 mixture of both the *cis*– and *trans*–carbonyl isomers. Both *cis*– and *trans*–carbonyl isomers contain whole molecule disorder and consequently the heavier Mo and I atoms were modeled and refined over several positions. Also, the *cis*–carbonyl isomer contains positional and compositional disorder between the CO ligands and terminal iodides within the equatorial plane of the molecule. The disorder was modeled such that the total of all ligand occupancy equals two CO ligands and two Iodides. The crystal structure of

$W(O_2CPh)_2(CO)_2(CNAr^{Dipp2})_2$ (**17**) contains isopropyl–group positional disorder, which was modeled and refined. The crystal structure of *trans*–$MoI_3(THF)(CNAr^{Dipp2})_2$ (**20**) contains positional disorder in one of the bound acetate ligands which was modeled and refined. The crystal structures of *trans*–$MoI_4(CNAr^{Dipp2})_2$ (**16**) and $(\eta^6–C_6H_6)Mo(N_2)(CNAr^{Dipp2})_2$ (**21**) contain positional disorder in toluene and $O(SiMe_3)_2$ molecules of cocrystalization, respectively. These disordered components were also modeled and refined.

Table 3.2. Crystallographic Data Collection and Refinement Information for *trans*–$W(NCMe)(CO)_3(CNAr^{Dipp2})_2 \cdot 2CH_2Cl_2$, *trans*–$W(CO)_4(CNAr^{Dipp2})_2$, and $WI_2(CO)_4(CNAr^{Dipp2})_2$

	trans–$W(NCMe)(CO)_3(CNAr^{Dipp2})_2 \cdot 2CH_2Cl_2$ (**11**·$2CH_2Cl_2$)	*trans*–$W(CO)_4(CNAr^{Dipp2})_2$ (**12**)	$WI_2(CO)_4(CNAr^{Dipp2})_2$ (**13**)
Formula	$C_{71}H_{85}Cl_{18}N_3O_3W$	$C_{66}H_{74}N_2O_4W$	$C_{65}H_{74}I_2N_2O_3W$
Crystal System	Monoclinic	Monoclinic	Monoclinic
Space Group	$P2_1/n$	C_2/c	$P2_1/c$
a, Å	15.870(3)	24.073(2)	19.3808(7)
b, Å	10.825(2)	23.997(2)	17.0361(6)
c, Å	22.399(7)	21.1748(17)	20.8151(8)
α, deg	90	90	90
β, deg	109.563(6)	108.2280(10)	116.4150(10)
γ, deg	90	90	90
V, Å^3	3625.9(15)	11618.0(17)	6155.1(4)
Z	2	8	4
Radiation (λ, Å)	Mo–K_α, 0.71073	Mo–K_α, 0.71073	Mo–K_α, 0.71073
ρ (calcd.), g/cm^3	1.370	1.307	1.477
μ, mm^{-1}	1.933	2.036	2.924
Temp, K	100(2)	100(2)	100(2)
θ max, deg	28.45	25.05	28.27
data/parameters	8308/0/404	10770/0/663	14311/0/674
R_1	0.0484	0.0422	0.0538
wR_2	0.1099	0.1230	0.1545
GOF	1.014	1.057	1.057

Table 3.3. Crystallographic Data Collection and Refinement Information for $MoI_2(CO)_2(CNAr^{Dipp2})_2$, $MoI_2(THF)(CO)_2(CNAr^{Dipp2})_2$, and *trans*–$MoI_4(CNAr^{Dipp2})_2{\cdot}(C_7H_8)$

	$MoI_2(CO)_2(CNAr^{Dipp2})_2$ (**14**)	$MoI_2(THF)(CO)_2(CNAr^{Dipp2})_2$ (**15**)	*trans*–$MoI_4(CNAr^{Dipp2})_2{\cdot}(C_7H_8)$ (**16**·(C_7H_8))
Formula	$C_{64}H_{74}I_{1.95}MoN_2O_2$	$C_{68}H_{82}I_2MoN_2O_3$	$C_{39}H_{47}I_2Mo_{0.5}N$
Crystal System	Monoclinic	Orthorhombic	Monoclinic
Space Group	*C*2/*c*	*Pbca*	*C*2/*m*
a, Å	24.3913(6)	27.6865(9)	20.601(5)
b, Å	24.3951(6)	17.4569(6)	16.167(4)
c, Å	21.1052(5)	29.1280(10)	15.491(7)
α, deg	90	90	90
β, deg	107.9900(10)	90	90
γ, deg	90	90	90
V, Å^3	11944.5(5)	14078.2(8)	4162(2)
Z	8	8	4
Radiation (λ, Å)	Cu–K_α, 1.54178	Cu–K_α, 1.54178	Mo–K_α, 0.71073
ρ (calcd.), g/cm^3	1.387	1.250	1.327
μ, mm^{-1}	10.044	8.718	1.678
Temp, K	100(2)	100(2)	100(2)
θ max, deg	70.87	65.24	27.14
data/parameters	10563/0/678	11666/0/701	4747/0/219
R_1	0.0601	0.0569	0.0416
wR_2	0.1816	0.1627	0.1196
GOF	1.070	1.054	1.084

Table 3.4. Crystallographic Data Collection and Refinement Information for $W(O_2CPh)_2(CO)_2(CNAr^{Dipp2})_2$, $W(O_2CMe)_2(CO)_2(CNAr^{Dipp2})_2$, and $Mo(O_2CMe)_2(CO)(CNAr^{Dipp2})_2$

	$W(O_2CPh)_2(CO)_2(CNAr^{Dipp2})_2$ (**17**)	$W(O_2CMe)_2(CO)_2(CNAr^{Dipp2})_2$ (**18**)	$Mo(O_2CMe)_2(CO)(CNAr^{Dipp2})_2$ (**19**)
Formula	$C_{78}H_{84}N_2O_6W$	$C_{68}H_{80}N_2O_6W$	$C_{67}H_{80}MoN_2O_5$
Crystal System	Triclinic	Triclinic	Triclinic
Space Group	*P*–1	*P*–1	*P*–1
a, Å	16.1462(6)	12.7672(9)	10.8652(7)
b, Å	16.9570(6)	18.9332(14)	14.4040(9)
c, Å	25.6350(9)	26.1549(19)	21.3033(13)
α, deg	106.364(2)	94.5690(10)	109.3830(10)
β, deg	90.527(3)	90.2100(10)	93.6950(10)
γ, deg	91.057(2)	101.2740(10)	101.9650(10)
V, Å^3	6732.4(4)	6179.4(8)	3044.6(3)
Z	4	4	2
Radiation (λ, Å)	Cu–K_α, 1.54178	Mo–K_α, 0.71073	Mo–K_α, 0.71073
ρ (calcd.), g/cm^3	1.312	1.295	1.188
μ, mm^{-1}	3.597	1.920	0.264
Temp, K	100(2)	100(2)	100(2)
θ max, deg	68.65	28.33	25.37
data/parameters	22977/6/1578	28160/12/1424	11135/0/694
R_1	0.0446	0.0370	0.0388
wR_2	0.0941	0.0923	0.1084
GOF	1.025	1.004	1.074

Table 3.5. Crystallographic Data Collection and Refinement Information for *trans*–$MoI_3(THF)(CNAr^{Dipp2})_2$, $(\eta^6–C_6H_6)Mo(N_2)(CNAr^{Dipp2})_2\cdot((Me_3Si)_2O)$, and $(\eta^6–C_6H_6)MoI_2(CNAr^{Dipp2})_2$

	trans–$MoI_3(THF)(CNAr^{Dipp2})_2$ (**20**)	$(\eta^6–C_6H_6)Mo(N_2)(CNAr^{Dipp2})_2\cdot((Me_3Si)_2O)$ (**21**·$((Me_3Si)_2O)$)	$(\eta^6–C_6H_6)MoI_2(CNAr^{Dipp2})_2$ (**22**)
Formula	$C_{66}H_{82}I_3MoN_2O$	$C_{71}H_{89}MoN_4OSi_2$	$C_{68}H_{80}I_2MoN_2$
Crystal System	Tetragonal	Triclinic	Monoclinic
Space Group	$P4_32_12$	*P*–1	$P2_1/c$
a, Å	17.956(6)	12.5493(10)	15.891(9)
b, Å	17.956(6)	12.7014(11)	18.193(10)
c, Å	41.03(2)	22.4890(19)	22.629(12)
α, deg	90	74.1840(10)	90
β, deg	90	74.6450(10)	110.253(7)
γ, deg	90	68.8530(10)	90
V, Å^3	13229(9)	3160.8(5)	6137(6)
Z	8	2	4
Radiation (λ, Å)	Mo–K_α, 0.71073	Mo–K_α, 0.71073	Mo–K_α, 0.71073
ρ (calcd.), g/cm^3	1.402	1.188	1.380
μ, mm^{-1}	1.637	0.271	1.260
Temp, K	100(2)	100(2)	100(2)
θ max, deg	27.29	25.35	25.44
data/parameters	14759/0/674	11568/722	11234/0/674
R_1	0.0640	0.0673	0.0353
wR_2	0.1519	0.1793	0.0836
GOF	1.021	1.026	1.027

3.8 Acknowledgements

Chapter 3 is adapted from Ditri, T. B.; Moore, C. E.; Rheingold, A. L.; Figueroa, J. S. "Oxidative Decarbonylation of *m*–Terphenyl Isocyanide Complexes of Molybdenum and Tungsten: Precursors to Low–Coordinate Isocyanide Complexes." *Inorg. Chem.* **2011,** *50*, 10448–10459. Copyright 2011 American Chemical Society. Permission to use copyrighted

images and data in the manuscript was also obtained from Moore, C. E.; Rheingold, A. L.; Figueroa, J. S. The dissertation author is the first author of this paper.

3.9 References

(1) Zhou, M.; Andrews, L.; Bauschlicher, C. W. *Chem. Rev.* **2001**, *101*, 1931–1962.

(2) Seder, T. A.; Church, S. P.; Weitz, E. *J. Am. Chem. Soc.* **1986**, *108*, 4721–4728.

(3) Perutz, R. N.; Turner, J. J. *J. Am. Chem. Soc.* **1975**, *97*, 4800–4804.

(4) Ishikawa, Y.; Kawakami, K. *J. Phys. Chem. A* **2007**, *111*, 9940–9944.

(5) Ishikawa, Y.; Hackett, P. A.; Rayner, D. M. *J. Phys. Chem.* **1988**, *92*, 3863–3869.

(6) Ishikawa, Y.; Brown, C. E.; Hackett, P. A.; Rayner, D. M. *J. Phys. Chem.* **1990**, *94*, 2404–2413.

(7) Ganske, J. A.; Rosenfeld, R. N. *J. Phys. Chem.* **1989**, *93*, 1959–1963.

(8) Fletcher, T. R.; Rosenfeld, R. N. *J. Am. Chem. Soc.* **1985**, *107*, 2203–2212.

(9) Burdett, J. K.; Graham, M. A.; Perutz, R. N.; Poliakoff, M.; Rest, A. J.; Turner, J. J.; Turner, R. F. *J. Am. Chem. Soc.* **1975**, *97*, 4805–4808.

(10) Andrews, L.; Zhou, M.; Gutsev, G. L.; Wang, X. *J. Phys. Chem. A* **2003**, *107*, 561–569.

(11) Andrews, L.; Zhou, M.; Gutsev, G. L. *J. Phys. Chem. A* **2003**, *107*, 990–999.

(12) Elian, M.; Hoffmann, R. *Inorg. Chem.* **1975**, *14*, 1058–1076.

(13) Burdett, J. K. *Inorg. Chem.* **1975**, *14*, 375–382.

(14) Burdett, J. K. *J.Chem. Soc., Faraday Trans. 2* **1974**, *70*, 1599–1613.

(15) Fox, B. J.; Sun, Q. Y.; DiPasquale, A. G.; Fox, A. R.; Rheingold, A. L.; Figueroa, J. S. *Inorg. Chem.* **2008**, *47*, 9010–9020.

(16) Ditri, T. B.; Fox, B. J.; Moore, C. E.; Rheingold, A. L.; Figueroa, J. S. *Inorg. Chem.* **2009**, *48*, 8362–8375.

(17) Yamamoto, Y. *Coord. Chem. Rev.* **1980**, *32*, 193–233.

(18) Sarapu, A. C.; Fenske, R. F. *Inorg. Chem.* **1974**, *14*, 247–253.

(19) Malatesta, L.; Bonati, F. *Isocyanide complexes of metals*; Wiley, 1969.

(20) Bonati, F.; Minghetti, G. *Inorg. Chim. Acta* **1974**, *9*, 95–112.

(21) Twamley, B.; Haubrich, S. T.; Power, P. P. *Adv. Organomet. Chem.* **1999**, *44*, 1–65.

(22) Clyburne, J. A. C.; McMullen, N. *Coord. Chem. Rev.* **2000**, *210*, 73–99.

(23) Wolf, R.; Ni, C.; Nguyen, T.; Brynda, M.; Long, G. J.; Sutton, A. D.; Fischer, R. C.; Fettinger, J. C.; Hellman, M.; Pu, L.; Power, P. P. *Inorg. Chem.* **2007**, *46*, 11277–11290.

(24) Wolf, R.; Brynda, M.; Ni, C.; Long, G. J.; Power, P. P. *J. Am. Chem. Soc.* **2007**, *129*, 6076–6077.

(25) Waterman, R.; Hillhouse, G. L. *Organometallics* **2003**, *22*, 5182–5184.

(26) Smith, R. C.; Shah, S.; Urnezius, E.; Protasiewicz, J. D. *J. Am. Chem. Soc.* **2002**, *125*, 40–41.

(27) Shah, S.; Simpson, M. C.; Smith, R. C.; Protasiewicz, J. D. *J. Am. Chem. Soc.* **2001**, *123*, 6925–6926.

(28) Robinson, G. H. *Chem. Commun.* **2000**, 2175–2181.

(29) Robinson, G. H. *Acc. Chem. Res.* **1999**, *32*, 773–782.

(30) Rivard, E.; Power, P. P. *Inorg. Chem.* **2007**, *46*, 10047–10064.

(31) Power, P. P. *Organometallics* **2007**, *26*, 4362–4372.

(32) Power, P. P. *Chem. Commun.* **2003**, 2091–2101.

(33) Power, P. P. *Chem. Rev.* **1999**, *99*, 3463–3504.

(34) Ni, C.; Power, P. In *Metal–Metal Bonding*; Parkin, G., Ed.; Springer Berlin Heidelberg: 2010; Vol. 136, p 59–111.

(35) Nguyen, T.; Sutton, A. D.; Brynda, M.; Fettinger, J. C.; Long, G. J.; Power, P. P. *Science* **2005**, *310*, 844–847.

(36) Klein, D. P.; Young, V. G.; Tolman, W. B.; Que, L. *Inorg. Chem.* **2006**, *45*, 8006–8008.

(37) Kays, D. L. *Dalton Trans.* **2011**, *40*, 769–778.

(38) Gavenonis, J.; Tilley, T. D. *Organometallics* **2004**, *23*, 31–43.

(39) Gavenonis, J.; Tilley, T. D. *Organometallics* **2002**, *21*, 5549–5563.

(40) Filippou, A. C.; Weidemann, N.; Philippopoulos, A. I.; Schnakenburg, G. *Angew. Chem., Int. Ed. Engl.* **2006**, *45*, 5987–5991.

(41) Carson, E. C.; Lippard, S. J. *Inorg. Chem.* **2006**, *45*, 828–836.

(42) Fox, B. J.; Millard, M. D.; DiPasquale, A. G.; Rheingold, A. L.; Figueroa, J. S. *Angew. Chem., Int. Ed.* **2009**, *48*, 3473–3477.

(43) Emerich, B. M.; Moore, C. E.; Fox, B. J.; Rheingold, A. L.; Figueroa, J. S. *Organometallics* **2011**, *30*, 2598–2608.

(44) Labios, L. A.; Millard, M. D.; Rheingold, A. L.; Figueroa, J. S. *J. Am. Chem. Soc.* **2009**, *131*, 11318–11319.

(45) Margulieux, G. W.; Weidemann, N.; Lacy, D. C.; Moore, C. E.; Rheingold, A. L.; Figueroa, J. S. *J. Am. Chem. Soc.* **2010**, *132*, 5033–5035.

(46) Wegman, R. W.; Brown, T. L. *J. Am. Chem. Soc.* **1980**, *102*, 2494–2495.

(47) Nalesnik, T. E.; Orchin, M. *Organometallics* **1982**, *1*, 222–223.

(48) Klingler, R. J.; Rathke, J. W. *J. Am. Chem. Soc.* **1994**, *116*, 4772–4785.

(49) Muetterties, E. L.; Stein, J. *Chem. Rev.* **1979**, *79*, 479–490.

(50) Heck, R. F.; Breslow, D. S. *J. Am. Chem. Soc.* **1961**, *83*, 4023–4027.

(51) Hebrard, F. d. r.; Kalck, P. *Chem. Rev.* **2009**, *109*, 4272–4282.

(52) Chiu, K. W.; Jones, R. A.; Wilkinson, G.; Galas, A. M. R.; Hursthouse, M. B. *J. Chem. Soc., Dalton Trans.* **1981**, 2088–2097.

(53) Mann, K. R.; Cimolino, M.; Geoffroy, G. L.; Hammond, G. S.; Orio, A. A.; Albertin, G.; Gray, H. B. *Inorg. Chim. Acta* **1976**, *16*, 97–101.

(54) Bassett, J.–M.; Berry, D. E.; Barker, G. K.; Green, M.; Howard, J. A. K.; Stone, F. G. A. *J. Chem. Soc., Dalton Trans.* **1979**, 1003–1011.

(55) Stoffelbach, F.; Saurenz, D.; Poli, R. *Eur. J. Inorg. Chem.* **2001**, *2001*, 2699–2703.

(56) Yamamoto, Y. *The Journal of Organic Chemistry* **2007**, *72*, 7817–7831.

(57) Singh, P. P.; Srivastava, S. K.; Srivastava, A. K. *Journal of Inorganic and Nuclear Chemistry* **1980**, *42*, 521–532.

(58) Colton, R.; Tomkins, I. *Aust. J. Chem.* **1966**, *19*, 1143–1146.

(59) Colton, R.; Tomkins, I. *Aust. J. Chem.* **1966**, *19*, 1519–1521.

(60) Anker, M.; Colton, R.; Tomkins, I. *Aust. J. Chem.* **1967**, *20*, 9–12.

(61) Colton, R.; Rix, C. *Aust. J. Chem.* **1968**, *21*, 1155–1158.

(62) Bowden, J.; Colton, R. *Aust. J. Chem.* **1968**, *21*, 2657–2661.

(63) Colton, R.; Rix, C. *Aust. J. Chem.* **1969**, *22*, 305–310.

(64) Drew, M.; Tomkins, I.; Colton, R. *Aust. J. Chem.* **1970**, *23*, 2517–2520.

(65) Filippou, A. C.; Grünleitner, W. *J. Organomet. Chem.* **1990**, *398*, 99–115.

(66) Coville, N. J.; Albers, M. O. *Inorg. Chim. Acta* **1982**, *65*, L7–L8.

(67) Albers, M. O.; Coville, N. J.; Ashworth, T. V.; Singleton, E.; Swanepoel, H. E. *J. Organomet. Chem.* **1980**, *199*, 55–62.

(68) Weidemann, N.; Margulieux, G. W.; Moore, C. E.; Rheingold, A. L.; Figueroa, J. S. *Inorg. Chim. Acta* **2010**, *364*, 238–245.

(69) Cotton, F. A.; Poli, R. *Inorg. Chem.* **1987**, *26*, 1514–1518.

(70) Poli, R.; Mui, H. D. *J. Am. Chem. Soc.* **1990**, *112*, 2446–2448.

(71) Hoffmann, R.; Beier, B. F.; Muetterties, E. L.; Rossi, A. R. *Inorg. Chem.* **1977**, *16*, 511–522.

(72) Drew, M. G. B. In *Prog. Inorg. Chem.*; John Wiley & Sons, Inc.: 2007, p 67–210.

(73) Shiu, K.–B.; Liou, K.–S.; Wang, S.–L.; Cheng, C. P.; Wu, F.–J. *J. Organomet. Chem.* **1989**, *359*, C1–C4.

(74) Shiu, K. B.; Liou, K. S.; Wang, S. L.; Wei, S. C. *Organometallics* **1990**, *9*, 669–675.

(75) Templeton, J. L.; Winston, P. B.; Ward, B. C. *J. Am. Chem. Soc.* **1981**, *103*, 7713–7721.

(76) Kubacek, P.; Hoffmann, R. *J. Am. Chem. Soc.* **1981**, *103*, 4320–4332.

(77) Colton, R. *Coord. Chem. Rev.* **1971**, *6*, 269–284.

(78) Davidson, J. L.; Vasapollo, G. *J. Chem. Soc., Dalton Trans.* **1985**, 2231–2238.

(79) Cotton, F. A.; Poli, R. *J. Am. Chem. Soc.* **1986**, *108*, 5628–5629.

(80) Colton, R.; Scollary, G.; Tomkins, I. *Aust. J. Chem.* **1968**, *21*, 15–19.

(81) Lyons, D.; Wilkinson, G.; Thornton–Pett, M.; Hursthouse, M. B. *J. Chem. Soc., Dalton Trans.* **1984**, 695–700.

(82) Alvarez, R.; Carmona, E.; Galindo, A.; Gutierrez, E.; Marin, J. M.; Monge, A.; Poveda, M. L.; Ruiz, C.; Savariault, J. M. *Organometallics* **1989**, *8*, 2430–2439.

(83) Green, M. L. H.; Parkin, G.; Chen, M.; Prout, K. *J. Chem. Soc., Dalton Trans.* **1986**, 2227–2236.

(84) Zhu, G.; Parkin, G. *Inorg. Chem.* **2005**, *44*, 9637–9639.

(85) Dreyer, E. B.; Lam, C. T.; Lippard, S. J. *Inorg. Chem.* **1979**, *18*, 1904–1908.

(86) Boyer, P. M.; Roy, C. P.; Bielski, J. M.; Merola, J. S. *Inorg. Chim. Acta* **1996**, *245*, 7–15.

(87) Cotton, F. A.; Dunbar, K. R.; Poli, R. *Inorg. Chem.* **1986**, *25*, 3700–3703.

(88) Green, M. L. H.; Silverthorn, W. E. *J. Chem. Soc., Dalton Trans.* **1973**, 301–306.

(89) Luck, R. L.; Morris, R. H.; Sawyer, J. F. *Organometallics* **1984**, *3*, 247–255.

(90) Luck, R.; Morris, R. H. *Inorg. Chem.* **1984**, *23*, 1489–1491.

(91) Ernst, M. F.; Roddick, D. M. *Organometallics* **1990**, *9*, 1586–1594.

(92) Hubig, S. M.; Lindeman, S. V.; Kochi, J. K. *Coord. Chem. Rev.* **2000**, *200–202*, 831–873.

(93) Atwood, J. L.; Hunter, W. E.; Rogers, R. D.; Carmona–Guzman, E.; Wilkinson, G. *J. Chem. Soc., Dalton Trans.* **1979**, 1519–1523.

(94) Radonovich, L. J.; Koch, F. J.; Albright, T. A. *Inorg. Chem.* **1980**, *19*, 3373–3379.

(95) Arney, D. J.; Wexler, P. A.; Wigley, D. E. *Organometallics* **1990**, *9*, 1282–1289.

(96) Wexler, P. A.; Wigley, D. E.; Koerner, J. B.; Albright, T. A. *Organometallics* **1991**, *10*, 2319–2327.

(97) Jones, N. G.; Green, M. L. H.; Vei, I. C.; Rees, L. H.; Pascu, S. I.; Watkin, D.; Cowley, A.; Morise, X.; Braunstein, P. *J. Chem. Soc., Dalton Trans.* **2002**, 2491–2500.

(98) Kuiper, D. S.; Wolczanski, P. T.; Lobkovsky, E. B.; Cundari, T. R. *Inorg. Chem.* **2008**, *47*, 10542–10553.

(99) Pangborn, A. B.; Giardello, M. A.; Grubbs, R. H.; Rosen, R. K.; Timmers, F. J. *Organometallics* **1996**, *15*, 1518–1520.

(100) Arnarego, W. L. F.; Chai, C. L. L. *Purification of Laboratory Chemicals*; 5th ed.; Elsevier, 2003.

(101) Kubas, G. J.; Van der Sluis, L. S. *Inorg. Synth.* **1990**, *28*, 29–33.

(102) Burla, M. C.; Caliandro, R.; Camalli, M.; Carrozzini, B.; Cascarano, G. L.; De Caro, L.; Giacovazzo, C.; Polidori, G.; Spagna, R. *J. Appl. Crystallogr.* **2005**, *38*, 381–388.

(103) Sheldrick, G. M. *Acta. Crystallogr.* **2008**, *64*, 112–122.

Chapter 4

Chloro– and Trifluoromethyl–Substituted Flanking–Ring *m*–Terphenyl Isocyanides: η^6–Arene Binding to Zerovalent Molybdenum Centers and Comparison to Alkyl–Substituted Derivatives

4.1 Introduction

Over the past two decades, the *m*–terphenyl group has become an important and extensively utilized ancillary framework for the stabilization of low–coordinate transition–metal and main–group complexes.[1–11] The appeal of the *m*–terphenyl framework as a ligand is derived from its ability to foster an encumbering and protective environment around a central atom or group of atoms. It has also found wide use because of the relative ease in which the steric properties of framework can be modified. Whereas *σ*–aryl *m*–terphenyl derivatives are convenient to prepare and have been broadly employed,[1–4,6–11] it is important to note that a

variety of donor atoms and groups have also been appended to the central framework ring to provide altered ligation properties. Accordingly, *m*–terphenyl–based aryloxides,[12–16] thiolates,[17–20] amidos[21–29], imidos,[30,31] and carboxylates,[32–38] have all been reported as ancillary ligands for either transition–metal and main–group systems. Our group has used the *m*–terphenyl framework in conjunction with the isocyanide functionality (CNR) in an effort to study a class of encumbering ligands that mimic the electronic properties of carbon monoxide (CO).[39–43] We have used these ligands for the generation of low–coordinate isocyanide complexes that are reminiscent of the binary unsaturated transition–metal carbonyls (*e.g.* $Co(CO)_4$, $Ni(CO)_3$ and $Pd(CO)_2$).[44–48]

During our studies of cobalt complexes supported by the *m*–terphenyl isocyanide ligand $CNAr^{Mes2}$ (Ar^{Mes2} = 2,6–(2,4,6–$Me_3C_6H_2)_2C_6H_3$), we uncovered that the flanking mesityl rings of this ligand could provide a robust η^6–arene interaction to low–valent cobalt centers.[48] Formation of this interaction clearly results as an effort to maximize coordinative saturation, especially in very low–coordinate environments. However, when coordinatively–unsaturated metal centers are the intended synthetic targets, the propensity of the *m*–terphenyl framework to engage in η^6–arene coordination is an undesirable property. Notably, 'η^6–capping' of low–coordinate metal fragments by flanking rings has been observed by Power, Dilworth, Rothwell and others for σ–aryl,[49,50] amido,[22] thiolate,[17,51–53] aryloxide,[54–57] phosphine,[58] and acetylene[59] *m*–terphenyl–based ligands. In these examples, the η^6–bound flanking arene rings are unsubstituted (C_6H_5) or feature 2,4,6–trimethyl (*i.e.* mesityl; Mes = 2,4,6–$Me_3C_6H_2$), 2,6–diisopropyl (*i.e.* Dipp = 2,6–(*i*–Pr)$_2C_6H_3$) or 2,4,6–triisopropyl (*i.e.* Tripp = 2,4,6–(*i*–Pr)$_3C_6H_2$) substitution patterns.

As an attempt to circumvent this problem, we reasoned that electron–withdrawing substituents on the flanking aryl rings of the *m*–terphenyl framework might provide a sufficiently deactivated arene system to resist η^6–coordination to low–coordinate and low–

valent metal centers. This idea stems from the fact that electron–deficient arenes are well known to foster kinetically labile η^6–interactions to low–valent, middle d–block transition–metals.[60–68] This behavior is especially pronounced when compared to arenes possessing electron–releasing alkyl groups. Furthermore, *m*–terphenyl groups featuring electron withdrawing substituents on the flanking rings are not common in coordination chemistry,[69–72] which warranted their synthesis and incorporation into an *m*–terphenyl isocyanide ligand. Such derivatives would additionally provide an important steric and electronic comparison to the alkyl–substituted *m*–terphenyl isocyanides $CNAr^{Mes2}$ and $CNAr^{Dipp2}$ (Ar^{Dipp2} = 2,6–(2,6–(*i*–Pr)$_2$C$_6$H$_3$)$_2$C$_6$H$_3$).[40,42,43] Presented in this report are the syntheses of the halo–substituted *m*–terphenyl isocyanide ligands, $CNAr^{Clips2}$ (Ar^{Clips2} = 2,6–(2,6–Cl$_2$C$_6$H$_3$)$_2$(4–*t*–Bu)C$_6$H$_2$) and $CNAr^{DArF2}$ (Ar^{DArF2} = 2,6–(3,5–(CF$_3$)$_2$C$_6$H$_3$)$_2$C$_6$H$_3$), and a demonstration of their coordination behavior towards zerovalent molybdenum centers. Furthermore, the abilities of $CNAr^{Clips2}$ and $CNAr^{DArF2}$ to foster a flanking–arene η^6–interaction are compared with those of $CNAr^{Mes2}$ and $CNAr^{Dipp2}$. While these halo–substituted *m*–terphenyls can bind in an η^6–fashion, the formation of such interactions is significantly less facile than for their alkyl–substituted counterparts. In addition, η^6–interactions from halo–substituted *m*–terphenyls are found to be fairly labile in some cases and therefore may be considered a potentially effective ‘masking’ strategy for reactive, low–valent metal centers.

4.2 Flanking–Ring Binding of the Isocyanides $CNAr^{Dipp2}$ and $CNAr^{Mes2}$ to Zerovalent Molybdenum

In a previous study, we reported our efforts to generate the two–coordinate molybdenum bis–isocyanide complex [Mo($CNAr^{Dipp2}$)$_2$] through a tandem oxidative–decarbonylation/reduction synthetic sequence.[42] This approach was not successful for its

intended target. Instead, zerovalent, bis–isocyanide–η^6–arene complexes of molybdenum were isolated when the reduction step was carried out in arene solvents, whereas intractable mixtures were produced when chemical reductions were performed in higher–polarity solvents such as Et_2O or THF. These observations, and the operational inconvenience of the tandem oxidative–decarbonylation/reduction sequence, prompted us to find a more direct synthetic route to low–coordinate, zerovalent molybdenum *m*–terphenyl isocyanide complexes. Accordingly, we turned molybdenum bis–naphthalene ($Mo(\eta^6–C_{10}H_8)_2$) as a synthetic precursor,[73] as this complex has been shown to serve as a source of zerovalent molybdenum upon reaction with monodentate neutral donor ligands such as isocyanides and phosphines (PR_3).[74,75]

Treatment of a benzene solution of $Mo(\eta^6–C_{10}H_8)_2$ with 3.0 equivalents of $CNAr^{Dipp2}$ proceeds to the trisisocyanide, η^6–arene complex $Mo(\eta^6–(Dipp)–\kappa^1–C–CNAr^{Dipp})(CNAr^{Dipp2})_2$ (**23**) with the loss of two equivalents of naphthalene (Scheme 4.1). Addition of 3.0 equivalents of the less encumbering isocyanide $CNAr^{Mes2}$ to $Mo(\eta^6–C_{10}H_8)_2$ in benzene similarly produces $Mo(\eta^6–(Mes)–\kappa^1–C–CNAr^{Mes})(CNAr^{Mes2})_2$ (**24**, Scheme 4.1), which possesses an η^6–bound mesityl ring. The ^1H NMR spectra of $Mo(\eta^6–(Dipp)–\kappa^1–C–CNAr^{Dipp})(CNAr^{Dipp2})_2$ (**23**) and $Mo(\eta^6–(Mes)–\kappa^1–C–CNAr^{Mes})(CNAr^{Mes2})_2$ (**24**) exhibit an overall C_s–symmetric pattern of Ar^{R2} residues and upfield–shifted arene resonances consistent with the η^6–binding of a single *m*–terphenyl flanking ring. Structural characterization of both $Mo(\eta^6–(Dipp)–\kappa^1–C–CNAr^{Dipp})(CNAr^{Dipp2})_2$ (**23**) and $Mo(\eta^6–(Mes)–\kappa^1–C–CNAr^{Mes})(CNAr^{Mes2})_2$ (**24**) (Figures 4.1 and 4.2) revealed that each adopts the three–legged piano stool motif typical for Group–6 metal (η^6–arene)ML_3 complexes. However, $Mo(\eta^6–(Dipp)–\kappa^1–C–CNAr^{Dipp})(CNAr^{Dipp2})_2$ (**23**) and $Mo(\eta^6–(Mes)–\kappa^1–C–CNAr^{Mes})(CNAr^{Mes2})_2$ (**24**) are unique with respect to the geometric constraints that η^6–binding of the flanking–arene ring places on the isocyanide unit to which it is attached. As

shown in Figures 4.1 and 4.2, η^6–binding of either a Dipp or Mes ring results in significantly bent C_{iso}–N–C_{ipso} angles of 120.4(7)˚ and 120.60(17)˚ in Mo(η^6–(Dipp)–κ^1–*C*–$CNAr^{Dipp}$)($CNAr^{Dipp2}$)$_2$ (**23**) and Mo(η^6–(Mes)–κ^1–*C*–$CNAr^{Mes}$)($CNAr^{Mes2}$)$_2$ (**24**), respectively. According to the Cambridge Structural Database, these values represent the most acute C_{iso}–N–C angles for structurally characterized isocyanide complexes to date.[76] The geometrically constrained isocyanide ligands in Mo(η^6–(Dipp)–κ^1–*C*–$CNAr^{Dipp}$)($CNAr^{Dipp2}$)$_2$ (**23**) and Mo(η^6–(Mes)–κ^1–*C*–$CNAr^{Mes}$)($CNAr^{Mes2}$)$_2$ (**24**) also feature greatly elongated isocyanide C–N bond lengths of 1.249(11) Å and 1.243(2) Å, respectively, and display very low energy ν_{CN} bands of 1652 cm^{-1} and 1643 cm^{-1}, respectively, in their IR spectra (Table 4.1). Importantly, we believe these structural and spectroscopic properties result from a disruption of N→C π–donation, rather than from significant M→ligand π back–donation, as a consequence of the geometric constraints placed on the isocyanide by flanking–ring η^6–binding. These observations, and the fact that the constrained C_{iso} atoms in Mo(η^6–(Dipp)–κ^1–*C*–$CNAr^{Dipp}$)($CNAr^{Dipp2}$)$_2$ (**23**) and Mo(η^6–(Mes)–κ^1–*C*–$CNAr^{Mes}$)($CNAr^{Mes2}$)$_2$ (**24**) give rise to very large down–field chemical shifts (**23** δ = 281.6 ppm (C_6D_6); **24** δ = 278.0 ppm (C_6D_6)), suggest that η^6–arene tethering imparts significant and static carbenic character on the isocyanide carbon of these ligands.

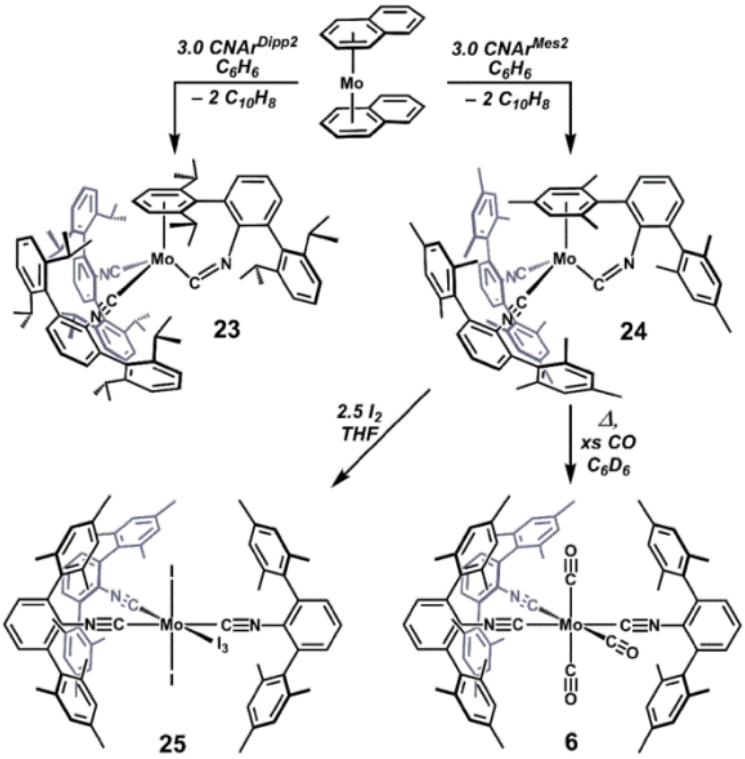

Scheme 4.1. Synthesis and reactivity of Mo(η^6–(Dipp)–κ^1–*C*–CNAr^{Dipp})(CNAr^{Dipp2})$_2$ (**23**) and Mo(η^6–(Mes)–κ^1–*C*–CNAr^{Mes})(CNAr^{Mes2})$_2$ (**24**).

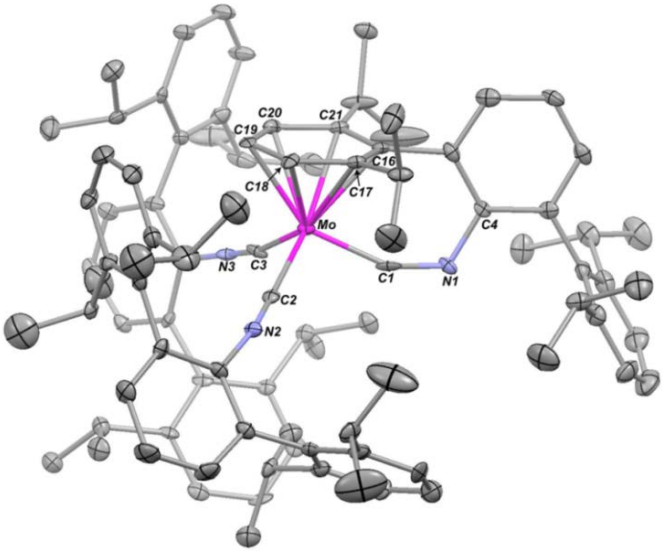

Figure 4.1. Molecular Structure of Mo(η^6–(Dipp)–κ^1–*C*–CNAr^{Dipp})(CNAr^{Dipp2})$_2$ (**23**). Selected bond distances (Å) and angles (Deg): Mo1–C1 = 1.939(9); Mo1–C2 = 2.042(6); Mo1–C3 = 2.060(7); Mo1–C16 = 2.317(6); Mo1–C17 = 2.361(6); Mo1–C18 = 2.295(6); Mo1–C19 = 2.329(6); Mo1–C20 = 2.296(6); Mo1–C21 = 2.346(5); C1–N1 = 1.244(9); N1–C4 = 1.417(7); Mo1–C1–N1 = 155.3(5); C1–N1–C4 = 120.3(6).

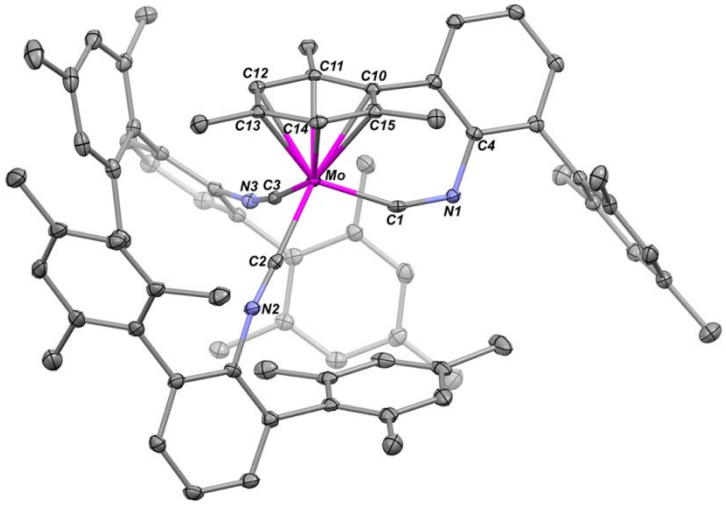

Figure 4.2. Molecular Structure of Mo(η^6–(Mes)–κ^1–*C*–CNAr^{Mes})(CNAr^{Mes2})$_2$ (**24**). Selected bond distances (Å) and angles (Deg): Mo1–C1 = 1.9360(19); Mo1–C2 = 2.0475(19); Mo1–C3 = 2.0045(19); Mo1–C10 = 2.3061(18); Mo1–C11 = 2.3225(18); Mo1–C12 = 2.3133(19); Mo1–C13 = 2.3424(18); Mo1–C14 = 2.3596(18); Mo1–C15 = 2.3667(18); C1–N1 = 1.244(2); N1–C4 = 1.414(2); C1–Mo1–C2 = 102.09(7); Mo1–C1–N1 = 152.63(15); C1–N1–C4 = 120.52(16).

Table 4.1. Spectroscopic and Structural Parameters for the Geometrically–Constrained Ligand in Mo(η^6–(R)–κ^1–*C*–CNAr^R)(CNAr^{R2})$_2$ complexes

Complex	ν_{CN} [a] (cm^{-1})	δC_{iso} [a] (ppm)	$\measuredangle(C_{iso}–N–C_{ipso})$ (deg)	$d(C_{iso}–N)$ (Å)
Mo(η^6–(Dipp)–κ^1–*C*–CNAr^{Dipp})(CNAr^{Dipp2})$_2$ (**23**)	1652	281.6	120.3(6)	1.244(9)
Mo(η^6–(Mes)–κ^1–*C*–CNAr^{Mes})(CNAr^{Mes2})$_2$ (**24**)	1643	278.0	120.52(16)	1.244(2)
Mo(η^6–(2,6–$Cl_2C_6H_3$)–κ^1–*C*–CNAr^{Clips})(CNAr^{Clips2})$_2$ (**29**)	1680	275.6	120.1(2)	1.236(4)
Mo((η^6–(3,5–$(CF_3)_2C_6H_3$)–κ^1–*C*–CNAr^{DArF})(CNAr^{DArF2})$_2$ (**33**)	1717	273.3	120.8(3)	1.229(4)

[a]Measured in C_6D_6 solution.

It is important to note that the flanking–ring η^6–arene interactions in Mo(η^6–(Dipp)–κ^1–*C*–CNAr^{Dipp})(CNAr^{Dipp2})$_2$ (**23**) and Mo(η^6–(Mes)–κ^1–*C*–CNAr^{Mes})(CNAr^{Mes2})$_2$ (**24**) readily form despite the use of benzene as a solvent. In addition, these η^6–arene interactions in Mo(η^6–(Dipp)–κ^1–*C*–CNAr^{Dipp})(CNAr^{Dipp2})$_2$ (**23**) and Mo(η^6–(Mes)–κ^1–*C*–CNAr^{Mes})(CNAr^{Mes2})$_2$ (**24**) cannot be displaced by external arene substrates after synthesis. For example, incorporation of benzene or toluene does not take place when pure Mo(η^6–(Dipp)–κ^1–*C*–CNAr^{Dipp})(CNAr^{Dipp2})$_2$ (**23**) and Mo(η^6–(Mes)–κ^1–*C*–CNAr^{Mes})(CNAr^{Mes2})$_2$ (**24**)

are heated in these solvents up to 120 ˚C for several days. The observation that benzene or toluene does not displace the substituted η^6–arene ligands in Mo(η^6–(Dipp)–κ^1–*C*–CNAr^{Dipp})(CNAr^{Dipp2})$_2$ (**23**) and Mo(η^6–(Mes)–κ^1–*C*–CNAr^{Mes})(CNAr^{Mes2})$_2$ (**24**) is consistent with findings that electron–rich arene ligands foster more thermodynamically stable η^6–arene interactions to transition–metal fragments than electron deficient arenes.[60–68] In the case of Mo(η^6–(Mes)–κ^1–*C*–CNAr^{Mes})(CNAr^{Mes2})$_2$ (**24**), the η^6–arene interaction can be disrupted oxidatively by excess I_2 to form the d^3 diiodo–triiodide complex *mer*–MoI$_2$(I$_3$)(CNAr^{Mes2})$_3$ (**25**, Scheme 4.2, Figure 4.3) or by treatment with an excess of CO under forcing conditions (100 ˚C, 5d) to form *mer*–Mo(CO)$_3$(CNAr^{Mes2})$_3$ (**6**).[43] Neither Mo(η^6–(Dipp)–κ^1–*C*–CNAr^{Dipp})(CNAr^{Dipp2})$_2$ (**23**) nor Mo(η^6–(Mes)–κ^1–*C*–CNAr^{Mes})(CNAr^{Mes2})$_2$ (**24**) react with H_2, H_2O or additional isocyanide ligand in benzene solution at elevated temperatures over the course of several days. The complexes also do not react with the coordinating solvents NCMe or THF at room temperature or above.

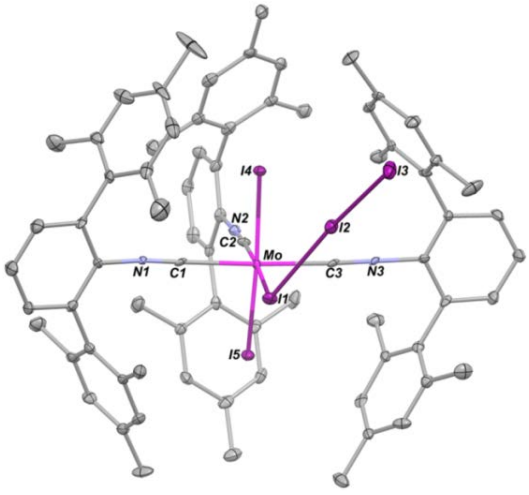

Figure 4.3. Molecular Structure of *mer*–MoI$_2$(I$_3$)(CNAr^{Mes2})$_3$. (**25**) Selected bond distances (Å) and angles (Deg): Mo1–C1 = 2.173(8); Mo1–C2 = 2.120(9); Mo1–C3 = 2.160(9); Mo1–I1 = 2.7756(9); Mo1–I4 = 2.6813(8); Mo1–I5 = 2.7133(8); C1–Mo1–C2 = 92.5(3); C1–Mo1–C3 = 173.1(3); C1–Mo1–I1 = 85.8(2); C1–Mo1–I4 = 88.1(2); C1–Mo1–I5 = 90.7(2); C2–Mo1–C3 = 93.2(3); C2–Mo1–I1 = 176.1(2); C2–Mo1–I4 = 88.1(2); C2–Mo1–I5 = 86.3(2); C3–Mo1–I1 = 88.8(2); C3–Mo1–I4 = 89.3(2); C3–Mo1–I5 = 93.5(2); I1–Mo1–I4 = 95.33(3); I1–Mo1–I5 = 90.26(2); I4–Mo1–I5 = 173.80(3).

4.3 Synthesis of the Halo–Substituted Isocyanide Ligands CNAr^{Clips2} and CNAr^{DArF2}

Despite possessing the empirical formula $Mo(CNR)_3$, the robust η^6–arene interactions in $Mo(\eta^6$–(Dipp)–κ^1–*C*–$CNAr^{Dipp})(CNAr^{Dipp2})_2$ (**23**) and $Mo(\eta^6$–(Mes)–κ^1–*C*–$CNAr^{Mes})(CNAr^{Mes2})_2$ (**24**) do not allow these complexes to serve as structural or functional mimics of the reactive binary carbonyl species $[Mo(CO)_3]$.[77–79] In order to weaken, or ideally prevent, η^6–arene interactions, we sought to synthetically amend electron–withdrawing substituents, such as halides, to the flanking ring of the *m*–terphenyl isocyanide framework. Halo–substituted *m*–terphenyl groups are uncommon, especially for substitution in the flanking rings. However, Protasiewicz has reported the synthesis of the 2,6–dichlorophenyl substituted *m*–terphenyl group 2,6–$(2,6–Cl_2C_6H_3)_2C_6H_3$ for the preparation of sterically protected diphosphenes[72]. Inspired by this report, we prepared the modified 2,6–dichlorophenyl–substituted *m*–terphenyl isocyanide $CNAr^{Clips2}$ from 2,6–$(2,6–Cl_2C_6H_3)_2C_6H_3I$ in five steps as outlined in Scheme 4.2. At the *m*–terphenyl iodide stage, a *para*–*tert*–butyl group was installed on the ligand framework via Friedel–Crafts alkylation to promote solubility and crystallinity, as well as to provide a convenient ^1H NMR handle. The free $CNAr^{Clips2}$ isocyanide is characterized by ν_{CN} stretch of 2132 cm^{-1} (KBr) and a C_{iso} $^{13}C\{^1H\}$ NMR chemical shift of δ = 172.0 ppm (C_6D_6).

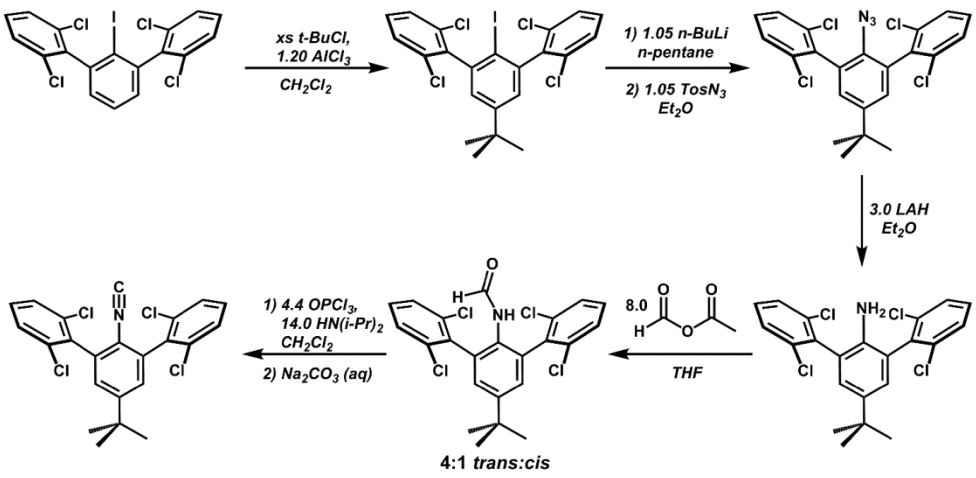

Scheme 4.2. Synthesis of $CNAr^{Clips2}$.

In addition to $CNAr^{Clips2}$, we sought to develop a *m*–terphenyl isocyanide in which the flanking aryl groups were further deactivated towards η^6–binding by the presence of trifluoromethyl (CF_3) groups. Accordingly, we targeted the bis–(trifluoromethyl)phenyl substituted isocyanide $CNAr^{DArF2}$ (Scheme 4.3), which we view as reminiscent of the weakly coordinating tetraarylborate anion $[B(3,5\text{–}(CF_3)_2C_6H_3)_4]^-$ ($[BAr^F{}_4]^-$).[80] Despite the widespread use of $[BAr^F{}_4]^-$ as a counterion,[81] η^6–coordination of one of its 3,5–$(CF_3)_2C_6H_3$ groups to a transition–metal center is currently limited to only two structurally characterized examples.[82,83] As shown in Scheme 4.3, $CNAr^{DArF2}$ is readily synthesized in good overall yield by palladium–catalyzed cross–coupling of 2,6–dibromoaniline with 3,5–$(CF_3)_2C_6H_3B(OH)_2$ and subsequent formylation/dehydration steps. Free $CNAr^{DArF2}$ gives rise to an isocyanide C_{iso} $^{13}C\{^1H\}$ NMR chemical shift of δ = 175.4 ppm in C_6D_6 solution, and its solid–state IR spectrum (KBr) exhibits a ν_{CN} band at 2119 cm^{-1}.

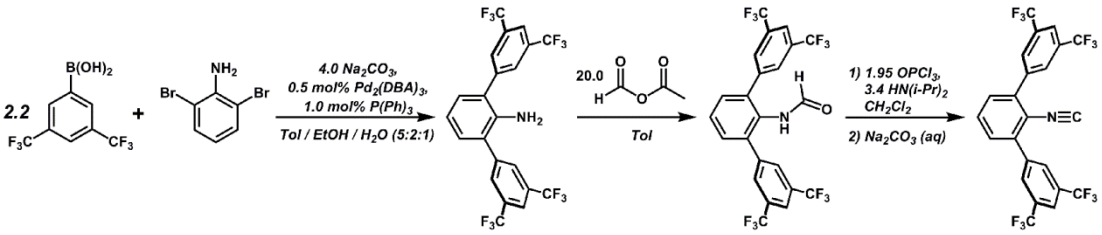

Scheme 4.3. Synthesis of $CNAr^{DArF2}$.

The solid–state IR ν_{CN} bands of $CNAr^{Clips2}$ (2132 cm^{-1}) and $CNAr^{DArF2}$ (2119 cm^{-1}) may also be compared with those of the alkyl–substituted isocyanides $CNAr^{Dipp2}$ and $CNAr^{Mes2}$. The latter exhibit solid–state ν_{CN} bands of 2124 cm^{-1} and 2120 cm^{-1}, respectively. This series of IR data thereby demonstrate that substituent changes on flanking rings or the *para*–position of the *m*–terphenyl framework can have a measured effect on the ν_{CN} band of the uncoordinated, terminal isocyano unit. This observation is in contrast to previous IR and computational studies on *para*– and *ortho*– mono–substituted aryl isocyanides, which have argued that the energy of ν_{CN} bands is not appreciably influenced by substituent changes.[84,85]

4.4 η^6–Arene Molybdenum Complexes Supported by $CNAr^{Clips2}$

Relative to $CNAr^{Dipp2}$ and $CNAr^{Mes2}$, dichlorophenyl–substituted $CNAr^{Clips2}$ displays a lower initial propensity for flanking–ring binding upon reaction with molybdenum η^6–arene starting materials. Treatment of $Mo(\eta^6\text{–}C_{10}H_8)_2$ with 3.0 equivalents of $CNAr^{Clips2}$ in *n*–pentane solution results in the formation of the η^6–naphthalene complex, $Mo(\eta^6\text{–}C_{10}H_8)(CNAr^{Clips2})_3$ (**26**, Scheme 4.4; Figure 4.4a). This outcome contrasts with the reactivity of both $CNAr^{Dipp2}$ and $CNAr^{Mes2}$ towards $Mo(\eta^6\text{–}C_{10}H_8)_2$, where flanking–ring η^6–arene binding is rapid and the corresponding η^6–naphthalene–tris(isocyanide) complexes are not observed (*i.e.* $Mo(\eta^6\text{–}C_{10}H_8)(CNR)_3$; R = Ar^{Dipp2} or Ar^{Mes2}). η^6–Binding of the 2,6–dichlorophenyl group in $CNAr^{Clips2}$ is also disfavored relative to the binding of benzene and

fluorobenzene when these solvents are used in conjunction with the Mo(η^6–$C_{10}H_8$)$_2$ starting material. Thus, treatment of Mo(η^6–$C_{10}H_8$)$_2$ with 3.0 equivalents of $CNAr^{Clips2}$ in either C_6H_6 or C_6H_5F at room temperature results in the rapid formation of the η^6–arene complexes, Mo(η^6–C_6H_6)($CNAr^{Clips2}$)$_3$ (**27**) and Mo(η^6–C_6H_5F)($CNAr^{Clips2}$)$_3$ (**28**), respectively (Scheme 4.4; Figure 4.4b–c). The molecular structures of Mo(η^6–$C_{10}H_8$)($CNAr^{Clips2}$)$_3$ (**26**), Mo(η^6–C_6H_6)($CNAr^{Clips2}$)$_3$ (**27**) and Mo(η^6–C_6H_5F)($CNAr^{Clips2}$)$_3$ (**28**) as determined by X–ray diffraction are shown in Figure 4.4. Each complex adopts the standard three–legged piano stool structural motif and exhibits a roughly C_3–symmetric orientation of $CNAr^{Clips2}$ ligands. The molybdenum centers in Mo(η^6–C_6H_6)($CNAr^{Clips2}$)$_3$ (**27**) and Mo(η^6–C_6H_5F)($CNAr^{Clips2}$)$_3$ display symmetric coordination of the η^6–arene carbon atoms. In contrast, Mo(η^6–$C_{10}H_8$)($CNAr^{Clips2}$)$_3$ (**26**) displays an asymmetric η^6–arene interaction that is ‘slipped’ away from the ring–junction carbon atoms of the naphthalene ligand. These so–called ‘flat–slipped’ η^6–interactions are well documented and arise to maximize orbital overlap between the metal center and the HOMO of naphthalene, which possesses a node at the ring–junction carbon atoms.[65,86]

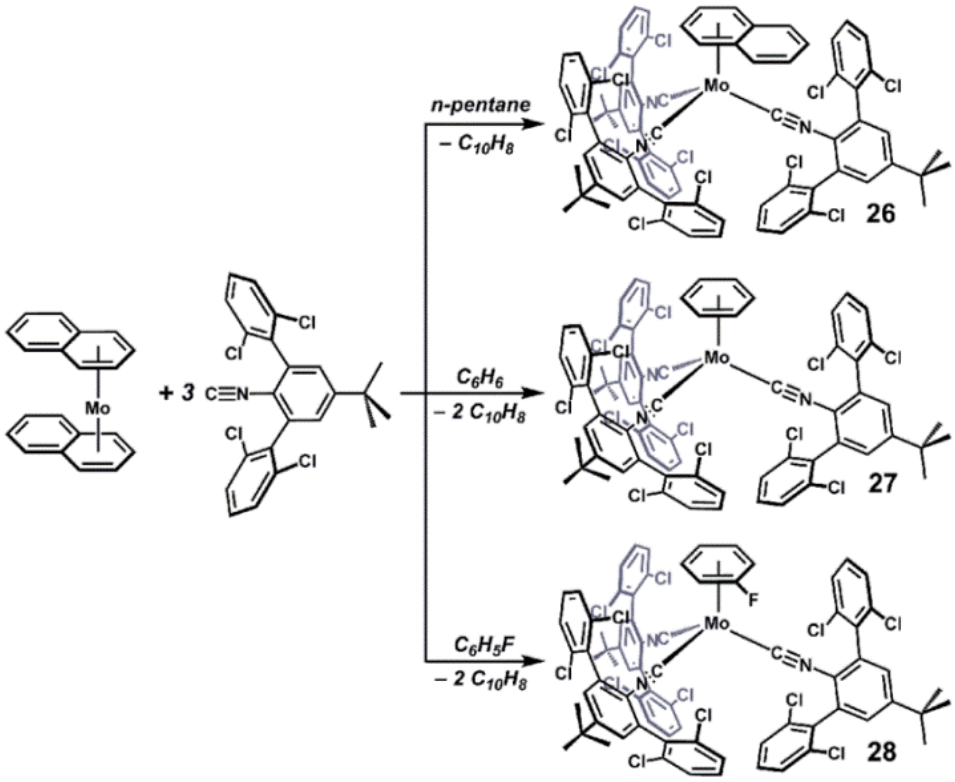

Scheme 4.4. Metathesis reactions between Mo(η^6–$C_{10}H_8$)$_2$ and CNAr^{Clips2}.

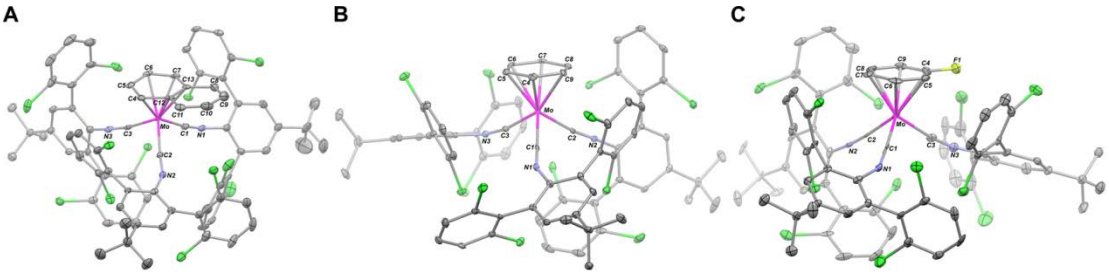

Figure 4.4. A) Molecular Structure of Mo(η^6–$C_{10}H_8$)(CNAr^{Clips2})$_3$ (**26**). Selected bond distances (Å) and angles (˚): Mo1–C1 = 2.035(8); Mo1–C2 = 2.015(7); Mo1–C3 = 1.998(8); Mo1–C4 = 2.325(8); Mo1–C5 = 2.319(8); Mo1–C6 = 2.313(8); Mo1–C7 = 2.287(7); Mo1–C12 = 2.461(8); Mo1–C13 = 2.424(8); C1–Mo1–C2 = 95.3(2); C1–Mo1–C3 = 90.9(3); C2–Mo1–C3 = 95.7(3). B) Molecular Structure of Mo(η^6–C_6H_6)(CNAr^{Clips2})$_3$ (**27**). Selected bond distances (Å) and angles (˚): Mo1–C1 = 2.020(4); Mo1–C2 = 2.013(4); Mo1–C3 = 1.995(4); Mo1–C4 = 2.322(4); Mo1–C5 = 2.358(4); Mo1–C6 = 2.310(4); Mo1–C7 = 2.326(4); Mo1–C8 = 2.302(4); Mo1–C9 = 2.352(4); C1–Mo1–C2 = 92.83(14); C1–Mo1–C3 = 96.17(14); C2–Mo1–C3 = 90.75(15). C) Molecular Structure of Mo(η^6–C_6H_5F)(CNAr^{Clips2})$_3$ (**28**). Selected bond distances (Å) and angles (˚): Mo1–C1 = 2.016(8); Mo1–C2 = 2.029(7); Mo1–C3 = 2.011(8); Mo1–C4 = 2.316(9); Mo1–C5 = 2.348(8); Mo1–C6 = 2.297(7); Mo1–C7 = 2.346(7); Mo1–C8 = 2.277(7); Mo1–C9 = 2.322(8); C1–Mo1–C2 = 89.8(3); C1–Mo1–C3 = 96.5(3); C2–Mo1–C3 = 89.1(3).

Although an η^6–dichlorophenyl interaction does not form upon reaction of $CNAr^{Clips2}$ with Mo(η^6–$C_{10}H_8$)$_2$ at room temperature, its formation can be induced from thermolysis of the resultant products. Accordingly, heating *n*–pentane solutions of either Mo(η^6–$C_{10}H_8$)($CNAr^{Clips2}$)$_3$ (**26**) or Mo(η^6–C_6H_6)($CNAr^{Clips2}$)$_3$ (**27**) at 60 ˚C for 12 h results in arene loss and formation of the η^6–dichlorophenyl complex, Mo(η^6–(2,6–$Cl_2C_6H_3$)–κ^1–*C*–$CNAr^{Clips}$)($CNAr^{Clips2}$)$_2$ (**29**, Scheme 4.5). Structural characterization of Mo(η^6–(2,6–$Cl_2C_6H_3$)–κ^1–*C*–$CNAr^{Clips}$)($CNAr^{Clips2}$)$_2$ (**29**, Figure 4.5) revealed a geometrically constrained isocyanide ligand similar to those found in Mo(η^6–(Dipp)–κ^1–*C*–$CNAr^{Dipp}$)($CNAr^{Dipp2}$)$_2$ (**23**) and Mo(η^6–(Mes)–κ^1–*C*–$CNAr^{Mes}$)($CNAr^{Mes2}$)$_2$ (**24**) (Table 4.1). The $^{13}C\{^1H\}$ NMR chemical shift and ν_{CN} IR stretch of the bent C_{iso} atom in Mo(η^6–(2,6–$Cl_2C_6H_3$)–κ^1–*C*–$CNAr^{Clips}$)($CNAr^{Clips2}$)$_2$ (**29**) are δ = 275.6 ppm (C_6D_6) and 1680 cm^{-1} (C_6D_6), respectively, which are also similar to the spectroscopic properties found for Mo(η^6–(Dipp)–κ^1–*C*–$CNAr^{Dipp}$)($CNAr^{Dipp2}$)$_2$ (**23**) and Mo(η^6–(Mes)–κ^1–*C*–$CNAr^{Mes}$)($CNAr^{Mes2}$)$_2$ (**24**) (Table 4.1). Furthermore, like its alkyl–substituted analogues, Mo(η^6–(2,6–$Cl_2C_6H_3$)–κ^1–*C*–$CNAr^{Clips}$)($CNAr^{Clips2}$)$_2$ (**29**) is resistant toward further reaction at room temperature with coordinating solvents, such as acetonitrile and THF, as well as arene solvents such as benzene and toluene. Thus, although the 2,6–dichlorophenyl group of $CNAr^{Clips2}$ does not readily displace η^6–coordinated arenes, once bound, it is not readily displaced from the molybdenum center by more electron–releasing arenes.

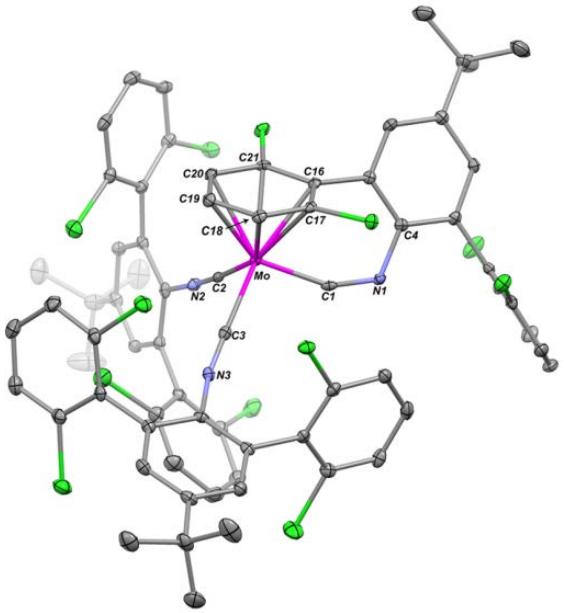

Figure 4.5. Molecular Structure Mo(η^6–(2,6–$Cl_2C_6H_3$)–κ^1–*C*–$CNAr^{Clips}$)($CNAr^{Clips2}$)$_2$ (**29**). Selected bond distances (Å) and angles (˚): Mo1–C1 = 1.928(3); Mo1–C2 = 2.036(3); Mo1–C3 = 2.051(3); C1–N1 = 1.235(4); N1–C4 = 1.408(4); Mo1–C16 = 2.316(3); Mo1–C17 = 2.323(3); Mo1–C18 = 2.333(3); Mo1–C19 = 2.334(3); Mo1–C20 = 2.330(3); Mo1–C21 = 2.314(3); C1–Mo1–C2 = 96.55(11); C1–Mo1–C3 = 98.50(11); C2–Mo1–C3 = 89.18(11); Mo1–C1–N1 = 153.5(2); C1–N1–C4 = 120.1(2).

While it can be isolated in pure form, it is important to note that the η^6–dichlorophenyl complex Mo(η^6–(2,6–$Cl_2C_6H_3$)–κ^1–*C*–$CNAr^{Clips}$)($CNAr^{Clips2}$)$_2$ (**29**) is not formed exclusively upon thermolysis of Mo(η^6–$C_{10}H_8$)($CNAr^{Clips2}$)$_3$ (**26**) or Mo(η^6–C_6H_6)($CNAr^{Clips2}$)$_3$ (**27**). As shown in Scheme 4.5, these thermolysis reactions produce Mo(η^6–(2,6–$Cl_2C_6H_3$)–κ^1–*C*–$CNAr^{Clips}$)($CNAr^{Clips2}$)$_2$ (**29**) along with the paramagnetic tetraisocyanide–dichloride complex *trans*–$MoCl_2(CNAr^{Clips2})_4$ (**30**) and the diphenanthridine (**31**). Thermolysis of either Mo(η^6–$C_{10}H_8$)($CNAr^{Clips2}$)$_3$ (**26**) or Mo(η^6–C_6H_6)($CNAr^{Clips2}$)$_3$ (**27**) produce Mo(η^6–(2,6–$Cl_2C_6H_3$)–κ^1–*C*–$CNAr^{Clips}$)($CNAr^{Clips2}$)$_2$ (**29**) and diphenanthridine (**31**) in roughly a 4:1 ratio as determined by ^{1}H NMR spectroscopy, and we presume that paramagnetic dichloride *trans*–$MoCl_2(CNAr^{Clips2})_4$ (**30**) is generated in roughly equimolar quantities to the diphenanthridine (**31**). Each compound can be isolated by successive

washings in benzene, thereby enabling their full characterization by NMR spectroscopic and X–ray diffraction methods (Figures 4.6 and 4.7). The formation of diphenanthridine (**31**) can be rationalized as a product resulting from chlorine–atom abstraction, phenyl–radical addition to an isocyanide unit and bimolecular coupling of two cyclized, Ar^{Clips}–based phenanthridine radicals. The initiation step in this sequence is likely chlorine–atom transfer from a $CNAr^{Clips2}$ ligand to a low–valent molybdenum center, which then enables the formation of *trans*–$MoCl_2(CNAr^{Clips2})_4$ (**30**). Contrastingly however, heating pure Mo(η^6–(2,6–$Cl_2C_6H_3$)–κ^1–*C*–$CNAr^{Clips}$)$(CNAr^{Clips2})_2$ (**29**) at 90 ˚C in cyclohexane–d_{12} produces only trace quantities of Mo(η^6–$C_{10}H_8$)$(CNAr^{Clips2})_3$ (**26**) and Mo(η^6–C_6H_6)$(CNAr^{Clips2})_3$ (**27**) after a 24 h period. This observation suggests that independent arene–displacement and chlorine–atom–abstraction pathways are available at elevated temperatures to the η^6–naphthalene and η^6–benzene complexes Mo(η^6–$C_{10}H_8$)$(CNAr^{Clips2})_3$ (**26**) and Mo(η^6–C_6H_6)$(CNAr^{Clips2})_3$ (**27**), respectively, whereas η^6–binding of a $CNAr^{Clips2}$ ligand by molybdenum evidently inhibits chlorine–atom abstraction.

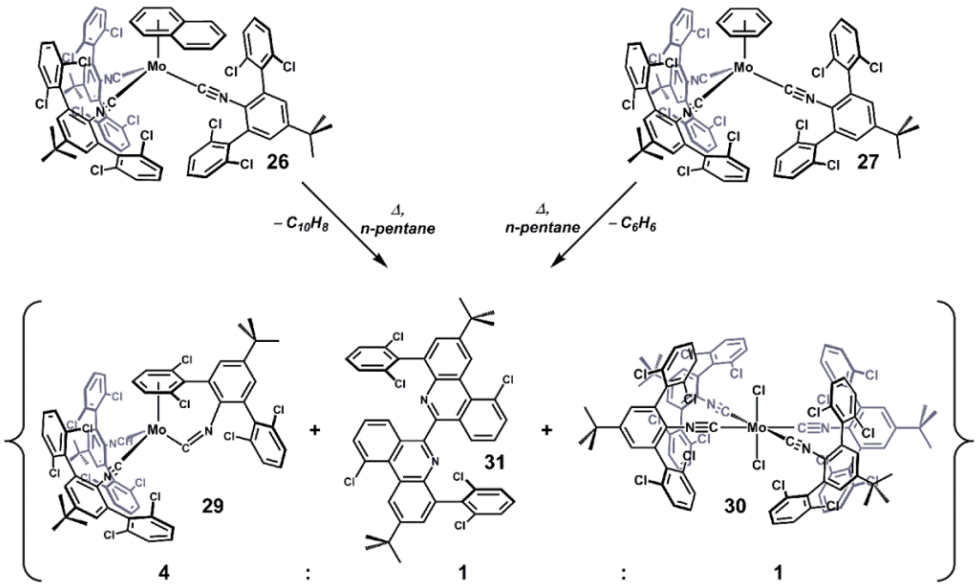

Scheme 4.5. Thermal decomposition products of Mo(η^6–$C_{10}H_8$)$(CNAr^{Clips2})_3$ (**26**) and Mo(η^6–C_6H_6)$(CNAr^{Clips2})_3$ (**27**).

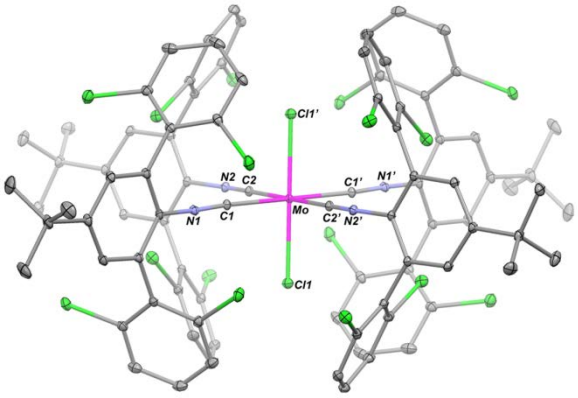

Figure 4.6. Molecular Structure of *trans*–$MoCl_2(CNAr^{Clips2})_4$ (**30**). Selected bond distances (Å) and angles (˚): Mo1–C1 = 2.1117(9); Mo1–C2 = 2.1129(9); Mo1–Cl1 = 2.4058(3); C1–Mo1–C2 = 88.99(3); C1–Mo1–Cl1 = 87.57(3); C2–Mo1–Cl1 = 89.79(3).

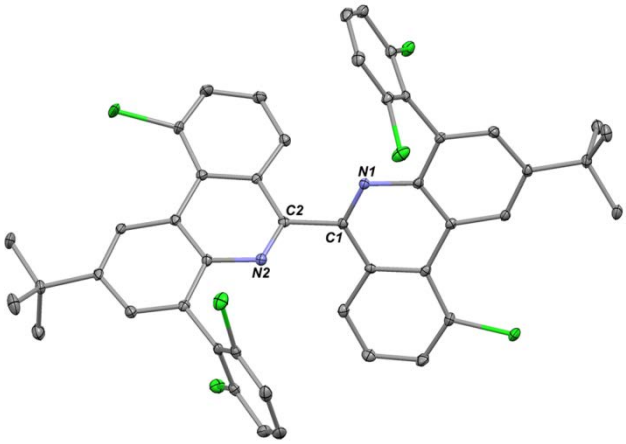

Figure 4.7. Molecular Structure of 2,2'–di–*tert*–butyl–10,10'–dichloro–4,4'–bis(Clips)–6,6'–biphenanthridine (**31**). Selected bond distances (Å) and angles (˚): C1–C2 = 1.500(3); C2–N2 = 1.303(3); C1–N1 = 1.303(3).

4.5 η^6–Arene Molybdenum Complexes Supported by $CNAr^{DArF2}$

The coordination properties of trifluoromethyl–substituted $CNAr^{DArF2}$ toward zerovalent molybdenum centers mirror those of $CNAr^{Clips2}$, but its resultant complexes display significantly different behavior. In analogy to the $CNAr^{Clips2}$ system, treatment of $Mo(\eta^6–C_{10}H_8)_2$ with three equivalents of $CNAr^{DArF2}$ in *n*–pentane generates the isolable η^6–naphthalene trisisocyanide complex, $Mo(\eta^6–C_{10}H_8)(CNAr^{DArF2})_3$ (**32**, Scheme 4.6). The latter

was characterized by X–ray diffraction (Figure 4.8) and possesses structural features largely similar to Mo(η^6–$C_{10}H_8$)($CNAr^{Clips2}$)$_3$ (**32**), including the 'flat–slipped' η^6–interaction of the coordinated naphthalene ring. However, the solid–state structure of Mo(η^6–$C_{10}H_8$)($CNAr^{DArF2}$)$_3$ (**32**) reveals, qualitatively, that the $CNAr^{DArF}$ ligand imparts a significantly higher degree of steric crowding around the central metal center than is found in similar $CNAr^{Mes2}$–, $CNAr^{Dipp2}$– or $CNAr^{Clips2}$–ligated systems.

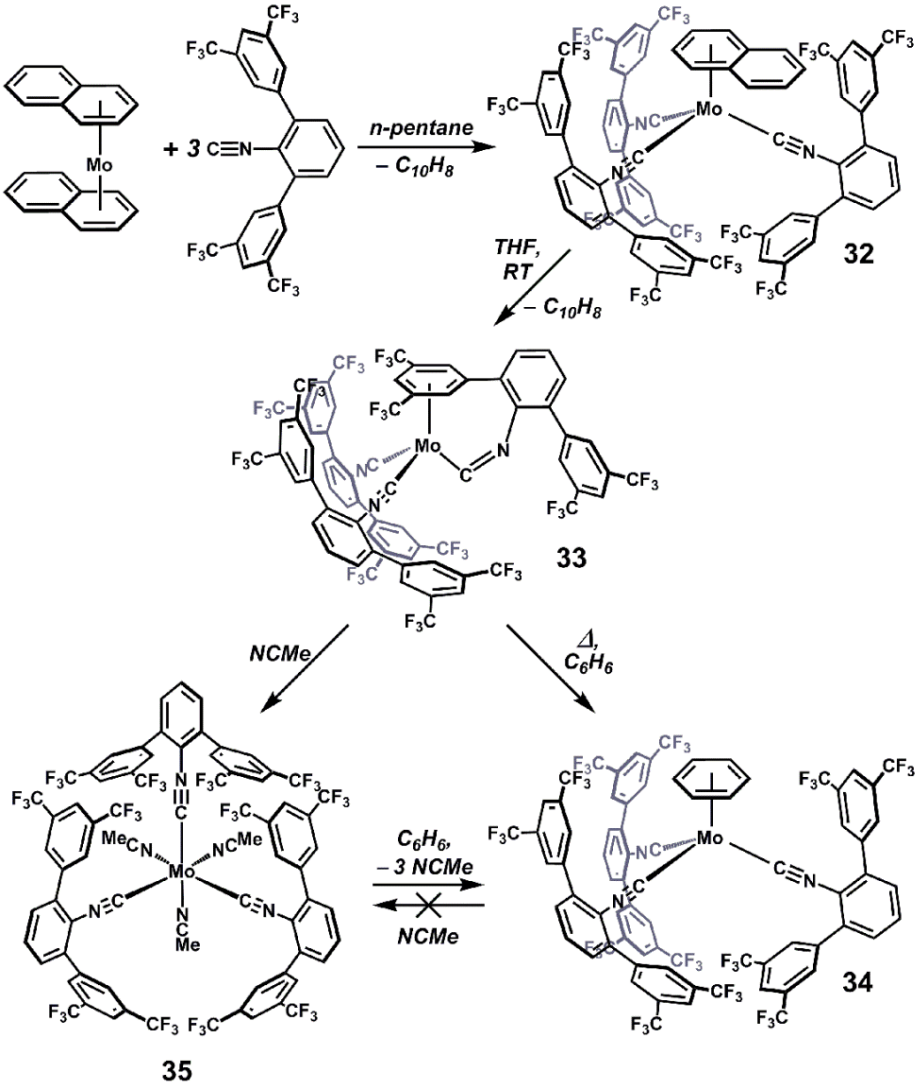

Scheme 4.6. Synthesis of Mo(η^6–$C_{10}H_8$)($CNAr^{DArF2}$)$_3$ (**32**), Mo(η^6–(3,5–$(CF_3)_2C_6H_3$)–κ^1–*C*–$CNAr^{DArF}$)($CNAr^{DArF2}$)$_2$ (**33**), Mo(η^6–C_6H_6)($CNAr^{DArF2}$)$_3$ (**34**), and *fac*–Mo(NCMe)$_3$($CNAr^{DArF2}$)$_3$ (**35**).

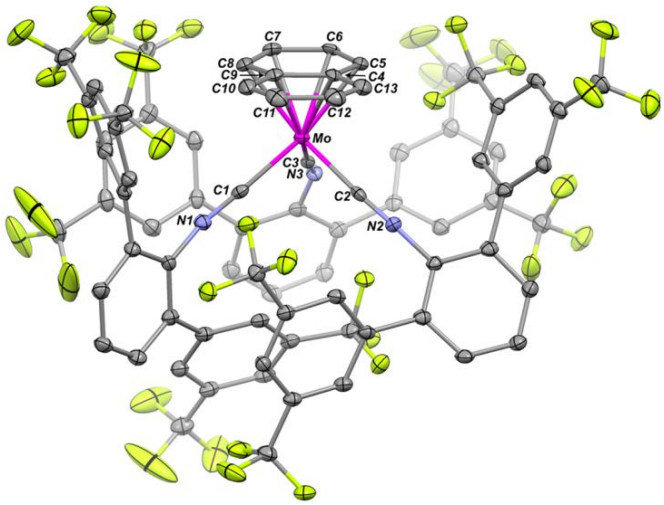

Figure 4.8. Molecular Structure of Mo(η^6–$C_{10}H_8$)($CNAr^{DArF2}$)$_3$ (**32**). Selected bond distances (Å) and angles (˚): Mo1–C1 = 2.012(4); Mo1–C2 = 2.011(4); Mo1–C3 = 1.961(5); Mo1–C4 = 2.441(4); Mo1–C5 = 2.343(4); Mo1–C6 = 2.331(4); Mo1–C7 = 2.325(4); Mo1–C8 = 2.319(4); Mo1–C9 = 2.440(4); C1–Mo1–C2 = 91.29(15); C1–Mo1–C3 = 90.00(15); C2–Mo1–C3 = 90.37(16).

Whereas Mo(η^6–$C_{10}H_8$)($CNAr^{DArF2}$)$_3$ (**32**) is isolable, it is found to cleanly form the η^6–bis–(trifluoromethyl)phenyl complex Mo(η^6–(3,5–$(CF_3)_2C_6H_3$)–κ^1–*C*–$CNAr^{DArF}$)($CNAr^{DArF2}$)$_2$ (**33**; Scheme 4.6) at room temperature over the course of 12 hours. As monitored by ^{1}H NMR spectroscopy, an equivalent of naphthalene is lost during upon η^6–bis–(trifluoromethyl)phenyl group binding. This behavior is clearly different that of $CNAr^{Clips2}$–ligated Mo(η^6–$C_{10}H_8$)($CNAr^{Clips2}$)$_3$ (**26**), which requires elevated temperatures to furnish a η^6–dichlorophenyl interaction. While 3,5–bis(trifluoromethyl)phenyl groups display a low propensity for η^6–arene binding,[82,83] we tentatively suggest that steric pressures[87] within the η^6–naphthalene complex Mo(η^6–$C_{10}H_8$)($CNAr^{DArF2}$)$_3$ (**32**) may provide for a low–energy pathway to flanking–ring η^6–binding of $CNAr^{DArF2}$ and naphthalene release. Alternatively, the peripheral CF_3 groups of the $CNAr^{DArF2}$ framework may provide a coordinatively assisted pathway to 3,5–bis(trifluoromethyl)phenyl group binding,[65] especially if η^6–naphthalene ring–slippage is facile within Mo(η^6–$C_{10}H_8$)($CNAr^{DArF2}$)$_3$ (**32**). However, evidence for such a process has not been obtained for Mo(η^6–$C_{10}H_8$)($CNAr^{DArF2}$)$_3$ (**32**) to date.

Crystallographic characterization of Mo(η^6–(3,5–$(CF_3)_2C_6H_3$)–κ^1–*C*–$CNAr^{DArF}$)$(CNAr^{DArF2})_2$ (**33**, Figure 4.9) revealed structural features similar to its $CNAr^{Mes2}$, $CNAr^{Dipp2}$ and $CNAr^{Clips2}$ analogues (Table 4.1), along with added steric congestion from the 3,5–CF_3 groups. The bent C_{iso} carbon in Mo(η^6–(3,5–$(CF_3)_2C_6H_3$)–κ^1–*C*–$CNAr^{DArF}$)$(CNAr^{DArF2})_2$ (**33**) also displays spectroscopic features consistent with the other geometrically–constrained isocyanide ligands presented in this study (Table 4.1.).

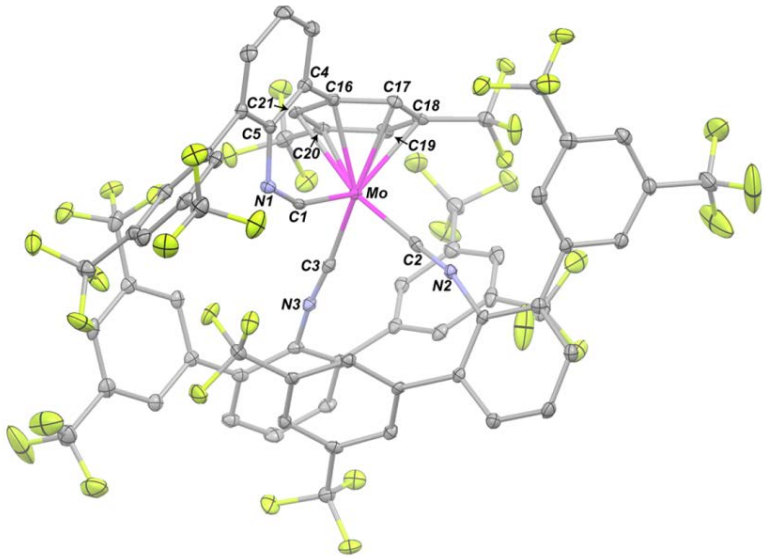

Figure 4.9. Molecular Structure of Mo(η^6–(3,5–$(CF_3)_2C_6H_3$)–κ^1–*C*–$CNAr^{DArF}$)$(CNAr^{DArF2})_2$ (**33**). Selected bond distances (Å) and angles (˚): Mo1–C1 = 1.947(3); Mo1–C2 = 2.048(3); Mo1–C3 = 2.037(3); C1–N1 = 1.229(4); N1–C5 = 1.410(4); Mo1–C16 = 2.307(3); Mo1–C17 = 2.340(3); Mo1–C18 = 2.316(3); Mo1–C19 = 2.334(3); Mo1–C20 = 2.292(3); Mo1–C21 = 2.300(3); C1–Mo1–C2 = 96.19(12); C1–Mo1–C3 = 90.74(12); C2–Mo1–C3 = 90.28(12); Mo1–C1–N1 = 153.9(2); C1–N1–C5 = 120.8(3).

Unlike the flanking–ring η^6–arene interactions in complexes Mo(η^6–(Dipp)–κ^1–*C*–$CNAr^{Dipp}$)$(CNAr^{Dipp2})_2$ (**23**), Mo(η^6–(Mes)–κ^1–*C*–$CNAr^{Mes}$)$(CNAr^{Mes2})_2$ (**24**) and Mo(η^6–(2,6–$Cl_2C_6H_3$)–κ^1–*C*–$CNAr^{Clips}$)$(CNAr^{Clips2})_2$ (**29**), the coordinated bis(trifluoromethyl)phenyl group in Mo((η^6–(3,5–$(CF_3)_2C_6H_3$)–κ^1–*C*–$CNAr^{DArF}$)$(CNAr^{DArF2})_2$ (**33**) can be released from the metal center upon addition of substrates. As shown in Scheme 4.6, dissolution of Mo(η^6–(3,5–$(CF_3)_2C_6H_3$)–κ^1–*C*–$CNAr^{DArF}$)$(CNAr^{DArF2})_2$ (**33**) in C_6H_6 solution followed by heating at

100 ˚C for 6 days provides the η^6–benzene complex (η^6–C_6H_6)Mo($CNAr^{DArF}$)$_3$ (**34**, Figure 4.10). Although displacement of the coordinated bis(trifluoromethyl)phenyl group in Mo(η^6–(3,5–$(CF_3)_2C_6H_3$)–κ^1–*C*–$CNAr^{DArF}$)($CNAr^{DArF2}$)$_2$ (**33**) by benzene is sluggish, it is in direct contrast to the behavior demonstrated by Mo(η^6–(Dipp)–κ^1–*C*–$CNAr^{Dipp}$)($CNAr^{Dipp2}$)$_2$ (**23**), Mo(η^6–(Mes)–κ^1–*C*–$CNAr^{Mes}$)($CNAr^{Mes2}$)$_2$ (**24**) and Mo(η^6–(2,6–$Cl_2C_6H_3$)–κ^1–*C*–$CNAr^{Clips}$)($CNAr^{Clips2}$)$_2$ (**29**) under similar conditions. This reactivity profile therefore demonstrates that the bis(trifluoromethyl)phenyl group of the $CNAr^{DArF2}$ ligand can be used to effectively mask the zerovalent molybdenum trisisocyanide fragment [Mo($CNAr^{DArF2}$)$_3$] in the form of the tethered η^6–arene complex Mo((η^6–(3,5–$(CF_3)_2C_6H_3$)–κ^1–*C*–$CNAr^{DArF}$)($CNAr^{DArF2}$)$_2$ (**33**). Furthermore, it is apparent that flanking–ring η^6–arene interactions to molybdenum from $CNAr^{Dipp2}$, $CNAr^{Mes2}$ and $CNAr^{Clips2}$ do not function similarly in this regard.

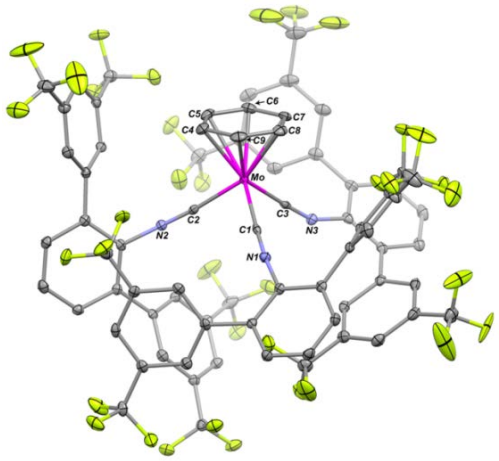

Figure 4.10. Molecular Structure of Mo(η^6–C_6H_6)($CNAr^{DArF2}$)$_3$ (**34**). Selected bond distances (Å) and angles (˚): Mo1–C1 = 1.989(3); Mo1–C2 = 1.991(3); Mo1–C3 = 1.998(3); Mo1–C4 = 2.297(17); Mo1–C5 = 2.289(16); Mo1–C6 = 2.289(16); Mo1–C7 = 2.299(17); Mo1–C8 = 2.307(18); Mo1–C9 = 2.306(18); C1–Mo1–C2 = 91.00(11); C1–Mo1–C3 = 87.55(11); C2–Mo1–C3 = 92.72(11).

While benzene reacts with Mo((η^6–(3,5–$(CF_3)_2C_6H_3$)–κ^1–*C*–$CNAr^{DArF}$)($CNAr^{DArF2}$)$_2$ (**33**) at elevated temperatures, it is far more notable that η^6– bis(trifluoromethyl)phenyl group

displacement is significantly more facile upon addition of stronger Lewis bases. Thus, dissolution of Mo((η^6–(3,5–$(CF_3)_2C_6H_3$)–κ^1–*C*–$CNAr^{DArF}$)$(CNAr^{DArF2})_2$ (**33**) in acetonitrile solution at room temperature results rapidly in a color change from orange to purple, concomitant with the formation of *fac*–$Mo(NCMe)_3(CNAr^{DArF2})_3$ (**35**). Structural characterization on purple single crystals of *fac*–$Mo(NCMe)_3(CNAr^{DArF2})_3$ (**35**) obtained from the reaction mixture confirmed that three acetonitrile molecules combine to displace the η^6–bound 3,5–$(CF_3)_2C_6H_3$ group in Mo((η^6–(3,5–$(CF_3)_2C_6H_3$)–κ^1–*C*–$CNAr^{DArF}$)$(CNAr^{DArF2})_2$ (**33**), resulting in three terminally–bound $CNAr^{DArF}$ ligands (Figure 4.11). ^{1}H NMR analysis of the Mo((η^6–(3,5–$(CF_3)_2C_6H_3$)–κ^1–*C*–$CNAr^{DArF}$)$(CNAr^{DArF2})_2$ (**33**) to *fac*–$Mo(NCMe)_3(CNAr^{DArF2})_3$ (**35**) conversion in acetonitrile–d_3 indicated that the displacement of η^6–bound 3,5–$(CF_3)_2C_6H_3$ group is complete upon mixing and that it does not reversibly coordinate over 3 days when excess acetonitrile is present. However, addition of an excess of benzene to a acetonitrile–d_3 solution of *fac*–$Mo(NCMe)_3(CNAr^{DArF2})_3$ (**35**), or dissolution of single crystalline *fac*–$Mo(NCMe)_3(CNAr^{DArF2})_3$ (**35**) in benzene, rapidly generates the η^6–benzene complex (η^6–C_6H_6)$Mo(CNAr^{DArF})_3$ (**34**, Scheme 4.6). Excess acetonitrile does not displace the η^6–benzene ligand from Mo(η^6–C_6H_6)$(CNAr^{DArF2})_3$ (**34**), which further highlights the lability of the η^6–(3,5–$(CF_3)_2C_6H_3$) group present in Mo((η^6–(3,5–$(CF_3)_2C_6H_3$)–κ^1–*C*–$CNAr^{DArF}$)$(CNAr^{DArF2})_2$ (**33**). We are currently probing the scope of coordinative displacement of η^6–(3,5–$(CF_3)_2C_6H_3$) group of Mo((η^6–(3,5–$(CF_3)_2C_6H_3$)–κ^1–*C*–$CNAr^{DArF}$)$(CNAr^{DArF2})_2$ (**33**) with additional substrates in order to ascertain whether this flanking–ring–bound *m*–terphenyl isocyanide complex serves reliably as a functional equivalent of [$Mo(CNAr^{DArF2})_3$].

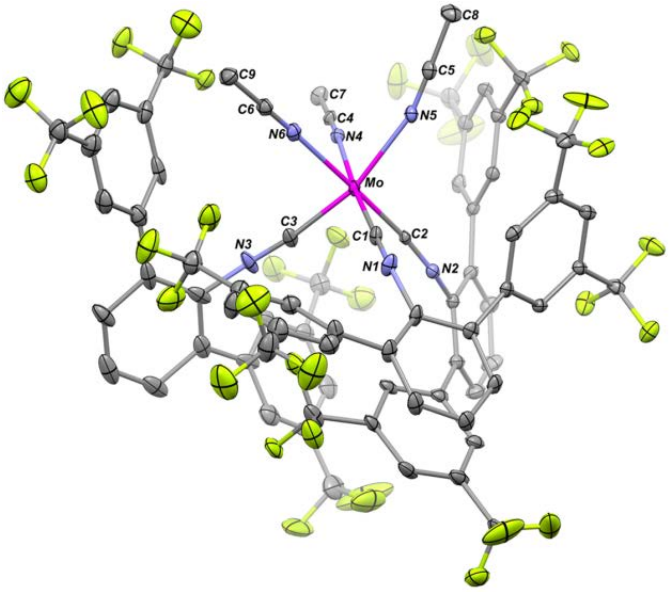

Figure 4.11. Molecular Structure of *fac*–Mo(NCMe)$_3$(CNAr^{DArF2})$_3$ (**35**). Selected bond distances (Å) and angles (˚): Mo1–C1 = 1.929(11); Mo1–C2 = 1.961(5); Mo1–C3 = 1.939(12); Mo1–N4 = 2.231(5); Mo1–N5 = 2.242(5); Mo1–N6 = 2.233(5); C1–Mo1–C2 = 86.8(4); C1–Mo1–C3 = 95.5(4); C1–Mo1–N4 = 173.9(2); C1–Mo1–N5 = 94.1(2); C1–Mo1–N6 = 95.1(18); C2–Mo1–C3 = 89.8(3); C2–Mo1–N4 = 88.69(19); C2–Mo1–N5 = 103.20(18); C2–Mo1–N6 = 177.44(19); C3–Mo1–N4 = 88.6(4); C3–Mo1–N5 = 164.3(3); C3–Mo1–N6 = 88.3(3); N4–Mo1–N5 = 82.93(16); N4–Mo1–N6 = 89.54(17); N5–Mo1–N6 = 78.42(17).

4.6 Electronic Comparison Chloro–, Trifluoromethyl– and Alkyl–Substituted *m*–Terphenyl Isocyanide Ligands

In addition to probing η^6–arene binding by alkyl–, chloro– and trifluoromethyl–substituted *m*–terphenyl isocyanides, we have also assessed the relative electronic influences these ligands impart on metal centers in their terminal–isocyanide binding mode. Given that their electron–withdrawing substituents are fairly distal to, and not π–conjugated with, the isocyanide unit, we were particularly interested in whether CNAr^{Clips2} and CNAr^{DArF2} displayed increased π–acceptor properties relative to isocyanides based on more traditional *m*–terphenyl frameworks. As a point of reference, it has previously been shown that the π–acceptor properties of coordinated aryl isocyanides can be modulated most broadly by the

identity of a substituent *para* to the isocyanide unit.[85,88,89] In general, the π–acceptor ability of *para*–substituted aryl isocyanides increase in the order MeO < Me < H < F < Cl < NO_2.[85] Modulation of *meta*–substituents has also been shown to affect the π–acceptor properties of aryl isocyanides, but to a lesser extent than found for similar substituent variation in the *para*–position. The electronic effects of *ortho*–substitution have not been studied systematically. However, computational work by Cooper has suggested that *ortho* substitutents have a more pronounced effect on the σ–donating ability of aryl isocyanides, rather than on their π–acceptor properties.[85]

To determine the electronic influences of $CNAr^{Clips2}$ and $CNAr^{DArF2}$, we targeted *fac*– and *mer*–tricarbonyl trisisocyanide complexes of molybdenum (*i.e.* $Mo(CO)_3(CNAr^{R2})_3$). Such targets allow for direct IR spectroscopic comparison to the previously reported $CNAr^{Mes2}$ derivatives *fac*–$Mo(CO)_3(CNAr^{Mes2})_3$ (**5**) and *mer*–$Mo(CO)_3(CNAr^{Mes2})_3$ (**6**).[43] Schemes 4.7 and 4.8 outline ligand–substitution and/or photochemical routes to the $CNAr^{Clips2}$ and $CNAr^{DArF2}$ complexes *fac*–$Mo(CO)_3(CNAr^{Clips2})_3$ (**36**), *mer*–$Mo(CO)_3(CNAr^{Clips2})_3$ (**37**) and *mer*–$Mo(CO)_3(CNAr^{DArF2})_3$ (**38**). Each complex has been crystallographically characterized (Figures 4.12 and 4.14) and exhibit NMR and IR spectroscopic features in solution consistent with their solid–state structures. To date, all attempts to prepare the *fac*–derivative of $Mo(CO)_3(CNAr^{DArF2})_3$ by thermal or photochemical methods have instead led to the isolation of its *mer* isomer. While steric pressures between three $CNAr^{DArF2}$ ligands may destabilize the *fac*–isomer of $Mo(CO)_3(CNAr^{DArF2})_3$,[43] it is important to note that the perfluorinated–isocyanide tungsten tricarbonyl complexes $W(CO)_3(CNCF_3)_3$ and $W(CO)_3(CNC_6F_5)_3$ prepared by Lentz exhibit a pronounced electronic preference for their *mer*–isomers.[90–92] Although it is presently unclear, a similar electronic preference for the *mer*–$Mo(CO)_3(CNR)_3$ isomer may potentially be displayed by the Ar^{DArF2} framework. It is also noteworthy that our attempts to prepare either *fac*– or *mer*–

$Mo(CO)_3(CNAr^{Dipp2})_3$ have been unsuccessful and have resulted typically in the formation of the bis–isocyanide tetracarbonyl complex $Mo(CO)_4(CNAr^{Dipp2})_2$.[42] Again, we believe that is observation is the result of steric pressures associated with the encumbering $CNAr^{Dipp2}$ framework. Accordingly, in this study, we limit the electronic comparison of $CNAr^{Clips2}$ and $CNAr^{DArF2}$ to the dimesityl derivative $CNAr^{Mes2}$.

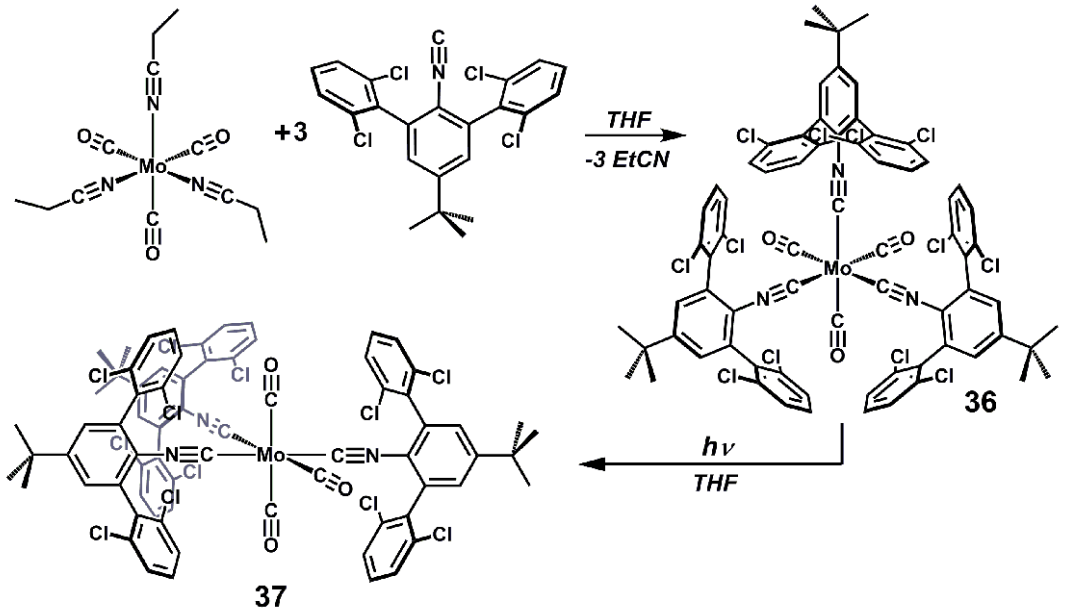

Scheme 4.7. Synthesis of *fac*–$Mo(CO)_3(CNAr^{Clips2})_3$ (**36**) and *mer*–$Mo(CO)_3(CNAr^{Clips2})_3$ (**37**).

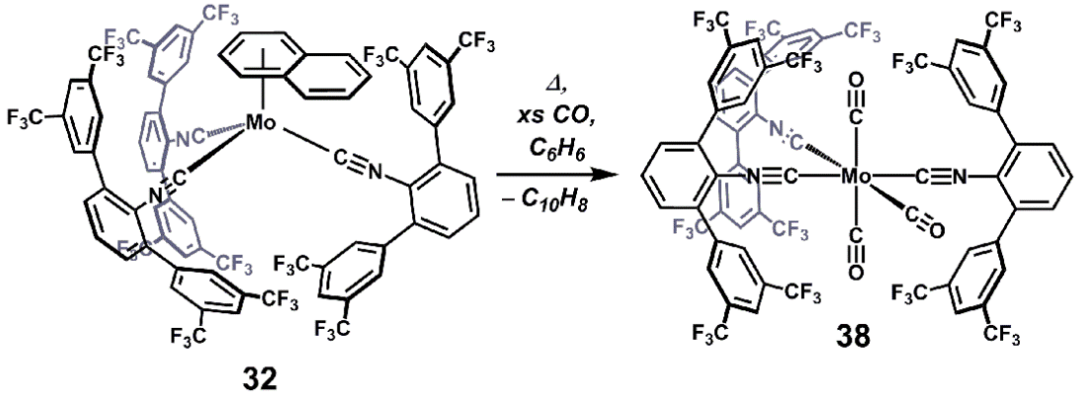

Scheme 4.8. Synthesis of *mer*–$Mo(CO)_3(CNAr^{DArF2})_3$ (**38**).

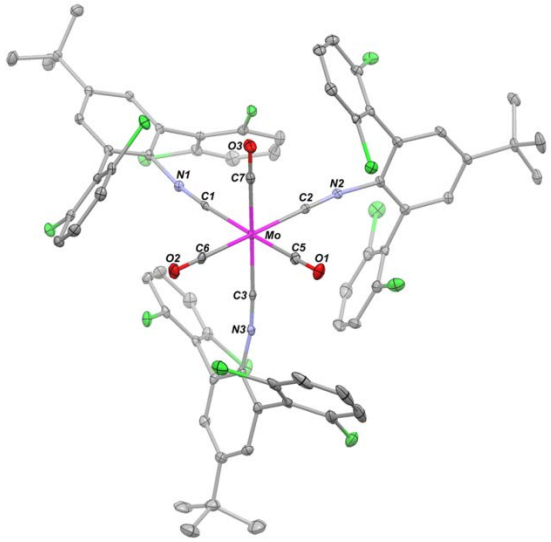

Figure 4.12. Molecular Structure of *fac*–Mo(CO)$_3$(CNAr^{Clips2})$_3$ (**36**). Selected bond distances (Å) and angles (˚): Mo1–C1 = 2.103(3); Mo1–C2 = 2.101(3); Mo1–C3 = 2.106(3); Mo1–C5 = 2.019(3); Mo1–C6 = 2.035(3); Mo1–C7 = 2.009(3); C1–Mo1–C2 = 93.12(11); C1–Mo1–C3 = 94.13(11); C1–Mo1–C5 = 175.79(11); C1–Mo1–C6 = 89.30(11); C1–Mo1–C7 = 87.34(11); C2–Mo1–C3 = 93.70(11); C2–Mo1–C5 = 88.15(11); C2–Mo1–C6 = 176.59(11); C2–Mo1–C7 = 88.15(11); C3–Mo1–C5 = 89.79(11); C3–Mo1–C6 = 88.52(12); C3–Mo1–C7 = 177.57(12); C5–Mo1–C6 = 89.27(12); C5–Mo1–C7 = 89.27(12); C6–Mo1–C7 = 89.55(12).

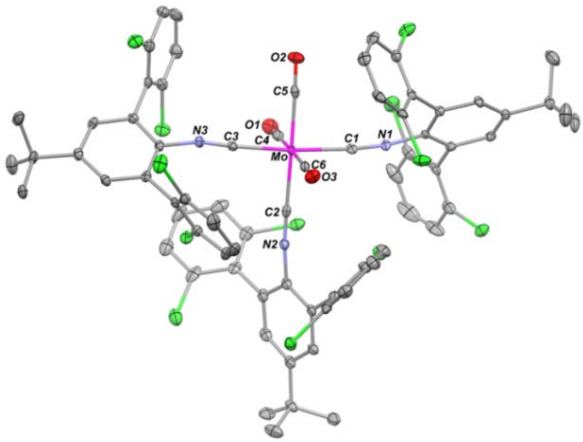

Figure 4.13. Molecular Structure of *mer*–Mo(CO)$_3$(CNAr^{Clips2})$_3$ (**37**). Selected bond distances (Å) and angles (˚): Mo1–C1 = 2.077(5); Mo1–C2 = 2.119(5); Mo1–C3 = 2.070(5); Mo1–C4 = 2.044(6); Mo1–C5 = 2.015(5); Mo1–C6 = 2.045(5); C1–Mo1–C2 = 92.88(17); C1–Mo1–C3 = 173.65(18); C1–Mo1–C4 = 91.59(19); C1–Mo1–C5 = 87.50(19); C1–Mo1–C6 = 88.30(19); C2–Mo1–C3 = 92.87(18); C2–Mo1–C4 = 89.57(19); C2–Mo1–C5 = 177.1(2); C2–Mo1–C6 = 88.92(19); C3–Mo1–C4 = 91.16(19); C3–Mo1–C5 = 86.90(18); C3–Mo1–C6 = 89.10(19); C4–Mo1–C5 = 87.55(19); C4–Mo1–C6 = 178.5(2); C5–Mo1–C6 = 93.96(19).

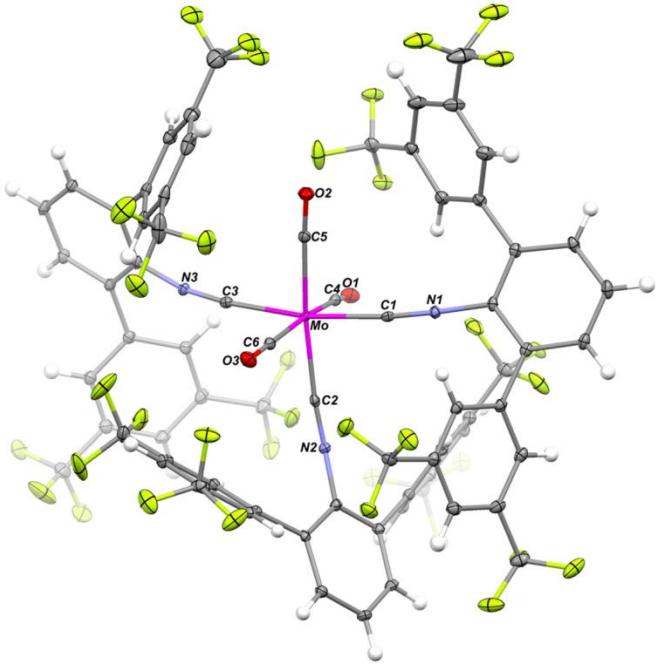

Figure 4.14. Molecular Structure of *mer*–$Mo(CO)_3(CNAr^{DArF2})_3$ (**38**). Selected bond distances (Å) and angles (˚): Mo1–C1 = 2.067(3); Mo1–C2 = 2.083(4); Mo1–C3 = 2.070(4); Mo1–C4 = 2.044(5); Mo1–C5 = 2.035(4); Mo1–C6 = 2.050(4); C1–Mo1–C2 = 88.46(13); C1–Mo1–C3 = 169.89(13); C1–Mo1–C4 = 88.08(13); C1–Mo1–C5 = 84.14(13); C1–Mo1–C6 = 96.70(13); C2–Mo1–C3 = 99.06(13); C2–Mo1–C4 = 85.63(13); C2–Mo1–C5 = 170.03(13); C2–Mo1–C6 = 86.72(13); C3–Mo1–C4 = 85.78(13); C3–Mo1–C5 = 88.91(14); C3–Mo1–C6 = 90.51(13); C4–Mo1–C5 = 99.15(14); C4–Mo1–C6 = 170.86(14); C5–Mo1–C6 = 89.11(14).

Table 4.2 lists the ν_{CO} bands for complexes $Mo(CO)_3(CNAr^{R2})_3$ determined in C_6D_6 solution. For the *fac* partners *fac*–$Mo(CO)_3(CNAr^{Mes2})_3$ (**5**) and *fac*–$Mo(CO)_3(CNAr^{Clips2})_3$ (**36**), it is evident that $CNAr^{Clips2}$ and $CNAr^{Mes2}$ exert a very similar electronic influence on the molybdenum center. Whereas the flanking 2,6–dichlorphenyl groups of $CNAr^{Clips2}$ may be expected to slightly increase the π–acidity of the isocyano group, the *para tert*–butyl substituent may act to oppose this increase. Comparison of the IR data for *mer*–$Mo(CO)_3(CNAr^{Mes2})_3$ (**6**), *mer*–$Mo(CO)_3(CNAr^{Clips2})_3$ (**37**) and *mer*–$Mo(CO)_3(CNAr^{DArF2})_3$ (**38**) is less straightforward because of the fact that both *mer*–$Mo(CO)_3(CNAr^{Clips2})_3$ (**37**) and *mer*–$Mo(CO)_3(CNAr^{DArF2})_3$ (**38**) give rise to only a single ν_{CO} band, rather than three as expected for a C_{2v}–symmetric geometry (Figures 4.15–4.17). However, relative to *mer*–

$Mo(CO)_3(CNAr^{Mes2})_3$ (**6**) and *mer*–$Mo(CO)_3(CNAr^{Clips2})_3$ (**37**), it is clear that *mer*–$Mo(CO)_3(CNAr^{DArF2})_3$ (**38**) gives rise to a significantly blue–shifted ν_{CO} band, thereby indicating that the flanking 3,5–bis(trifluoromethyl)phenyl groups of $CNAr^{DArF}$ can indeed increase the π–acceptor properties of the isocyano group. Most importantly, this finding suggests that isocyanide ligands can be prepared that offer a large degree of steric encumbrance, while providing π–acceptor properties that begin to match that of CO. We believe the ligand design strategy will prove useful for the generation of low–coordinate isocyanide complexes that more accurately mimic the functional and spectroscopic behavior of the unsaturated binary metal carbonyls.[93]

Table 4.2. Solution (C_6D_6) ν_{CN} and Stretching Frequencies for $Mo(CO)_3(CNAr^{R2})_3$.

Complex	ν_{CN} (cm^{-1})	ν_{CO} (cm^{-1})
fac–$Mo(CO)_3(CNAr^{Mes2})_3$ (**5**)[a]	2046 (s)	1942 (s)
	2000 (m)	1910 (s)
fac–$Mo(CO)_3(CNAr^{Clips2})_3$ (**36**)	2042(s)	1943 (s)
	2023 (m sh)	1909 (vs)
mer–$Mo(CO)_3(CNAr^{Mes2})_3$ (**6**)[a]	2046 (m)	1926 (vs)
	2024 (s)	1902 (m)
	1993 (s)	
mer–$Mo(CO)_3(CNAr^{Clips2})_3$ (**37**)	2038 (m sh)	1917 (vs)
	2010 (s)	
	1979 (w sh)	
mer–$Mo(CO)_3(CNAr^{DArF2})_3$ (**38**)	2040 (m sh)	1941 (vs)
	2006 (s)	
	1979 (m sh)	

[a] Data from reference 42.

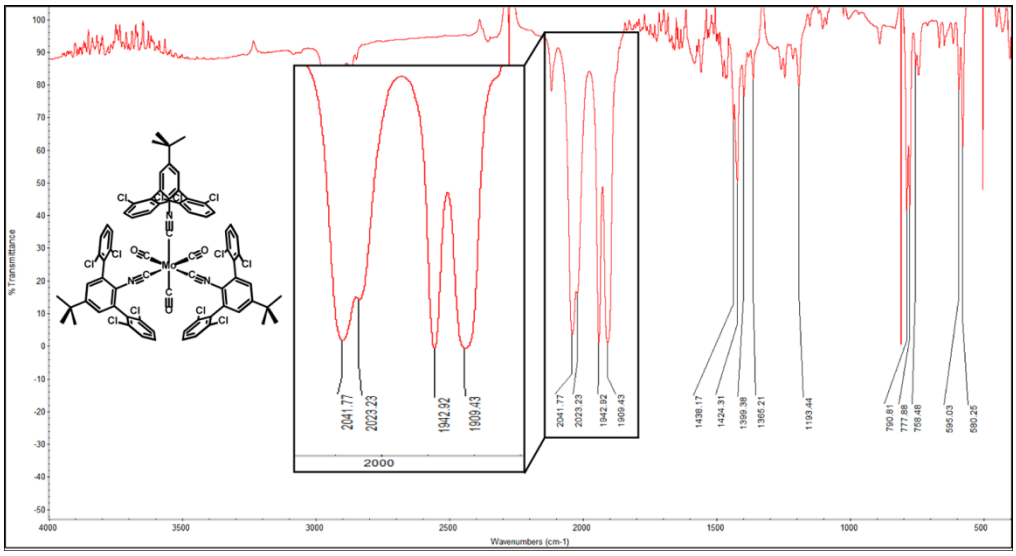

Figure 4.15. FTIR spectra of *fac*–$Mo(CO)_3(CNAr^{Clips2})_3$ (**36**).

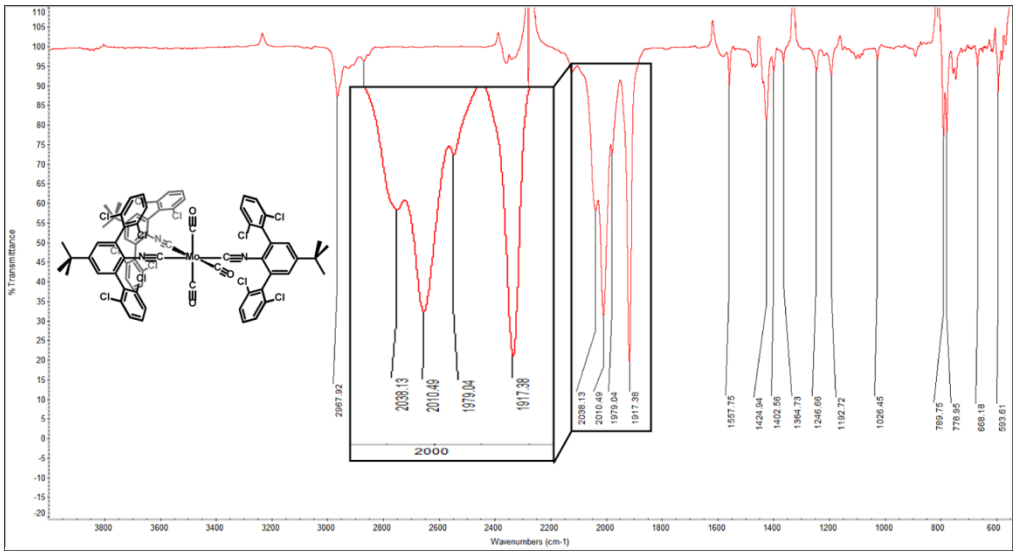

Figure 4.16. FTIR spectra of *mer*–$Mo(CO)_3(CNAr^{Clips2})_3$ (**37**).

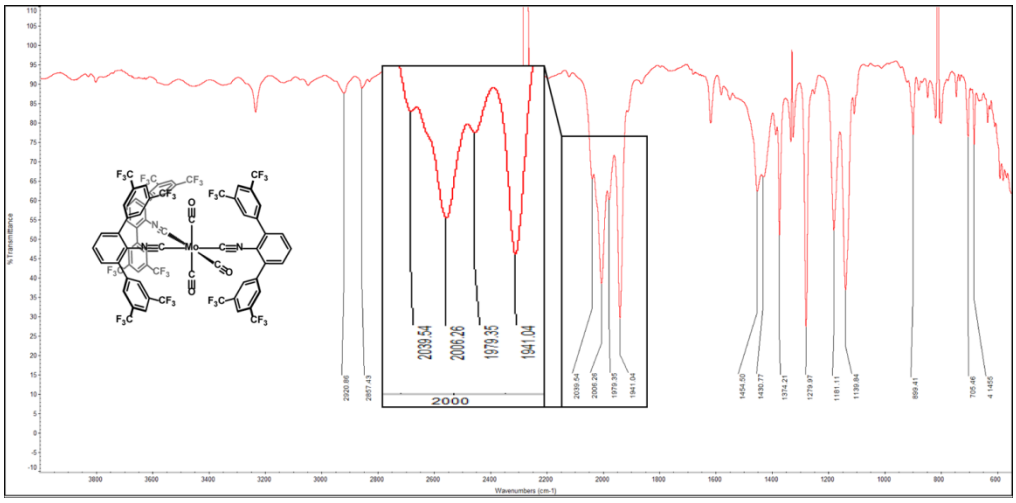

Figure 4.17. FTIR spectra of *mer*–$Mo(CO)_3(CNAr^{DArF2})_3$ (**38**).

4.7 Synthetic Procedures

General Considerations. All manipulations were carried out under an atmosphere of dry dinitrogen using standard Schlenk and glovebox techniques. Solvents were dried and deoxygenated according to standard procedures.[94] Unless otherwise stated, reagent–grade starting materials were purchased from commercial sources and either used as received or purified by standard procedures.[95] The *m*–terphenyl derivatives $CNAr^{Dipp2}$, $CNAr^{Mes2}$ and 2,6–$(2,6\text{–}Cl_2C_6H_3)_2C_6H_3I$ were prepared according to literature procedures.[41,43,72] *p*–Tolylsulfonyl azide ($TosN_3$) was prepared as described previously.[96] Benzene–d_6 and cyclohexane–d_{12} (Cambridge Isotope Laboratories) were degassed and stored over 4 Å molecular sieves under N_2 for 2 d prior to use. Chloroform–*d* (Cambridge Isotope Laboratories) was vacuum distilled from NaH and then stored over 3 and 4 Å molecular sieves under N_2 for 2 d prior to use. Celite 405 (Fisher Scientific) was dried under vacuum (24 h) at a temperature above 250 ˚C and stored in the glovebox prior to use. Solution ^1H, $^{13}C\{^1H\}$ and ^{19}F spectra were recorded on Varian Mercury 300 and 400 spectrometers, a Varian X–Sens500 spectrometer, or a JEOL ECA–500 spectrometer. ^1H and $^{13}C\{^1H\}$ chemical shifts are reported in ppm relative to $SiMe_4$

(^{1}H and ^{13}C δ = 0.0 ppm) with reference to residual solvent resonances of 7.16 ppm (^{1}H) and 128.06 ppm (^{13}C) for benzene–d_6, 1.38 ppm (^{1}H) and 26.43 ppm (^{13}C) for cyclohexane–d_{12} and 7.24 ppm (^{1}H) and 77.23 ppm (^{13}C) for chloroform–*d*. ^{19}F{^{1}H} NMR chemical shifts were referenced internally via capillary to neat trifluoroacetic acid $F_3CC(O)OH$ (δ = –78.5 ppm vs. $CFCl_3$ = 0.0 ppm). FTIR spectra were recorded on a Thermo–Nicolet iS10 FTIR spectrometer. Samples were prepared as C_6D_6, C_6D_{12} and $CDCl_3$ solutions injected into a ThermoFisher solution cell equipped with KBr windows or as KBr pellets. For solution FTIR spectra, solvent peaks were digitally subtracted from all spectra by comparison with an authentic spectrum obtained immediately prior to that of the sample. The following abbreviations were used for the intensities and characteristics of important IR absorption bands: vs = very strong, s = strong, m = medium, w = weak, vw = very weak; b = broad, vb = very broad, sh = shoulder. High resolution mass spectrometry (HRMS) was performed using an Agilent 6230 ESI–TOFMS instrument running in positive ion mode. Combustion analyses were performed by Robertson Microlit Laboratories of Madison, NJ (USA).

Synthesis of IAr^{Clips2}. To 100 mL of CH_2Cl_2 was added solid 2,6–(2,6–$Cl_2C_6H_3)_2C_6H_3I$ (8.500 g, 17.2 mmol). To this solution was sequentially added 20 equivalent portions each of $AlCl_3$ (2.747 g, 20.6 mmol, 1.2 equiv) and 2–methyl–2–chloropropane (31.7 g, 0.345 mol, 20.0 equiv). The addition of $AlCl_3$ was followed by the addition of 2–methyl–2–chloropropane 1 min later, followed by a 3 min interval after witch both regents were added again with the 1 min separation. This sequence was continued until all of the $AlCl_3$ and 2–methyl–2–chloropropane was added. Following the last addition, the resulting purple CH_2Cl_2 solution was cooled to 0 ˚C and 100 mL of a saturated aqueous solution of NaCl was added. The reaction mixture was allowed to stir for 20 min. The organic and aqueous layers were then separated and the organic layer was washed with CH_2Cl_2 (3 x 50 mL). The

combined CH_2Cl_2 extracts were stirred over $MgSO_4$, filtered and dried *in vacuo*, affording a brown semi–solid that was used without further purification. Yield: 7.00 g, 12.72 mmol, 73%. ^{1}H NMR (400.1 MHz, C_6D_6, 20 ˚C): δ = 7.27 (s, 2H, *m*–Ph), 7.08 (d, 4H, *J* = 8 Hz, *m*–Clips), 6.62 (t, 2H, *J* = 8 Hz, *p*–Clips), 1.11 (s, 9H, C(C*H*$_3$)$_3$) ppm. ^{13}C{^{1}H} NMR (100.6 MHz, C_6D_6, 20 °C): δ = 152.6, 143.8, 143.2, 135.8, 135.7, 127.4, 127.3, 126.5, 34.8 (*C*(CH$_3$)$_3$), 31.0 (C(*C*H$_3$)$_3$) ppm. FTIR (C_6D_6, KBr windows): 2966 (s), 2907 (w), 2871 (w), 1590 (w), 1559 (m), 1477 (w), 1430 (vs), 1410 (m), 1391 (m), 1245 (m), 1193 (m), 1091 (w), 1007 (m), 813 (m), 791 (s), 777 (s), 724 (w) cm^{-1}. Anal. Calcd for $C_{22}H_{17}Cl_4I$: C, 48.04; H, 3.12; N, 0.00. Found: C, 47.71; H, 2.97; N, < 0.02.

Synthesis of LiAr^{Clips2}. To a thawing *n*–pentane solution of IAr^{Clips2} (7.00 g, 12.7 mmol, 400 mL) was added 8.35 mL of 1.6 M *n*–bultlyllitium in hexanes (13.3 mmol, 1.05 equiv.) and the mixture was allowed to stir for 1 h. The reaction mixture was concentrated to a volume of 100 mL, filtered and the resulting white solid was washed with thawing *n*–pentane (2 x 50 mL) before being dried *in vacuo*. Yield: 5.49 g, 12.7 mmol, 99%. ^{1}H NMR (400.1 MHz, C_6D_6, 20 ˚C): δ = 7.13 (s, 2H, *m*–Ph), 6.94 (d, 4H, *J* = 8 Hz, *m*–Clips), 6.52 (t, 2H, *J* = 8 Hz, *p*–Clips), 1.24 (s, 9H, C(C*H*$_3$)$_3$) ppm. ^{13}C{^{1}H} NMR (100.6 MHz, C_6D_6, 20 °C): δ = 149.9, 148.6, 146.1, 137.0, 135.6, 134.0, 129.9, 129.4, 34.5 (*C*(CH$_3$)$_3$), 31.4 (C(*C*H$_3$)$_3$) ppm. Anal. Calcd for $C_{22}H_{17}LiCl_4$: C, 61.43; H, 3.98; N, 0.00. Found: C, 59.60; H, 3.93; N, <0.02.

Synthesis of N$_3$Ar^{Clips2}. To an Et_2O solution of LiAr^{Clips2} (5.45 g, 12.6 mmol, 400 mL) was added an Et_2O solution of $TosN_3$ (2.624 g, 13.3 mmol, 1.05 equiv, 20 mL). The opaque yellow solution was allowed to stir at room temperature for 2 h, after which 100 mL of H_2O was added and the reaction mixture was stirred for an additional 20 min. The organic

and aqueous layers were separated, and the aqueous layer was washed with Et_2O (3 x 80 mL). The combined Et_2O extracts were stirred over $MgSO_4$, filtered, and dried *in vacuo*, affording N_3Ar^{Clips2} as a yellow solid that was used without further purification. Yield: 5.47 g, 11.8 mmol, 93%. ^{1}H NMR (400.1 MHz, C_6D_6, 20 ˚C): δ = 7.36 (s, 2H, *m*–Ph), 7.28 (d, 4H, *J* = 8 Hz, *m*–Clips), 6.90 (t, 2H, *J* = 8 Hz, *p*–Clips), 1.24 (s, 9H, C(CH_3)$_3$) ppm. ^{13}C{^{1}H} NMR (100.6 MHz, C_6D_6, 20 °C): δ = 149.0, 137.0, 136.3, 133.8, 131.2, 130.2, 128.9, 128.2, 34.7 (*C*(CH$_3$)$_3$), 31.2 (C(*C*H$_3$)$_3$) ppm. FTIR (C_6D_6, KBr windows): ν_{N3} = 2110 (vs) cm^{-1}, also, 2965 (s), 2904 (m), 2869 (m), 1557 (s), 1466 (m), 1430 (s), 1396 (w), 1363 (w), 1327 (w), 1244 (s), 1147 (w), 1091 (w), 1027 (w), 889 (w), 841 (w), 744 (w), 719 (w) cm^{-1}. Anal. Calcd for $C_{22}H_{17}N_3Cl_4$: C, 56.80; H, 3.68; N, 9.04. Found: C, 56.52; H, 3.71; N, 8.78.

Synthesis of NH_2Ar^{Clips2}. Under an N_2 atmosphere, an Et_2O solution of N_3Ar^{Clips2} (5.47g, 11.8 mmol, 50 mL) was added dropwise via a pressure–equalizing addition funnel to an Et_2O slurry of $LiAlH_4$ (1.0 g, 35.4 mmol, 3.0 equiv, 150 mL) over 10 min, The reaction mixture was allowed to stir for 1 h and then cooled to 0 ˚C. To the cooled solution was added 70 mL of H_2O dropwise via a pressure–equalizing addition funnel addition funnel over the course of 20 min. The reaction was allowed to warm to room temperature, after which it was neutralized with 35 mL of 1 M aqueous HCl. The organic layer was decanted from the aqueous layer and the aqueous layer was then washed with Et_2O (2 x 50 mL). The combined Et_2O extracts were stirred over $MgSO_4$, filtered, and dried *in vacuo*, affording NH_2Ar^{Clips2} as a colorless solid. Yield: 5.16 g, 11.2 mmol, 95%. ^{1}H NMR (400.1 MHz, C_6D_6, 20 ˚C): δ = 7.21 (s, 2H, *m*–Ph), 7.08 (d, 4H, *J* = 8 Hz, *m*–Clips), 6.59 (t, 2H, *J* = 8 Hz, *p*–Clips), 2.96 (s, 2H, N*H*$_2$), 1.23 (s, 9H, C(C*H*$_3$)$_3$) ppm. ^{13}C{^{1}H} NMR (100.6 MHz, C_6D_6, 20 ˚C): δ = 141.2, 139.3, 137.9, 136.7, 129.6, 128.5, 127.6, 123.4, 34.2 (*C*(CH$_3$)$_3$), 31.7 (C(*C*H$_3$)$_3$) ppm. FTIR (C_6D_6, KBr windows): ν_{NH} = 3472 (m) and 3392 (m) cm^{-1}, also 2964 (s), 2903 (w), 2866 (w),

1612 (m), 1597 (w), 1554 (s), 1480 (m), 1443 (w), 1428 (s), 1330 (m), 1258 (m), 1241 (m), 1189 (m), 814 (w), 789 (s) cm^{-1}. Anal. Calcd for $C_{22}H_{19}NCl_4$: C, 60.16; H, 4.36; N, 3.19. Found: C, 59.91; H, 4.28; N, 3.14.

Synthesis of HC(O)NHAr^{Clips2}. Neat acetic anhydride (9.65 g, 94.5 mmol, 8 equiv) was cooled to 0 ˚C under an N_2 atmosphere and formic acid (5.44 g, 118 mmol, 10 equiv) was added via syringe over 20 min. The resulting colorless solution was heated for 3 h at 60 ˚C and then allowed to cool to room temperature. To this mixture containing formyl acetic anhydride, was added a THF solution of NH_2Ar^{Clips2} (5.16 g, 11.81 mmol, 1 equiv) and the reaction mixture was allowed to stir for 12 h. All volatile materials were then removed under reduced pressure. The resultant pale–yellow residue was then slurried in cold hexanes (–30 ˚C, 50 mL) and filtered to afford HC(O)NHAr^{Clips2} as a colorless solid, which was dried *in vacuo* and collected. Yield: 4.6 g, 9.85 mmol, 83%. ^{1}H NMR analysis at 20 ˚C of HC(O)NHAr^{Clips2} as isolated above indicated a 4:1 mixture of *trans*– and *cis*– isomers (see the Supporting Information for full details). This isomeric mixture was used in the subsequent dehydration step without separation. Spectroscopic data for *trans*–isomer: ^{1}H NMR (400.1 MHz, C_6D_6, 20 ˚C): δ = 8.23 (d, 1H, J = 11 Hz, NHC(O)*H*), 7.32 (s, 2H, *m*–Ph), 7.21 (d, 1H, J = 11 Hz, N*H*C(O)H), 6.95 (d, 4H, J = 8 Hz, *m*–Clips), 6.51 (t, 2H, J = 8 Hz, *p*–Clips), 1.11 (s, 9H, C(C*H*$_3$)$_3$) ppm. ^{13}C{^{1}H} NMR (100.6 MHz, C_6D_6, 20 ˚C): δ = 162.6, 150.9, 137.0, 135.4, 134.7, 130.2, 130.1, 129.5, 128.7, 34.7 (*C*(CH$_3$)$_3$), 31.1 (C(*C*H$_3$)$_3$) ppm. Spectroscopic data for *cis*–isomer: ^{1}H NMR (400.1 MHz, C_6D_6, 20 ˚C): δ = 7.43 (s, 2H, *m*–Ph), 7.07 (d, 4H, J = 8 Hz, *m*–Clips), 7.05 (s, 1H, NC*H*OH), 6.59 (t, 2H, J = 8 Hz, *p*–Clips), 6.14 (s, 1H, J = 8 Hz, NCHO*H*), 1.17 (s, 9H, C(C*H*$_3$)$_3$) ppm. ^{13}C{^{1}H} NMR (100.6 MHz, C_6D_6, 20 ˚C): δ = 157.7, 150.5, 138.1, 135.9, 135.3, 131.0, 130.7, 129.5, 34.8 *C*(CH$_3$)$_3$, 31.2 C(*C*H$_3$)$_3$ ppm. FTIR isomeric mixture (C_6D_6, KBr windows): ν_{NH} = 3385 (w) cm^{-1}, ν_{CO} = 1702 (vs b) cm^{-1},

also 3079 (w), 2966 (s), 2906 (w), 1484 (w), 1460 (w), 1445 (w), 1429 (s), 1397 (m), 1245 (m), 1193 (m), 1092 (w), 790 (s) cm^{-1}. HRMS isomeric mixture (ESI, Acetone): m/z Found = 462.39 $[M+H]^+$. Anal. Calcd for $C_{23}H_{19}NOCl_4$ (bulk sample, isomeric mixture): C, 59.13; H, 4.10; N, 3.00. Found: C, 58.34; H, 3.83; N, 2.89.

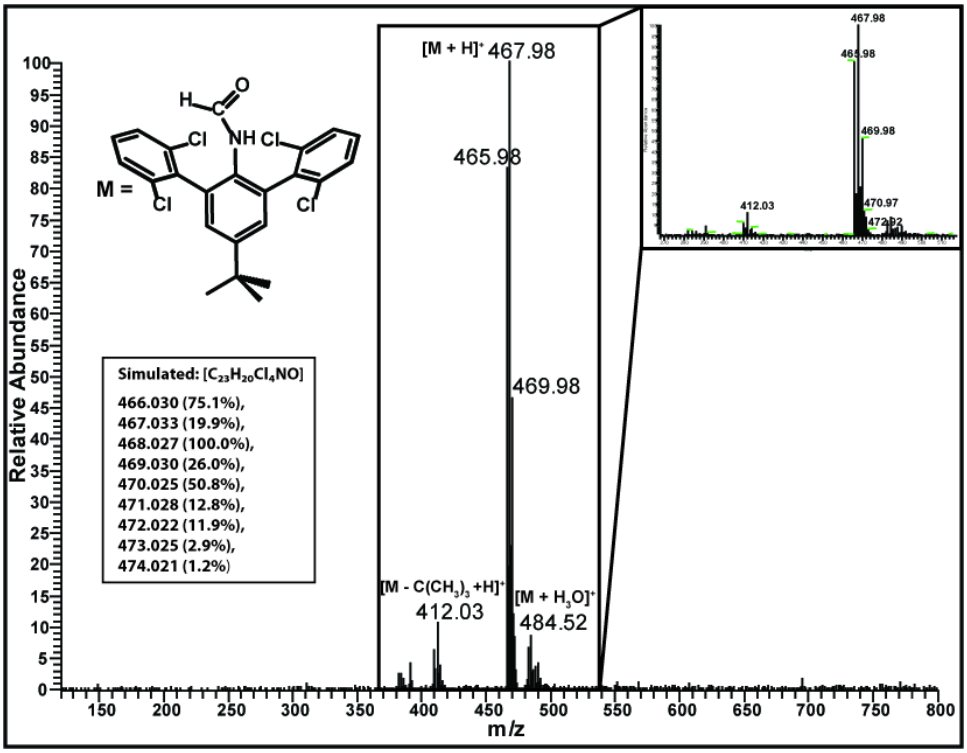

Figure 4.18. Full HRMS (ESI/positive ion mode, acetone) mass spectrum of $HC(O)NHAr^{Clips2}$.

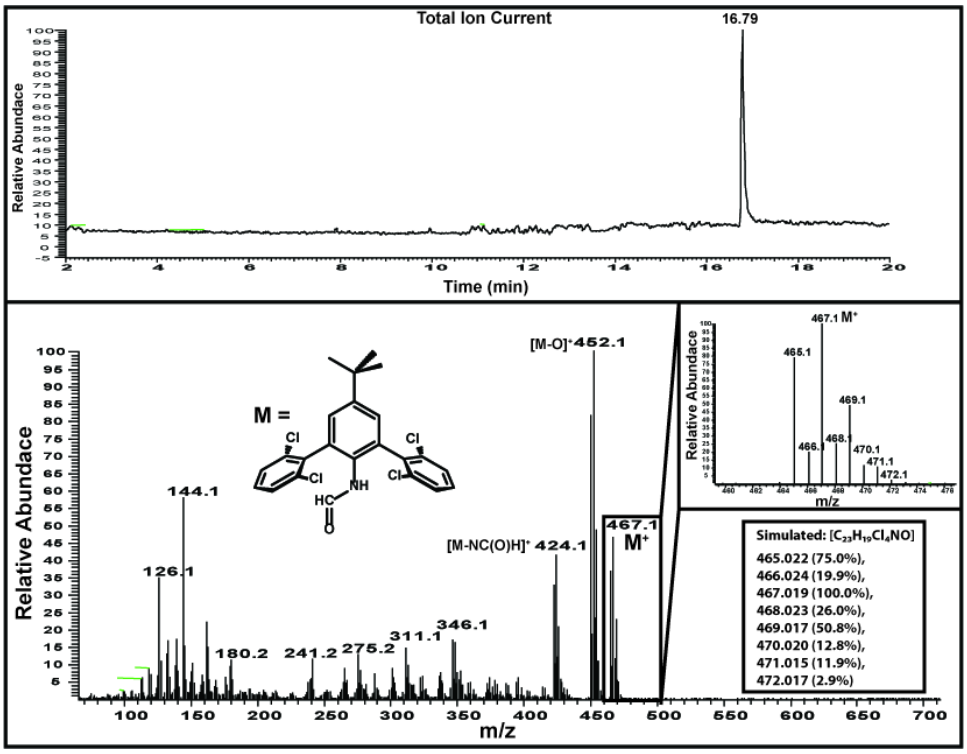

Figure 4.19. GCMS data of HC(O)NHAr^{Clips2}. The *cis*– and *trans*–isomers of HC(O)NHAr^{Clips2} were found to elute with the same retention time.

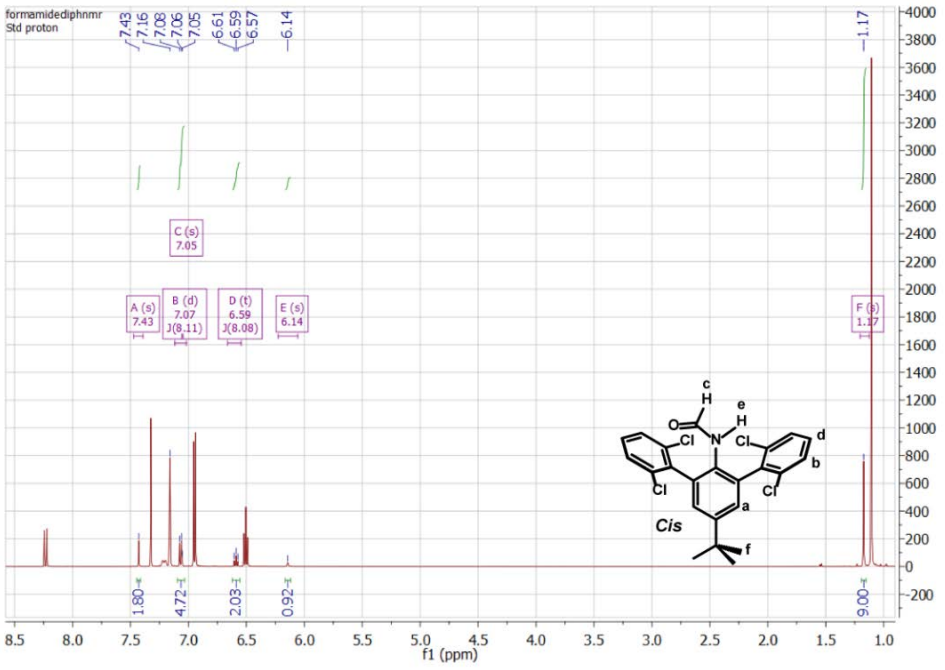

Figure 4.20. ^{1}H NMR data of *cis/trans* mixture highlighting *trans*–HC(O)NHAr^{Clips2} peak assignments.

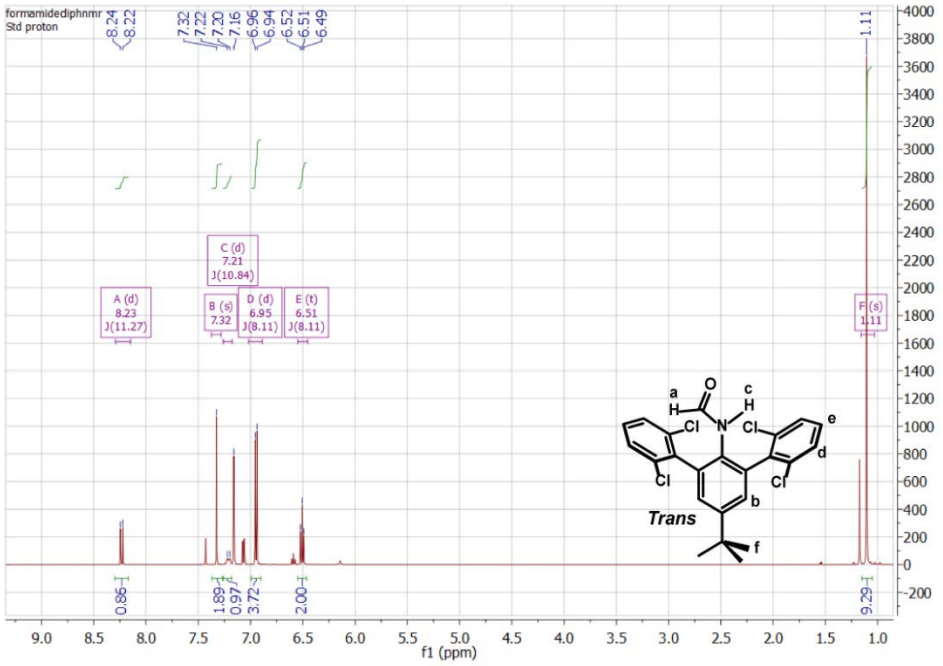

Figure 4.21. ^{1}H NMR data of *cis/trans* mixture highlighting *cis*–HC(O)NHAr^{Clips2} peak assignments.

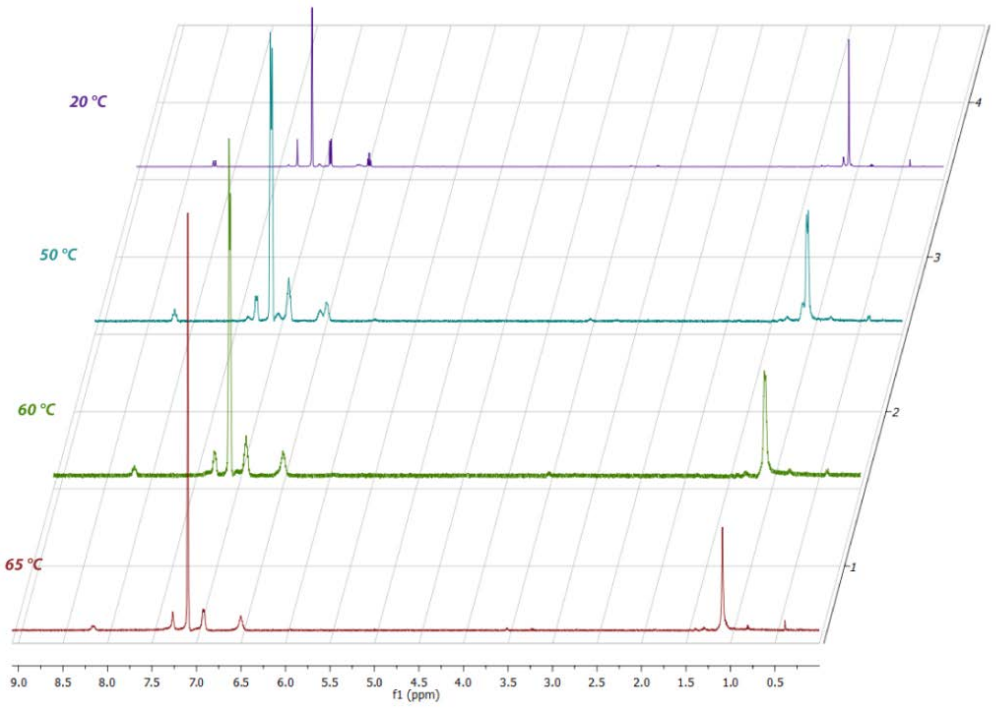

Figure 4.22. Variable temperature ^{1}H NMR spectra (500.1 MHz) of *cis/trans* mixture of HC(O)NHAr^{Clips2}. The temperature for onset of free rotation (*i.e.* coalescence temperature) was determined to be *ca.* 60 ˚C.

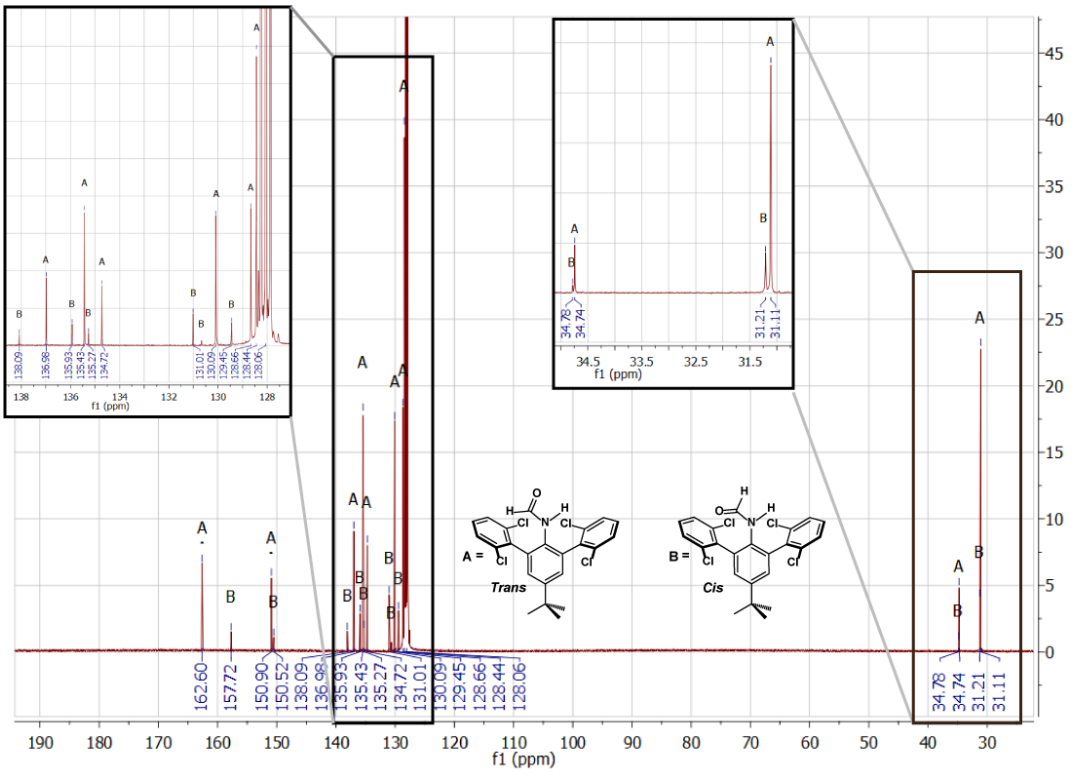

Figure 4.23. ^{13}C NMR spectra of *cis/trans* mixture of HC(O)NHAr^{Clips2}.

Synthesis of CNAr^{Clips2}. To a CH_2Cl_2 solution of HC(O)NHAr^{Clips2} (4:1 mixture of *trans/cis* isomers; 4.60 g, 9.85 mmol, 100 mL) was added diisopropylamine (13.95 g, 137 mmol, 14.0 equiv). The solution was cooled to 0 ˚C under an N_2 atmosphere and $POCl_3$ (4 mL, 6.64 g, 43.3 mmol, 4.4 equiv) was added dropwise via syringe. The resulting mixture was allowed to stir for 12 h, after which 70 mL of an aqueous 0.9 M Na_2CO_3 was added. After an additional 1 h of stirring, the organic and aqueous layers were separated, and the aqueous layer was washed with CH_2Cl_2 (3 x 70 mL). The combined organic extracts were stirred over $MgSO_4$, filtered, and dried *in vacuo*. The resulting residue was slurried in cold acetonitrile (40 mL, 0 ˚C), filtered and dried *in vacuo* to afford isocyanide CNAr^{Clips2} as a colorless solid. Yield: 3.80 g, 8.45 mmol, 86%. ^{1}H NMR (400.1 MHz, C_6D_6, 20 ˚C): δ = 7.33 (s, 2H, *m*–Ph), 6.99 (d, 4H, J = 8 Hz, *m*–Clips), 6.53 (t, 2H, J = 8 Hz, *p*–Clips), 1.07 (s, 9H, C(CH_3)$_3$) ppm. ^{13}C{^{1}H} NMR (100.6 MHz, C_6D_6, 20 ˚C): δ = 172.0 (*C*≡N), 153.0, 136.1,

135.5, 135.3, 130.6, 128.4, 128.0, 35.1, 30.9 ppm. FTIR (KBr pellet): ν_{CN} = 2132 (s) cm^{-1}, also 2965 (s), 1599 (w), 1558 (m), 1424 (vs), 1399 (w), 1366 (w), 1247 (w), 1193 (m), 1091 (w), 1027 (w), 889 (w), 781 (vs), 651 (w), and 622 (w) cm^{-1}. FTIR (C_6D_6, KBr windows): ν_{CN} = 2119 (s) cm^{-1}, also 2968 (s b), 1598 (w), 1557 (w), 1428 (m), 1400 (w), 1247 (m), 791 (s), 779 (s), 742 (w), 707 (w), 654 (w), 625 (w) cm^{-1}. Anal. Calcd for $C_{23}H_{17}NCl_4$: C, 61.50; H, 3.81; N, 3.12. Found: C, 61.32; H, 3.82; N, 2.97.

Synthesis of H_2NAr^{DArF2}: A re–sealable ampoule was charged with 2,6–dibromoaniline (0.915 g, 3.60 mmol), 3,5–bis(trifluoromethyl)phenylboronic acid (2.04 g, 8.00 mmol, 2.2 equiv), Na_2CO_3 (1.56 g, 0.015 mol, 4.4 equiv) and placed under an N_2 atmosphere. A toluene (25 mL) solution containing $Pd_2(dba)_3$ (0.017 g, 0.018 mmol, 0.5 mol%) and PPh_3 (0.009 g, 0.036 mmol, 1 mol%) was then added, followed by H_2O (5 mL) and EtOH (10 mL). The ampoule was sealed and heated at 90 °C for 16 h. The reaction mixture was cooled to room temperature and filtered through a medium porosity frit packed with Celite. Water (20 mL) was added to the filtrate and 1 M aqueous HCl was then added to achieve a pH 7.0. The aqueous and organic phases were then separated and the aqueous layer was then washed with Et_2O (3 x 10 mL). The combined organic phases were dried over $MgSO_4$ and then all volatile materials were removed by rotary evaporation. The resulting yellow oil was purified by column chromatography (silica gel) using hexanes to elute the principle contaminants and then 0.5% EtOAc in hexanes to elute H_2NAr^{DArF2}. Fractions containing H_2NAr^{DArF2} were combined and volatile materials were removed by rotary evaporation to afford a colorless solid. Yield: 1.206 g, 2.30 mmol, 65%. ^{1}H NMR (499.8 MHz, C_6D_6, 20 °C): δ = 7.76 (s, 2H, *p*–ArF), 7.67 (s, 4H, *o*–ArF), 6.64 (m, 3H, *p*–Ph + *m*–Ph), 2.71 (s, 2H, NH_2) ppm. ^{13}C{^{1}H} NMR (125.7 MHz, C_6D_6, 20 °C): δ = 141.9, 140.7, 132.5 (q, $^2J_{C–F}$ = 33 Hz, *m*–ArF), 131.3, 129.7, 125.1, 123.8 (q, $^1J_{C–F}$ = 273 Hz, CF_3), 121.4

(septet, $^{3}J_{C–F}$ = 4 Hz, *p*–ArF), 119.3 ppm. ^{19}F NMR (470.6 MHz, C_6D_6, 20 ˚C): δ = –63.38 (s, C*F*$_3$) ppm. FTIR (C_6D_6, KBr windows): ν_{NH} = 3487 (w), 3398 (m) cm^{-1}, also 3065 (w), 2962 (vw), 2915 (w), 1805 (m), 1783 (m), 1675 (m), 1616 (s), 1377 (vs), 1283 (vs), 1211 (s), 1178 (vs), 1142 (vs), 906 (s), 845 (m), 751 (m), 709 (m), 681 (m), 637 (m) cm^{-1}. Anal. Calcd For $C_{22}H_{11}F_{12}N$: C, 51.08; H, 2.14; N, 2.71. Found: C, 50.83; H, 2.28; N, 2.78.

Synthesis of HC(O)NHAr^{DArF2}: Neat acetic anhydride (5.9 g, 58.0 mmol, 20 equiv) was cooled to 0 ˚C under an N_2 atmosphere and formic acid (3.33 g, 73.0 mmol, 25 equiv) was added via syringe over 20 min. The resulting colorless solution was heated for 3 h at 60 ˚C and then allowed to cool to room temperature. This mixture now containing formyl acetic anhydride was then cooled to room temperature and added, via syringe, to a toluene solution of H_2NAr^{DArF2} (1.01 g, 1.95 mmol, 50 mL). The resulting mixture was stirred for 16 h. All volatile materials were then removed by rotary evaporation to afford a colorless solid that was used without further purification. Yield: 0.880 g, 1.60 mmol, 82%. ^{1}H NMR (499.8 MHz, C_6D_6, 20 ˚C): δ = 7.76 (s, 2H, *p*–ArF), 7.59 (s, 4H, *o*–ArF), 6.96 (s, 1H, *H*C(O)NHAr^{DArF2}), 6.91 (t, 1H, *J* = 8 Hz, *p*–Ph), 6.72 (d, 2H, *J* = Hz, *m*–Ph), 4.60 (s, 1H, HC(O)N*H*Ar^{DArF2}) ppm. ^{13}C{^{1}H} NMR (125.7 MHz, C_6D_6, 20 ˚C): δ = 159.1 (H*C*(O)NHAr^{ArF2}), 141.5, 138.1, 131.9 (q, $^{2}J_{C–F}$ = 33 Hz, *m*–ArF), 130.9, 130.4, 129.4, 127.5, 123.8 (q, $^{1}J_{C–F}$ = 273 Hz, *C*F$_3$), 121.6 (septet, $^{3}J_{C–F}$ = 4 Hz, *p*–ArF) ppm. ^{19}F NMR (470.6 MHz, C_6D_6, 20 ˚C): δ = –63.34 (s, C*F*$_3$) ppm. FTIR (C_6D_6, KBr windows): ν_{NH} = 3367 (w), ν_{CO} = 1707 (s) cm^{-1}; also 2917 (w), 2851 (w), 1680 (s), 1374 (s), 1277 (vs), 1208 (sh), 1183 (vs), 1138 (vs), 903 (m), 850 (m), 800 (m), 725 (m), 705 (w), 633 (w) cm^{-1}. Anal. Calcd for $C_{23}H_{11}F_{12}NO$: C, 50.66; H, 2.03; N, 2.57. Found: C, 50.77; H, 1.84; N, 2.66.

Synthesis of $CNAr^{DArF2}$: Diisopropylamine ($HN(i\text{–}Pr)_2$; 0.520 g, 5.13 mmol, 3.4 equiv) was added, via syringe, to a CH_2Cl_2 solution of $HC(O)NHAr^{DArF2}$ (0.800 g, 1.50 mmol, 60 mL). The resulting mixture was cooled to 0 ˚C and $POCl_3$ (0.450 g, 2.93 mmol, 1.95 equiv) was added by syringe. The reaction mixture was allowed to warm slowly to room temperature and then stirred for 16 h. Aqueous Na_2CO_3 (1.5 M, 40 mL) was then added and the resulting mixture stirred for 1 h. The organic and aqueous layers were separated and the aqueous layer was washed with CH_2Cl_2 (3 x 20 mL). The combined organic layers were dried over $MgSO_4$ and then all volatile materials were removed by rotary evaporation. The resulting solid was dissolved in a minimal amount of MeCN and cooled to –40 ˚C to produce a colorless precipitate. Cold filtration of the mixture then afforded $CNAr^{DArF2}$ a colorless solid. Yield: 0.400 g, 0.75 mmol, 51%. ^{1}H NMR (499.8 MHz, C_6D_6, 20 ˚C): δ = 7.83 (s, 2H, *p*–ArF), 7.75 (s, 4H, *o*–ArF), 6.86 (t, 1H, J = 8 Hz, *p*–Ph), 6.62 (d, 2H, J = 8 Hz, *m*–Ph) ppm. $^{13}C\{^1H\}$ NMR (125.7 MHz, C_6D_6, 20 ˚C): δ = 175.4 (*C*NR), 139.0, 136.8, 132.2 (q, $^2J_{C–F}$ = 34 Hz, *m*–ArF), 130.4, 129.7, 129.6, 127.5, 123.6 (q, $^1J_{C–F}$ = 273 Hz, *C*F_3), 122.6 (septet, $J_{C–F}$ = 4 Hz, *p*–ArF) ppm. ^{19}F NMR (470.4 MHz, C_6D_6, 20 ˚C): δ = –63.25 (s, C*F*$_3$) ppm. FTIR (C_6D_6, KBr windows): ν_{CN} = 2112 (s) cm^{-1} also, 3087 (w), 3056(w), 2956 (w), 2923 (w), 1624 (w), 1483 (w), 1459 (m), 1372 (vs), 1279 (vs), 1250 (m), 1182 (vs), 1142 (vs), 1110 (m), 1073 (w), 1060 (w), 900 (m), 847 (w), 803 (m), 749 (m), 683 (m), 637 (w) cm^{-1}. FTIR (C_6D_6, KBr Pellet): ν_{CN} = 2119 (s) cm^{-1} also, 3097 (m), 2967 (w), 2929 (w), 1627 (m), 1465 (m), 1374 (vs), 1280, (vs), 1250 (s), 1193 (s), 1169 (s), 1118 (vs), 1069 (m), 908 (s), 850 (m),747 (s), 708 (s), 683 (s), 633 (m), 545 (w) cm^{-1}. Anal. Calcd for $C_{23}H_9F_{12}N$: C, 52.39; H, 1.72; N, 2.66. Found: C, 52.07; H, 1.65; N, 2.70.

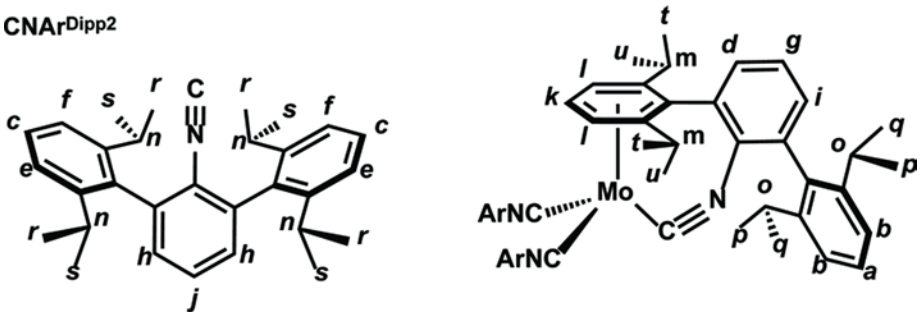

Figure 4.24. Labeling scheme for ^{1}H NMR assignments in Mo(η^6–(Dipp)–κ^1–*C*–CNAr^{Dipp})(CNAr^{Dipp2})$_2$ (**23**).

Synthesis of Mo(η^6–(Dipp)–κ^1–*C*–CNAr^{Dipp})(CNAr^{Dipp2})$_2$ (23). A mixture of Mo(η^6–$C_{10}H_8$)$_2$ (0.028 g, 0.079 mmol) and CNAr^{Dipp2} (0.100 g, 0.235 mmol, 3 equiv) was dissolved in C_6H_6 (20 mL) and heated at 60 ˚C for 24 h. The resulting orange solution was filtered and all volatiles were removed *in vacuo*. The remaining orange residue was dissolved in Et_2O (5 mL), filtered, and stored at –35 ˚C for 1 d, whereupon orange crystals of Mo(η^6–(Dipp)–κ^1–*C*–CNAr^{Dipp})(CNAr^{Dipp2})$_2$ (**23**) were obtained. Yield: 0.060 g, 0.044 mmol, 55%. X–ray diffraction quality crystals were grown from saturated acetonitrile solution stored at –35 ˚C for 1 d. ^{1}H NMR (500.1 MHz, C_6D_6, 20 ˚C): δ = 7.46 (t, 1H, J = 8 Hz, H_a), 7.39 (d, 2H, J = 8 Hz, H_b), 7.26 (t, 4H, J = 8 Hz, H_c), 7.18 (d, 1H, J = 8 Hz, H_d), 7.16 (d, 4H, J = 7 Hz , H_e), 7.14 (d, 4H, J = 8 Hz, H_f), 7.06 (d, 1H, J = 8 Hz, H_g), 6.91 (d, 4H, J = 8 Hz, H_h), 6.80 (t, 1H, J = 7 Hz, H_i), 6.74 (t, 2H, J = 8 Hz, H_j), 4.20 (t, 1H, J = 6 Hz, H_k), 4.07 (d, 2H, J = 5 Hz, H_l), 2.88 (m, 2H, J = 7 Hz, H_m), 2.81 (m, 8H, J = 7 Hz, H_n), 1.96 (m, 2H, J = 7 Hz, H_o), 1.43 (d, 6H, J = 7 Hz, H_p), 1.25 (d, 6H, J = 7 Hz, H_q), 1.11 (d, 12H, J = 8 Hz, H_r), 1.07 (d, 12H, J = 7 Hz, H_s), 0.85 (d, 6H, J = 7 Hz, H_t), 0.78 (d, 6H, J = 7 Hz, H_u) ppm. ^{13}C{^{1}H} NMR (125.7 MHz, C_6D_6, 20 ˚C): δ = 281.6 (*C*≡N), 194.4 (*C*≡N), 153.7, 147.2, 147.0, 138.6, 137.1, 136.6, 133.2, 131.8, 131.6, 130.1, 129.2, 128.9, 128.6, 127.7, 127.7, 127.5, 114.8, 95.3, 89.5, 85.2, 32.0, 31.1, 31.0, 30.9, 26.1, 25.6, 25.4, 25.2, 24.8, 24.1, 23.9, 23.3 ppm. FTIR (C_6D_6, KBr windows): ν_{CN} = 2017 (w), 1991 (w), 1928 (s), and 1652 (s) cm^{-1}, also 2962 (m), 2923 (w),

2867 (w), 1563 (m), 1462 (m), 1431 (m b), 1404 (m), 880 (w), 760 (w) cm^{-1}. Anal. Calcd for $C_{93}H_{111}N_3Mo$: C, 81.72; H, 8.19; N, 3.08. Found: C, 81.65; H, 8.45; N, 3.13.

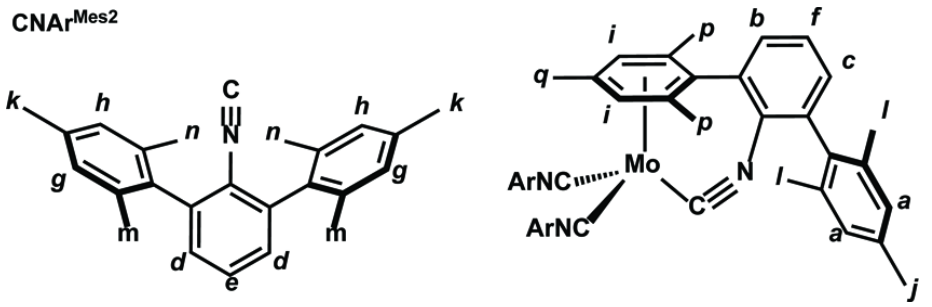

Figure 4.25. Labeling scheme for ^{1}H NMR assignments in Mo(η^6–(Mes)–κ^1–*C*–$CNAr^{Mes2}$)($CNAr^{Mes2}$)$_2$ (**24**).

Mo(η^6–(Mes)–κ^1–*C*–$CNAr^{Mes}$)($CNAr^{Mes2}$)$_2$ (24). A mixture of Mo(η^6–$C_{10}H_8$)$_2$ (0.421 g, 1.20 mmol) and $CNAr^{Mes2}$ (1.217 g, 3.59 mmol, 3 equiv) was dissolved in C_6H_6 (100 mL) and heated at 60 ˚C for 24 h. The resulting orange solution was filtered and all volatiles were removed *in vacuo*. The remaining orange residue was subjected to three cycles of *n*–pentane (20 mL) wash, followed by drying under reduced pressure. After the last cycle, Mo(η^6–(Mes)–κ^1–*C*–$CNAr^{Mes}$)($CNAr^{Mes2}$)$_2$ (**24**) was obtained as an orange powder. Yield: 1.015 g, 0.911 mmol, 76%. X–ray diffraction quality crystals were grown from a saturated fluorobenzene solution stored at –35 ˚C for 1 d. ^{1}H NMR (500.1 MHz, C_6D_6, 20 ˚C): δ = 7.06 (s, 2H, H_a), 7.03 (d, 1H, J = 7 Hz, H_b), 6.99 (d, 1H, J = 7 Hz, H_c), 6.93 (d, 4H, J = 9 Hz, H_d), 6.91 (t, 2H, J = 9 Hz, H_e), 6.90 (t, 1H, J = 7 Hz, H_f), 6.88 (s, 4H, H_g) 6.87 (s, 4H, H_h), 4.10 (s, 2H, H_i), 2.40 (s, 3H , H_j), 2.27 (s, 12H, H_k), 2.27 (s, 6H, H_l), 2.11 (s, 12H, H_m), 2.03 (s, 12H, H_n), 1.43 (s, 6H, H_o), 1.41 (s, 6H, H_p) ppm. ^{13}C{^{1}H} NMR (125.7 MHz, C_6D_6, 20 °C): δ = 278.0 (*C*≡N), 197.3 (*C*≡N), 153.5, 138.6, 137.1, 137.0, 136.4, 136.2, 135.9, 135.9, 135.9, 134.9, 130.1, 130.1, 129.6, 129.1, 128.9, 127.7, 127.5, 125.1, 122.2, 108.6, 100.5, 91.3, 89.2, 21.5, 21.4, 21.3, 20.9, 20.6, 19.4 ppm. FTIR (C_6D_6, KBr windows): ν_{CN} = 2035 (m), 2004 (m), 1940 (vs), and 1643 (s) cm^{-1}, also 3037 (w), 2918 (w), 2851 (w), 1566 (m), 1483 (w),

1402 (w), 1374 (w), 1194 (w), 1036 (w), 852 (w), 752 (w), 680 (m) cm^{-1}. Anal. Calcd for $C_{75}H_{75}N_3Mo$: C, 80.83; H, 6.78; N, 3.77. Found: C, 82.02; H, 7.11; N, 3.28.

Synthesis of *mer*–$MoI_2(I_3)(CNAr^{Mes2})_3$ (25). A mixture of Mo(η^6–(Mes)–κ^1–*C*–$CNAr^{Mes}$)$(CNAr^{Mes2})_2$ (**24**, 0.050 g, 0.045 mmol, 100 mL) and I_2 (0.029 g, 0.114 mmol, 2.55 equiv) was dissolved in THF (10 mL) and then allowed to stir for 12 h. The resulting brown solution was filtered through Celite and all volatiles were removed under reduced pressure to afford *mer*–$MoI_2(I_3)(CNAr^{Mes2})_3$ (**25**) as a brown solid. Yield: 0.064 g, 0.037 mmol, 81%. X–ray diffraction quality crystals were grown from a saturated Et_2O solution. ^{1}H NMR (400.1 MHz, $CDCl_3$, 20 ˚C): δ = 29.03 (d, 2H, *J* = 8 Hz, *m*–Ph), 25.65 (d, 4H, *J* = 8 Hz, *m*–Ph), 7.80 (s, 8H, *m*–Mes), 7.57 (s, 4H, *m*–Mes), 5.92 (s, 24H, *o*–CH_3), 4.46 (s, 12H, *p*–CH_3), 0.24 (s, 6H, *p*–CH_3), –0.29 (s, 12H, *o*–CH_3), –17.16 (s, 2H, *o*–Ph), –35.14 (s, 12H, *o*–Ph) ppm. μ_{eff} (Evans Method, $CDCl_3$ with $O(SiMe_3)_2$, 400.1 MHz, 20 ˚C) = 3.68(9) μ_B (average of 3 independent measurements). FTIR ($CDCl_3$, KBr windows): ν_{CN} = 2142 (vs) cm^{-1}, also 3027 (w), 2974 (w), 2949 (w), 2918 (m), 2859 (w), 1613 (w), 1376 (w), 1274 (w), 1030 (w), 849 (m), 605 (w) cm^{-1}. Anal. Calcd for $C_{75}H_{75}N_3I_5Mo$: C, 53.01; H, 4.32; N, 2.41. Found: C, 53.01; H, 4.33; N, 1.97.

Synthesis of Mo(η^6–$C_{10}H_8$)$(CNAr^{Clips2})_3$ (26). A mixture of Mo(η^6–$C_{10}H_8$)$_2$ (0.026 g, 0.074 mmol) and $CNAr^{Clips2}$ (0.100 g, 0.223 mmol, 3 equiv) was slurried in 20 mL of *n*–pentane for 12 h. The reaction mixture was then concentrated to 10 mL under reduced pressure and filtered. The resulting brown solid was then subjected to three cycles of thawing–*n*–pentane wash (2 mL), followed by drying *in vacuo*. After the last cycle, Mo(η^6–$C_{10}H_8$)$(CNAr^{Clips2})_3$ (**26**) was obtained as a brown powder. Yield: 0.055 g, 0.035 mmol, 47%. X–ray diffraction quality crystals were grown from a concentrated cyclohexane solution. ^{1}H

NMR (500.1 MHz, C_6D_6, 20 ˚C): δ = 7.33 (s, 6H, *m*–Ph), 7.16 (dd, 2H, J = 6 Hz, J = 6 Hz, $C_{10}H_8$), 7.12 (d, 12H, J = 8 Hz, *m*–Clips), 6.83 (dd, 2H, J = 6 Hz, J = 6 Hz, $C_{10}H_8$), 6.77 (t, 6H, J = 8 Hz, *p*–Clips), 4.40 (dd, 2H, J = 5 Hz, J = 3 Hz, $C_{10}H_8$), 3.91 (dd, 2H, J = 5 Hz, J = 3 Hz, $C_{10}H_8$), 1.14 (s, 27H, C(CH_3)$_3$) ppm. $^{13}C\{^1H\}$ NMR (125.7 MHz, C_6D_6, 20 ˚C): δ = 203.6 (*C*≡N), 146.2, 138.4, 136.4, 132.6, 129.4, 129.4, 127.2, 126.2, 108.4, 87.2, 83.7, 34.6 (*C*(CH$_3$)$_3$), 31.4 (C(*C*H$_3$)$_3$) ppm. FTIR (C_6D_6, KBr windows): ν_{CN} = 1998 (s), 1905 (s), and 1862 (s) cm^{-1}, also 2960 (m), 2904 (w), 2868 (w), 1557 (w), 1419 (m), 1329 (w), 1188 (w), 783 (m), 757 (m), 672 (w) cm^{-1}. Anal. Calcd for $C_{79}H_{59}N_3Cl_{12}Mo$: C, 60.37; H, 3.78; N, 2.67. Found: C, 56.25; H, 3.91; N, 2.67.

Synthesis of Mo(η^6–C_6H_6)(CNAr^{Clips2})$_3$ (27). To a C_6H_6 solution of Mo(η^6–$C_{10}H_8$)$_2$ (**26**, 0.039 g, 0.111 mmol, 5 mL) was added a C_6H_6 solution of CNAr^{Clips2} (0.150 g, 0.334 mmol, 3 equiv, 10 mL). The reaction mixture was allowed to stir for 2 h, after which all volatile materials were removed under reduced pressure. Dissolution of the resulting red residue in *n*–pentane (15 mL) followed by filtration and storage at –35 ˚C for 24 h resulted in red crystals, which were collected and dried *in vacuo*. Yield: 0.097 g, 0.064 mmol, 57%. X–ray diffraction quality crystals were grown from a concentrated cyclohexane solution. ^1H NMR (500.1 MHz, C_6D_6, 20 ˚C): δ = 7.32 (s, 6H, *m*–Ph), 7.18 (d, 12H, J = 8 Hz, *m*–Clips), 6.78 (t, 6H, J = 8 Hz, *p*–Clips), 4.14 (s, 6H, C_6H_6), 1.14 (s, 27H, C(CH_3)$_3$) ppm. $^{13}C\{^1H\}$ NMR (125.7 MHz, C_6D_6, 20 ˚C): δ = 205.6 (*C*≡N), 146.6, 138.4, 136.3, 132.8, 129.5, 129.1, 129.0, 88.0, 34.6 (*C*(CH$_3$)$_3$), 31.2 (C(*C*H$_3$)$_3$) ppm. FTIR (C_6D_6, KBr windows): ν_{CN} = 2003 (m), 1903 (vs), and 1850 (s) cm^{-1}, also 2964 (w), 2928 (w), 2908 (w), 2870 (w), 1421 (m), 1245 (w), 1190 (w), 789 (w), 778 (w), 756 (w) cm^{-1}. Anal. Calcd for $C_{23}H_{17}NCl_4$: C, 59.20; H, 3.78; N, 2.76. Found: C, 58.93; H, 4.04; N, 2.51.

Synthesis of Mo(η^6–C_6H_5F)($CNAr^{Clips2}$)$_3$ (28). To a C_6H_5F solution of Mo(η^6–$C_{10}H_8$)$_2$ (**26**, 0.026 g, 0.074 mmol, 5 mL) was added a C_6H_5F solution of $CNAr^{Clips2}$ (0.100 g, 0.223 mmol, 3 equiv, 5 mL). The reaction mixture was allowed to stir for 2 h, after which all volatile materials were removed under reduced pressure. Dissolution of the resulting red residue in *n*–pentane (10 mL) followed by filtration and storage at –35 ˚C for 24 h resulted in red crystals, which were collected and dried *in vacuo*. Yield: 0.071 g, 0.046 mmol, 62%. X–ray diffraction quality crystals were grown from a concentrated cyclohexane solution. ^{1}H NMR (500.1 MHz, C_6D_6, 20 ˚C): δ = 7.33 (s, 6H, *m*–Ph), 7.17 (d, 12H, *J* = 8 Hz, *m*–Clips), 6.77 (t, 6H, *J* = 8 Hz, *p*–Clips), 4.04 (m, 2H, *o*–C_6H_5F), 3.86 (m, 2H, *m*–C_6H_5F), 3.65 (m, 1H, *p*–C_6H_5F), 1.13 (s, 27H, C(CH_3)$_3$) ppm. ^{13}C{^{1}H} NMR (125.7 MHz, C_6D_6, 20 °C): δ = 204.0 (*C*≡N), 147.0, 138.3, 136.4, 132.9, 129.6, 129.2, 128.8, 128.6, 88.5, 88.4, 78.9, 71.6, 71.4, 34.6 (*C*(CH$_3$)$_3$), 31.1 (C(*C*H$_3$)$_3$) ppm. FTIR (C_6D_6, KBr windows): ν_{CN} = 2012 (s), 1916 (s), and 1873 (s) cm^{-1}, also 2963 (m), 2905 (w), 2868 (w), 1558 (w), 1441 (w), 1421 (m), 1202 (w), 792 (w), 779 (w), 757 (w), 669 (w) cm^{-1}. Anal. Calcd for $C_{75}H_{65}N_3Cl_{12}FMo$: C, 58.51; H, 3.67; N, 2.73. Found: C, 57.16; H, 3.92; N, 2.51.

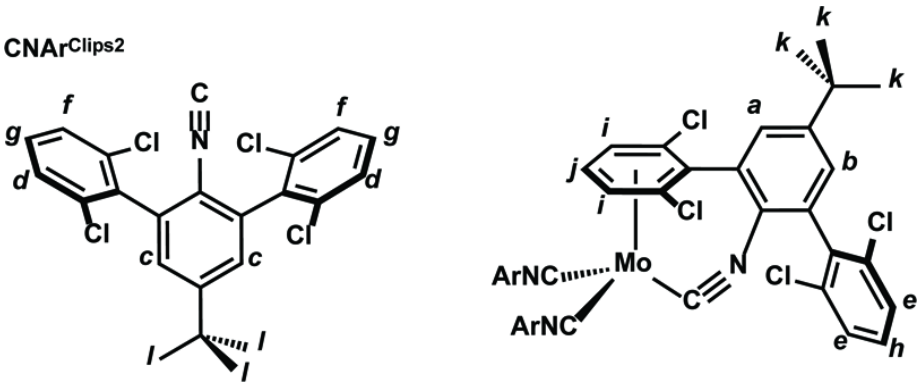

Figure 4.26. Labeling scheme for ^{1}HNMR assignments in Mo(η^6–(2,6–$Cl_2C_6H_3$)–κ^1–*C*–$CNAr^{Clips}$)($CNAr^{Clips2}$)$_2$ (**29**).

Synthesis of Mo(η^6–(2,6–$Cl_2C_6H_3$)–κ^1–*C*–$CNAr^{Clips}$)($CNAr^{Clips2}$)$_2$ (29). An *n*–pentane slurry of Mo(η^6–$C_{10}H_8$)($CNAr^{Clips2}$)$_3$ (**26**, 0.200 g, 0.127 mmol, 50 mL) was heated at 60 ˚C for 12 h. The resulting brown solution was filtered over a medium porosity frit and all volatile materials were removed from the filtrate under reduced pressure. ^{1}H NMR spectroscopic analysis (C_6D_6) of resultant crude brown material revealed a mixture three products, Mo(η^6–(2,6–$Cl_2C_6H_3$)–κ^1–*C*–$CNAr^{Clips}$)($CNAr^{Clips2}$)$_2$ (**29**), $MoCl_2(CNAr^{Clips2})_4$ (**30**) , and 2,2'–di–*tert*–butyl–10,10'–dichloro–4,4'–bis(Clips)–6,6'–biphenanthridine (**31**) in an approximate 4:1:1 distribution, respectively. Dissolution of the crude material in acetonitrile (10 mL), followed by filtration and storage at –35 ˚C for 24 h resulted in the selective crystallization of orange crystals of Mo(η^6–(2,6–$Cl_2C_6H_3$)–κ^1–*C*–$CNAr^{Clips}$)($CNAr^{Clips2}$)$_2$ (**29**), which were collected and dried *in vacuo*. ^{1}H NMR analysis indicated that these crystals were free of compounds Mo(η^6–(2,6–$Cl_2C_6H_3$)–κ^1–*C*–$CNAr^{Clips}$)($CNAr^{Clips2}$)$_2$ (**29**) and $MoCl_2(CNAr^{Clips2})_4$ (**30**). Yield: 0.044 g, 0.030 mmol, 24%. ^{1}H NMR (500.1 MHz, C_6D_6, 20 ˚C): δ = 7.65 (d, 1H, J = 2 Hz, H_a), 7.37 (d, 1H, J = 2 Hz, H_b), 7.34 (s, 4H, H_c), 7.26 (d, 4H, J = 8 Hz, H_d), 7.21 (d, 2H, J = 8 Hz, H_e), 7.18 (d, 4H, J = 8 Hz, H_f), 6.83 (t, 4H, J = 8 Hz, H_g), 6.74 (t, 1H, J = 8 Hz, H_h), 4.69 (d, 2H, J = 6 Hz, H_i), 4.17 (t, 1H, J = 6 Hz, H_j), 1.20 (s, 9H, H_k), 1.10 (s, 18H, H_l) ppm. ^{13}C{^{1}H} NMR (125.7 MHz, C_6D_6, 20 ˚C): δ = 275.6 (*C*≡N), 190.6 (*C*≡N), 149.9, 149.4, 146.2, 139.8, 136.8, 136.4, 136.3, 135.8, 133.2, 130.4, 130.0, 129.0, 128.2, 127.7, 127.7, 126.6, 126.0, 115.6, 115.4, 106.5, 89.9, 86.5, 81.2, 34.9, 34.7, 31.4, 31.1 ppm. FTIR (C_6D_6, KBr windows): ν_{CN} = 2060 (s), 1999 (s), and 1680 (s) cm^{-1}, also 2962 (m), 2360, 1591 (w), 1559 (w), 1427 (m), 1247 (w), 1191 (w), 789 (w), 775 (w) cm^{-1}. Anal. Calcd for $C_{75}H_{57}N_3Cl_{12}Mo$: C, 59.20; H, 3.78; N, 2.51. Found: C, 58.93; H, 4.04; N, 2.51.

Synthesis of a mixture of $MoCl_2(CNAr^{Clips2})_4$ (30) and 2,2'–di–*tert*–butyl–10,10'–dichloro–4,4'–bis(Clips)–6,6'–biphenanthridine (31). A mixture of Mo(η^6–$C_{10}H_8$)$_2$ (0.078

g, 0.223 mmol) and $CNAr^{Clips2}$ (0.300 g, 0.668 mmol, 3 equiv) was dissolved in Et_2O (100 mL) and heated at 90 °C for 24 h. This procedure first forms $Mo(\eta^6–C_{10}H_8)(CNAr^{Clips2})_3$ (**26**), which is then exhaustively thermolyzed to $MoCl_2(CNAr^{Clips2})_4$ (**30**) and the biphenanthridine (**31**). The reaction mixture was filtered and all volatiles were removed under reduced pressure. ^1H NMR analysis of the resulting brown residue revealed the presence of naphthalene and 2,2'–di–*tert*–butyl–10,10'–dichloro–4,4'–bis(Clips)–6,6'–biphenanthridine (**31**) in a 2:3 ratio respectively, and also *trans*–$MoCl_2(CNAr^{Clips2})_4$ (**30**) as a paramagnetic product.

Isolation of $MoCl_2(CNAr^{Clips2})_4$ (30) from a mixture of $MoCl_2(CNAr^{Clips2})_4$, 2,2'–di–*tert*–butyl–10,10'–dichloro–4,4'–bis(Clips)–6,6'–biphenanthridine (31) and naphthalene. A mixture of $Mo(\eta^6–C_{10}H_8)_2$ (0.078 g, 0.223 mmol) and $CNAr^{Clips2}$ (0.300 g, 0.668 mmol, 3 equiv) was dissolved in Et_2O (100 mL) and heated at 90 ˚C for 24 h. The reaction mixture was filtered and all volatiles were removed under reduced pressure. The resulting brown solid was then subjected to five cycles of C_6H_6 wash (3 mL), followed by drying *in vacuo*. After the last cycle, *trans*–$MoCl_2(CNAr^{Clips2})_4$ (**30**) was obtained as an orange powder. Yield: 0.040 g, 0.021 mmol, 9%. X–ray diffraction quality crystals were grown from a saturated C_6H_6 solution. ^1H NMR (400.1 MHz, $CDCl_3$, 20 ˚C): δ = 15.43 (s, 8H), 7.04 (s, 16H, *m*–Clips), 6.29 (s, 8H), 1.54 (s, 36H, $C(CH_3)_3$) ppm. FTIR ($CDCl_3$, KBr windows): ν_{CN} = 2062 (vs) cm^{-1}, also 2967 (m), 2907 (w), 2872 (w), 1560 (w), 1478 (w), 1463 (w), 1440 (m), 1423 (w), 1400 (w), 1365 (w), 1248 (w), 1213 (w), 1195 (w), 791 (m), 776 (m) cm^{-1}. Anal. Calcd for $C_{92}H_{68}N_4Cl_{18}Mo$: C, 56.27; H, 3.49; N, 2.85. Found: C, 57.17; H, 3.29; N, 2.83.

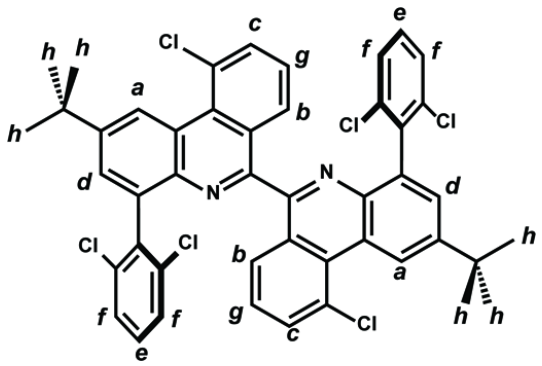

Figure 4.27. Labeling scheme for ^{1}H NMR assignments in 2,2'–di–*tert*–butyl–10,10'–dichloro–4,4'–bis(Clips)–6,6'–biphenanthridine (**31**).

Isolation of 2,2'–di–*tert*–butyl–10,10'–dichloro–4,4'–bis(Clips)–6,6'–biphenanthridine (31) from a mixture of $MoCl_2(CNAr^{Clips2})_4$ (30), 2,2'–di–*tert*–butyl–10,10'–dichloro–4,4'–bis(Clips)–6,6'–biphenanthridine and naphthalene. A mixture of $Mo(\eta^6–C_{10}H_8)_2$ (0.078 g, 0.223 mmol) and $CNAr^{Clips2}$ (0.300 g, 0.668 mmol, 3 equiv) was dissolved in Et_2O (100 mL) and heated at 90 ˚C for 24 h. The reaction mixture was filtered and all volatiles were removed under reduced pressure. The resulting brown solid was washed with C_6H_6 (5 x 3 mL) and the first two washes were discarded, while the latter three were combined and dried under reduced pressure. The remaining tan solid was dissolved in *n*–pentane (10 mL) and filtered. Storage of this solution at –35 °C for 3 d resulted in the formation of a tan precipitate. The *n*–pentane supernatant was decanted away from the solids and filtered. Following the removal of all volatile materials from the filtrate under reduced pressure, 2,2'–di–*tert*–butyl–10,10'–dichloro–4,4'–bis(Clips)–6,6'–biphenanthridine (**31**) was isolated as an off–white solid. Yield: 0.011 g, 0.012 mmol, 5%. X–ray diffraction quality crystals were grown from a saturated Et_2O solution of the crude reaction mixture stored at –35 ˚C for 1 d. A sample for X–ray analysis was obtained by manually separating the colorless crystals from bulk sample on a microscope slide. ^{1}H NMR (500.1 MHz, $CDCl_3$, 20 ˚C): δ = 10.00 (d, 2H, J = 2 Hz, H_a), 8.19 (d, 2H, J = 8 Hz, H_b), 7.88 (d, 2H, J = 8 Hz, H_c), 7.74 (d,

2H, J = 2 Hz, H_d), 7.38 (t, 2H, J = 7 Hz, H_e), 7.25 (d, 4H, J = 8 Hz, H_f), 7.06 (t, 2H, J = 8 Hz, H_g) 1.52 (w, 18H, H_h) ppm. $^{13}C\{^1H\}$ NMR (125.7 MHz, $CDCl_3$, 20 ˚C): δ = 156.9, 149.4, 140.3, 139.2, 136.8, 135.6, 134.3, 130.8, 130.8, 129.0, 128.7, 128.7, 127.6, 126.6, 123.2, 122.9, 35.8 ($C(CH_3)_3$), 31.6 ($C(CH_3)_3$) ppm. HRMS (ESI, acetone): m/z Found = 827.24 $[M+H]^+$.

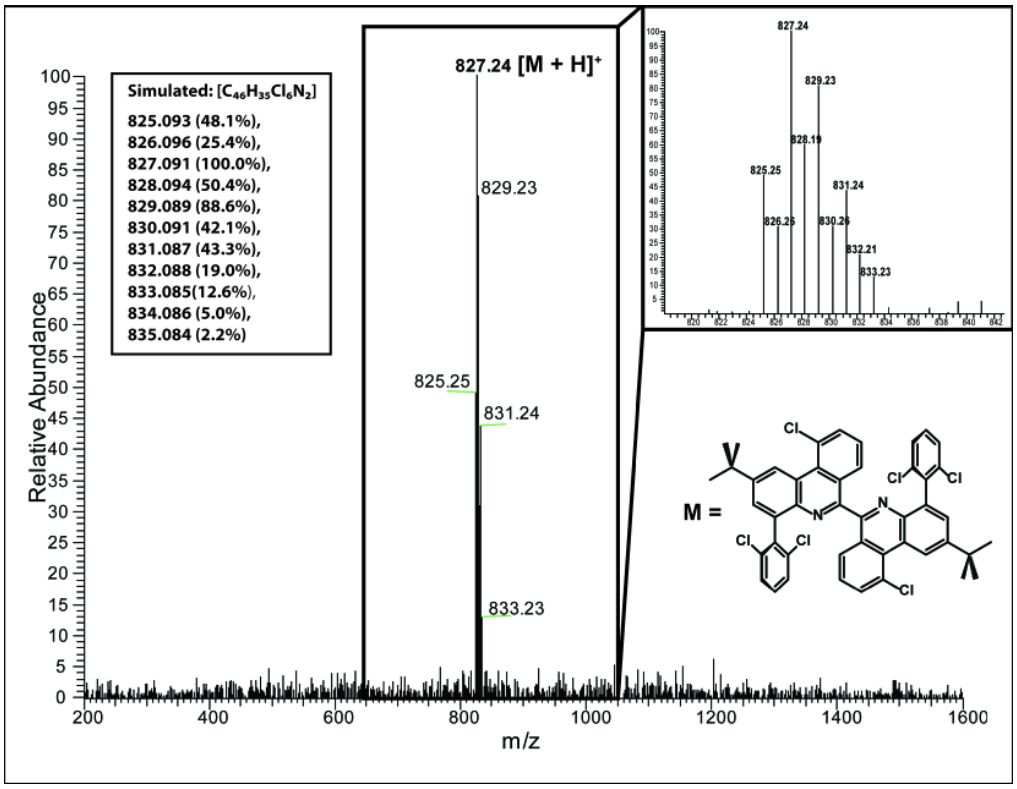

Figure 4.28. Full HRMS (ESI/positive ion mode, acetone) mass spectrum of 2,2'–di–*tert*–butyl–10,10'–dichloro–4,4'–bis(Clips)–6,6'–biphenanthridine (**31**).

Synthesis of Mo(η^6–$C_{10}H_8$)($CNAr^{DArF2}$)$_3$ (32). To an Et_2O solution of Mo(η^6–$C_{10}H_8$)$_2$ (0.029 g, 0.082 mmol, 5 mL) was added an Et_2O solution of $CNAr^{DArF2}$ (0.130 g, 0.247 mmol, 3 equiv, 5 mL). The reaction mixture was allowed to stir for 30 min, after which all volatile materials were removed under reduced pressure. Dissolution of the resulting purple residue in cyclohexane (10 mL), followed by filtration and storage at room temperature for 24

h resulted in purple crystals, which were collected and dried *in vacuo*. Yield: 0.083 g, 0.046 mmol, 56%. ^{1}H NMR (500.1 MHz, C_6D_6, 20 ˚C): δ = 7.76 (s, 12H, *o*–ArF), 7.60 (s, 6H, *p*–ArF), 6.76 (t, 3H, J = 8 Hz, *p*–Ph), 6.72 (d, 6H, J = 8 Hz, *m*–Ph), 6.30 (dd, 2H, J = 6 Hz, J = 3 Hz, $C_{10}H_8$), 5.90 (dd, 2H, J = 6 Hz, J = 3 Hz, $C_{10}H_8$), 4.48 (dd, 2H, J = 5 Hz, J = 3 Hz $C_{10}H_8$), 3.96 (dd, 2H, J = 5 Hz, J = 3 Hz, $C_{10}H_8$) ppm. ^{13}C{^{1}H} NMR (125.7 MHz, C_6D_6, 20 ˚C): δ = 203.5 (*C*≡N), 141.9, 134.7, 131.7, 131.5 (q, $^{2}J_{C-F}$ = 33 Hz, *m*–ArF), 129.8, 127.0, 126.3, 125.1, 123.7 (q, $^{1}J_{C-F}$ = 273 Hz, *C*F_3), 121.0 (b, *p*–ArF), 108.6, 90.9, 85.3 ppm. ^{19}F NMR (470.4 MHz, C_6D_6, 20 ˚C): δ = −63.1 ppm. FTIR (C_6D_6, KBr windows): ν_{CN} = 2009 (m), 1990 (w sh), and 1911(s b) cm^{-1}, also 2923 (w), 2851 (w), 1578 (w), 1429 (s b), 1373 (vs), 1280 (s), 1180 (m), 1138 (s), 899 (w), 848 (w), 743 (w), 704 (w) cm^{-1}. Anal. Calcd for $C_{79}H_{35}N_3F_{36}Mo$: C, 52.53; H, 1.95; N, 2.33. Found: C, 52.25; H, 1.87; N, 2.26.

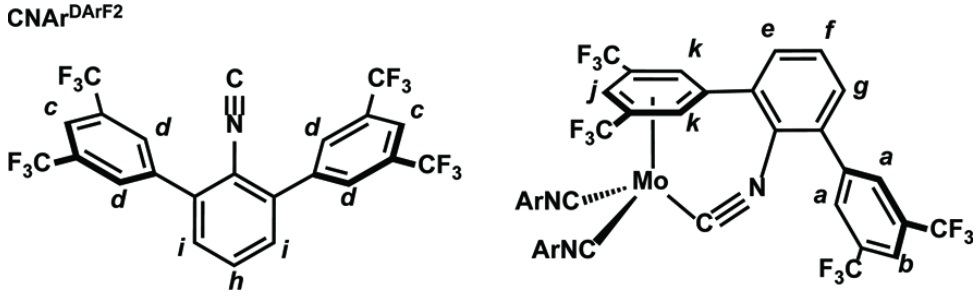

Figure 4.29. Labeling scheme for ^{1}H NMR assignments in Mo(η^6–(3,5–$(CF_3)_2C_6H_3$)–κ^1–*C*–$CNAr^{DArF}$)$(CNAr^{DArF2})_2$ (**33**).

Synthesis of Mo(η^6–(3,5–$(CF_3)_2C_6H_3$)–κ^1–*C*–$CNAr^{DArF}$)$(CNAr^{DArF2})_2$ (33). **Method A.** A THF solution of Mo(η^6–$C_{10}H_8$)$(CNAr^{DArF2})_3$ (**32**, 0.120 g, 0.066 mmol, 8 mL) was allowed to stir for 12 h. The resulting orange solution was filtered and all volatiles materials were removed under reduced pressure. The resulting orange solid was then subjected to three cycles of thawing *n*–pentane wash (1 mL), followed by drying *in vacuo*. After the last cycle, Mo(η^6–(3,5–$(CF_3)_2C_6H_3$)–κ^1–*C*–$CNAr^{DArF}$)$(CNAr^{DArF2})_2$ (**33**) was isolated as an orange powder. Yield: 0.067 g, 0.040 mmol, 60%. X–ray diffraction quality crystals

were grown from a saturated cyclohexane solution. ^{1}H NMR (500.1 MHz, C_6D_6, 20 ˚C): δ = 7.98 (s, 2H, H_a), 7.85 (s, 1H, H_b), 7.77 (s, 4H, H_c), 7.60 (s, 8H, H_d), 6.98 (d, 1H, J = 7 Hz, H_e), 6.92 (t, 1H, J = 8 Hz, H_f), 6.89 (s, 1H, J = 7 Hz, H_g) 6.75 (t, 2H, J = 8 Hz, H_h), 7.71 (d, 4H, J = 8 Hz, H_i), 4.55 (s, 1H, H_j), 4.35 (s, 2H, H_k) ppm. ^{13}C{^{1}H} NMR (125.7 MHz, C_6D_6, 20 ˚C): δ = 273.3 (*C*≡N), 187.7 (*C*≡N), 146.9, 141.3, 140.2, 136.0, 133.6, 132.1 (q, $^{2}J_{C–F}$ = 33 Hz, *m*–ArF), 131.4 (q, $^{2}J_{C–F}$ = 33 Hz, *m*–ArF), 130.9, 130.5, 130.2, 129.9, 129.4, 125.9, 124.7, 124.4 (q, $^{1}J_{C–F}$ = 273 Hz, *C*F_3), 123.5 (q, $^{1}J_{C–F}$ = 273 Hz, *C*F_3), 123.1 (q, $^{1}J_{C–F}$ = 273 Hz, *C*F_3), 122.2, 121.1, 105.1, 89.4 (q, $^{2}J_{C–F}$ = 37 Hz, *m*–ArF coordinated), 75.7, 70.7 ppm (two aryl resonances obscured by C_6D_6 solvent). ^{19}F NMR (282.3 MHz, C_6D_6, 20 ˚C): δ = –61.9, –63.3 and –63.5 ppm. FTIR (C_6D_6, KBr windows): ν_{CN} = 2063 (s), 2005 (s), 1984 (ws) and 1717 (s) cm^{-1}, also 3090 (w), 3067 (w), 2959 (w), 2926 (w), 1577 (m), 1374 (m), 1280 (s), 1179 (s), 1140 (vs), 900 (m), 848 (w), 799 (w), 746 (w), 704 (w), 682 (w) cm^{-1}. Anal. Calcd for $C_{69}H_{27}N_3F_{36}Mo$: C, 49.39; H, 1.62; N, 2.50. Found: C, 50.51; H, 1.79; N, 2.38.

Method B. A mixture of Mo(η^6–$C_{10}H_8$)$_2$ (0.045 g, 0.126 mmol) and CNAr^{DArF2} (0.200 g, 0.379 mmol, 3 equiv) was slurried in *n*–pentane (40 mL) and heated at 90 °C for 12 h. The reaction mixture was then concentrated to 10 mL under reduced pressure and filtered. The resulting orange solid was the subjected to three cycles of thawing *n*–pentane wash (2 mL), followed by drying *in vacuo*. After the last cycle, Mo(η^6–(3,5–$(CF_3)_2C_6H_3$)–κ^1–*C*–CNAr^{DArF})(CNAr^{DArF2})$_2$ (**33**) was isolated as an orange powder. Yield: 0.105 g, 0.063 mmol, 50%.

Synthesis of Mo(η^6–C_6H_6)(CNAr^{DArF2})$_3$ (34) via thermolysis in benzene. A C_6H_6 solution of Mo(η^6–(3,5–$(CF_3)_2C_6H_3$)–κ^1–*C*–CNAr^{DArF})(CNAr^{DArF2})$_2$ (**33**, 0.070 g, 0.042 mmol, 15 mL) was placed in a sealed ampoule and heated at 110 ˚C for 6 d. All volatiles were removed under reduced pressure. The remaining red semi–solid was dissolved in Et_2O

(2 mL), filtered, layered with $O(SiMe_3)_2$ (6 mL) and stored at –35 ˚C for 1 day, whereupon fine red crystals of Mo(η^6–C_6H_6)($CNAr^{DArF2}$)$_3$ (**34**) were obtained. Yield: 0.032 g, 0.018 mmol, 44%. ^{1}H NMR (500.1 MHz, C_6D_6, 20 ˚C): δ = 7.78 (s, 12H, *o*–ArF), 7.60 (s, 6H, *p*–ArF), 6.78 (t, 3H, *J* = 8 Hz, *p*–Ph), 6.72 (d, 6H, *J* = 8 Hz, *m*–Ph), 3.64 (s, 6H, C_6H_6) ppm. ^{13}C{^{1}H} NMR (125.7 MHz, C_6D_6, 20 ˚C): δ = 202.6 (*C*≡N), 141.9, 134.9, 131.6, 131.6 (q, $^2J_{C–F}$ = 33 Hz, *m*–ArF), 129.8, 127.2, 125.2, 123.7 (q, $^1J_{C–F}$ =273 Hz, *C*F_3), 121.1 (b, *p*–ArF), 89.7 ppm. ^{19}F NMR (470.4 MHz, C_6D_6, 20 ˚C): δ = –63.2 ppm. FTIR (C_6D_6, KBr windows): ν_{CN} = 2012 (m), 1995 (w sh), and 1903(vs b) cm^{-1}, also 2958 (w), 2921 (w), 2859 (w), 2830 (w), 1618 (m), 1373 (m), 1332 (m), 1280 (s), 1180 (m), 1138 (s), 704 (w), 683 (w) cm^{-1}. Anal. Calcd for $C_{75}H_{33}N_3F_{36}Mo$: C, 51.30; H, 1.89; N, 2.39. Found: C, 48.61; H, 1.80; N, 2.45.

Synthesis of *fac*–Mo(NCMe)$_3$($CNAr^{DArF2}$)$_3$ (35). To Et_2O solution of Mo(η^6–(3,5–$(CF_3)_2C_6H_3$)–κ^1–*C*–$CNAr^{DArF}$)($CNAr^{DArF2}$)$_2$ (**33**, 0.045 g, 0.026 mmol, 5 mL) was added acetonitrile (MeCN; 0.786 g, 19.14 mmol, 736 equiv, 1 mL), which resulted in a rapid color change from orange to purple. The reaction mixture was stirred for 1 h, after which all volatiles were removed *in vacuo*. The resulting purple solid was dissolved in Et_2O (2 mL total), filtered, layered with MeCN (3 mL), and stored at –35 ˚C for 1 day, whereupon fine purple crystals of *fac*–Mo(NCMe)$_3$($CNAr^{DArF2}$)$_3$ were obtained. Yield: 0.25 g, 0.088 mmol, 60%. ^{1}H NMR (500.2 MHz, C_6D_{12}, 20 ˚C): δ = 7.96 (s, 6H, *p*–ArF), 7.95 (s, 12H, *o*–ArF), 7.51 (t, 3H, *J* = 8 Hz, *p*–Ph), 7.42 (d, 6H, *J* = 8 Hz, *m*–Ph), 1.29 (s, 9H, NCC*H*$_3$) ppm. ^{13}C{^{1}H} NMR (125.7 MHz, C_6D_{12}, 20 ˚C): δ = 178.1 (*C*≡N), 139.8, 138.4, 133.7 (q, $^2J_{C–F}$ = 34 Hz, *m*–ArF), 130.7, 131.0 (N*C*–CH_3, tentative), 129.9, 124.5, 123.8 (q, $^1J_{C–F}$ = 273 Hz, *C*F_3), 124.5, 123.2 (b, *p*–ArF), 30.6 (NC–*C*H_3) ppm. FTIR (KBr pellet): ν_{CN} = 1905 (vs b) and 1864 (w sh) cm^{-1}; ν_{NC} = 2189 (m br) cm^{-1}, also 3095 (w), 2929 (w), 2854 (w), 1622 (w),

1577 (s), 1459 (m), 1408 (m), 1375 (m), 1278 (m), 1774 (m), 1136 (m) cm^{-1}. Solid–state samples of *fac*–Mo(NCMe)$_3$(CNAr^{DArF2})$_3$ (**35**) exhibit limited thermal stability at room temperature, which precluded the acquisition of a satisfactory combustion analysis.

Synthesis of Mo(η^6–C$_6$H$_6$)(CNAr^{DArF2})$_3$ (34) from *fac*–Mo(NCMe)$_3$(CNAr^{DArF2})$_3$ (35) and benzene. Method A: An acetonitrile solution of Mo(η^6–(3,5–(CF$_3$)$_2$C$_6$H$_3$)–κ^1–*C*–CNAr^{DArF2})(CNAr^{DArF2})$_2$ (**33**, 0.050 g, 0.030 mmol, 5 mL) was allowed to stir for 30 min, during which time the solution changed from orange to purple indicating the formation of *fac*–Mo(NCMe)$_3$(CNAr^{DArF2})$_3$ (**35**). All volatiles were then removed *in vacuo.* The remaining purple solid was dissolved in C$_6$H$_6$, and allowed to stir for 30 min resulting in a color change from purple to red. Following the removal of all volatile materials under reduced pressure, Mo(η^6–C$_6$H$_6$)(CNAr^{DArF2})$_3$ (**34**) was isolated as a red solid as determined by ^{1}H NMR spectroscopy in C$_6$D$_6$.

Method B: Purple single crystals of *fac*–Mo(NCMe)$_3$(CNAr^{DArF2})$_3$ (**8**^{DArF}, 0.010 g, 0.005 mmol) were dissolved in C$_6$D$_6$ (0.8 mL), which resulted in the formation of a red solution. Analysis of the solution by ^{1}H NMR spectroscopy revealed CNAr^{DArF2} resonances consistent with the formation of Mo(η^6–C$_6$H$_6$)(CNAr^{DArF2})$_3$ (**4**^{DArF}) along with resonances corresponding to free NCMe (0.60 ppm).

Synthesis of *fac*–Mo(CO)$_3$(CNAr^{Clips2})$_3$ (36). To an Et$_2$O slurry of Mo(CO)$_3$(NCEt)$_3$ (0.045 g, 0.148 mmol, 5 mL) was added Et$_2$O solution of CNAr^{Clips2} (0.200 g, 0.445 mmol, 3 equiv, 10 mL). The mixture was stirred for 1 h, after which all volatiles were removed *in vacuo*. The remaining yellow solid was dissolved in a 1:5 mixture of THF/Et$_2$O (6 mL total), filtered, layered with *n*–pentane (5 mL), and stored at –35 ˚C for 1 day, whereupon fine yellow crystals of *fac*–Mo(CO)$_3$(CNAr^{Clips2})$_3$ (**36**) were obtained. Yield: 0.135 g, 0.088 mmol,

60%. ^{1}H NMR (500.2 MHz, C_6D_6, 20 ˚C): δ = 7.36 (s, 6H, *m*–Ph), 7.28 (d, 12H, *J* = 8 Hz, *m*–Clips), 6.90 (t, 6H, *J* = 8 Hz, *p*–Clips), 1.12 (s, 27H, C(CH_3)$_3$) ppm. ^{13}C{^{1}H} NMR (125.7 MHz, C_6D_6, 20 ˚C): δ = 209.8 (*C*≡O), 177.7 (*C*≡N), 150.2, 136.0, 135.6, 134.0, 130.6, 128.8, 128.7, 128.4, 126.0, 34.9 (*C*(CH$_3$)$_3$), 31.0 (C(*C*H$_3$)$_3$) ppm. FTIR (C_6D_6, KBr windows): ν_{CN} = 2042 (s) and 2023 (m sh) cm^{-1}; ν_{CO} = 1943 (s) and 1909 (vs) cm^{-1}, also 2967 (m), 2915 (s), 2870 (s), 1438 (w), 1424 (m), 1399 (w), 1365 (w), 1193 (w), 791 (m), 778 (m), 758 (w), 595 (w), 580 (w) cm^{-1}. Anal. Calcd for $C_{72}H_{51}N_3O_3Cl_{12}Mo$: C, 56.61; H, 3.37; N, 2.75. Found: C, 56.87; H, 3.37; N, 2.69.

Synthesis of *mer*–Mo(CO)$_3$(CNAr^{Clips2})$_3$ (37). A THF solution of *fac*–Mo(CO)$_3$(CNAr^{Clips2})$_3$ (**36**; 0.100 g, 0.065 mmol, 10 mL) was placed in a sealed ampoule and irradiated with a 254 nm Hg lamp for 6 h. All volatiles were removed under reduced pressure. The remaining orange solid was dissolved in fluorobenzene (2 mL), filtered, layered with *n*–pentane (2 mL) and stored at –35 ˚C for 1 day, whereupon fine orange crystals of *mer*–Mo(CO)$_3$(CNAr^{Clips2})$_3$ were obtained. Yield: 0.042 g, 0.027 mmol, 42%. ^{1}H NMR (500.2 MHz, C_6D_6, 20 ˚C): δ = 7.38 (s, 2H, *m*–Ph), 7.33 (d, 4H, *J* = 7 Hz, *m*–Clips), 7.32 (s, 4H, *m*–Ph), 7.26 (d, 8H, *J* = 8 Hz, *m*–Clips), 7.0 (t, 2H, *J* = 7 Hz, *p*–Clips), 6.79 (t, 4H, *J* = 8 Hz, *p*–Clips), 1.08 (s, 18H, C(CH_3)$_3$), 1.08 (s, 9H, C(CH_3)$_3$) ppm. ^{13}C{^{1}H} NMR (125.7 MHz, C_6D_6, 20 ˚C): δ = 209.9 (*C*≡O), 206.7(*C*≡O), 178.3 (*C*≡N), 176.7 (*C*≡N), 150.0, 149.8, 136.6, 136.0, 135.8, 135.7, 134.1, 134.0, 128.6, 128.6, 128.5, 128.4, 34.9 (*C*(CH$_3$)$_3$), 34.9 (*C*(CH$_3$)$_3$), 31.1 (C(*C*H$_3$)$_3$), 31.0 (C(*C*H$_3$)$_3$) ppm. FTIR (C_6D_6, KBr windows): ν_{CN} = 2038 (m sh), 2010 (s), and 1979 (m sh) cm^{-1}; ν_{CO} = 1917 (vs) cm^{-1}, also 2968 (m), 2869 (w), 1558 (w), 1425 (m), 1403 (w), 1365 (w), 1247 (w), 1193 (w), 1026 (w), 790 (m), 779 (m), 668 (w), 594 (w) cm^{-1}. Anal. Calcd for $C_{72}H_{51}N_3O_3Cl_{12}Mo$: C, 56.61; H, 3.37; N, 2.75. Found: C, 56.36; H, 3.61; N, 2.66.

Synthesis of *mer*–Mo(CO)$_3$(CNAr^{DArF2})$_3$ (38). To a C_6H_6 solution of Mo(η^6–$C_{10}H_8$)(CNAr^{DArF2})$_3$ (**32**, 0.120 g, 0.066 mmol, 15 mL) was added CO gas (0.035 mL, 1.455 mmol, 22 equiv). The reaction mixture was heated at 70 ˚C for 12 h, after which all volatiles were removed under reduced pressure. The remaining yellow solid was dissolved in a 2:5 mixture of THF/Et_2O (7 mL total), filtered, layered with *n*–pentane (7 mL), and stored at –35 ˚C for 1 d, whereupon fine yellow crystals of *mer*–Mo(CO)$_3$(CNAr^{DArF2})$_3$ (**38**) were obtained. Yield: 0.080 g, 0.045 mmol, 69%. ^{1}H NMR (500.2 MHz, C_6D_6, 20 ˚C): δ = 7.76 (s, 2H, *p*–ArF), 7.75 (s, 4H, *o*–ArF), 7.67 (s, 8H, *o*–ArF), 7.62 (s, 4H, *p*–ArF), 6.81 (t, 1H, *J* = 8 Hz, *p*–Ph), 6.74 (t, 2H, *J* = 8 Hz, *p*–Ph), 6.68 (d, 2H, *J* = 8 Hz, *m*–Ph), 6.59 (d, 4H, *J* = 8 Hz, *m*–Ph) ppm. ^{13}C{^{1}H} NMR (125.7 MHz, C_6D_6, 20 ˚C): δ = 207.4 and 205.2 (*C*≡O), 178.6 and 177.3 (*C*≡N), 140.2, 139.8, 136.4, 136.3, 132.3 (q, $^2J_{C–F}$ = 33 Hz, *m*–ArF), 132.1 (q, $^2J_{C–F}$ = 34 Hz, *m*–ArF), 130.9, 130.8, 129.4, 129.3, 127.0, 126.9, 125.1, 123.9, 123.6 (q, $^1J_{C–F}$ = 273 Hz, *C*F_3), 123.5 (q, $^1J_{C–F}$ = 273 Hz, *C*F_3), 122.2 (b, 2 x *p*–ArF) ppm. ^{19}F NMR (470.4 MHz, C_6D_6, 20 ˚C): δ = –63.4 and –63.4 ppm. FTIR (C_6D_6, KBr windows): ν_{CN} = 2040 (m sh), 2006 (s), and 1979 (m sh) cm^{-1}; ν_{CO} = 1941 (vs) cm^{-1}, also 2921 (w), 2857 (w), 1455 (s b), 1430 (s sh), 1374 (m), 1280 (s), 1181 (m), 1140 (s), 899 (w), 705 (w), 683 (w) cm^{-1}. Anal. Calcd for $C_{72}H_{27}N_3O_3F_{36}Mo$: C, 49.08; H, 1.54; N, 2.29. Found: C, 49.33; H, 1.49; N, 2.42.

4.8 Crystallographic Structure Determinations

General Considerations. Single crystal X–ray structure determinations were carried out at low temperature on a Bruker Platform or Kappa Diffractometers equipped with a Bruker APEX, APEX II, and Photon 100 area detectors. All structures were solved via direct methods with SIR 2004[97] and refined by full–matrix least–squares procedures utilizing SHELXL–2013.[98] Crystallographic data collection and refinement information are listed in

Table 4.3 through 4.8. The crystallographic routine SQUEEZE[99] was used to account for disordered solvent of cocrystallization in the crystal structures of Mo(η^6–(Dipp)–κ^1–*C*–$CNAr^{Dipp}$)($CNAr^{Dipp2}$)$_2$ (**23**), Mo(η^6–$C_{10}H_8$)($CNAr^{Clips2}$)$_3$ (**26**), and Mo(η^6–C_6H_6)($CNAr^{Clips2}$)$_3$ (**27**). The crystal structure of Mo(η^6–C_6H_6)($CNAr^{DArF2}$)$_3$ (**34**) contains a two–site positional disorder of the η^6–C_6H_6 ligand. The disorder was modeled such that the η^6–C_6H_6 ligands are present at 50% occupancy at each of the two sites. The crystal structure Mo(η^6–(Mes)–κ^1–*C*–$CNAr^{Mes}$)($CNAr^{Mes2}$)$_2$ (**24**) exhibits a 2% whole molecule disorder. Only the metal center was modeled because of the low percentage. The crystal structure of *fac*–Mo$(NCMe)_3$($CNAr^{DArF2}$)$_3$ (**35**) exhibits whole–molecule disorder of the ligand framework, which was modeled. All disorder was modeled and refined using standard crystallographic techniques.

Table 4.3. Crystallographic Data Collection and Refinement Information for Mo(η^6–(Dipp)–κ^1–*C*–CNAr^{Dipp})(CNAr^{Dipp2})$_2$·Et$_2$O·3(MeCN), Mo(η^6–(Mes)–κ^1–*C*–CNAr^{Mes})(CNAr^{Mes2})$_2$·C$_6$H$_5$F, and *mer*–MoI$_2$(I$_3$)(CNAr^{Mes2})$_3$·Et$_2$O

	Mo(η^6–(Dipp)–κ^1–*C*–CNAr^{Dipp})(CNAr^{Dipp2})$_2$·Et$_2$O·3(MeCN) (**23**· Et$_2$O·2.5(MeCN))	Mo(κ^1–*C*–CNAr^{Mes}(η^6–Mes))(CNAr^{Mes2})$_2$·C$_6$H$_5$F·*n*–pentane (**24**·C$_6$H$_5$F·*n*–pentane)	*mer*–MoI$_2$(I$_3$)(CNAr^{Mes2})$_3$·Et$_2$O (**25**·Et$_2$O)
Formula	$MoC_{102}H_{128.5}N_{5.5}O$	$MoC_{86}H_{92}N_3F$	$MoC_{79}H_{85}I_5N_3O$
Crystal System	Monoclinic	Triclinic	Triclinic
Space Group	$P2_1/n$	$P\bar{1}$	$P1$
a, Å	18.281(3)	12.409(2)	11.8544(9)
b, Å	12.0656(12)	14.486(3)	13.7194(9)
c, Å	41.545(5)	20.300(3)	13.9351(9)
α, deg	90	78.447(6)	66.634(3)
β, deg	99.526(8)	82.824(6)	74.122(3)
γ, deg	90	72.219(4)	66.577(4)
V, Å^3	9045.9(19)	3396.4(10)	1890.9(2)
Z	4	2	1
Radiation (λ, Å)	Mo–Kα, 0.71073	Mo–Kα, 0.71073	Cu–Kα, 1.54178
ρ (calcd.), g/cm^3	1.133	1.254	1.601
μ, mm^{-1}	0.194	0.245	17.774
Temp, K	100(2)	100(2)	100(2)
θ max, deg	25.382	25.607	65.618
data/parameters	12714 / 3 / 1010	12534 / 0 / 797	8693 / 3 /823
R_1	0.0712	0.0324	0.0308
wR_2	0.1435	0.0759	0.0751
GOF	1.015	1.031	1.013

Table 4.4. Crystallographic Data Collection and Refinement Information for Mo(η^6–$C_{10}H_8$)($CNAr^{Clips2}$)$_3$·1.5(Et_2O), Mo(η^6–C_6H_6)($CNAr^{Clips2}$)$_3$·2C_6H_{12}, and Mo(η^6–C_6H_5F)($CNAr^{Clips2}$)·2(C_6H_{12})

	Mo(η^6–$C_{10}H_8$)($CNAr^{Clips2}$)$_3$·1.5(Et_2O) (**26**·1.5(Et_2O))	Mo(η^6–C_6H_6)($CNAr^{Clips2}$)$_3$·2C_6H_{12} (**27**·2(C_6H_{12}))	Mo(η^6–C_6H_5F)($CNAr^{Clips2}$)·2(C_6H_{12}) (**28**·2(C_6H_{12}))
Formula	$MoC_{85}H_{74}Cl_{12}N_3O_{1.5}$	$MoC_{87}H_{81}Cl_{12}N_3$	$MoC_{87}H_{80}Cl_{12}FN_3$
Crystal System	Monoclinic	Monoclinic	Triclinic
Space Group	$P2_1$	$P2_1/n$	P–1
a, Å	18.5055(8)	17.4444(5)	11.6130(9)
b, Å	11.8182(6)	23.2637(7)	17.6893(16)
c, Å	19.9431(9)	21.8457(6)	20.1556(16)
α, deg	90	90	94.558(3)
β, deg	110.772(3)	112.5250(10)	90.406(3)
γ, deg	90	90	102.177(3)
V, Å^3	4078.1(3)	8189.1(4)	4033.3(6)
Z	2	4	2
Radiation (λ, Å)	Cu–Kα, 1.54178	Mo–Kα, 0.71073	Mo–Kα, 0.71073
ρ (calcd.), g/cm^3	1.370	1.371	1.406
μ, mm^{-1}	5.304	0.598	0.610
Temp, K	100(2)	100(2)	100(2)
θ max, deg	63.80	26.390	25.405
data/parameters	10392 / 7 / 864	16692 / 0 / 896	14298 / 2 /954
R_1	0.0476	0.0567	0.0837
wR_2	0.1200	0.1169	0.1576
GOF	1.063	1.071	1.064

Table 4.5. Crystallographic Data Collection and Refinement Information for Mo(η^6–(2,6–$Cl_2C_6H_3$)–κ^1–*C*–$CNAr^{Clips}$)($CNAr^{Clips2}$)$_2$·3(MeCN), $MoCl_2(CNAr^{Clips2})_4$·3(C_6H_6), and 2,2'–di–*tert*–butyl–10,10'–dichloro–4,4'–bis(Clips)–6,6'–biphenanthridine

	Mo(η^6–(2,6–$Cl_2C_6H_3$)–κ^1–*C*–$CNAr^{Clips}$)($CNAr^{Clips2}$)$_2$ ·3(MeCN) (**29**·3(MeCN))	$MoCl_2(CNAr^{Clips2})_4$ ·3(C_6H_6) (**30**·6(C_6H_6))	2,2'–di–*tert*–butyl–10,10'–dichloro–4,4'–bis(Clips)–6,6'–biphenanthridine (**31**)
Formula	$MoC_{75}H_{60}Cl_{12}N_6$	$MoC_{128}H_{104}Cl_{18}N_4$	$C_{46}H_{34}Cl_6N_2$
Crystal System	Triclinic	Triclinic	Monoclinic
Space Group	*P*–1	*P*–1	$P2_1/c$
a, Å	11.1298(9)	13.4390(11)	14.9326(8)
b, Å	18.6393(17)	14.2602(12)	20.1177(16)
c, Å	19.9418(17)	16.6204(14)	14.8086(10)
α, deg	117.464(3)	110.610(4)	90
β, deg	94.760(4)	94.686(3)	117.189(2)
γ, deg	90.755(4)	100.299(3)	90
V, Å^3	3615.2(5)	2896.9(4)	3957.1(5)
Z	2	1	4
Radiation (λ, Å)	Mo–Kα, 0.71073	Mo–Kα, 0.71073	Mo–Kα, 0.71073
ρ (calcd.), g/cm^3	1.439	1.394	1.389
μ, mm^{-1}	0.672	0.581	0.471
Temp, K	100(2)	100(2)	100(2)
θ max, deg	25.410	36.421	25.431
data/parameters	13163 / 0 / 870	28121 / 0 / 688	7236 / 0 / 493
R_1	0.0374	0.0337	0.0400
wR_2	0.0775	0.0792	0.0829
GOF	1.042	1.027	1.019

Table 4.6. Crystallographic Data Collection and Refinement Information for Mo(η^6–$C_{10}H_8$)($CNAr^{DArF2}$)$_3$, Mo(η^6–(3,5–$(CF_3)_2C_6H_3$)–κ^1–*C*–$CNAr^{DArF}$)($CNAr^{DArF2}$)$_2$·0.5(*n*–hexane), and Mo(η^6–C_6H_6)($CNAr^{DArF2}$)$_3$

	Mo(η^6–$C_{10}H_8$)($CNAr^{DArF2}$)$_3$ (**32**)	Mo(η^6–(3,5–$(CF_3)_2C_6H_3$)–κ^1–*C*–$CNAr^{DArF}$) ($CNAr^{DArF2}$)$_2$·0.5(*n*–hexane) (**33**·0.5(*n*–hexane))	Mo(η^6–C_6H_6)($CNAr^{DArF2}$)$_3$ (**34**)
Formula	$MoC_{79}H_{35}F_{36}N_3$	$MoC_{72}H_{34}F_{36}N_3$	$MoC_{75}H_{33}F_{36}N_3$
Crystal System	Orthorhombic	Monoclinic	Orthorhombic
Space Group	*Pbca*	$P2_1/n$	*Pbca*
a, Å	21.817(3)	14.3929(9)	16.5715(13)
b, Å	22.2232(4)	23.181(2)	23.656(2)
c, Å	29.0539(5)	20.4299(13)	35.706(3)
α, deg	90	90	90
β, deg	90	102.026(3)	90
γ, deg	90	90	90
V, Å^3	14084.5(4)	6666.6(9)	13997(2)
Z	8	4	8
Radiation (λ, Å)	Cu–Kα, 1.54178	Mo–Kα, 0.71073	Mo–Kα, 0.71073
ρ (calcd.), g/cm^3	1.703	1.715	1.667
μ, mm^{-1}	2.850	0.346	0.331
Temp, K	100(2)	100(2)	100(2)
θ max, deg	67.761	25.422	25.394
data/parameters	11549 / 4 / 1113	12161 / 0 / 1010	12858 / 27 / 1102
R_1	0.0503	0.0414	0.0424
wR_2	0.1117	0.0799	0.0890
GOF	1.016	1.004	1.016

Table 4.7. Crystallographic Data Collection and Refinement Information for *fac*–$Mo(MeCN)_3(CNAr^{DArF2})_3$·MeNC, *fac*–$Mo(CO)_3(CNAr^{Clips2})_3$·*n*–pentane, and *mer*–$Mo(CO)_3(CNAr^{Clips2})_3$·3($C_6H_5F$)

	fac–$Mo(MeCN)_3(CNAr^{DArF2})_3$·MeNC (**35**·MeNC)	*fac*–$Mo(CO)_3(CNAr^{Clips2})_3$·*n*–pentane (**36**·*n*–pentane)	*mer*–$Mo(CO)_3(CNAr^{Clips2})_3$·3($C_6H_5F$) (**37**·3($C_6H_5F$))
Formula	$MoC_{77}H_{39}F_{36}N_7$	$MoC_{77}H_{63}Cl_{12}N_3O_3$	$MoC_{90}H_{66}Cl_{12}F_3N_3O_3$
Crystal System	Triclinic	Triclinic	Monoclinic
Space Group	*P*–1	*P*–1	*Pn*
a, Å	11.7056(9)	11.0785(15)	14.4864(8)
b, Å	15.6512(11)	15.886(2)	16.1022(10)
c, Å	21.5669(16)	22.426(9)	18.1710(10)
α, deg	80.373(4)	105.310(6)	90
β, deg	76.557(3)	92.152(7)	96.779(2)
γ, deg	88.860(3)	95.241(6)	90
V, $Å^3$	3788.1(5)	3783.2(9)	4209.0(4)
Z	2	2	4
Radiation (λ, Å)	Mo–Kα, 0.71073	Mo–Kα, 0.71073	Mo–Kα, 0.71073
ρ (calcd.), g/cm^3	1.615	1.404	1.433
μ, mm^{-1}	0.312	0.646	0.595
Temp, K	100(2)	100(2)	100(2)
θ max, deg	25.404	25.446	25.379
data/parameters	13887 / 51 / 1209	13835 / 0 / 876	12866 / 308 / 1037
R_1	0.0771	0.0392	0.0346
wR_2	0.1921	0.0862	0.0766
GOF	1.029	1.052	1.033

Table 4.8. Crystallographic Data Collection and Refinement Information for *mer*–$Mo(CO)_3(CNAr^{DArF2})_3$

	mer–$Mo(CO)_3(CNAr^{DArF2})_3$ (**38**)
Formula	$MoC_{82}H_{27}F_{36}N_3O_3$
Crystal System	Monoclinic
Space Group	*C*2/*c*
a, Å	26.1623(18)
b, Å	16.5584(11)
c, Å	31.990(2)
α, deg	90
β, deg	100.681(3)
γ, deg	90
V, Å^3	13617.9(16)
Z	8
Radiation (λ, Å)	Mo–Kα, 0.71073
ρ (calcd.), g/cm^3	1.719
μ, mm^{-1}	0.344
Temp, K	100(2)
θ max, deg	25.490
data/parameters	12563 / 0 / 1052
R_1	0.0454
wR_2	0.1228
GOF	1.073

4.9 Acknowledgements

Chapter 4 is adapted from Ditri, T. B.; Carpenter, A. E.; Ripatti, D. S.; Moore, C. E.; Rheingold, A. L.; Figueroa, J. S. "Chloro– and Trifluoromethyl–Substituted Flanking–Ring *m*–Terphenyl Isocyanides: η^6–Arene Binding to Zerovalent Molybdenum Centers and Comparison to Alkyl–Substituted Derivatives" *Inorg. Chem.* **2013,** *52,* 13216–13229.

in the manuscript was also obtained from Carpenter, A. E., Ripatti, D. S., Moore, C. E., Rheingold, A. L., and Figueroa, J. S. The dissertation author is the first author of this paper.

4.10 References

(1) Twamley, B.; Haubrich, S. T.; Power, P. P. *Adv. Organomet. Chem.* **1999**, *44*, 1–65.

(2) Robinson, G. H. *Chem. Commun.* **2000**, 2175–2181.

(3) Robinson, G. H. *Acc. Chem. Res.* **1999**, *32*, 773–782.

(4) Rivard, E.; Power, P. P. *Inorg. Chem.* **2007**, *46*, 10047–10064.

(5) Power, P. P. *Chem. Rev.* **2012**, *112*, 3482–3507.

(6) Power, P. P. *Organometallics* **2007**, *26*, 4362–4372.

(7) Power, P. P. *Chem. Commun.* **2003**, 2091–2101.

(8) Power, P. P. *Chem. Rev.* **1999**, *99*, 3463–3504.

(9) Kays, D. L. *Dalton Trans.* **2011**, *40*, 769–778.

(10) Kays, D. L. In *Organometallic Chemistry: Volume 36*; The Royal Society of Chemistry: 2010; Vol. 36, p 56–76.

(11) Clyburne, J. A. C.; McMullen, N. *Coord. Chem. Rev.* **2000**, *210*, 73–99.

(12) Stanciu, C.; Olmstead, Marilyn M.; Phillips, Andrew D.; Stender, M.; Power, Philip P. *Eur. J. Inorg. Chem.* **2003**, *2003*, 3495–3500.

(13) Ni, C.; Power, P. P. *Chem. Commun.* **2009**, 5543–5545.

(14) Hill, J. E.; Fanwick, P. E.; Rothwell, I. P. *Organometallics* **1991**, *10*, 15–16.

(15) Hill, J. E.; Fanwick, P. E.; Rothwell, I. P. *Organometallics* **1990**, *9*, 2211–2213.

(16) Hill, J. E.; Balaich, G. J.; Fanwick, P. E.; Rothwell, I. P. *Organometallics* **1991**, *10*, 3428–3430.

(17) S. Buyuktas, B.; P. Power, P. *Chem. Commun.* **1998**, 1689–1690.

(18) Rekken, B. D.; Brown, T. M.; Olmstead, M. M.; Fettinger, J. C.; Power, P. P. *Inorg. Chem.* **2013**, *52*, 3054–3062.

(19) Rekken, B. D.; Brown, T. M.; Fettinger, J. C.; Lips, F.; Tuononen, H. M.; Herber, R. H.; Power, P. P. *J. Am. Chem. Soc.* **2013**, *135*, 10134–10148.

(20) Ellison, J. J.; Ruhlandt–Senge, K.; Power, P. P. *Angew. Chem., Int. Ed. Engl.* **1994**, *33*, 1178–1180.

(21) Ni, C.; Rekken, B.; Fettinger, J. C.; Long, G. J.; Power, P. P. *Dalton Trans.* **2009**, 8349–8355.

(22) Ni, C.; Fettinger, J. C.; Long, G. J.; Power, P. P. *Inorg. Chem.* **2009**, *48*, 2443–2448.

(23) Merrill, W. A.; Wright, R. J.; Stanciu, C. S.; Olmstead, M. M.; Fettinger, J. C.; Power, P. P. *Inorg. Chem.* **2010**, *49*, 7097–7105.

(24) Merrill, W. A.; Steiner, J.; Betzer, A.; Nowik, I.; Herber, R.; Power, P. P. *Dalton Trans.* **2008**, 5905–5910.

(25) Li, J.; Song, H.; Cui, C.; Cheng, J.–P. *Inorg. Chem.* **2008**, *47*, 3468–3470.

(26) Bryan, A. M.; Merrill, W. A.; Reiff, W. M.; Fettinger, J. C.; Power, P. P. *Inorg. Chem.* **2012**, *51*, 3366–3373.

(27) Boynton, J. N.; Merrill, W. A.; Reiff, W. M.; Fettinger, J. C.; Power, P. P. *Inorg. Chem.* **2012**, *51*, 3212–3219.

(28) Boynton, J. N.; Guo, J.–D.; Fettinger, J. C.; Melton, C. E.; Nagase, S.; Power, P. P. *J. Am. Chem. Soc.* **2013**, *135*, 10720–10728.

(29) Alexander Merrill, W.; Stich, T. A.; Brynda, M.; Yeagle, G. J.; Fettinger, J. C.; Hont, R. D.; Reiff, W. M.; Schulz, C. E.; Britt, R. D.; Power, P. P. *J. Am. Chem. Soc.* **2009**, *131*, 12693–12702.

(30) Gavenonis, J.; Tilley, T. D. *J. Am. Chem. Soc.* **2002**, *124*, 8536–8537.

(31) Gavenonis, J.; Tilley, T. D. *Organometallics* **2002**, *21*, 5549–5563.

(32) Yoon, S.; Lippard, S. J. *J. Am. Chem. Soc.* **2005**, *127*, 8386–8397.

(33) Klein, D. P.; Young, V. G.; Tolman, W. B.; Que, L. *Inorg. Chem.* **2006**, *45*, 8006–8008.

(34) Hagadorn, J. R.; Que, L.; Tolman, W. B.; Prisecaru, I.; Münck, E. *J. Am. Chem. Soc.* **1999**, *121*, 9760–9761.

(35) Hagadorn, J. R.; Que, L.; Tolman, W. B. *Inorg. Chem.* **2000**, *39*, 6086–6090.

(36) Carson, E. C.; Lippard, S. J. *Inorg. Chem.* **2006**, *45*, 828–836.

(37) Carson, E. C.; Lippard, S. J. *Inorg. Chem.* **2005**, *45*, 837–848.

(38) Carson, E. C.; Lippard, S. J. *J. Am. Chem. Soc.* **2004**, *126*, 3412–3413.

(39) Weidemann, N.; Margulieux, G. W.; Moore, C. E.; Rheingold, A. L.; Figueroa, J. S. *Inorg. Chim. Acta* **2010**, *364*, 238–245.

(40) Stewart, M. A.; Moore, C. E.; Ditri, T. B.; Labios, L. A.; Rheingold, A. L.; Figueroa, J. S. *Chem. Commun.* **2011**, *47*, 406–408.

(41) Fox, B. J.; Sun, Q. Y.; DiPasquale, A. G.; Fox, A. R.; Rheingold, A. L.; Figueroa, J. S. *Inorg. Chem.* **2008**, *47*, 9010–9020.

(42) Ditri, T. B.; Moore, C. E.; Rheingold, A. L.; Figueroa, J. S. *Inorg. Chem.* **2011**, *50*, 10448–10459.

(43) Ditri, T. B.; Fox, B. J.; Moore, C. E.; Rheingold, A. L.; Figueroa, J. S. *Inorg. Chem.* **2009**, *48*, 8362–8375.

(44) Margulieux, G. W.; Weidemann, N.; Lacy, D. C.; Moore, C. E.; Rheingold, A. L.; Figueroa, J. S. *J. Am. Chem. Soc.* **2010**, *132*, 5033–5035.

(45) Labios, L. A.; Millard, M. D.; Rheingold, A. L.; Figueroa, J. S. *J. Am. Chem. Soc.* **2009**, *131*, 11318–11319.

(46) Fox, B. J.; Millard, M. D.; DiPasquale, A. G.; Rheingold, A. L.; Figueroa, J. S. *Angew. Chem., Int. Ed.* **2009**, *48*, 3473–3477.

(47) Emerich, B. M.; Moore, C. E.; Fox, B. J.; Rheingold, A. L.; Figueroa, J. S. *Organometallics* **2011**, *30*, 2598–2608.

(48) Carpenter, A. E.; Margulieux, G. W.; Millard, M. D.; Moore, C. E.; Weidemann, N.; Rheingold, A. L.; Figueroa, J. S. *Angew. Chem., Int. Ed.* **2012**, *51*, 9412–9416.

(49) Nguyen, T.; Merrill, W. A.; Ni, C.; Lei, H.; Fettinger, J. C.; Ellis, B. D.; Long, G. J.; Brynda, M.; Power, P. P. *Angew. Chem., Int. Ed.* **2008**, *47*, 9115–9117.

(50) Lei, H.; Ellis, B. D.; Ni, C.; Grandjean, F.; Long, G. J.; Power, P. P. *Inorg. Chem.* **2008**, *47*, 10205–10207.

(51) Ohki, Y.; Takikawa, Y.; Sadohara, H.; Kesenheimer, C.; Engendahl, B.; Kapatina, E.; Tatsumi, K. *Chem.–Asian J.* **2008**, *3*, 1625–1635.

(52) Dilworth, J. R.; Zheng, Y.; Lu, S.; Wu, Q. *Inorg. Chim. Acta* **1992**, *194*, 99–103.

(53) Bishop, P. T.; Dilworth, J. R.; Nicholson, T.; Zubieta, J. *J. Chem. Soc., Dalton Trans.* **1991**, 385–392.

(54) Lockwood, M. A.; Fanwick, P. E.; Rothwell, I. P. *Organometallics* **1997**, *16*, 3574–3575.

(55) Lentz, M. R.; Vilardo, J. S.; Lockwood, M. A.; Fanwick, P. E.; Rothwell, I. P. *Organometallics* **2004**, *23*, 329–343.

(56) Kerschner, J. L.; Torres, E. M.; Fanwick, P. E.; Rothwell, I. P.; Huffman, J. C. *Organometallics* **1989**, *8*, 1424–1431.

(57) Kerschner, J. L.; Rothwell, I. P.; Huffman, J. C.; Streib, W. E. *Organometallics* **1988**, *7*, 1871–1873.

(58) Buster, B.; Diaz, A. A.; Graham, T.; Khan, R.; Khan, M. A.; Powell, D. R.; Wehmschulte, R. J. *Inorg. Chim. Acta* **2009**, *362*, 3465–3474.

(59) Ni, C.; Long, G. J.; Power, P. P. *Organometallics* **2009**, *28*, 5012–5016.

(60) Sievert, A. C.; Muetterties, E. L. *Inorg. Chem.* **1981**, *20*, 489–501.

(61) Schroeter, K.; Wesendrup, R.; Schwarz, H. *Eur. J. Org. Chem.* **1998**, *1998*, 565–571.

(62) Pasynkiewicz, S.; Giezyński, R.; Dzierzgowski, S. *J. Organomet. Chem.* **1973**, *54*, 203–205.

(63) Nolan, S. P.; Lopez de la Vega, R.; Hoff, C. D. *Organometallics* **1986**, *5*, 2529–2537.

(64) Mukerjee, S. L.; Lang, R. F.; Ju, T.; Kiss, G.; Hoff, C. D. *Inorg. Chem.* **1992**, *31*, 4885–4889.

(65) Muetterties, E. L.; Bleeke, J. R.; Wucherer, E. J.; Albright, T. *Chem. Rev.* **1982**, *82*, 499–525.

(66) Muetterties, E. L.; Bleeke, J. R.; Sievert, A. C. *J. Organomet. Chem.* **1979**, *178*, 197–216.

(67) Klabunde, K. J.; Anderson, B. B.; Bader, M.; Radonovich, L. J. *J. Am. Chem. Soc.* **1978**, *100*, 1313–1314.

(68) Adedeji, F. A.; Lalage, D.; Brown, S.; Connor, J. A.; Leung, M. L.; Paz–Andrade, I. M.; Skinner, H. A. *J. Organomet. Chem.* **1975**, *97*, 221–228.

(69) Wolf, R.; Ni, C.; Nguyen, T.; Brynda, M.; Long, G. J.; Sutton, A. D.; Fischer, R. C.; Fettinger, J. C.; Hellman, M.; Pu, L.; Power, P. P. *Inorg. Chem.* **2007**, *46*, 11277–11290.

(70) Smith, Rhett C.; Ren, T.; Protasiewicz, John D. *Eur. J. Inorg. Chem.* **2002**, *2002*, 2779–2783.

(71) Protasiewicz, J. D. *J. Chem. Soc., Chem. Commun.* **1995**, 1115–1116.

(72) Peng, Y.; Fischer, R. C.; Merrill, W. A.; Fischer, J.; Pu, L.; Ellis, B. D.; Fettinger, J. C.; Herber, R. H.; Power, P. P. *Chem. Sci.* **2010**, *1*, 461–468.

(73) Pomije, M. K.; Kurth, C. J.; Ellis, J. E.; Barybin, M. V. *Organometallics* **1997**, *16*, 3582–3587.

(74) Kundig, E. P.; Timms, P. L. *J. Chem. Soc., Chem. Commun.* **1977**, 912–913.

(75) Thi, N. P. D.; Spichiger, S.; Paglia, P.; Bernardinelli, G.; Kündig, E. P.; Timms, P. L. *Helv. Chim. Acta* **1992**, *75*, 2593–2607.

(76) Shapiro, P. J.; Zehnder, R.; Foo, D. M.; Perrotin, P.; Budzelaar, P. H. M.; Leitch, S.; Twamley, B. *Organometallics* **2006**, *25*, 719–732.

(77) Perutz, R. N.; Turner, J. J. *J. Am. Chem. Soc.* **1975**, *97*, 4800–4804.

(78) Perutz, R. N.; Turner, J. J. *Inorg. Chem.* **1975**, *14*, 262–270.

(79) Ishikawa, Y.; Kawakami, K. *J. Phys. Chem. A* **2007**, *111*, 9940–9944.

(80) Nishida, H.; Takada, N.; Yoshimura, M.; Sonoda, T.; Kobayashi, H. *Bull. Chem. Soc. Jpn.* **1984**, *57*, 2600–2604.

(81) Brookhart, M.; Grant, B.; Volpe, A. F. *Organometallics* **1992**, *11*, 3920–3922.

(82) Powell, J.; Lough, A.; Saeed, T. *J. Chem. Soc., Dalton Trans.* **1997**, 4137–4138.

(83) Douglas, T. M.; Molinos, E.; Brayshaw, S. K.; Weller, A. S. *Organometallics* **2006**, *26*, 463–465.

(84) Connor, J. A.; Jones, E. M.; McEwen, G. K.; Lloyd, M. K.; McCleverty, J. A. *J. Chem. Soc., Dalton Trans.* **1972**, 1246–1253.

(85) Johnston, R. F.; Cooper, J. C. *J. Mol. Struct. Theochem* **1991**, *236*, 297–307.

(86) Zhu, G.; Janak, K. E.; Figueroa, J. S.; Parkin, G. *J. Am. Chem. Soc.* **2006**, *128*, 5452–5461.

(87) Smith, R. C.; Shah, S.; Urnezius, E.; Protasiewicz, J. D. *J. Am. Chem. Soc.* **2002**, *125*, 40–41.

(88) Essenmacher, G. J.; Treichel, P. M. *Inorg. Chem.* **1977**, *16*, 800–806.

(89) Treichel, P. M.; Mueh, H. J. *Inorg. Chem.* **1977**, *16*, 1167–1169.

(90) Lentz, D.; Anibarro, M.; Preugschat, D.; Bertrand, G. *J. Fluorine Chem.* **1998**, *89*, 73–81.

(91) Lentz, D. *Angew. Chem., Int. Ed. Engl.* **1994**, *33*, 1315–1331.

(92) Lentz, D. *J. Organomet. Chem.* **1990**, *381*, 205–212.

(93) Zhou, M.; Andrews, L.; Bauschlicher, C. W. *Chem. Rev.* **2001**, *101*, 1931–1962.

(94) Pangborn, A. B.; Giardello, M. A.; Grubbs, R. H.; Rosen, R. K.; Timmers, F. J. *Organometallics* **1996**, *15*, 1518–1520.

(95) Arnarego, W. L. F.; Chai, C. L. L. *Purification of Laboratory Chemicals*; 5th ed.; Elsevier, 2003.

(96) McElwee–White, L.; Dougherty, D. A. *J. Am. Chem. Soc.* **1984**, *106*, 3466–3474.

(97) Burla, M. C.; Caliandro, R.; Camalli, M.; Carrozzini, B.; Cascarano, G. L.; De Caro, L.; Giacovazzo, C.; Polidori, G.; Spagna, R. *J. Appl. Crystallogr.* **2005**, *38*, 381–388.

(98) Sheldrick, G. M. *Acta. Crystallogr.* **2008**, *64*, 112–122.

(99) van der Sluis, P.; Spek, A. L. *Acta Crystallogr.* **1990**, *A46*, 194.

Chapter 5

Synthesis of η^6–Arene–Tethered *m*–Terphenyl Isocyanide Complexes of Chromium and Molybdenum: Activation of Isocyanides towards Electrophilic Addition

5.1 Introduction

Over the past 20 years the *m*–terphenyl group has proven a viable ligand framework towards the isolation of novel main–group[1–5] and transition–metal[6–9] complexes. The ability of the *m*–terphenyl group to foster an encumbering and protective environment around a metal center has elicited its use as a supporting ancillary for a vast array of ligand types including thiolates,[10–14] amidos,[15–22] imidos,[23,24] aryloxides,[25–29] and carboxylates[30–36]. With interest in isolating low–coordinate zerovalent metal isocyanide analogues to the binary unsaturated metal carbonyls (i.e., $[Cr(CO)_3]$, $[Cr(CO)_4]$, $[Fe(CO)_4]$ and $[Ni(CO)_3]$)[37–39], our group has developed a library *m*–terphenyl supported isocyanide ligands that host a range of sterically and electronically modified *m*–terphenyl functionalities.[40–42] For our goals, *m*–

terphenyl isocyanides are particularly suitable surrogates for CO because they are isolobal with CO, and featuring an aryl constitution, their π–acidity more closely mimics that of CO when compared to their alkyl counterparts.[43] Additionally, modification of the *m*–terphenyl backbone through introduction of sterically bulky substituents,[41] and/or electron–releasing/–withdrawing functionalities,[40,41] has proven effective at both: (i) controlling the extent of isocyanide ligation to transition–metal centers,[41,44–46] and (ii) influencing the donor/acceptor properties of the isocyanide ligand.[40] To date, our group has successfully utilized the *m*–terphenyl isocyanides $CNAr^{Mes2}$ and $CNAr^{Dipp2}$ (Ar^{Mes2} = 2,6–(2,4,6–$Me_3C_6H_2)_2C_6H_3$,[42] and Ar^{Dipp2} = 2,6–(2,6–(*i*–$Pr)_2C_6H_3)_2C_6H_3$))[41] ligands for the generation of isolable isocyanide analogues of the coordinatively unsaturated metal carbonyls $Co(CO)_4$,[47] $Ni(CO)_3$,[46,48] and $Pd(CO)_2$.[49]

In an effort to extend our studies to include isocyanide analogues of the unsaturated group 6 metal carbonyls (i.e., $[M(CO)_4]$, $[M(CO)_3]$, and $[M(CO)_2]$), we discovered that the coordinatively unsaturated molybdenum isocyanide intermediates $[Mo(CNAr^{R2})_2]$, and $[Mo(CNAr^{R2})_3]$ (Ar^{R2} = *m*–terphenyl) were appreciably susceptible to the η^6–binding of arenes. This phenomenon was initially observed in the reduction of the tetraiodide complex $MoI_4(CNAr^{Dipp2})_2$ in C_6H_6 solution under an N_2 atmosphere.[41] Under the latter conditions, isolation of $[Mo(CNAr^{Dipp2})_2]$ was precluded by concomitant binding of C_6H_6 and dinitrogen, resulting in the η^6–benzene, dinitrogen, isocyanide complex (η^6–C_6H_6)$Mo(N_2)(CNAr^{Dipp2})_2$ (**21**).[45] More recently, we observed similar η^6–binding to zerovalent molybdenum centers, however, in these examples the η^6–interactions were fostered by the secondary coordination of one of the flanking aryl rings of a metal–bound *m*–terphenyl isocyanide as opposed to solvent.[40] Accordingly, a series of zerovalent, trisisocyanide, η^6–arene complexes with the general formula $Mo(\eta^6$–(R)–κ^1–*C*–$CNAr^R)(CNAr^{R2})_2$ (Ar^{R2} = Ar^{Dipp2}, Ar^{Mes2}, Ar^{Clips2}, and Ar^{DArF2}) were isolated and characterized.[40] Importantly, the arene–"tethered" isocyanides

featured in the Mo(η^6–(R)–κ^1–*C*–CNAr^{R})(CNAr^{R2})$_2$ complexes were shown to be both structurally and spectroscopically distinct from their untethered isocyanide counterparts. As consequence of η^6–capping, extensive contraction of the C_{iso}–N–C_{ipso} bond angle (ca. 60°) coupled with marginal shortening of the N–C_{ipso} bond length (ca. 0.016 Å) is observed. Furthermore, elongated C_{iso}–N bonds (ranging from 1.229 to 1.244 Å), consistent with red shifted ν_{CN} FTIR bands (ranging from 1652 to 1717 cm^{-1}), and remarkably short M–C_{iso} bond lengths (ca. 1.938 Å), corroborated by significantly downfield–shifted ^{13}C isocyanide resonances (ranging from 273.3 to 281.6 ppm) reveal that the arene–tethered isocyanide ligands have substantial carbenic character. In total, the data suggested that the arene–tethered isocyanides featured in the Mo(η^6–(R)–κ^1–*C*–CNAr^{R})(CNAr^{R2})$_2$ complexes may effectively enhance the reactivity of these molecules.

We focused our efforts on the study the trisisocyanide complex Mo(η^6–(Mes)–κ^1–*C*–CNAr^{Mes})(CNAr^{Mes2})$_2$. It is important to note that the η^6–coordination of the *m*–terphenyl isocyanides prominent in the Mo(η^6–(R)–κ^1–*C*–CNAr^{R})(CNAr^{R2})$_2$ complexes supported by halo–substituted ligands were shown to have increased lability relative to their alkyl–substituted counterparts. Therefore, we reasoned that the trimethyl–substitution of the flanking mesityl rings featured in the Mo(η^6–(Mes)–κ^1–*C*–CNAr^{Mes})(CNAr^{Mes2})$_2$ complex would result in the most persistent metal–arene interaction in the Mo(η^6–(R)–κ^1–*C*–CNAr^{R})(CNAr^{R2})$_2$ series. Additionally, we were intrigued to discover what effect replacing molybdenum with chromium in the M(η^6–(Mes)–κ^1–*C*–CNAr^{Mes})(CNAr^{Mes2})$_2$ type complexes would have on the structure and reactivity of the molecule. Herein, we report the synthesis of M(η^6–(Mes)–κ^1–*C*–CNAr^{Mes})(CNAr^{Mes2})$_2$ (M = Cr and Mo) complexes via an oxidative–decarbonylation/reduction methodology. The chemistry of the M(η^6–(Mes)–κ^1–*C*–CNAr^{Mes})(CNAr^{Mes2})$_2$ (M = Cr and Mo) towards electrophiles is explored and the origin of

the preferential addition of electrophilic substrates to the geometrically–constrained η^6–tethered isocyanide featured in these complexes is discussed.

5.2 Synthesis of *mer*–$MI_2(I_3)(CNAr^{Mes2})_3$ Complexes

Previously, we reported the use of molybdenum bis–naphthalene ($Mo(\eta^6–C_{10}H_8)_2$)) as a synthetic precursor for the synthesis zerovalent, trisisocyanide, η^6–arene $Mo(\eta^6–(R)–\kappa^1–C–CNAr^R)(CNAr^{R2})_2$ complexes. However, in this study, a tandem oxidative–decarbonylation/reduction synthetic sequence was employed for the synthesis of $M(\eta^6–(Mes)–\kappa^1–C–CNAr^{Mes})(CNAr^{Mes2})_2$ (M = Mo and Cr) complexes. Although procedurally cumbersome, the oxidative–decarbonylation/reduction strategy alleviates the necessity to separate $C_{10}H_8$ from $M(\eta^6–(Mes)–\kappa^1–C–CNAr^{Mes})(CNAr^{Mes2})_2$, which can become especially problematic when large quantities of $M(\eta^6–(Mes)–\kappa^1–C–CNAr^{Mes})(CNAr^{Mes2})_2$ are desired. Moreover, this strategy provides a straightforward approach for the inclusion of chromium in our studies of both the $M(CO)_3(CNAr^{Mes2})_3$ and $M(\eta^6–(Mes)–\kappa^1–C–CNAr^{Mes})(CNAr^{Mes2})_2$ systems. The target molecule $Cr(\eta^6–(Mes)–\kappa^1–C–CNAr^{Mes})(CNAr^{Mes2})_2$ was of particular interest because we reasoned that the shorter metal–ligand bonds expected for Cr(0) relative to Mo(0),[50] could render the $C_{iso}–N–C_{ipso}$ bond angle of the geometrically constrained isocyanide ligand in $Cr(\eta^6–(Mes)–\kappa^1–C–CNAr^{Mes})(CNAr^{Mes2})_2$ more acute than that of its molybdenum counterpart $Mo(\eta^6–(Mes)–\kappa^1–C–CNAr^{Mes})(CNAr^{Mes2})_2$ ($C_{iso}–N–C_{ipso}$ = 120.4(7)°**)**.[40] We speculated that increased strain on the $C_{iso}–N–C_{ipso}$ bond angle of arene–tethered isocyanide ligand in $Cr(\eta^6–(Mes)–\kappa^1–C–CNAr^{Mes})(CNAr^{Mes2})_2$ could: (i) increase the lability of the η^6–Mes interaction and (ii) further attenuate the reactivity of the arene–tethered isocyanide C≡N bond.

In a previous report, the coordination chemistry between the *m*–terphenyl isocyanides $CNAr^{Mes2}$ and $CNAr^{Dipp2}$ with *fac*–$Mo(CO)_3(NCMe)_3$ was investigated.[41] These studies

unveiled that the [$Mo(CO)_3$] fragment can accommodate three of the less sterically encumbering *m*–terphenyl isocyanide $CNAr^{Mes2}$, whereas with the more sterically encumbering $CNAr^{Dipp2}$, maximal isocyanide ligation was limited to two units. Similarly, it was of interest to discern whether or not the smaller covalent radii of Cr(0) relative to Mo(0) could also influence extent of $CNAr^{R2}$ ligation.[50] Accordingly, treatment of *fac*–$Cr(CO)_3(NCMe)_3$ with 3.0 equiv of $CNAr^{Mes2}$ in Et_2O results in complete consumption of $CNAr^{Mes2}$ providing $Cr(CO)_3(CNAr^{Mes2})_3$ (**39**, Scheme 5.1). Although $Cr(CO)_3(CNAr^{Mes2})_3$ (**39**) eluded crystallographic characterization, the ^1H NMR spectra of $Cr(CO)_3(CNAr^{Mes2})_3$ (**39**) in $CDCl_3$ reveals a single set of Ar^{Mes2} resonances and the solution phase ($CDCl_3$) FTIR spectrum gives rise to two ν_{CO} and two ν_{CN} frequencies, both consistent with $Cr(CO)_3(CNAr^{Mes2})_3$ possessing a *fac* conformation (Table 5.1). Unvarying from its molybdenum congener, upon heating (C_6D_6, 90°C, 2 days), *fac*–$Cr(CO)_3(CNAr^{Mes2})_3$ (**39**) undergoes a *fac–mer* isomerization and converts to the less sterically congested *mer*–conformer, *mer*–$Cr(CO)_3(CNAr^{Mes2})_3$ (Scheme 5.1, Figure 5.1, **40**). X–Ray crystallography of yellow crystals of *mer*–$Cr(CO)_3(CNAr^{Mes2})_3$ (**40**) confirms its meridional conformation, and that the [$Cr(CO)_3$] fragment can indeed accommodate three of the sterically encumbering $CNAr^{Mes2}$ ligands despite the more crowded ligand environment resulting from shorter M–C bonds (0.143(80) Å shorter on average). Also, both ^1H NMR and FTIR analysis of *mer*–$Cr(CO)_3(CNAr^{Mes2})_3$ showed the expected spectroscopic signatures for the *mer* isomer (Table 5.1).

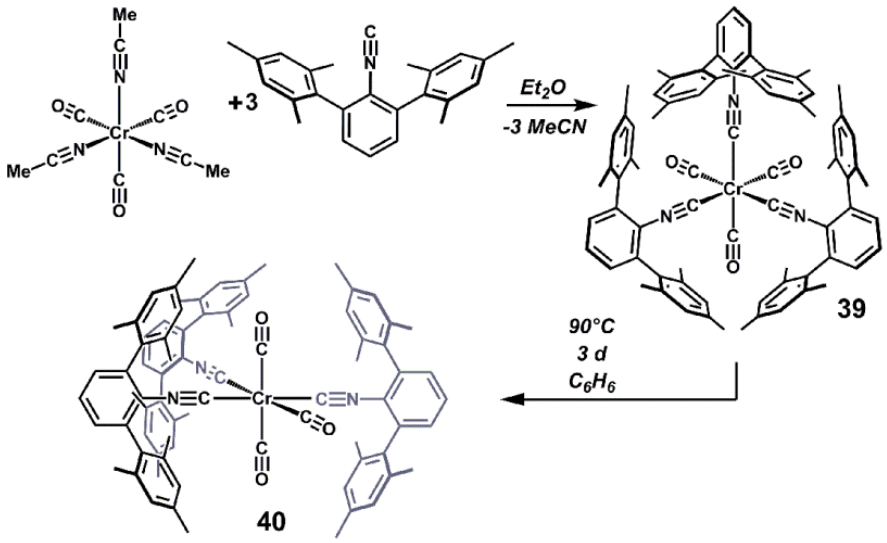

Scheme 5.1. Synthesis of *fac*–$Cr(CO)_3(CNAr^{Mes2})_3$, and *mer*–$Cr(CO)_3(CNAr^{Mes2})_3$.

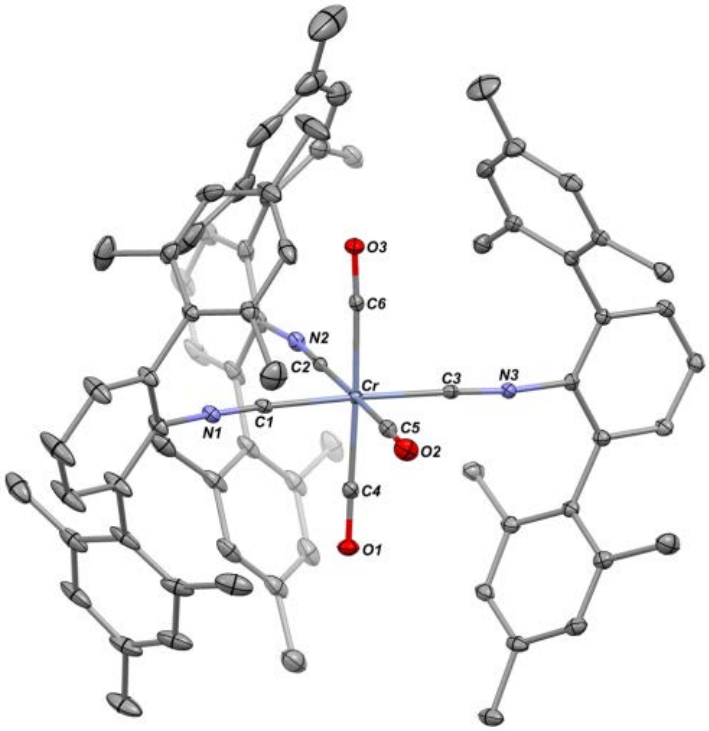

Figure 5.1. Molecular Structure of *mer*–$Cr(CO)_3(CNAr^{Mes2})_3$ (**40**). Selected bond distances (Å) and angles (Deg): Cr1–C1 = 1.948(4); Cr1–C2 = 1.974(4); Cr1–C3 = 1.949(4); Cr1–C4 = 1.902(4); Cr1–C5 = 1.880(4); Cr1–C6 = 1.914(4); C1–Cr1–C2 = 92.98(16); C1–Cr1–C3 = 175.08(16); C1–Cr1–C4 = 89.41(16); C1–Cr1–C5 = 85.93(17); C1–Cr1–C6 = 88.69(16); C2–Cr1–C3 = 91.89(15); C2–Cr1–C4 = 90.83(16); C2–Cr1–C5 = 178.90(16); C2–Cr1–C6 = 87.57(16); C3–Cr1–C4 = 89.84(16); C3–Cr1–C5 = 89.20(17); C3–Cr1–C6 = 92.19(15); C4–Cr1–C5 = 89.01(17); C4–Cr1–C6 = 177.45(17); C5–Cr1–C6 = 92.55(17).

Table 5.1. Solution ν_{CN} and ν_{CO} Stretching Frequencies for $M(CO)_3(CNAr^{Mes2})_3$ (M = Cr and Mo)

Complex	ν_{CN} (cm^{-1})	ν_{CO} (cm^{-1})
fac–$Mo(CO)_3(CNAr^{Mes2})_3$ (**5**)[a,b]	2046 (s)	1942 (s)
	2000 (m)	1910 (s)
fac–$Cr(CO)_3(CNAr^{Mes2})_3$ (**39**)[c]	2042 (vs)	1943 (vs)
	1999 (w sh)	1913 (vs)
mer–$Mo(CO)_3(CNAr^{Mes2})_3$ (**6**)[a,b]	2046 (m)	1926 (vs)
	2024 (s)	1902 (m)
	1993 (s)	
mer–$Cr(CO)_3(CNAr^{Mes2})_3$ (**40**)[c]	2052 (m)	1924 (vs)
	2024 (m)	1902 (s)
	2002 (s)	

[a]Data from reference[41], [b]Measured in C_6D_6 solution, [c]Measured in $CDCl_3$ solution.

There was some debate as to whether $M(CO)_3(CNAr^{Mes2})_3$ complexes would be suitable for oxidative decarbonylation by molecular iodine. Previously, we had discovered that while the bis–isocyanide *trans*–$M(NCMe)(CO)_3(CNAr^{Dipp2})$ (M = Mo or W) complexes readily react with I_2, the tetracarbonyl *trans*–$M(CO)_4(CNAr^{Dipp2})$ (M = Mo or W) complexes were found to be resistant towards chemical oxidation by molecular iodine.[51] We speculated that a labile NCMe ligand was necessary to promote inner–sphere oxidation events in the Mo– and W–$CNAr^{Dipp2}$ systems. Interestingly, however, despite lacking a labile solvent ligand, complete oxidative–decarbonylation of *fac*–$Mo(CO)_3(CNAr^{Mes2})_3$ (**5**) and *fac*–$Cr(CO)_3(CNAr^{Mes2})_3$ (**39**) can be achieved. Accordingly, treatment of *fac*–$M(CO)_3(CNAr^{Mes2})_3$ (M = Cr or Mo) with 2.55 equivalents of I_2 proceeds with the loss of three equivalents of CO, affording the diiodo–triiodide complexes *mer*–$MI_2(I_3)(CNAr^{Mes2})_3$ (M = Cr or Mo), as determined by determined by X–ray diffraction (Schemes 5.2 and 5.3, Figure 5.2). $CrI_2(I_3)(CNAr^{Mes2})_3$ (**41**) is isostructural to $MoI_2(I_3)(CNAr^{Mes2})_3$ (**25**), and features meridional isocyanides, and a coordinated I_3^- molecule, which although rare is not unknown for tri–valent group 6 molecules.[52,53] As expected, both *mer*–$CrI_2(I_3)(CNAr^{Mes2})_3$ (**41**) and *mer*–$MoI_2(I_3)(CNAr^{Mes2})_3$ (**25**) are paramagnetic and give rise to a solution magnetic

moments (Evans Method, $CDCl_3$ with $O(SiMe_3)_2$, 400.1 MHz, 20 ˚C) of μ_{eff} = 3.77(2) μ_B and μ_{eff} = 3.68(1) μ_B respectively, consistent with S = 1 1/2, d^3 metal centers.

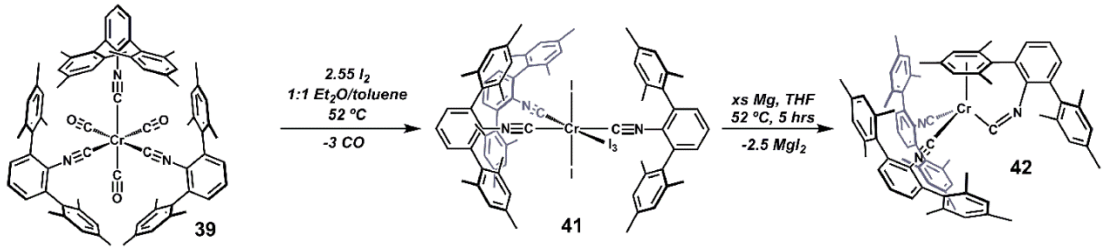

Scheme 5.2. Synthesis of *mer*–$CrI_2(I_3)(CNAr^{Mes2})_3$ (**41**), and $Cr(\eta^6$–(Mes)–κ^1–*C*–$CNAr^{Mes})(CNAr^{Mes2})_2$ (**42**).

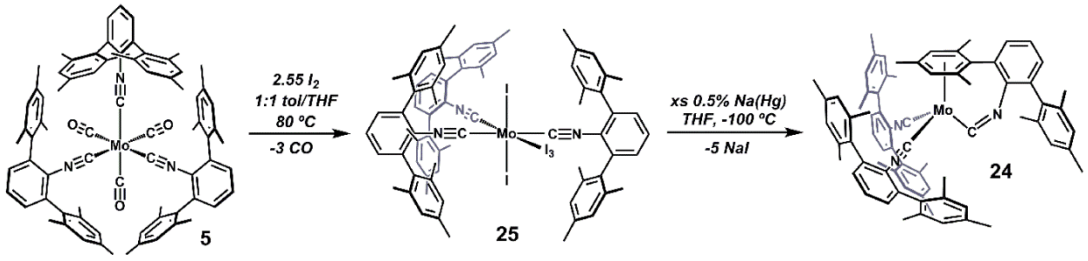

Scheme 5.3. Synthesis of *mer*–$MoI_2(I_3)(CNAr^{Mes2})_3$ (**25**), and $Mo(\eta^6$–(Mes)–κ^1–*C*–$CNAr^{Mes})(CNAr^{Mes2})_2$ (**24**).

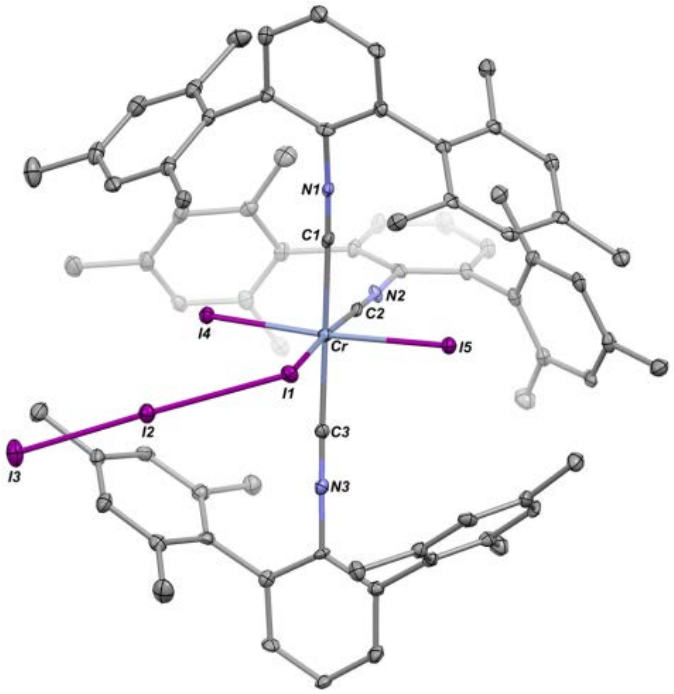

Figure 5.2. Molecular Structure of *mer*–$CrI_2(I_3)(CNAr^{Mes2})_3$ (**41**). Selected bond distances (Å) and angles (Deg): Cr1–C1 = 2.173(8); Cr1–C2 = 2.114(7); Cr1–C3 = 2.157(8); Cr1–I1 = 2.7760(8); Cr1–I4 = 2.6809(7); Cr1–I5 = 2.7135(7); C1–Cr1–C2 = 92.4(3); C1–Cr1–C3 = 173.1(3); C1–Cr1–I1 = 85.80(19); C1–Cr1–I4 = 86.99(17); C1–Cr1–I5 = 90.75(18); C2–Cr1–C3 = 93.3(3); C2–Cr1–I1 = 176.06(19); C2–Cr1–I4 = 88.11(19); C2–Cr1–I5 = 86.24(19); C3–Cr1–I1 = 88.7(2); C3–Cr1–I4 = 89.31(18); C3–Cr1–I5 = 93.50(18); I1–Cr1–I4 = 95.32(2); I1–Cr1–I5 = 90.25(2); I4–Cr1–I5 = 173.82(3).

The divergent oxidation chemistry observed for the *fac*–$M(CO)_3(CNAr^{Mes2})_3$ (M = Cr, Mo) and *trans*–$M(CO)_4(CNAr^{Dipp2})$ (M = Mo, W) complexes is likely governed by the relative lability of the isocyanide ligands in these systems. The generation of a 5–coordinate intermediate, requisite for inner–sphere oxidation, is likely more facile for *fac*–$M(CO)_3(CNAr^{Mes2})_3$ complexes, where isocyanide departure is facilitated by the strong *trans*–effect imparted by the CO ligands oriented *trans* to the isocyanides. The *trans*–$M(CO)_4(CNAr^{Dipp2})$ complexes, lacking isocyanides *trans* to CO, cannot as easily generate five–coordinate intermediates and are therefore resistant towards inner–sphere oxidation by I_2. Furthermore, electrochemical investigations of several permutations of group 6 M(CO)*n*(CNR)*m* (*m* = 6 – *n*, *n* = 1–3) complexes has revealed that the ease of oxidation

increases markedly as carbonyl substitution increases.[54] This trend suggest that the ease of outer–sphere oxidation is likely not a relevant factor in the dissimilar oxidative behavior exhibited in the *fac*–$M(CO)_3(CNAr^{Mes2})_3$ and *trans*–$M(CO)_4(CNAr^{Dipp2})$ complexes.[54,55]

5.3 Synthesis of Mo(η^6–(R)–κ^1–*C*–$CNAr^R$)$(CNAr^{R2})_2$ Complexes

The conditions for the reduction of *mer*–$CrI_2(I_3)(CNAr^{Mes2})_3$ (**41**) and *mer*–$MoI_2(I_3)(CNAr^{Mes2})_3$ (**25**) to zerovalent, η^6–arene isocyanide M(η^6–(Mes)–κ^1–*C*–$CNAr^{Mes}$)$(CNAr^{Mes2})_2$ (M = Cr or Mo) complexes are outlined in Schemes 5.2 and 5.3, respectively. Not surprisingly, whereas the complete reduction of *mer*–$CrI_2(I_3)(CNAr^{Mes2})_3$ (**41**) is achieved by the addition of excess Mg(0) in Et_2O/Tol solution, the trivalent mer–$MoI_2(I_3)(CNAr^{Mes2})_3$ (**25**) requires more forcing conditions (THF, 0.5% Na/Hg). As determined by X–ray crystallography, the trisisocyanide, η^6–arene complex Cr(η^6–(Mes)–κ^1–*C*–$CNAr^{Mes}$)$(CNAr^{Mes2})_2$ (**42**, Figure 5.3) is isostructural with Mo(η^6–(Mes)–κ^1–*C*–$CNAr^{Mes}$)$(CNAr^{Mes2})_2$ (**24**), however, subtle variations in the crystallographic data are noteworthy, and are summarized in Table 5.2. As expected, the shorter C_{iso}–metal bond distance and the contracted η^6–arene centroid–metal bond distance have the combined effect of rendering the C_{iso}–N–C_{ipso} bond angle of the geometrically constrained isocyanide ligand in Cr(η^6–(Mes)–κ^1–*C*–$CNAr^{Mes}$)$(CNAr^{Mes2})_2$ (**42**) more acute (118.3(2)°) than its molybdenum counterpart (120.52(16)°, Table 5.2).[40] Also noteworthy, the reduction of the C_{iso}–N–C_{ipso} bond angle in the arene–tethered isocyanide ligand is concomitant with a more linear M–C_{ipso}–N bond angle (157.1(2)°), which is ca. 4.5° greater than its molybdenum congener (152.63(15)°, Table 5.2).[40] Therefore, the aggregate changes in the C_{iso}–N–C_{ipso} and M–C_{ipso}–N bond angles for the geometrically constrained isocyanide ligand featured in Cr(η^6–(Mes)–κ^1–*C*–$CNAr^{Mes}$)$(CNAr^{Mes2})_2$ (**42**) relative to its molybdenum complement make it challenging to assess which of the complexes furnishes a more strained M–C_{iso}–N–C_{ipso} bond.

Nevertheless, similar to Mo(η^6–(Mes)–κ^1–*C*–CNAr^{Mes})(CNAr^{Mes2})$_2$ (**24**), the flanking–ring η^6–arene interaction in Cr(η^6–(Mes)–κ^1–*C*–CNAr^{Mes})(CNAr^{Mes2})$_2$ (**42**) is persistent. Accordingly, analogous to Mo(η^6–(Mes)–κ^1–*C*–CNAr^{Mes})(CNAr^{Mes2})$_2$ (**24**), extended heating of Cr(η^6–(Mes)–κ^1–*C*–CNAr^{Mes})(CNAr^{Mes2})$_2$ (**42**) in either benzene or toluene solution (120°C, 2 days) does not promote solvent induced displacement of the η^6–Mes interaction.[40] Moreover, both M(η^6–(Mes)–κ^1–*C*–CNAr^{Mes})(CNAr^{Mes2})$_2$ complexes are resistant to further CNAr^{Mes2} incorporation under both thermolytic and photolytic conditions (C_6D_6, 120 °C, 3 d and C_6D_6, low–pressure Hg lamp (254 nm), 3 d, respectively).

Table 5.2. Spectroscopic and Structural Parameters for the Geometrically Constrained Isocyanide Ligands in M(η^6–(R)–κ^1–*C*–CNAr^{R})(CNAr^{R2})$_2$ (M = Cr and Mo) Complexes

Complex	ν_{CN} (cm^{-1})	ν_{NH} (cm^{-1})	δC (ppm)	∠(*C*-N-C_{ipso}) (deg)	∠(*M*-*C*-*N*) (deg)	*d*(*C*-N) (Å)	*d*(*C*-M) (Å)	*d*(*M*-*centroid*) (Å)
Cr(η^6-(Mes)-κ^1-*C*-CNAr^{Mes})(CNAr^{Mes2})$_2$ (**42**)[a]	1647		295.7	118.3(2)	157.1(2)	1.244(3)	1.882(3)	1.714
Mo(η^6-(Mes)-κ^1-*C*-CNAr^{Mes})(CNAr^{Mes2})$_2$ (**24**)[b]	1645		278.3	120.52(16)	152.63(15)	1.244(2)	1.9360(19)	1.851
[Cr(η^6-(Mes)-κ^1-*C*-CN(H)Ar^{Mes})(CNAr^{Mes2})$_2$]OTf (**43**)[a]	1493	3323	292.6	121.6(2)	150.9(2)	1.314(4)	1.747(3)	1.736
[Mo(η^6-(Mes)-κ^1-*C*-CN(H)Ar^{Mes})(CNAr^{Mes2})$_2$]OTf (**44**)[a]	1416	3323	280.7	122.7(2)	149.76(19)	1.339(3)	1.828(2)	1.900
[Mo(η^6-(Mes)-κ^1-*C*-CN(CH$_3$)Ar^{Mes})(CNAr^{Mes2})$_2$]OTf (**45**)[a]	1483		282.7	119.5(4)	153.5(4)	1.336(6)	1.820(6)	1.892
[Mo(η^6-(Mes)-κ^1-*C*-C(H)N(H)Ar^{Mes})(CNAr^{Mes2})$_2$](OTf)$_2$ (**46**)[a]	1507	3267	260.6	129.2(7)	135.1(6)	1.306(10)	2.177(8)	1.874
Mo(η^6-(Mes)-κ^1-*C*-C(H)N(H)Ar^{Mes})(CNAr^{Mes2})$_2$ (**47**)[c]	1576	3345	261.7	130.34(17)	131.36(14)	1.372(3)	2.036(2)	1.858

[a]Measured in $CDCl_3$ solution. [b]Measured in CD_2Cl_2 solution. [c]Measured in C_6D_6 solution.

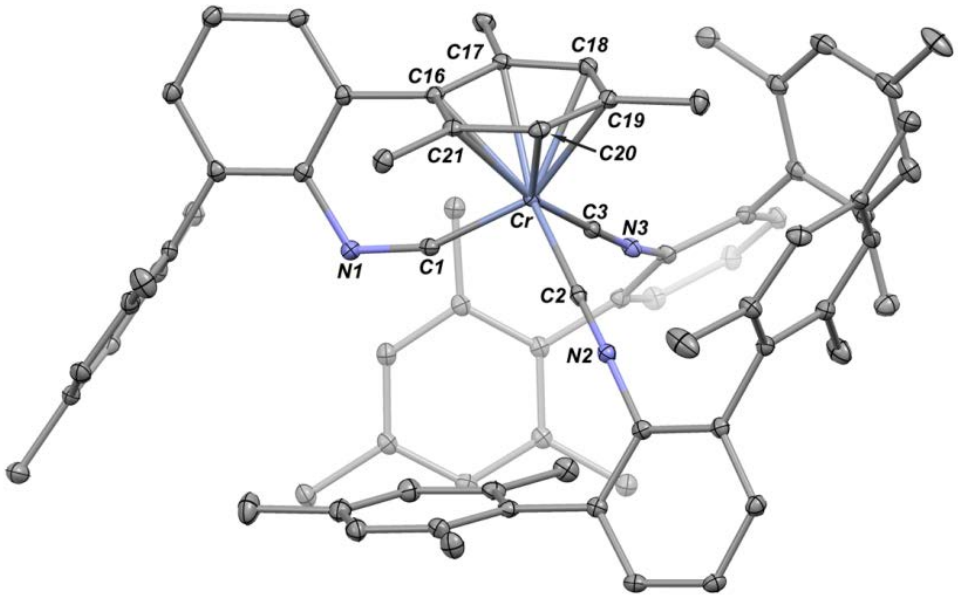

Figure 5.3. Molecular Structure of [Cr(κ^1–*C*–CN(H)Ar^{Mes}(η^6–Mes))(CNAr^{Mes2})$_2$]OTf (**43**). Selected bond distances (Å) and angles (Deg): Cr1–C1 = 1.747(3); Cr1–C2 = 1.926(3); Cr1–C3 = 1.937(3); C1–N1 = 1.314(4); N1–C4 = 1.420(3); C1–Cr1–C2 = 93.33(12); C1–Cr1–C3 = 95.77(12); C2–Cr1–C3 = 93.70(10); Cr1–C1–N1 = 150.9(2); C1–N1–C4 = 121.6(2).

Akin to its molybdenum counterpart, the geometrically constrained isocyanide ligand in Cr(η^6–(Mes)–κ^1–*C*–CNAr^{Mes})(CNAr^{Mes2})$_2$ (**42**) possesses considerable carbenic character. Notably, the elongated C_{iso}–N bond and contracted M–C_{iso} bond (1.244(3) Å and 1.882(3) Å, respectively), coupled with a very low energy ν_{CN} band of 1647 cm^{-1}, indicate a substantial degree of metal→ligand π–backdonation from chromium to the tethered–isocyanide. Previous studies have revealed a correlation between the ^{13}C NMR chemical shift of isocyanide ligands and the magnitude of metal→isocyanide π–backbonding.[43,56,57] Remarkably, to the best our knowledge, the geometrically constrained isocyanide ligand featured in Cr(η^6–(Mes)–κ^1–*C*–CNAr^{Mes})(CNAr^{Mes2})$_2$ (**42**) possess the most acute C–N–C angle for a structurally characterized isocyanide complex according to the Cambridge Structural Database.[58] Moreover, it also gives rise to the largest down–field ^{13}C NMR chemical shift reported for an isocyanide ($CDCl_3$, δ = 295.7 ppm , Table 5.2).

In an attempt to place the structural and spectroscopic characteristics found in the M(η^6–(Mes)–κ^1–*C*–CNAr^{Mes})(CNAr^{Mes2})$_2$ complexes in context with reported literature values for metal isocyanides also exhibiting a considerable degree of metal→isocyanide π–backdonation (as indicated by significantly bent C–N–C bond angles), a search of Cambridge Structural Data Base for metal complexes featuring non–bridging isocyanide ligands exhibiting C–N–C bond angles ≤ 160° was performed.[58] This inquiry revealed that, generally, ^{13}C isocyanide resonances shift down–field as C–N–C bond angles become increasingly acute (Figures 5.4 and 5.5). Unfortunately, although 163 structures matched our search criteria, ^{13}C chemical shifts were reported for only 44 of these compounds.[40,44,59–86] Nevertheless, construction of (x, y) scatterplots of this data revealed a roughly linear relationship between the C–N–C bond angle and ^{13}C CNR chemical shift of the isocyanides. Moreover, when (x, y) scatter plots are limited to isocyanides supported by group 6 metals, an appreciably better linear correlation in the data is observed (Figure 5.5). Most notably, the location of the trisisocyanide η^6–arene M(η^6–(Mes)–κ^1–*C*–CNAr^{Mes})(CNAr^{Mes2})$_2$ complexes at the uttermost confines of these plots highlights how astonishingly unique they are both structurally and chemically.

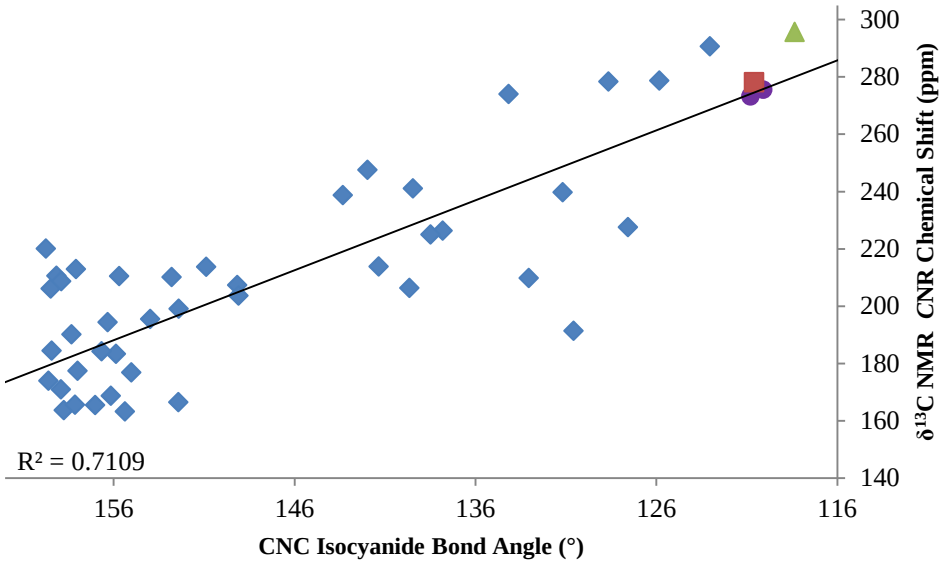

Figure 5.4. (x, y) scatter plot of C–N–C isocyanide bond angles versus isocyanide ^{13}C CNR chemical shifts for isocyanide complexes (▲Cr(η^6–(Mes)–κ^1–*C*–CNAr^{Mes})(CNAr^{Mes2})$_2$ (**42**), ■ Mo(η^6–(Mes)–κ^1–*C*–CNAr^{Mes})(CNAr^{Mes2})$_2$ (**24**), ● other Mo(η^6–(R)–κ^1–*C*–CNAr^{R})(CNAr^{R2})$_2$ synthesized by our group,[40] ♦ literature values for isocyanide complexes[44,59–86]).

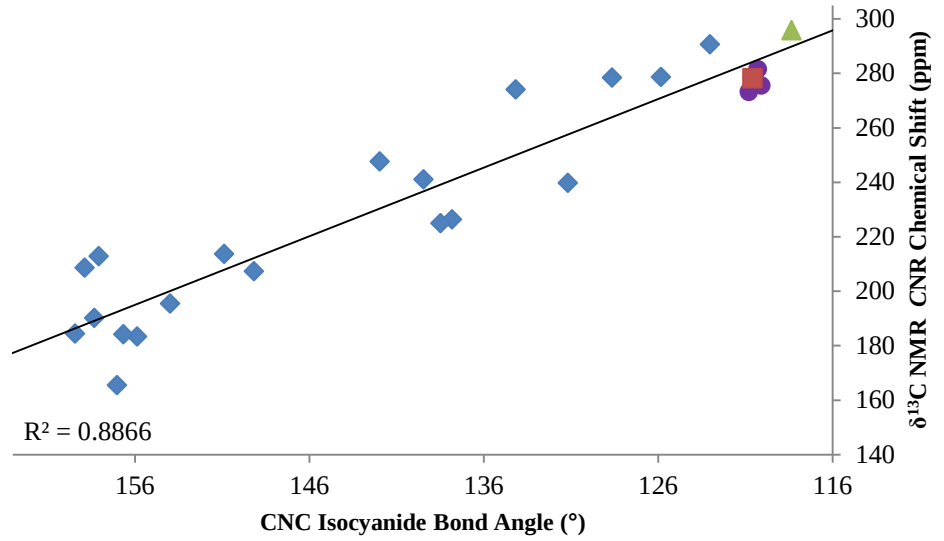

Figure 5.5. (x, y) scatter plot of C–N–C isocyanide bond angles versus isocyanide ^{13}C CNR chemical shifts for group 6 isocyanide complexes (▲Cr(η^6–(Mes)–κ^1–*C*–CNAr^{Mes})(CNAr^{Mes2})$_2$ (**42**), ■ Mo(η^6–(Mes)–κ^1–*C*–CNAr^{Mes})(CNAr^{Mes2})$_2$ (**24**), ● other Mo(η^6–(R)–κ^1–*C*–CNAr^{R})(CNAr^{R2})$_2$ synthesized by our group,[40] ♦ literature values for group 6 isocyanide complexes[44,59–69]).

Historically, control of the donor/acceptor properties of aryl isocyanides has been achieved through introduction of electron–releasing or –withdrawing substituents to the aromatic ring.[54,87–91] Nevertheless, to date, little attention has been focused on attenuating donor/acceptor properties of isocyanides by constraining their ability to bond linearly to transition–metals. Therefore, the constrained C_{iso}–N–C_{ipso} bond angle resulting from the flanking–ring η^6–interaction observed in the M(η^6–(Mes)–κ^1–*C*–$CNAr^{Mes}$)($CNAr^{Mes2}$)$_2$ complexes is unprecedented. Although a multitude of mononuclear/polydentate isocyanides complexes have been structurally characterized, to our knowledge, significant bending of an isocyanide C–N–C bond angle due secondary coordination events has only been observed in one previous example.[74] Liu and co–workers isolated the iron, cylopentyldienyl carbonyl salt [FeCp(CO)(κ^1–*C*–CN$(CH_2)_3$–κ^1–*P*–PPh_2)]I, which features a bidentate phosphine–tethered isocyanide ligand. The tethered–isocyanide host a short three–atom ($(CH_2)_3$) linker joining the PPh_2 and C≡N moieties which lends to a geometrically constrained C–N–C isocyanide bond angle of 141(2)°. Interestingly, however, [FeCp(CO)(κ^1–*C*–CN$(CH_2)_3$–κ^1–*P*–PPh_2)]I reacts with propylamine to afford the aminocarbene complex [FeCp(CO)(κ^1–*C*($(CH_2)_2CH_3$)–CN(H)$(CH_2)_3$–κ^1–*P*–PPh_2)]I.[74] This reactivity contrast that of the M(η^6–(Mes)–κ^1–*C*–$CNAr^{Mes}$)($CNAr^{Mes2}$)$_2$ complexes in this study, which were shown to be unreactive towards both amines and more potent nucleophiles (i.e. methyl lithium (LiMe) and lithium bis(trimethylsilyl)amide ($LiN(SiMe_3)_2$).

5.4 Mono–Addition of Electrophilic Substrates to Mo(η^6–(R)–κ^1–*C*–$CNAr^R$)($CNAr^{R2}$)$_2$ Complexes

The reactivity of isocyanides ligated to transition–metals has been well established,[92–96] and can be generalized into three categories; those reactive towards nucleophiles,[92]

electrophiles,[93] or neither. The broad scope of isocyanide reactivity is owed to its ability to function as both a σ–donor and a π–acid,[97–99] and it's the interplay of these two binding modes that dictate where on the reactivity spectrum an isocyanide will fall when ligated to a metal.[92–96] Representing one extreme, nucleophic addition at the α–carbon of a transition–metal isocyanide is common, contrastingly, however, electrophilic addition at the β–nitrogen of a transition–metal isocyanide is far less observed.[93] Reactivity of the latter type requires low–valent, electron–releasing metal–centers,[100–116] often supported by strong donor ligands,[100,102–104,107,109,111–113,115,116] and is almost exclusively limited to metal–centers supported by alkyl isocyanides.[102,105,116] These requirements can be rationalized by considering that (i) an appreciably π–basic metal–center is imperative for an electron rich nitrogen atom and (ii) the arene π*–orbitals of aryl isocyanides can syphon electron density away from the nitrogen atom.

It is generally accepted that an approximate indication to the extent of M→ligand π–donation is reflected by the magnitude an isocyanide C–N–C bond angle deviates from linearity. The contraction of the C–N–C bond angle results from charge localization on the electronegative nitrogen atom and paring effects, which induce a sp toward sp^2 rehybridization at the nitrogen atom of the C–N–C linkage.[88] Expectedly, these distortions are diminished with aryl isocyanides, where the *p*–orbitals of the aromatic ring can delocalize charge away from both the metal–center and the nitrogen atom along the M–C_{iso}–N–C_{ipso} bond. Interestingly, however, frontier molecular orbital calculations have indicated this phenomenon can be negated, and that contraction of the C_{iso}–N–C_{ipso} bond angle in aryl isocyanides may effectively inhibit metal→arene π–donation.[117] Bennet and co–workers reported that the π–acidity (as determined by the relative energy of the isocyanide π* orbitals) of aryl isocyanides decrease as a function of decreasing C_{iso}–N–C_{ipso} bond angle (180° → 120°), and although more pronounced when the C≡N group was bent out of the plane of the

aromatic ring, in plane bending demonstrated a similar but lesser effect.[117] Consistent with theory, on average, a 0.0275(13) Å and 0.0245(10) Å increase in N–C_{ipso} bond length is observed for the geometrically constrained isocyanide ligands when compared to the untethered isocyanides of Cr(η^6–(Mes)–κ^1–*C*–$CNAr^{Mes}$)($CNAr^{Mes2}$)$_2$ (**42**) and Mo(η^6–(Mes)–κ^1–*C*–$CNAr^{Mes}$)($CNAr^{Mes2}$)$_2$ (**24**), respectively. The relative lengthening N–C_{ipso} bond implies that metal→ligand π–donation along the N–C_{ipso} bond is indeed disrupted by C_{iso}–N–C_{ipso} bending in the M(η^6–(Mes)–κ^1–*C*–$CNAr^{Mes}$)($CNAr^{Mes2}$)$_2$ complexes, albeit marginally. In total, we speculated that geometrically constrained η^6–arene isocyanide ligand featured in the M(η^6–(Mes)–κ^1–*C*–$CNAr^{Mes}$)($CNAr^{Mes2}$)$_2$ complexes should demonstrate enhanced reactivity toward electrophiles.

Accordingly, addition of trifluoromethylsulfonic acid (HOTf) to a thawing Et_2O solution (–116 °C) of the trisisocyanide, η^6–arene M(η^6–(Mes)–κ^1–*C*–$CNAr^{Mes}$)($CNAr^{Mes2}$)$_2$ proceeds via rapid β–N–protonation of the geometrically constrained isocyanide ligand leading to precipitation of the trisisocyanide, aminocarbyne salt [M(η^6–(Mes)–κ^1–*C*–$CN(H)Ar^{Mes}$)($CNAr^{Mes2}$)$_2$](OTf) (M = Cr, Mo) as determined by X–ray diffraction (Schemes 5.4 and 5.5, Figures 5.6 and 5.7). The aminocarbyne ligands in [Cr(η^6–(Mes)–κ^1–*C*–$CN(H)Ar^{Mes}$)($CNAr^{Mes2}$)$_2$](OTf) (**43**) and [Mo(η^6–(Mes)–κ^1–*C*–$CN(H)Ar^{Mes}$)($CNAr^{Mes2}$)$_2$](OTf) (**44**) feature long C_{iso}–N bond lengths of 1.314(3) Å and 1.339(3) Å, respectively, and short C_{iso}–M bond lengths of 1.747(3) Å and 1.828(2) Å, respectively, both consistent with a aminocarbyne formalism (Table 5.2). Moreover, solution FTIR spectra of [Cr(η^6–(Mes)–κ^1–*C*–$CN(H)Ar^{Mes}$)($CNAr^{Mes2}$)$_2$](OTf) (**43**, $CDCl_3$) and [Mo(η^6–(Mes)–κ^1–*C*–$CN(H)Ar^{Mes}$)($CNAr^{Mes2}$)$_2$](OTf) (**44**, CD_2Cl_2) reveal ν_{NH} bands at 3323 cm^{-1} and 3323 cm^{-1}, respectively, and ν_{CN} bands at 1493 cm^{-1} and 1416 cm^{-1}, respectively, both diagnostic of β–N–protonation of the arene–tethered isocyanide ligand in these complexes (Table 5.2). The most remarkable structural feature of [Cr(η^6–(Mes)–κ^1–*C*–

$CN(H)Ar^{Mes})(CNAr^{Mes2})_2](OTf)$ (**43**) and $[Mo(\eta^6–(Mes)–\kappa^1–C–CN(H)Ar^{Mes})(CNAr^{Mes2})_2](OTf)$ (**44**) is the notably bent N–C–M bond angles of 150.9(2)° and 149.76(19)°, respectively (Table 5.2). According to the Cambridge Structural Database,[58] the most acute N–C–M bond angle previously reported for a structurally characterized aminocarbyne was 170.199°, nearly 20° more obtuse than that found for the tethered–aminocarbynes in this report.[118] Although the acute M–C–N aminocarbyne bond angles found in the $[M(\eta^6–(Mes)–\kappa^1–C–CN(H)Ar^{Mes})(CNAr^{Mes2})_2](OTf)$ complexes are compelling, the remainder of the spectroscopic features of these compounds (i.e. $^{13}C\{^1H\}$ NMR, ^1H NMR and FTIR) fall well within the range of published values for similar aminocarbyne complexes (Table 5.2).[103,112,113,116]

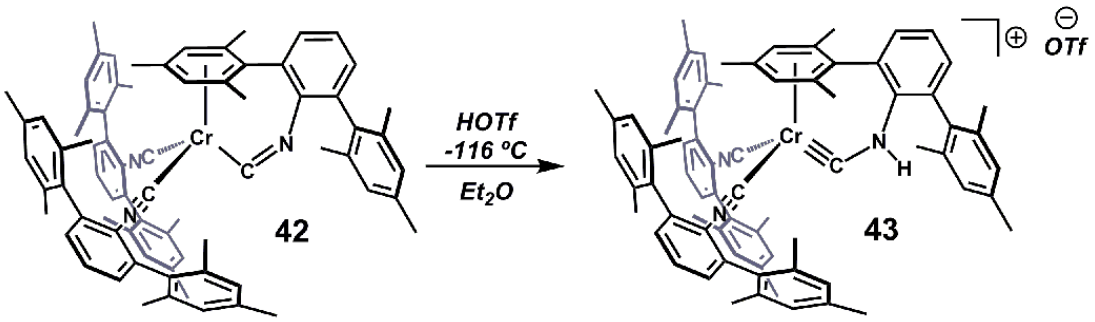

Scheme 5.4. Synthesis of $[Cr(\eta^6–(Mes)–\kappa^1–C–CN(H)Ar^{Mes})(CNAr^{Mes2})_2](OTf)$ (**43**).

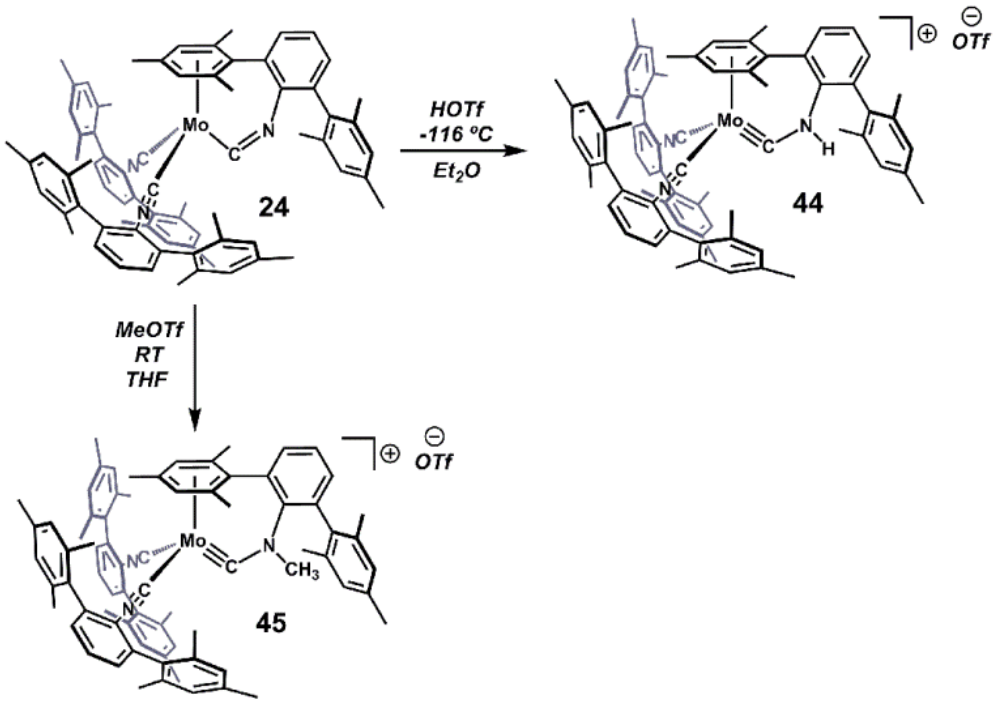

Scheme 5.5. Synthesis of [Mo(η^6–(Mes)–κ^1–*C*–CN(H)Ar^{Mes})(CNAr^{Mes2})$_2$](OTf) (**44**) and [Mo(η^6–(Mes)–κ^1–*C*–CN(CH$_3$)Ar^{Mes})(CNAr^{Mes2})$_2$](OTf) (**45**).

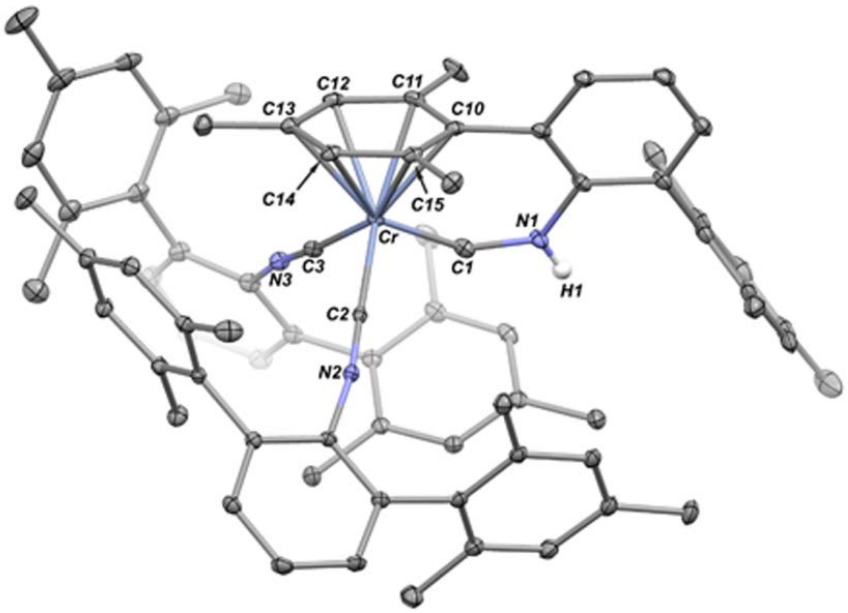

Figure 5.6. Molecular Structure of [Cr(κ^1–*C*–CN(H)Ar^{Mes}(η^6–Mes))(CNAr^{Mes2})$_2$]OTf (**43**). Selected bond distances (Å) and angles (Deg): Cr1–C1 = 1.747(3); Cr1–C2 = 1.926(3); Cr1–C3 = 1.937(3); C1–N1 = 1.314(4); N1–C4 = 1.420(3); C1–Cr1–C2 = 93.33(12); C1–Cr1–C3 = 95.77(12); C2–Cr1–C3 = 93.70(10); Cr1–C1–N1 = 150.9(2); C1–N1–C4 = 121.6(2).

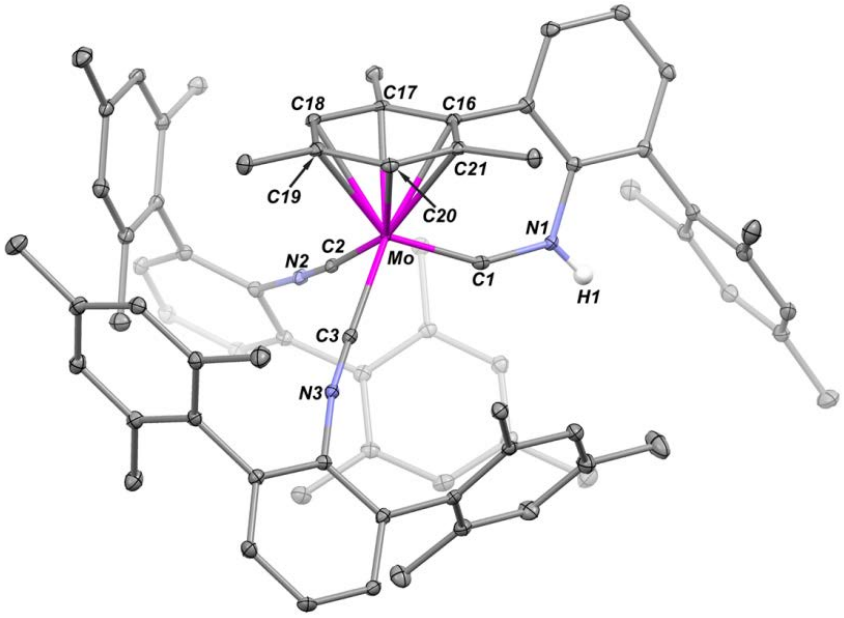

Figure 5.7. Molecular Structure of [Mo(κ^1–*C*–CN(H)Ar^{Mes}(η^6–Mes))(CNAr^{Mes2})$_2$]OTf (**44**). Selected bond distances (Å) and angles (Deg): Mo1–C1 = 1.828(2); Mo1–C2 = 2.036(2); Mo1–C3 = 2.083(2); C1–N1 = 1.339(3); N1–C4 = 1.413(2); C1–Mo1–C2 = 91.81(9); C1–Mo1–C3 = 102.52(9); C2–Mo1–C3 = 91.81(9); Mo1–C1–N1 = 149.76(19); C1–N1–C4 = 122.7(2).

In order to further assess the reactivity of the trisisocyanide, η^6–arene complex Mo(η^6–(Mes)–κ^1–*C*–CNAr^{Mes})(CNAr^{Mes2})$_2$ (**24**), we next pursued alkylating reagents that could deliver equivalents of (CH_3^+), specifically methyl iodide (MeI) and methyl triflate (MeOTf). Contrasting to reactions between HOTf and Mo(η^6–(Mes)–κ^1–*C*–CNAr^{Mes})(CNAr^{Mes2})$_2$ (**24**), which proceed rapidly, Mo(η^6–(Mes)–κ^1–*C*–CNAr^{Mes})(CNAr^{Mes2})$_2$ (**24**) was found to be unreactive towards MeI at room temperature. However, when Mo(η^6–(Mes)–κ^1–*C*–CNAr^{Mes})(CNAr^{Mes2})$_2$ (**24**) is treated with MeOTf in lieu of MeI, the N–methylated aminocarbyne complex [Mo(η^6–(Mes)–κ^1–*C*–CN(CH_3)Ar^{Mes})(CNAr^{Mes2})$_2$](OTf) (**45**) is formed within 24h at ambient temperatures, as determined by X–ray crystallography (Scheme 5.5, Figure 5.8). The presence of an aminocarbyne ligand was confirmed by ^{13}C NMR analysis, which revealed a down–field chemical shift of 282.7 ppm ($CDCl_3$) and by FTIR spectroscopy ($CDCl_3$) which revealed a

low–energy ν_{CN} stretch at 1483 cm^{-1}. One prominent difference between the N–methylated and N–protonated aminocarbynes is that the ν_{CN} band for the tethered–aminocarbyne in [Mo(η^6–(Mes)–κ^1–*C*–CN(CH_3)Ar^{Mes})($CNAr^{Mes2}$)$_2$](OTf) (**45**) is shifted 69 cm^{-1} to higher energy relative to its N–protonated counterpart (1416 cm^{-1}, Table 5.2). Interestingly, in other studies, where both the product of N–protonation and N–methylation of a metal isocyanide were isolated, a similar upwards shift of the N–alkylated aminocarbyne ν_{CN} stretch was observed, but to a lesser extent.[103,104]

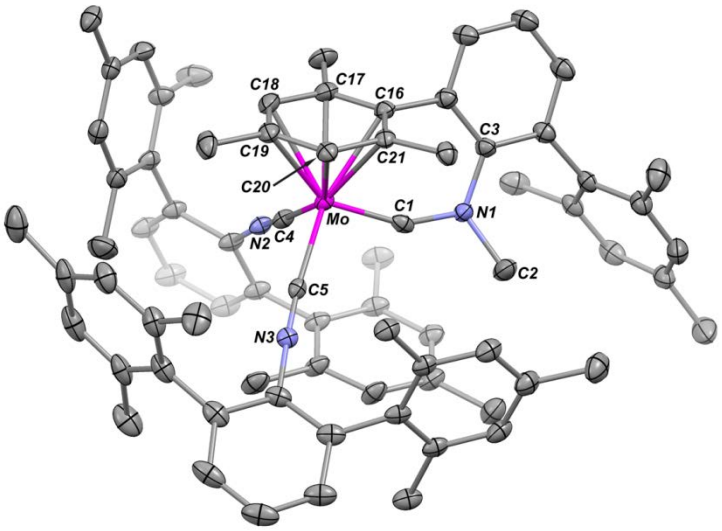

Figure 5.8. Molecular Structure of [Mo(κ^1–*C*–CN(CH_3)Ar^{Mes}(η^6–Mes))($CNAr^{Mes2}$)$_2$]OTf (**45**). Selected bond distances (Å) and angles (Deg): Mo1–C1 = 1.820(6); Mo1–C4 = 2.022(5); Mo1–C5 = 2.073(5); C1–N1 = 1.336(6); N1–C2 = 1.490(6); N1–C3 = 1.441(6); C1–Mo1–C4 = 91.8(2); C1–Mo1–C5 = 98.28(19); C4–Mo1–C5 = 93.07(18); Mo1–C1–N1 = 153.5(4); C1–N1–C4 = 119.5(4); C1–N1–C2 = 122.7(2); C2–N1–C3 = 125.4(4).

As mentioned earlier, due to the increased π–acidity of aryl isocyanides relative to their alkyl counterparts, electrophilic addition is rarely observed in complexes supported by these ligands. Generally, the addition of acid to aryl isocyanides leads to the formation of metal–hydrides,[45,102,105,116,119,120] and in the rare examples aminocarbynes are formed, they are frequently unstable, and decompose to metal–hydrides.[105,116,121] To our knowledge, the only

persistent N–protonated or N–alkylated arylaminocarbynes were isolated by Masanobu and co–workers.[116] In these reports, aryl isocyanides supported by the electron–rich $Mo(dppe)_2$ (dppe = $Ph_2PCH_2CH_2PPh_2$) fragment were demonstrated to form isolable arylaminocarbynes upon both protonation and methylation.[116] [Cr(η^6–(Mes)–κ^1–*C*–CN(H)Ar^{Mes})($CNAr^{Mes2}$)$_2$](OTf) (**43**) and [Mo(η^6–(Mes)–κ^1–*C*–CN(H)Ar^{Mes})($CNAr^{Mes2}$)$_2$](OTf) (**44**) also display marked stability ($CDCl_3$, 25 °C, 3 days), but in contrast to the aforementioned, lack an appreciably π–basic metal center. Evidently, the constrained C_{iso}–N–C_{ipso} bond serves to not only activate the arene–tethered isocyanide towards electrophilic addition, but also stabilizes the resulting aryl–aminocarbyne by inhibiting proton transfer to the metal center. We speculate that the stability exhibited in the arylaminocarbyne [M(η^6–(Mes)–κ^1–*C*–CN(H)Ar^{Mes})($CNAr^{Mes2}$)$_2$](OTf) complexes is likely because η^6–tethering does not allow for rotation along the C_{iso}–N bond or bending of the C_{iso}–N–C_{ipso} bond, therefore molecular movement that could place the proton into close proximity with the metal–center is inhibited, and proton transfer is suppressed.

It is noteworthy that, although aminocarbynes have been proposed as intermediates in the protic–coupling of isocyanides supported by chromium metal–centers,[114] to the best of our knowledge, [Cr(η^6–(Mes)–κ^1–*C*–CN(H)Ar^{Mes})($CNAr^{Mes2}$)$_2$](OTf) (**43**) is the first isolated example of a chromium aminocarbyne complex synthesized via β–N–protonation of either an alkyl or aryl isocyanide. Also noteworthy, [Mo(η^6–(Mes)–κ^1–*C*–CN(CH_3)Ar^{Mes})($CNAr^{Mes2}$)$_2$](OTf) (**45**) is the first example of a structurally characterized N–alkylated arylaminocarbyne according to the Cambridge Structural Database.[58]

5.5 Protonation of [Mo(η^6–(Mes)–κ^1–*C*–CN(H)Ar^{Mes})(CNAr^{Mes2})$_2$](OTf) and [Mo(η^6–(Mes)–κ^1–*C*–CN(CH$_3$)Ar^{Mes})(CNAr^{Mes2})$_2$](OTf)

The pioneering work of Lippard and Pombeiro demonstrated that the addition of two equivalents of acid to electron–rich, metal complexes supported by two or more isocyanides often leads to protic coupling of isocyanides.[101,106,108,110,112–115,122,123] The above reactions have been shown to proceed by route of two successive isocyanide N–protonations to afford bis–aminocarbyne intermediates, which rearrange to form diaminoacetylene complexes.[112,115,123] With respect to the limited number of examples of N–protonation of aryl isocyanides, it is not surprising that there are no known reports of the protic coupling of two aryl isocyanides. In addition to diaminoacetylenes, aminocarbenes have also been isolated by addition of two equivalents of acid to monoisocyanide complexes, however, the double protonation of isocyanides observed in these reports were not shown to occur through aminocarbyne intermediates.[116,124] Furthermore, although aminocarbenes have been derived from the protonation of aminocarbynes,[125–128] the aminocarbyne precursors in the latter examples were not derived from isocyanides. Nevertheless, whether addition of a second equivalent of acid to [Mo(η^6–(Mes)–κ^1–*C*–CN(H)Ar^{Mes})(CNAr^{Mes2})$_2$](OTf) or [Mo(η^6–(Mes)–κ^1–*C*–CN(CH$_3$)Ar^{Mes})(CNAr^{Mes2})$_2$](OTf) resulted in the coupling of two aryl isocyanides, formation of a bis–arylaminocarbyne, or preferential protonation of a carbyne over an isocyanide ligand, the reaction would be unprecedented.

Thus, treatment of the aminocarbyne [Mo(η^6–(Mes)–κ^1–*C*–CN(H)Ar^{Mes})(CNAr^{Mes2})$_2$](OTf) (**44**) with 0.9 equiv of HOTf in a 2:1 toluene/THF mixture proceeds via α–carbon protonation of the aminocarbyne ligand resulting in the formation of the Mo(II) aminocarbene salt [Mo(THF)(η^6–(Mes)–κ^1–*C*–

C(H)N(H)Ar^{Mes})(CNAr^{Mes2})$_2$](OTf)$_2$ (**46**, Scheme 5.6, Figure 5.9, Table 5.2). [Mo(THF)(η^6–(Mes)–κ^1–*C*–C(H)N(H)Ar^{Mes})(CNAr^{Mes2})$_2$](OTf)$_2$ (**46**) was characterized by X–ray crystallography, and both the C*H* and N*H* protons of the aminocarbene functionality were unequivocally found in the Fourier map, thus confirming the presence of an aminocarbene. Further corroborating the carbene assignment, ^{1}H NMR spectra of the diamagnetic complex [Mo(THF)(η^6–(Mes)–κ^1–*C*–C(H)N(H)Ar^{Mes})(CNAr^{Mes2})$_2$](OTf)$_2$ (**46**) ($CDCl_3$) revealed a pair of doublets at 8.83 and 10.38 ppm for the C*H* and N*H* protons of the aminocarbene, respectively. Moreover, a ν_{NH} stretch at 3267 cm^{-1} was detected by solution FTIR ($CDCl_3$, Table 5.3). Interestingly, despite possessing a Mo(II) metal–center, the η^6–Mes binding in [Mo(THF)(η^6–(Mes)–κ^1–*C*–C(H)N(H)Ar^{Mes})(CNAr^{Mes2})$_2$](OTf)$_2$ (**46**) is persistent in solution (^{1}H NMR, $CDCl_3$) as evidenced by an upfield–shifted arene resonance at 4.84 ppm.

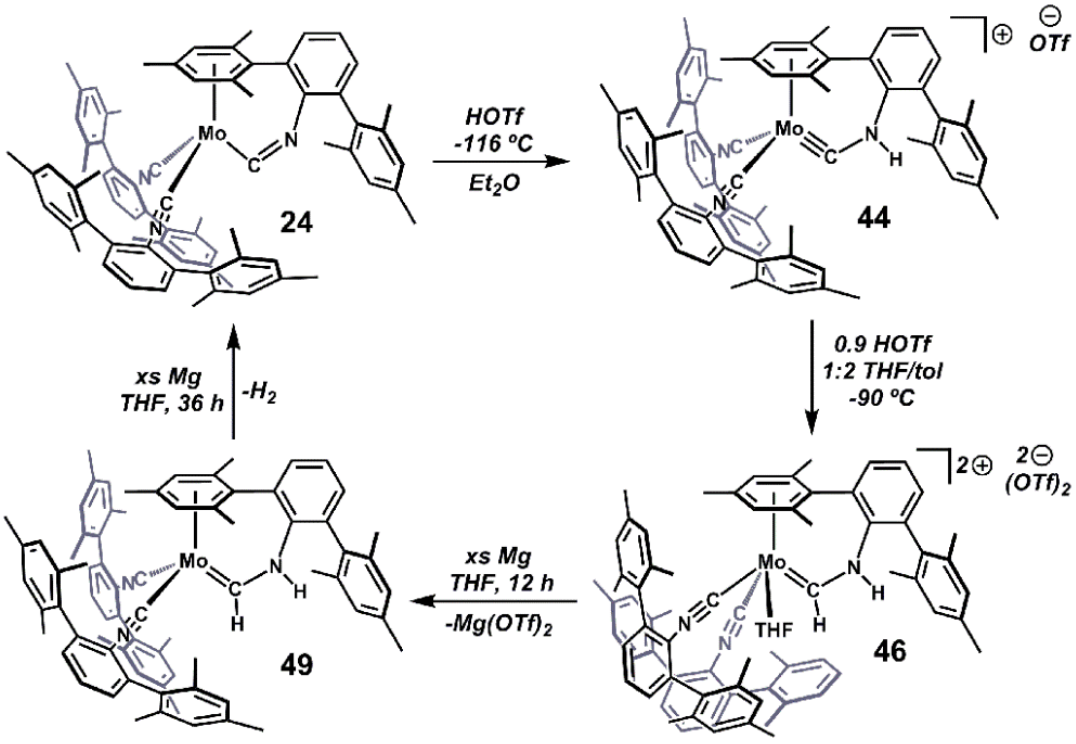

Scheme 5.6. Synthesis of [Mo(THF)(η^6–(Mes)–κ^1–*C*–C(H)N(H)Ar^{Mes})(CNAr^{Mes2})$_2$](OTf)$_2$ (**46**) and Mo(η^6–(Mes)–κ^1–*C*–C(H)N(H)Ar^{Mes})(CNAr^{Mes2})$_2$] (**49**).

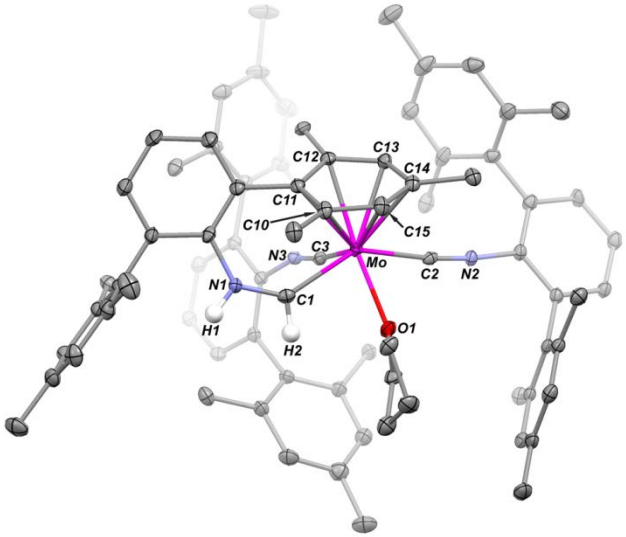

Figure 5.9. Molecular Structure of [Mo(THF)(κ^1–*C*–C(H)N(H)Ar^{Mes}(η^6–Mes))(CNAr^{Mes2})$_2$](OTf)$_2$ (**46**). Selected bond distances (Å) and angles (Deg): Mo1–C1 = 2.117(8); Mo1–C2 = 2.150(7); Mo1–C3 = 2.019(7); Mo1–O1 = 2.210(5); C1–N1 = 1.306(10); N1–C4 = 1.422(9); C1–Mo1–C2 = 137.7(3); C1–Mo1–C3 = 75.8(3); C1–Mo1–O1 = 75.6(3); C2–Mo1–C3 = 84.6(3); C2–Mo1–O1 = 75.4(2); C3–Mo1–O1 = 107.9(3); Mo1–C1–N1 = 135.1(6); C1–N1–C4 = 129.2(7).

Selectivity for α–carbon protonation of an aminocarbyne over β–nitrogen protonation of a second isocyanide in an aminocarbyne/isocyanide metal complex to the best of our knowledge has not been previously reported. Although it is generally accepted that the carbon atoms of aminocarbynes are nucleophilic, the credence of this "rule" is put into question by a number of examples of α–carbon protonation of aminocarbynes.[125–128] We suspect that exclusive protonation of the aminocarbyne ligand in [Mo(η^6–(Mes)–κ^1–*C*–CN(H)Ar^{Mes})(CNAr^{Mes2})$_2$](OTf) (**44**) is likely because the isocyanide ligands are markedly deactivated towards electrophilic addition, as indicated by the high–energy isocyanide ν_{CN} stretches that range from 2011 to 2110 cm^{-1}. None the less, it is impossible to rule out that the mechanism for the formation of the aminocarbene complex [Mo(THF)(η^6–(Mes)–κ^1–*C*–C(H)N(H)Ar^{Mes})(CNAr^{Mes2})$_2$](OTf)$_2$ (**46**) does not proceed via protonation of the metal center followed by hydride migration from the metal to the aminocarbyne carbon. The validity of

this mechanism is supported by claims that the addition of $LiAlH_4$ to aminocarbynes resulted in aminocarbene formation.[105]

Whereas the protonation of [Mo(η^6–(Mes)–κ^1–*C*–CN(H)Ar^{Mes})($CNAr^{Mes2}$)$_2$](OTf) (**44**) by addition of HOTf proceeds smoothly to afford a single aminocarbene product, addition of HOTf to [Mo(η^6–(Mes)–κ^1–*C*–CN(CH_3)Ar^{Mes})($CNAr^{Mes2}$)$_2$](OTf) (**45**) results in a complex mixture as determined by ^{1}H NMR spectroscopy (Scheme 5.7). Crystallographic structure determination of orange and red crystals grown from a concentrated 1:1 THF/*n*–pentane solution of the crude reaction mixture revealed the aminocarbene salt [Mo(OTf)(η^6–(Mes)–κ^1–*C*–C(H)N(CH_3)Ar^{Mes})($CNAr^{Mes2}$)$_2$](OTf) (**47**, Figure 5.10), and the allylimine salt [Mo(η^6–(Mes)–η^3–(CH_2CHN)–Ar^{Mes})($CNAr^{Mes2}$)$_2$](OTf)$_2$ (**48**, Figure 5.11), respectively. Despite our efforts, conditions for the exclusive isolation of either [Mo(OTf)(η^6–(Mes)–κ^1–*C*–C(H)N(CH_3)Ar^{Mes})($CNAr^{Mes2}$)$_2$](OTf)$_2$ (**47**), or [Mo(η^6–(Mes)–η^3–(CH_2CHN)–Ar^{Mes})($CNAr^{Mes2}$)$_2$](OTf)$_2$ (**48**) were not found, and further spectroscopic characterization of these compounds was not obtained. The isolation of [Mo(OTf)(η^6–(Mes)–κ^1–*C*–C(H)N(CH_3)Ar^{Mes})($CNAr^{Mes2}$)$_2$](OTf) (**47**) indicates that akin to its N–protonated counterpart, the aminocarbyne carbon atom of [Mo(η^6–(Mes)–κ^1–*C*–CN(CH_3)Ar^{Mes})($CNAr^{Mes2}$)$_2$](OTf) is indeed nucleophilic. However, it's uncertain what factors are culpable for the markedly divergent reactivity observed in [Mo(η^6–(Mes)–κ^1–*C*–CN(CH_3)Ar^{Mes})($CNAr^{Mes2}$)$_2$](OTf) (**45**) relative to [Mo(η^6–(Mes)–κ^1–*C*–CN(H)Ar^{Mes})($CNAr^{Mes2}$)$_2$](OTf) (**44**). Investigations concerning the reactivity of [Mo(η^6–(Mes)–κ^1–*C*–CN(CH_3)Ar^{Mes})($CNAr^{Mes2}$)$_2$](OTf) (**45**) towards electrophiles are ongoing.

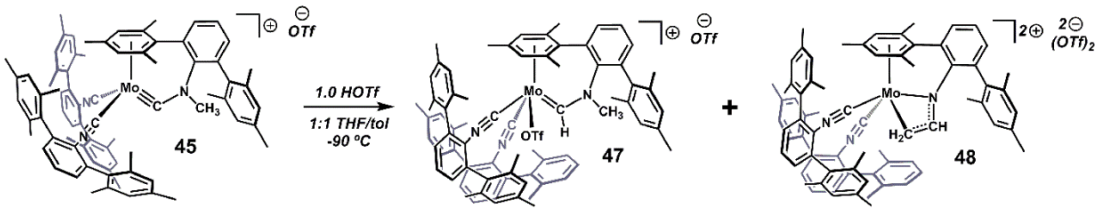

Scheme 5.6. Synthesis of [Mo(OTf)(η^6–(Mes)–κ^1–*C*–C(H)N(CH_3)Ar^{Mes})($CNAr^{Mes2}$)$_2$](OTf)$_2$ (**47**), and [Mo(η^6–(Mes)–η^3–(CH_2CHN–Ar^{Mes})($CNAr^{Mes2}$)$_2$](OTf)$_2$ (**48**).

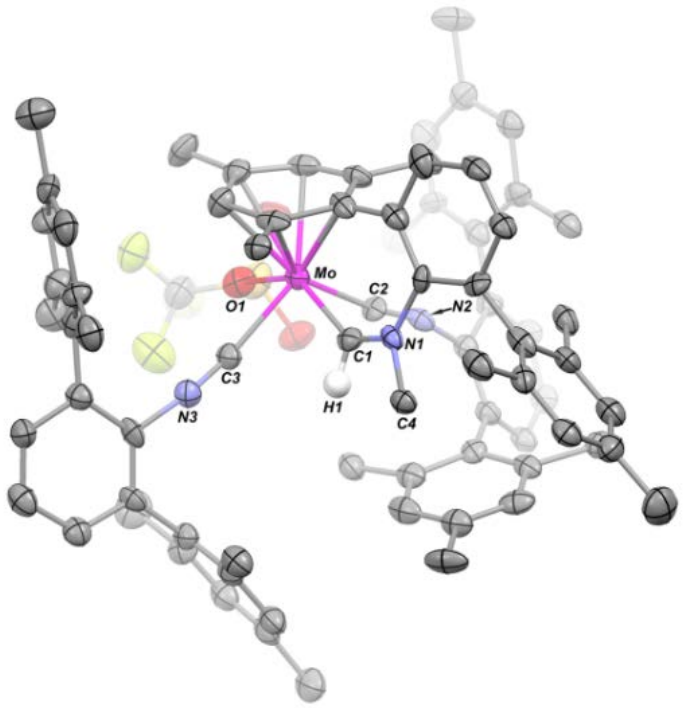

Figure 5.10. Molecular Structure of [Mo(OTf)(η^6–(Mes)–κ^1–*C*–C(H)N(CH_3)Ar^{Mes})($CNAr^{Mes2}$)$_2$](OTf) (**47**) (OTf counterion is omitted). Selected bond distances (Å) and angles (Deg): Mo1–C1 = 2.18(3); Mo1–C2 = 2.029(15); Mo1–C3 = 2.128(19); Mo1–O1 = 2.218(11); C1–N1 = 1.23(2); N1–C4 = 1.497(17); C1–Mo1–C2 = 78.3(5); C1–Mo1–C3 = 81.0(7); C1–Mo1–O1 = 143.6(7); C2–Mo1–C3 = 108.8(5); C2–Mo1–O1 = 85.2(5); C3–Mo1–O1 = 74.0(5); Mo1–C1–N1 = 148.2(15); C1–N1–C4 = 117.3(13).

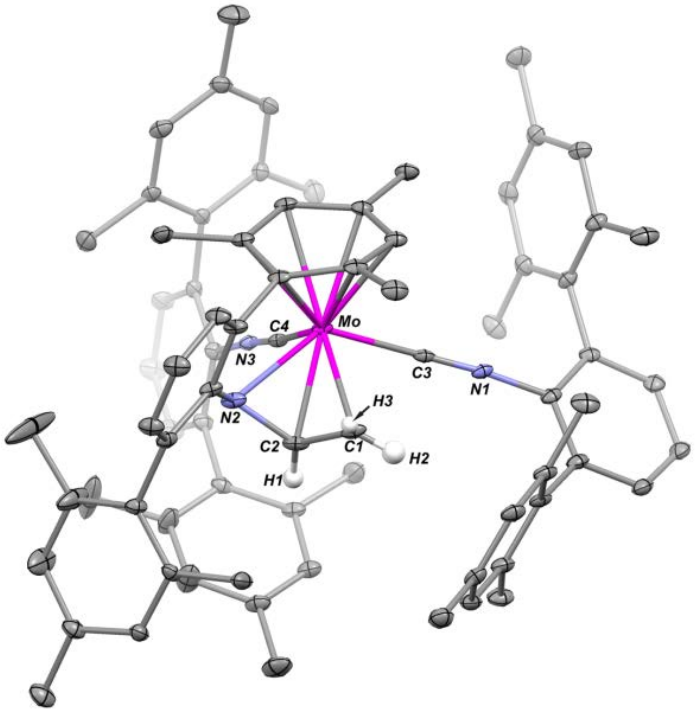

Figure 5.11. Molecular Structure of [Mo(η^6–(Mes)–η^3–(CH_2CHN)–Ar^{Mes})($CNAr^{Mes2}$)$_2$]$(OTf)_2$ (**48**) (OTf counterions are omitted). Selected bond distances (Å) and angles (Deg): Mo1–C1 = 2.304(6); Mo1–C2 = 2.199(6); Mo1–C3 = 2.129(7); Mo1–C4 = 2.057(6); Mo1–N2 = 2.198(6); C3–N1 = 1.154(8); C4–N3 = 1.158(8); N2–C5 = 1.475(8); C3–Mo1–C4 = 87.0(2); C4–Mo1–N2 = 84.8(2); C1–Mo1–C3 = 77.9(3); N2–C2–C1 = 113.9(6).

5.6 Reductions of [Mo(η^6–(Mes)–κ^1–*C*–CN(H)Ar^{Mes})($CNAr^{Mes2}$)$_2$](OTf) and [Mo(THF)(η^6–(Mes)–κ^1–*C*–C(H)N(H)Ar^{Mes})($CNAr^{Mes2}$)$_2$]$(OTf)_2$

In addition to probing the reactivity of [Mo(η^6–(Mes)–κ^1–*C*–CN(H)Ar^{Mes})($CNAr^{Mes2}$)$_2$](OTf) (**44**) towards HOTf, we have also chemically assessed its electrochemistry. DFT single point energy calculations of the atom coordinates obtained from the X–ray analysis of [Mo(η^6–(Mes)–κ^1–*C*–CN(H)Ar^{Mes})($CNAr^{Mes2}$)$_2$](OTf) (**44**) revealed low lying π^* orbitals for η^6–bound mesityl ring (Figure 5.12, B and C). Therefore, we reasoned that the η^6–bound mesityl ring in [Mo(η^6–(Mes)–κ^1–*C*–CN(H)Ar^{Mes})($CNAr^{Mes2}$)$_2$](OTf) (**44**)

could potentially be reduced to a dianionic 1,4–cyclohexa–2,5–dienyl moiety. Furthermore, we were intrigued to see if dearomatization of the tethered mesityl ring had an appreciable effect on the tethered aminocarbyne ligand. Disappointingly, treatment of [Mo(η^6–(Mes)–κ^1–*C*–CN(H)Ar^{Mes})(CNAr^{Mes2})$_2$](OTf) with 10 equiv of 1% Na(Hg) in THF solution results in the slow regeneration of the trisisocyanide complex Mo(η^6–(Mes)–κ^1–*C*–CNAr^{Mes})(CNAr^{Mes2})$_2$ (**24**) over a 24 h period. It's important to note that aliquots of the reaction mixture taken before complete formation of Mo(η^6–(Mes)–κ^1–*C*–CNAr^{Mes})(CNAr^{Mes2})$_2$ (**24**) (ca. 12h) revealed the presence of only the aminocarbyne starting material [Mo(η^6–(Mes)–κ^1–*C*–CN(H)Ar^{Mes})(CNAr^{Mes2})$_2$](OTf) (**44**) and the trisisocyanide product Mo(η^6–(Mes)–κ^1–*C*–CNAr^{Mes})(CNAr^{Mes2})$_2$ (**24**) (^{1}H NMR spectroscopy). Our observations are in agreement with electrochemical cyclic voltammetry studies of others, which revealed aminocarbynes are converted to isocyanides via H^+ reduction.[129,130] It is accepted, that when dissolved in a mildly basic solvent such as THF, the aminocarbyne becomes marginally acidic, and an equilibrium between the aminocarbyne and the deprotonated anionic isocyanide complexes is formed.[129] The latter equilibrium highly favors the aminocarbyne, which rationalizes the slow transformation of [Mo(η^6–(Mes)–κ^1–*C*–CN(H)Ar^{Mes})(CNAr^{Mes2})$_2$](OTf) (**44**) to Mo(η^6–(Mes)–κ^1–*C*–CNAr^{Mes})(CNAr^{Mes2})$_2$ (**24**) observed in our studies.

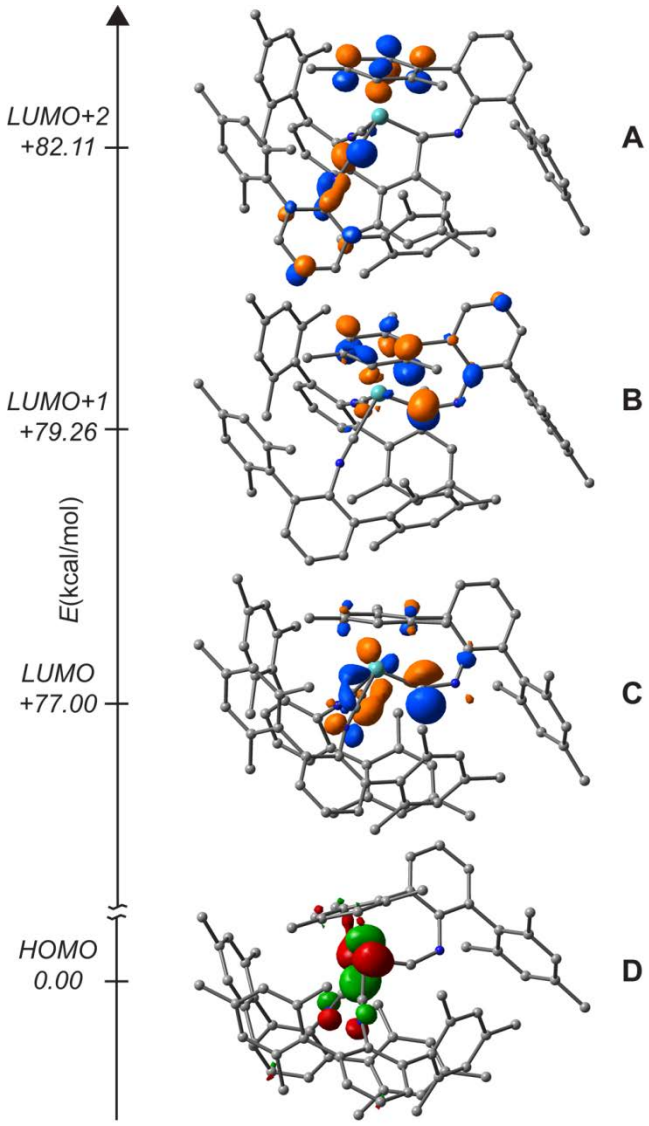

Figure 5.12. Selected frontier molecular orbitals calculated for [Mo(η^6–(Mes)–κ^1–*C*–CN(H)Ar^{Mes})(CNAr^{Mes2})$_2$](OTf) (**44**). ORCA 3.01; B3LYP/D3BJ RIJCOSX defbas–4 ZORA.

In order to discern whether reductive deprotonation was limited to only the aminocarbyne complex [Mo(η^6–(Mes)–κ^1–*C*–CN(H)Ar^{Mes})(CNAr^{Mes2})$_2$](OTf) (**44**), we extended our electrochemical survey to include [Mo(THF)(η^6–(Mes)–κ^1–*C*–C(H)N(H)Ar^{Mes})(CNAr^{Mes2})$_2$](OTf)$_2$ (**46**). The reduction of [Mo(THF)(η^6–(Mes)–κ^1–*C*–C(H)N(H)Ar^{Mes})(CNAr^{Mes2})$_2$](OTf)$_2$ (**46**) is outlined in Scheme 5.6, and although reductive deprotonation to the trisisocyanide complex Mo(η^6–(Mes)–κ^1–*C*–CNAr^{Mes})(CNAr^{Mes2})$_2$ (**24**)

was observed, the reaction proceeds through an intermediate that was isolated and identified as the zerovalent, bisisocyanide aminocarbene complex Mo(η^6–(Mes)–κ^1–*C*–C(H)N(H)Ar^{Mes})(CNAr^{Mes2})$_2$ (**49**) as determined by X–ray crystallography (Figure 5.13). Comparison of the aminocarbene ligand featured in the divalent aminocarbene complex [Mo(THF)(η^6–(Mes)–κ^1–*C*–C(H)N(H)Ar^{Mes})(CNAr^{Mes2})$_2$](OTf)$_2$ (**46**), with that of the zerovalent complex Mo(η^6–(Mes)–κ^1–*C*–C(H)N(H)Ar^{Mes})(CNAr^{Mes2})$_2$ (**49**) revealed that accompanied with the reduction of Mo(II) → Mo(0) there is a marked contraction (2.1778(8) → 2.036(2) Å) in the M–C$_{iso}$ bond length, consistent with a more π–basic metal center. The increased π–basicity of the zerovalent aminocarbene complex Mo(η^6–(Mes)–κ^1–*C*–C(H)N(H)Ar^{Mes})(CNAr^{Mes2})$_2$ (**49**) is also reflected in the low energy ν_{CN} bands at 1967 and 1874 cm^{-1} observed for the untethered isocyanides. It's important to note, that upon complete reduction of [Mo(THF)(η^6–(Mes)–κ^1–*C*–C(H)N(H)Ar^{Mes})(CNAr^{Mes2})$_2$](OTf)$_2$ (**46**), only trace quantities (ca. < 3 %) of the trisisocyanide complex Mo(η^6–(Mes)–κ^1–*C*–CNAr^{Mes})(CNAr^{Mes2})$_2$ (**24**) are detected (^{1}H NMR spectroscopy), suggesting that reductive deprotonation is operative only with the zerovalent aminocarbene Mo(η^6–(Mes)–κ^1–*C*–C(H)N(H)Ar^{Mes})(CNAr^{Mes2})$_2$ (**49**) and not the divalent aminocarbene [Mo(THF)(η^6–(Mes)–κ^1–*C*–C(H)N(H)Ar^{Mes})(CNAr^{Mes2})$_2$](OTf)$_2$ (**46**). Nevertheless, the mechanism for the reductive deprotonation of Mo(η^6–(Mes)–κ^1–*C*–C(H)N(H)Ar^{Mes})(CNAr^{Mes2})$_2$ (**49**) is unknown to us, and is currently under investigation. The reductive deprotonation of [Mo(THF)(η^6–(Mes)–κ^1–*C*–C(H)N(H)Ar^{Mes})(CNAr^{Mes2})$_2$](OTf)$_2$ (**46**) is notable because although previous reports have outlined the oxidation of zerovalent group 6 carbene complexes to divalent species while preserving carbene ligation,[131,132] to our knowledge, ours is the first example of the reverse process.

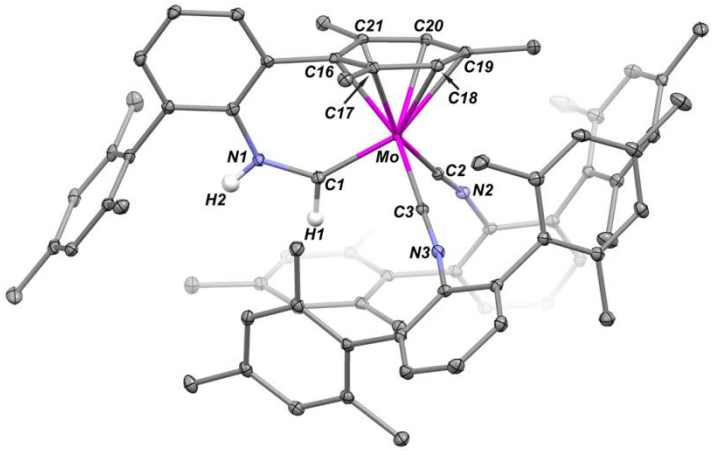

Figure 5.13. Molecular Structure of Mo(κ^1–*C*–C(H)N(H)Ar^{Mes}(η^6–Mes))(CNAr^{Mes2})$_2$ (**49**). Selected bond distances (Å) and angles (Deg): Mo1–C1 = 2.096(2); Mo1–C2 = 2.0029(19); Mo1–C3 = 2.0083(19); C1–N1 = 1.372(3); N1–C4 = 1.403(3); C1–Mo1–C2 = 88.27(8); C1–Mo1–C3 = 91.27(8); C2–Mo1–C3 = 84.47(7); Mo1–C1–N1 = 131.36(14); C1–N1–C4 = 130.34(17).

5.7 Synthetic Procedures

General Considerations. All manipulations were carried out under an atmosphere of dry dinitrogen using standard Schlenk and glovebox techniques. Solvents were dried and deoxygenated according to standard procedures.[133] Unless otherwise stated, reagent–grade starting materials were purchased from commercial sources and either used as received or purified by standard procedures.[134] The *m*–terphenyl derivatives CNAr^{Dipp2}, CNAr^{Mes2} and 2,6–(2,6–$Cl_2C_6H_3$)$_2C_6H_3$I were prepared according to literature procedures.[41,42,135] *p*–Tolylsulfonyl azide ($TosN_3$) was prepared as described previously.[136] Benzene–d_6 and cyclohexane–d_{12} (Cambridge Isotope Laboratories) were degassed and stored over 4 Å molecular sieves under N_2 for 2 d prior to use. Chloroform–*d* (Cambridge Isotope Laboratories) was vacuum distilled from NaH and then stored over 3 and 4 Å molecular sieves under N_2 for 2 d prior to use. Celite 405 (Fisher Scientific) was dried under vacuum (24 h) at a temperature above 250 ˚C and stored in the glovebox prior to use. Solution ^{1}H,

$^{13}C\{^{1}H\}$ and ^{19}F spectra were recorded on Varian Mercury 300 and 400 spectrometers, a Varian X–Sens500 spectrometer, or a JEOL ECA–500 spectrometer. ^{1}H and $^{13}C\{^{1}H\}$ chemical shifts are reported in ppm relative to $SiMe_4$ (^{1}H and ^{13}C δ = 0.0 ppm) with reference to residual solvent resonances of 7.16 ppm (^{1}H) and 128.06 ppm (^{13}C) for benzene–d_6, 1.38 ppm (^{1}H) and 26.43 ppm (^{13}C) for cyclohexane–d_{12} and 7.24 ppm (^{1}H) and 77.23 ppm (^{13}C) for chloroform–*d*. $^{19}F\{^{1}H\}$ NMR chemical shifts were referenced internally via capillary to neat trifluoroacetic acid $F_3CC(O)OH$ (δ = –78.5 ppm vs. $CFCl_3$ = 0.0 ppm). FTIR spectra were recorded on a Thermo–Nicolet iS10 FTIR spectrometer. Samples were prepared as C_6D_6, C_6D_{12} and $CDCl_3$ solutions injected into a ThermoFisher solution cell equipped with KBr windows or as KBr pellets. For solution FTIR spectra, solvent peaks were digitally subtracted from all spectra by comparison with an authentic spectrum obtained immediately prior to that of the sample. The following abbreviations were used for the intensities and characteristics of important IR absorption bands: vs = very strong, s = strong, m = medium, w = weak, vw = very weak; b = broad, vb = very broad, sh = shoulder. High resolution mass spectrometry (HRMS) was performed using an Agilent 6230 ESI–TOFMS instrument running in positive ion mode. Combustion analyses were performed by Robertson Microlit Laboratories of Madison, NJ (USA).

Synthesis of *fac*–$Cr(CO)_3(CNAr^{Mes2})_3$ (39). To an Et_2O solution of $CNAr^{Mes2}$ (3.037 g, 8.947 mmol, 3 equiv, 200 mL) was added to an Et_2O slurry of $Cr(CO)_3(NCMe)_3$ (0.773 g, 2.982 mmol, 1 equiv, 30 mL). The mixture was stirred for 3 h, after which the reaction mixture was then concentrated to ca. 1/2 its original volume under reduced pressure and cooled to –78°C, resulting in the precipitation of an bright yellow solid. This solid was collected via filtration over medium posterity frit, slurried in Et_2O (20 mL), filtered, dried *in vacuo*, and collected. Yield: 2.692g, 2.332 mmol, 78%. ^{1}H NMR (400.1 MHz, $CDCl_3$, 20 ˚C):

δ = 7.28 (t, 3H, *J* = 8 Hz, *o*–Ph), 7.05 (d, 6H, *J* = 8 Hz, *m*–Ph), 6.82 (s, 12H, *m*–Mes), 2.21 (s, 18H, *p*–C*H*$_3$), 1.90 (s, 36H, *o*–C*H*$_3$) ppm. ^{13}C{^{1}H} NMR (100.6 MHz, CD_2Cl_2, 20 °C): δ = 219.3, (*C*≡O), 184.9 (*C*≡N), 138.1, 137.0, 135.8, 134.7, 130.1, 128.7, 128.2, 126.6, 21.3, 20.4 ppm. FTIR ($CDCl_3$, KBr windows): (ν_{CN}) 2042 (vs) cm^{-1}, 1999 (vw sh) cm^{-1}, (ν_{CO}) 1943 (vs) cm^{-1}, 1913 (vs) cm^{-1}, also 2960, 2923, 2871, 2859, 1612, 1579, 1462, 1416, 1379 cm^{-1}. Anal. Calcd for $C_{78}H_{75}N_3O_3Cr$: C, 81.85; H, 6.55; N, 3.64. Found: C, 79.95; H, 6.63; N, 3.52.

Synthesis of *mer*–Cr(CO)$_3$(CNAr^{Mes2})$_3$ (40). A benzene solution of *fac*–Cr(CO)$_3$(CNAr^{Mes2})$_3$ (**39**, 0.100 g, 0.083 mmol, 20 mL) was stirred at 90 °C for 72 h, after which all volatile materials were removed under reduced pressure. Dissolution of the resulting orange residue in a toluene/*n*–pentane mixture (1:3, 4 mL total) followed by filtration and storage at −35 °C for 24 h resulted in orange crystals, which were collected and dried *in vacuo*. Yield: 0.065 g, 0.054 mmol, 65%. ^{1}H NMR (400.1 MHz, $CDCl_3$, 20 °C): δ = 6.95 (s, 4H, *m*–Mes), 6.94 (s, 8H, *m*–Mes), 6.92 (t, 2H, *J* = 8 Hz, *p*–Ph), 6.88 (d, 2H, *J* = 8 Hz, *m*–Ph), 6.87 (t, 1H, *J* = 8 Hz, *p*–Ph), 6.83 (d, 4H, *J* = 8 Hz, *m*–Ph), 2.48 (s, 6H, *p*–CH_3), 2.42 (s, 12H, *p*–CH_3), 2.09 (s, 24H, *o*–CH_3), 2.00 (s, 12H, *o*–CH_3) ppm. ^{13}C{^{1}H} NMR (100.6 MHz, $CDCl_3$, 20 °C): FTIR (C_6D_6, NaCl windows): (ν_{CN}) 2052 (m), 2024 (m), and 2002 (s) cm^{-1}, (ν_{CO}) 1924 (vs) and 1902 (s) cm^{-1} also 2918, 2854, 2390, 1619, 1582, 1452, 1410, 1330, and 1158 cm^{-1}. Anal. Calcd for $C_{78}H_{75}N_3O_3Cr$: C, 81.85; H, 6.55; N, 3.64. Found:

Synthesis of *mer*–CrI$_2$(I$_3$)(CNAr^{Mes2})$_3$ (41). To a toluene solution of I_2 (0.266 g, 10.47 mmol, 2.55 equiv, 40 mL) was added a 1:1 Et_2O/toluene solution of *fac*–Cr(CO)$_3$(CNAr^{Mes2})$_3$ (**39**, 0.700 g, 0.606 mmol, 1 equiv, 200 mL). The reaction mixture was stirred for 8 h at 52^{o}C. The reaction mixture was concentrated to 20 mL under reduced

pressure and 150 mL of pentane was added, followed by storage at –30°C. The next day, the red pentane/toluene solution was filtered over a medium posterity frit, and the resulting burgundy power slurried in pentane (20mL), filtered, and dried *in vacuo*, affording *mer*–$CrI_2(I_3)(CNAr^{Mes2})_3$ (**41**). Yield: .814 g, 0.477 mmol, 78%. X–ray diffraction quality crystals were grown from saturated Et_2O solution. ^{1}H NMR (400.1 MHz, $CDCl_3$, 20 ˚C): δ = 20.26 (s, 2H, *m*–Ph), 18.61 (s, 4H, *m*–Ph), 7.21 (s, 4H, *m*–Mes), 7.92 (s, 8H, *m*–Mes), 3.73 (s, 24H, *o*–CH_3), 3.56 (s, 12H, *p*–CH_3), 1.54 (s, 6H, *p*–CH_3), 0.84 (s, 12H, *o*–CH_3), –10.54 (s, 4H, *o*–Ph), –18.31 (s, 1H, *o*–Ph) ppm. μ_{eff} (Evans Method, $CDCl_3$ with $O(SiMe_3)_2$, 400.1 MHz, 20 ˚C) = 3.77(±0.02) μ_B (average of 5 independent measurements). FTIR ($CDCl_3$, KBr windows): (ν_{CN}) 2176 (vs) cm^{-1}, 2973, 2951, 2920, 2859, 1613, 1496, 1457, 1378, 1277, 1189 cm^{-1}. Anal. Calcd for $C_{75}H_{75}N_3I_5Cr$: C, 52.83; H, 4.43; N, 2.47. Found: C, 52.23; H, 4.49; N, 2.20.

Synthesis of *mer*–$MoI_2(I_3)(CNAr^{Mes2})_3$ (25). To a toluene solution of *fac*–$Mo(CO)_3(CNAr^{Mes2})_3$ (**5**, 3.917 g, 3.302 mmol, 1 equiv, 100 mL) was added a toluene solution of I_2 (2.137 g, 8.419 mmol, 2.55 equiv, 200 mL) and the resulting reaction mixture was heated to 80° C under Ar purge for 24 hrs. Concentration of the mixture to a volume of 100 mL, followed by the addition of *n*–pentane (200 mL), resulted in the precipitation of a magenta solid. The mixture was then stirred for 1 h, filtered and the solids were washed with 30 mL of *n*–pentane before being dried *in vacuo* and collected. Yield: 5.020 g, 2.870 mmol, 87%. X–ray diffraction quality crystals were grown from saturated Et_2O solution. ^{1}H NMR (400.1 MHz, $CDCl_3$, 20 ˚C): δ = 29.03 (d, 2H, *J* = 8 Hz, *m*–Ph), 25.65 (d, 4H, *J* = 8 Hz, *m*–Ph), 7.80 (s, 8H, *m*–Mes), 7.57 (s, 4H, *m*–Mes), 5.92 (s, 24H, *o*–CH_3), 4.46 (s, 12H, *p*–CH_3), 0.24 (s, 6H, *p*–CH_3), –0.29 (s, 12H, *o*–CH_3), –17.16 (s, 2H, *o*–Ph), –35.14 (s, 12H, *o*–Ph) ppm. μ_{eff} (Evans Method, $CDCl_3$ with $O(SiMe_3)_2$, 400.1 MHz, 20 ˚C) = 3.68 (±0.09) μ_B

(average of 3 independent measurements). FTIR ($CDCl_3$, KBr windows): (ν_{CN}) 2142 (vs) cm^{-1}, also 3027 (w), 2974 (w), 2949 (w), 2918 (m), 2859 (w), 1613 (w), 1376 (w), 1274 (w), 1030 (w), 849 (m), 605 (w) cm^{-1}. Anal. Calcd for $C_{75}H_{75}N_3I_5Mo$: C, 53.01; H, 4.32; N, 2.41. Found: C, 53.01; H, 4.33; N, 1.97.

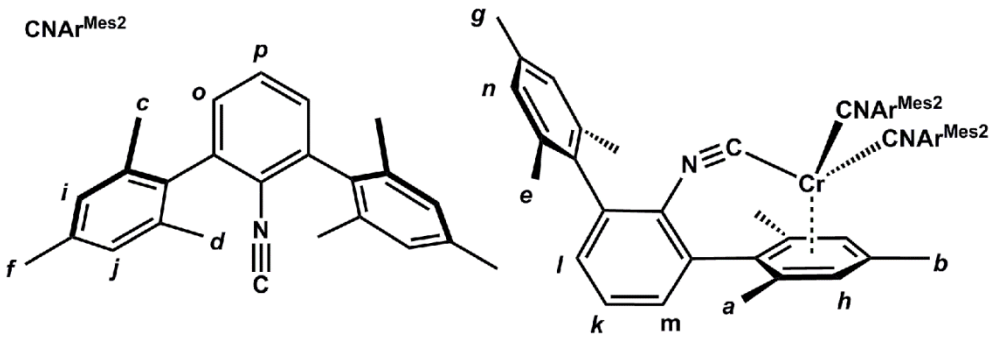

Figure 5.14. Labeling scheme for ^{1}H NMR assignments in Cr(κ^1–*C*–$CNAr^{Mes}$(η^6–Mes))($CNAr^{Mes2}$)$_2$ (**42**).

Synthesis of Cr(κ^1–*C*–$CNAr^{Mes}$(η^6–Mes))($CNAr^{Mes2}$)$_2$ (42). To a stirred mixture of excess Mg turnings (1.0 g, 41.14 mmol, 70 equiv) in THF (100 mL) was added a THF solution of *mer*–$CrI_2(I_3)(CNAr^{Mes2})_3$ (**41**, 1.000 g, 0.587 mmol, 300 mL). The resulting solution was heated at 52^{o}C for 8 h, after which all volatiles were removed *in* vacuo. The remaining solids were slurried in pentane (20 mL), filtered over a medium porosity frit and the resulting orange pentane solution was then evaporated under reduced pressure. The remaining orange solid was dissolved in fluorobenzene (3 mL), filtered, and stored at –35 ˚C for 1 d, whereupon orange crystals were obtained, collected and dried *in vacuo*. Yield: 0.840 g, 0.785 mmol, 67%. ^{1}H NMR (500.1 MHz, CD_3Cl, 20 ˚C): δ = 7.12 (t, 2H, J = 7 Hz, H_p), 7.02 (d, 4H, J = 7 Hz, H_o), 6.99 (s, 2H, H_n), 6.99 (d, 1H, J = 7 Hz, H_m), 6.91 (d, 1H, J = 7 Hz, H_l), 6.88 (t, 1H, J = 7 Hz, H_k), 6.84 (s, 4H, H_j), 6.79 (s, 4H, H_i), 3.81 (s, 2H, H_h), 2.40 (s, 3H, H_g), 2.18 (s, 12H, H_f) 2.09 (s, 6H, H_e), 1.97 (s, 12H, H_d), 1.90 (s, 12H, H_c), 1.33 (s, 3H, H_b),

1.20 (s, 6H, H_a) ppm. $^{13}C\{^1H\}$ NMR (100.6 MHz, CD_3Cl, 20 °C): δ = 295.7, (*C*≡N), 208.5 (*C*≡N), 166.8, 137.8, 137.2, 137.0, 136.7, 136.2, 136.0, 135.8, 135.7, 135.6, 129.4, 129.2, 128.7, 128.5, 128.3, 127.8, 125.4, 124.7, 121.5, 110.8, 93.1, 89.5, 34.3, 22.5, 21.3, 21.3, 21.2, 20.7, 20.3, 19.1, 18.7 ppm. FTIR ($CDCl_3$, KBr windows): (ν_{CN}) 2036 (s), 2004 (s), 1946 (vs), 1647 (s) cm^{-1}, also 2972, 2950, 2917, 2859, 1630, 1565, 1494, 1377, 1221, 1199, 1155, 850, 805 cm^{-1}. Anal. Calcd for $C_{75}H_{75}N_3Cr$: C, 84.15; H, 7.06; N, 33.93. Found: C, 83.53; H, 7.13; N, 3.80.

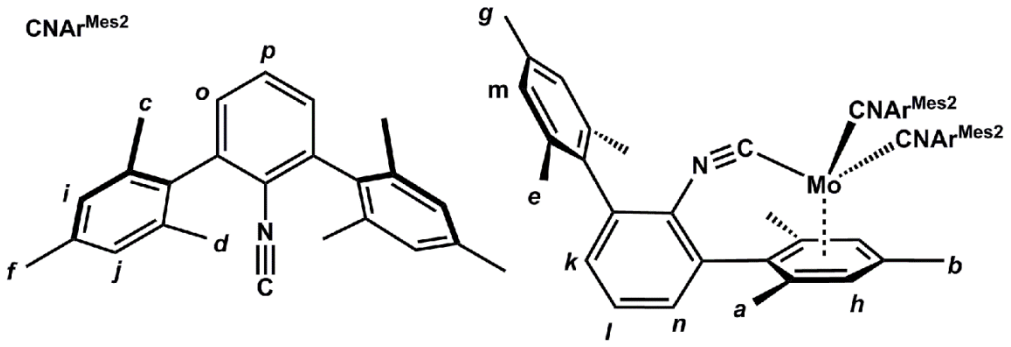

Figure 5.15. Labeling scheme for ^1H NMR assignments in Mo(κ^1–*C*–$CNAr^{Mes}$(η^6–Mes))($CNAr^{Mes2}$)$_2$ (**24**).

Synthesis of Mo(κ^1–*C*–$CNAr^{Mes}$(η^6–Mes))($CNAr^{Mes2}$)$_2$ (24). To a stirred mixture of sodium amalgam (Na/Hg) (Na: 0.617 g, 26.9 mmol; Hg: 124.0 g; 0.5% w/w; 10 equiv Na/Mo) in THF (100 mL) was added a THF solution of *mer*–$MoI_2(I_3)(CNAr^{Mes2})_3$ (**25**, 4.700 g, 2.69 mmol, 300 mL). The resulting solution was allowed to stir for 20 min and gradually changed in color from magenta to orange. The solution was then decanted from the residual amalgam and all volatile materials were removed under reduced pressure. The resulting orange residue was then slurried in toluene (300 mL) and filtered through Celite. The filtrate was concentrated to a volume of 100 mL, layered with *n*–pentane (100 mL) and stored at –35 ˚C for 1 d, whereupon orange crystals were obtained, collected and dried *in vacuo*. Yield:

2.01 g, 1.803 mmol, 67%. ^{1}H NMR (500.1 MHz, CD_2Cl_2, 20 ˚C): δ = 7.17 (t, 2H, J = 7 Hz, H_p), 7.01 (d, 4H, J = 7 Hz, H_o), 7.00 (d, 1H, J = 7 Hz, H_n), 7.94 (s, 2H, H_m), 6.91 (t, 1H, J = 7 Hz, H_l), 6.87 (d, 1H, J = 7 Hz, H_k), 6.81 (s, 4H, H_j), 6.76 (s, 4H, H_i), 3.99 (s, 2H, H_h), 2.36 (s, 3H, H_g), 2.17 (s, 12H, H_f) 1.99 (s, 6H, H_e), 1.95 (s, 12H, H_d), 1.87 (s, 12H, H_c), 1.30 (s, 3H, H_b), 1.29 (s, 6H, H_a) ppm. ^{13}C{^{1}H} NMR (100.6 MHz, CD_2Cl_2, 20 °C): δ = 278.3, (*C*≡N), 196.6 (*C*≡N), 153.4, 138.3, 137.1, 136.8, 136.4, 136.2, 136.1, 136.0, 135.7, 134.3, 129.9, 129.8, 129.7, 128.8, 128.6, 128.2, 127.9, 125.0, 121.7, 108.3, 101.0, 91.3, 89.1, 21.2, 21.2, 20.8, 20.4, 19.3, 19.2 ppm. FTIR ($CDCl_3$, KBr windows): (ν_{CN}) 2034 (s), 2004 (s), 1945 (vs), 1645 (s) cm^{-1}, also 2970, 2950, 2918, 2856, 1564, 1488, 1415, 1403, 1378, 1199, 1071, 1032, 852, 755 cm^{-1}. Anal. Calcd for $C_{75}H_{75}N_3Mo$: C, 80.83; H, 6.78; N, 3.77. Found: C, 82.02; H, 7.11; N, 3.28.

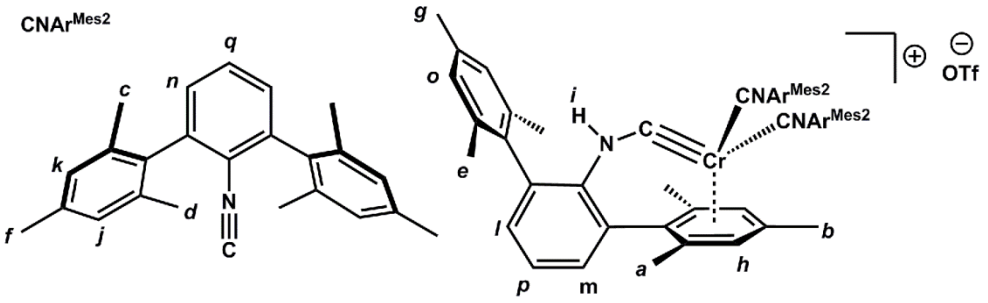

Figure 5.16. Labeling scheme for ^{1}H NMR assignments in [Cr(κ^1–*C*–CN(H)Ar^{Mes}(η^6–Mes))(CNAr^{Mes2})$_2$]OTf (**43**).

Synthesis of [Cr(κ^1–*C*–CN(H)Ar^{Mes}(η^6–Mes))(CNAr^{Mes2})$_2$]OTf (43). To a thawing Et_2O solution of Cr(κ^1–*C*–CNAr^{Mes}(η^6–Mes))(CNAr^{Mes2})$_2$ (**42**, 0.100 g, 0.093 mmol, 1.0 equiv, 15 mL) was added a thawing Et_2O solution of HOTf (0.015 g, 0.098 mmol, 1.05 equiv, 20 mL) dropwise over 2 mins. The reaction mixture was allowed to stir for 3 h, after which it was cooled to –78ºC and filtered, washed with pentane (10 mL) and dried *in vacuo* to afford [Cr(κ^1–*C*–CN(H)Ar^{Mes}(η^6–Mes))(CNAr^{Mes2})$_2$]OTf as a bright red powder. Yield: 0.070 g,

0.057 mmol, 62%. X–ray diffraction quality crystals were grown from saturated THF solution. ^{1}H NMR (500.1 MHz, CD_3Cl, 20 ˚C): δ = 7.40 (t, 2H, J = 8 Hz, H_q), 7.20 (t, 2H, J = 7 Hz, H_p), 7.14 (s, 2H, H_o) 7.12 (d, 4H, J = 8 Hz, H_n), 7.02 (d, 1H, J= 7Hz, H_m), 7.03 (d, 1H, J = 7 Hz, H_l), 6.92 (s, 4H, H_k), 6.80 (s, 4H, H_j), 6.77 (s, 1H, H_i), 4.61 (s, 2H, H_h), 2.44 (s, 3H, H_g), 2.18 (s, 12H, H_f) 2.02 (s, 6H, H_e), 1.96 (s, 12H, H_d), 1.89 (s, 12H, H_c), 1.53 (s, 6H, H_b), 1.20 (s, 3H, H_a) ppm. ^{13}C{^{1}H} NMR (100.6 MHz, $CDCl_3$, 20 ˚C): δ = 292.6 (M≡*C*NH), 189.3 (*C*≡N), 142.1, 139.3, 137.3, 137.0, 136.5, 136.0, 136.0, 134.5, 131.70, 131.6, 129.9, 129.5, 129.1, 128.7, 128.6, 128.5, 128.3, 126.4, 125.2, 119.2, 114.8, 113.4, 102.7, 100.1, 21.3, 21.0, 20.8, 20.6, 20.2, 19.5, 18.6 ppm. FTIR ($CDCl_3$, KBr windows): (ν_{NH}) 3323 (m) cm^{-1}, (ν_{CN}) 2109 (vs), 2068 (vs) and 2011 (w sh) cm^{-1}, ($\nu_{C–NH}$) 1493 (s) cm $^{-1}$, also 2977, 2950, 2921, 2858, 1596, 1416, 1379, 1267, 1223, 1156, 1031, 855, 805, 519 cm^{-1}. Anal. Calcd for $C_{76}H_{76}F_3N_3O_3SCr$: C, 74.79; H, 6.28; N, 3.44. Found: C, 64.40; H, 5.83; N, 2.82.

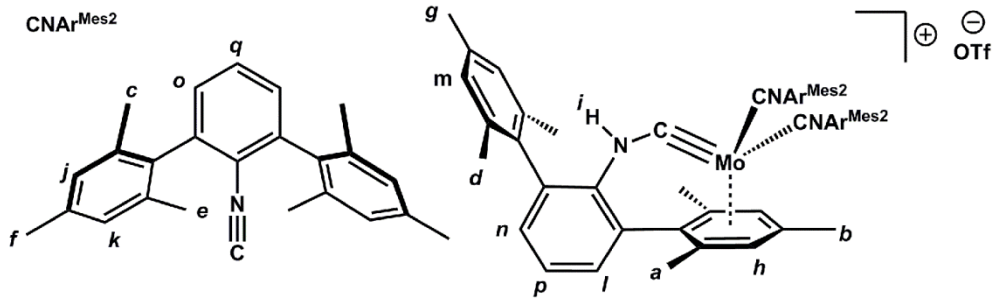

Figure 5.17. Labeling scheme for ^{1}H NMR assignments in[Mo(κ^1–*C*–CN(H)Ar^{Mes}(η^6–Mes))(CNAr^{Mes2})$_2$]OTf (**44**).

Synthesis of [Mo(κ^1–*C*–CN(H)Ar^{Mes}(η^6–Mes))(CNAr^{Mes2})$_2$]OTf (44). To a thawing Et_2O solution of Mo(κ^1–*C*–CNAr^{Mes}(η^6–Mes))(CNAr^{Mes2})$_2$ (**24**, 0.300 g, 0.269 mmol, 200 mL) was added a thawing Et_2O solution of HOTf (0.043 g, 0.282 mmol, 1.05 equiv, 20 mL) dropwise over 5 mins. The reaction mixture was allowed to stir for 20 min, resulting in the formation of an orange precipitate. This precipitate was collected by filtration, washed

with Et_2O (20 mL) and dried *in vacuo* to afford [Mo(κ^1–*C*–CN(H)Ar^{Mes}(η^6–Mes))($CNAr^{Mes2}$)$_2$]OTf (**44**) as an orange powder. Yield: 0.210 g, 0.086 mmol, 53%. X–ray diffraction quality crystals were grown from saturated DME solution. ^{1}H NMR (500.1 MHz, CD_3Cl, 20 ˚C): δ = 7.42 (t, 2H, J = 8 Hz, H_q), 7.20 (t, 1H, J = 7 Hz, H_p), 7.16 (d, 4H, J = 8 Hz, H_o) 7.15 (d, 1H, J = 7 Hz, H_n), 7.11 (s, 2H, H_m), 7.03 (d, 1H, J = 7 Hz, H_l), 6.90 (s, 4H, H_k), 6.76 (s, 4H, H_j), 6.74 (s, 1H, H_i), 5.04 (s, 2H, H_h), 2.42 (s, 3H, H_g), 2.17 (s, 12H, H_f) 1.97 (s, 12H, H_e), 1.97 (s, 6H, H_d), 1.88 (s, 12H, H_c), 1.65 (s, 6H, H_b), 1.35 (s, 3H, H_a) ppm. ^{13}C{^{1}H} NMR (100.6 MHz, $CDCl_3$, 20 ˚C): δ = 280.7 (M≡*C*NH), 179.5 (*C*≡N), 139.7, 139.2, 137.2, 136.8, 136.6, 136.0, 136.0, 134.3, 131.8, 131.3, 129.8, 129.8, 129.7, 129.4, 128.6, 128.5, 128.5, 128.2, 126.6, 124.8, 118.9, 116.6, 112.8, 100.9, 100.7, 21.3, 21.1, 20.6, 20.5, 20.1, 19.7, 18.9 ppm. FTIR ($CDCl_3$, KBr windows): (ν_{NH}) 3323 (m) cm^{-1}, (ν_{CN}) 2110 (vs), 2060 (vs) and 2011 (m sh) cm^{-1}, ($\nu_{C–NH}$) 1416 (s) cm $^{-1}$, also 2977, 2951, 2920, 2859, 1379, 1267, 1225, 1203, 1101, 1031, 854, 802, 634 cm^{-1}. Anal. Calcd for $C_{76}H_{76}F_3N_3O_3SMo$: C, 72.19; H, 6.06; N, 3.32. Found: C, 75.81; H, 6.26; N, 3.13.

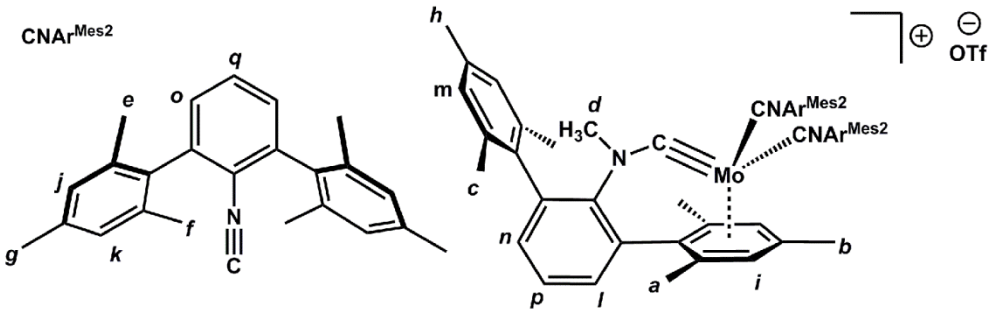

Figure 5.18. Labeling scheme for ^{1}H NMR assignments in[Mo(κ^1–*C*–CN(CH_3)Ar^{Mes}(η^6–Mes))($CNAr^{Mes2}$)$_2$]OTf (**45**).

Synthesis of [Mo(κ^1–*C*–CN(CH_3)Ar^{Mes}(η^6–Mes))($CNAr^{Mes2}$)$_2$]OTf (45). To a THF solution of Mo(κ^1–*C*–$CNAr^{Mes}$(η^6–Mes))($CNAr^{Mes2}$)$_2$ (**24**, 0.200 g, 0.180 mmol, 1.00 equiv, 10 mL) was added a THF solution of methyl trifluoromethanesulfonate (0.147 g, 0.897 mmol,

5.00 equiv, 10 mL). The reaction mixture was allowed to stir for 1 day, after which all volatiles were removed *in vacuo*. The remaining orange solid was dissolved in THF (5 mL), filtered, layered with *n*–pentane (10 mL) and stored at –35 °C for 1 d, whereupon orange crystals of [Mo(κ^1–*C*–CN(CH$_3$)Ar^{Mes}(η^6–Mes))(CNAr^{Mes2})$_2$]OTf were obtained. Yield: 0.100 g, 0.078 mmol, 43%. X–ray diffraction quality crystals were grown from saturated toluene solution. ^{1}H NMR (500.1 MHz, CD_3Cl, 20 ˚C): δ = 7.42 (t, 2H, J = 8 Hz, H_q), 7.18 (t, 1H, J = 8 Hz, H_p), 7.15 (d, 4H, J = 8 Hz, H_o) 7.07 (d, 1H, J = 7 Hz, H_n), 7.00 (s, 2H, H_m), 6.99 (d, 1H, J = 8 Hz, H_l), 6.92 (s, 4H, H_k), 6.83 (s, 4H, H_j), 5.13 (s, 2H, H_i), 2.41 (s, 3H, H_h), 2.23 (s, 12H, H_g), 2.01 (s, 12H, H_f) 1.92 (s, 12H, H_e), 1.89 (s, 3H, H_d), 1.87 (s, 6H, H_c), 1.59 (s, 6H, H_b), 1.43 (s, 3H, H_a) ppm. ^{13}C{^{1}H} NMR (100.6 MHz, $CDCl_3$, 20 ˚C): δ = 282.7 (M≡*C*NMe), 178.8 (*C*≡N), 142.6, 138.2, 137.3, 137.0, 136.1, 036.0, 135.9, 135.8, 134.4, 133.9, 131.6, 130.0, 129.9, 128.5, 128.4, 128.4, 126.4, 125.4, 122.0, 114.3, 112.3, 102.0, 99.5, 37.0, 21.2, 21.1, 20.7, 20.5, 20.2, 20.1, 18.7 ppm. FTIR ($CDCl_3$, KBr windows): (ν_{CN}) 2107 (vs), 2057 (vs) and 2015 (m sh) cm^{-1}, ($\nu_{C–NCH3}$) 1483 (m) cm $^{-1}$, also 2950, 2922, 2860, 1611, 1453, 1414, 1393, 1379, 1265, 1225, 1159, 1124, 1032, 566 cm^{-1}. Anal. Calcd for $C_{77}H_{79}F_3N_3O_3SMo$: C, 72.28; H, 6.22; N, 3.29. Found: C, 69.56; H, 5.89; N, 3.00.

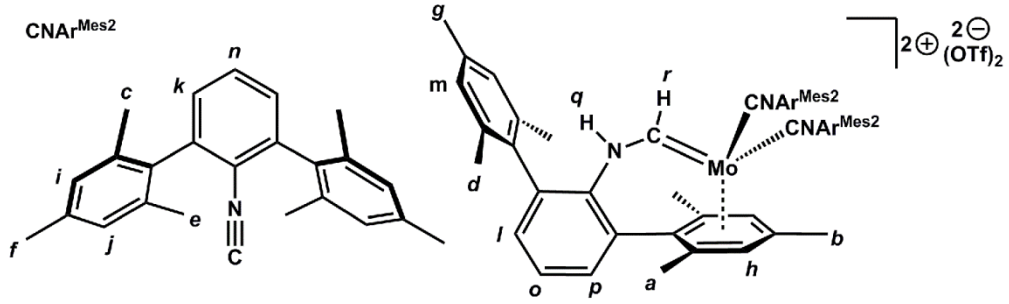

Figure 5.19. Labeling scheme for ^{1}HNMR assignments in [Mo(THF)(κ^1–*C*–C(H)N(H)Ar^{Mes}(η^6–Mes))(CNAr^{Mes2})$_2$](OTf)$_2$ (**46**).

Synthesis of [Mo(THF)(κ^1–*C*–C(H)N(H)Ar^{Mes}(η^6–Mes))(CNAr^{Mes2})$_2$](OTf)$_2$ (46). To a thawing toulene/THF solution (2:1, *ca*. 15 mL total) of [Mo(κ^1–*C*–CN(H)Ar^{Mes}(η^6–Mes))(CNAr^{Mes2})$_2$]OTf (**44**, 0.100 g, 0.079 mmol, 1.00 equiv) was added a thawing toluene solution of HOTf (0.011 g, 0.071 mmol, 0.9 equiv, 5 mL) dropwise over 3 min. The reaction mixture was allowed to stir for 20 min, resulting in the formation of a brown precipitate. This precipitate was collected by filtration, washed with THF (10 mL) and dried *in vacuo* to afford [Mo(THF)(κ^1–*C*–C(H)N(H)Ar^{Mes}(η^6–Mes))(CNAr^{Mes2})$_2$](OTf)$_2$ as a brown powder. Yield: 0.070 g, 0.049 mmol, 62%. X–ray diffraction quality crystals were grown from saturated CH_2Cl_2 solution. ^{1}H NMR (500.1 MHz, CD_3Cl, 20 ˚C): δ = 10.38(d, 1H, J=12 Hz, H_r), 8.83 (d, 1H, J = 13 Hz, H_q), 7.70 (d, 1H, J = 8 Hz, H_p), 7.50 (t, 1H, J = 8 Hz, H_o) 7.45 (t, 2H, J = 8 Hz, H_n), 7.18 (s, 2H, H_m), 7.16 (d, 1H, J = 7 Hz, H_l), 7.01 (d, 4H, J = 8 Hz, H_k), 6.75 (s, 4H, H_j), 6.70 (s, 4H, H_i), 4.84 (s, 2H, H_h), 2.47 (s, 3H, H_g), 2.22 (s, 12H, H_f) 1.95 (s, 12H, H_e), 1.89 (s, 6H, H_d), 1.87 (s, 12H, H_c), 1.61 (s, 3H, H_b), 1.47 (s, 6H, H_a) ppm. ^{13}C{^{1}H} NMR (100.6 MHz, $CDCl_3$, 20 ˚C): δ = 260.6 (M≡*C*NH), 179.1 (*C*≡N), 140.0, 139.1, 138.3, 136.9, 136.8, 136.7, 135.0, 134.9, 133.4, 133.0, 132.2, 131.0, 130.8, 130.7, 130.2, 129.3, 128.9, 128.5, 128.4, 126.7, 119.9, 109.1, 105.1, 104.6, 21.4, 21.0, 21.0, 20.9, 20.3, 20.0, 19.6 ppm. FTIR ($CDCl_3$, KBr windows): (ν_{NH}) 3267 (m) cm^{-1}, (ν_{CN}) 2101 (m) and 2061 (vs) cm^{-1}, (ν_{CNH}) 1507 (m) cm $^{-1}$, also 2976, 2954, 2924, 1610, 1457, 1382, 1328, 1267, 1230, 1201, 1161, 1033, 1008, 858, 808, 517 cm^{-1}. Anal. Calcd for $C_{77}H_{77}F_6N_3O_6S_2Mo$: C, 65.38; H, 5.46; N, 2.97. Found: C, 59.57; H, 65.05; N, 2.57.

Synthesis of a mixture of [Mo(OTf)(η^6–(Mes)–κ^1–*C*–C(H)N(CH$_3$)Ar^{Mes})(CNAr^{Mes2})$_2$](OTf) (47), and [Mo(η^6–(Mes)–η^3–(CH$_2$CHN)–Ar^{Mes})(CNAr^{Mes2})$_2$](OTf)$_2$ (48). To a thawing toulene/THF solution (1:1, *ca*. 10 mL total) of [Mo(κ^1–*C*–CN(CH$_3$)Ar^{Mes}(η^6–Mes))(CNAr^{Mes2})$_2$]OTf (**44**, 0.200 g, 0.162 mmol, 1.00 equiv)

was added a thawing toluene solution of HOTf (0.026 g, 0.164 mmol, 1.0 equiv, 5 mL) dropwise over 10 min. The reaction mixture was allowed to stir for 1 h, after which, all volatiles were remove under reduced pressure. The resulting orange semi–solid was dissolved in 3 mL of THF, filtered, layered with 3 mL of *n*–pentane, and stored at –35 °C for 4 d, whereupon orange and red crystals of [Mo(OTf)(η^6–(Mes)–κ^1–*C*–C(H)N(CH_3)Ar^{Mes})($CNAr^{Mes2}$)$_2$](OTf) (**47**), and [Mo(η^6–(Mes)–η^3–(CH_2CHN)–Ar^{Mes})($CNAr^{Mes2}$)$_2$](OTf)$_2$ (**48**), respectively, were obtained. Samples for X–ray analysis were obtained by manually separating orange and red crystals from the bulk sample on a microscope slide.

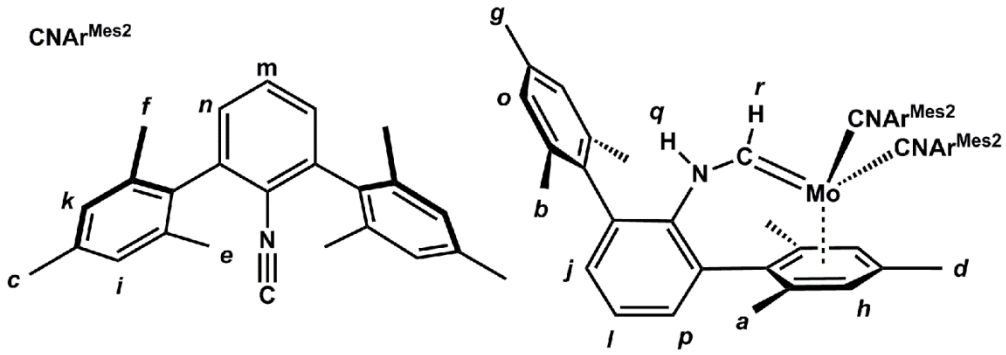

Figure 5.20. Labeling scheme for ^{1}HNMR assignments in Mo(κ^1–*C*–C(H)N(H)Ar^{Mes}(η^6–Mes))($CNAr^{Mes2}$)$_2$ (**49**).

Synthesis of Mo(κ^1–*C*–C(H)N(H)Ar^{Mes}(η^6–Mes))($CNAr^{Mes2}$)$_2$ (49). To a THF slurry of [Mo(THF)(κ^1–*C*–C(H)N(H)Ar^{Mes}(η^6–Mes))($CNAr^{Mes2}$)$_2$](OTf)$_2$ (**46**, 0.200 g, 0.141 mmol, 1 equiv, 15 mL) was added freshly I_2 activated magnesium turnings (0.086 g, 3.53 mmol, 25 equiv). The reaction mixture was allowed to stir for 10 h during which the turbid mixture became translucent and red–brown in color. The resulting solution was decanted away from the residual magnesium turnings and then dried under reduced pressure. The residue was slurried in pentane (15 mL), stirred for 20 min, filtered through celite, and then dried *in vacuo*. The resulting brown solid was dissolved in pentane (10 mL), filtered and

stored at –35 °C for 1 d, whereupon brown crystals of Mo(κ^1–*C*–C(H)N(H)Ar^{Mes}(η^6–Mes))(CNAr^{Mes2})$_2$ were obtained. Yield: 0.070 g, 0.062 mmol, 44%. ^{1}H NMR (500.1 MHz, C_6D_6, 20 ˚C): δ = 9.70(d, 1H, J = 10 Hz, H_r), 8.86 (d, 1H, J = 9 Hz, H_q), 7.01 (d, 1H, J = 8 Hz, H_p), 6.98 (s, 2H, H_o) 6.95 (d, 4H, J = 8 Hz, H_n), 6.93 (t, 2H, J = 8 Hz, H_m), 6.90 (t, 1H, J = 7 Hz, H_l), 6.89 (s, 4H, H_k), 6.84 (d, 1H, J = 8 Hz, H_j), 6.76 (s, 4H, H_i), 4.01 (s, 2H, H_h), 2.30 (s, 3H, H_g), 2.23 (s, 12H, H_f) 2.19 (s, 12H, H_e), 2.16 (s, 3H, H_d), 2.04 (s, 12H, H_c), 2.00 (s, 6H, H_b), 1.26 (s, 6H, H_a) ppm. ^{13}C{^{1}H} NMR (100.6 MHz, C_6D_6, 20 ˚C): δ = 261.7 (M≡*C*NH), 210.0 (*C*≡N), 138.6, 137.8, 137.3, 137.2, 137.1, 136.5, 136.4, 135.7, 134.7, 131.7, 131.4, 130.8, 129.5, 129.3, 128.4, 128.4, 128.4, 128.3, 123.5, 122.0, 121.5, 101.2, 94.5, 93.9, 30.3, 21.2, 21.2, 20.9, 20.8, 20.5, 19.3 ppm. FTIR (C_6D_6, KBr windows): (ν_{NH}) 3345 (m) cm^{-1}, (ν_{CN}) 1967 (s) and 1874 (s) cm^{-1}, (ν_{CNH}) 1576 (m) cm^{-1}, also 2975, 2919, 2857, 1611, 1497, 1414, 1376, 1262, 1228, 1152, 1071, 908, 852, 752, 624 cm^{-1}. Solid–state samples of Synthesis of Mo(κ^1–*C*–C(H)N(H)Ar^{Mes}(η^6–Mes))(CNAr^{Mes2})$_2$ (**49**) exhibit limited thermal stability at room temperature, which precluded the acquisition of a satisfactory combustion analysis.

5.8 Crystallographic Structure Determinations.

General Considerations. Single crystal X–ray structure determinations were carried out at low temperature on a Bruker Platform or Kappa Diffractometers equipped with a Bruker APEX, APEX II, and Photon 100 area detectors. All structures were solved via direct methods with SIR 2004[137] and refined by full–matrix least–squares procedures utilizing SHELXL–2013.[138] Crystallographic data collection and refinement information are listed in Tables 5.3 to 5.6.

Table 5.3. Crystallographic Data Collection and Refinement Information for *Mer*–$Cr(CO)_3(CNAr^{Mes2})_3{\cdot}2CH_2Cl_2$, *mer*–$CoI_2(I_3)(CNAr^{Mes2})_3{\cdot}C_7H_8$, and $Cr(\eta^6\text{–(Mes)–}\kappa^1\text{–}C\text{–}CNAr^{Mes})(CNAr^{Mes2})_2$

	Mer–$Cr(CO)_3(CNAr^{Mes2})_3{\cdot}2CH_2Cl_2$ (**40**$\cdot 2CH_2Cl_2$)	*mer*–$CoI_2(I_3)(CNAr^{Mes2})_3{\cdot}C_7H_8$ (**41**$\cdot C_7H_8$)	$Cr(\eta^6\text{–(Mes)–}\kappa^1\text{–}C\text{–}CNAr^{Mes})(CNAr^{Mes2})_2$ (**42**)
Formula	$CrC_{80}H_{79}Cl_{14}N_3O_3$	$CrC_{82}H_{83}N_3I_5$	$CrC_{75}H_{75}N_3$
Crystal System	Triclinic	Triclinic	Triclinic
Space Group	*P*–1	*P*–1	*P*–1
a, Å	14.892(4)	14.8121(6)	11.599(2)
b, Å	16.146(4)	14.8164(7)	15.534(3)
c, Å	16.483(4)	19.1845(7)	18.746(4)
α, deg	74.831(3)	70.4190(10)	66.797(2)
β, deg	71.803(3)	82.8760(10)	72.917(3)
γ, deg	72.644(3)	74.6010(10)	74.551(2)
V, $Å^3$	3531.1(14)	3821.5(3)	2923.5(10)
Z	2	2	2
Radiation (λ, Å)	Mo–Kα, 0.71073	Mo–Kα, 0.71073	Mo–Kα, 0.71073
ρ (calcd.), g/cm^3	1.246	1.562	1.216
μ, mm^{-1}	0.363	2.213	0.243
Temp, K	100(2)	100(2)	100(2)
θ max, deg	25.52	25.45	25.49
data/parameters	12986 / 0 / 838	13934/0/839	10583/0/730
R_1	0.0887	0.0545	0.0528
wR_2	0.1049	0.1130	0.0720
GOF	1.072	0.999	1.042

Table 5.4. Crystallographic Data Collection and Refinement Information for [Cr(η^6–(Mes)–κ^1–*C*–CN(H)Ar^{Mes})(CNAr^{Mes2})$_2$](OTf)·THF, [Mo(η^6–(Mes)–κ^1–*C*–CN(H)Ar^{Mes})(CNAr^{Mes2})$_2$](OTf)·DME, and [Mo(η^6–(Mes)–κ^1–*C*–CN(CH$_3$)Ar^{Mes})(CNAr^{Mes2})$_2$](OTf)·2C$_7$H$_8$

	[Cr(η^6–(Mes)–κ^1–*C*–CN(H)Ar^{Mes})(CNAr^{Mes2})$_2$](OTf)·THF ((**43**)·THF)	[Mo(η^6–(Mes)–κ^1–*C*–CN(H)Ar^{Mes})(CNAr^{Mes2})$_2$](OTf)·DME ((**44**)·DME)	[Mo(η^6–(Mes)–κ^1–*C*–CN(CH$_3$)Ar^{Mes})(CNAr^{Mes2})$_2$](OTf)·2C$_7$H$_8$ ((**45**)·2C$_7$H$_8$)
Formula	$CrC_{80}H_{84}N_3O_4F_3S$	$MoC_{84}H_{96}N_3O_7F_3S$	$MoC_{91}H_{94}N_3O_3F_3S$
Crystal System	Monoclinic	Monoclinic	Monoclinic
Space Group	$P2_1/n$	$P2_1/n$	$P2_1/c$
a, Å	14.0275(16)	15.167(6)	17.3440(8)
b, Å	29.935(3)	32.6715(14)	15.3450(7)
c, Å	16.2126(18)	16.6486(7)	29.9680(14)
α, deg	90	90	90
β, deg	90.110(6)	109.8640(10)	97.7840(10)
γ, deg	90	90	90
V, Å^3	6807.9(13)	7682.1(6)	7902.3(6)
Z	4	4	4
Radiation (λ, Å)	Mo–Kα, 0.71073	Cu–Kα, 1.54178	Mo–K$_\alpha$, 0.71073
ρ (calcd.), g/cm^3	1.261	1.249	1.229
μ, mm^{-1}	0.260	0.260	0.250
Temp, K	100(2)	100(2)	100(2)
θ max, deg	28.46	25.39	25.47
data/parameters	17049/0/807	14036/0/918	14585/0/940
R_1	0.0951	0.0423	0.0804
wR_2	0.1168	0.0533	0.1130
GOF	1.029	1.023	1.019

Table 5.5. Crystallographic Data Collection and Refinement Information for [Mo(THF)(η^6–(Mes)–κ^1–*C*–C(H)N(H)Ar^{Mes})(CNAr^{Mes2})$_2$](OTf)$_2$, [Mo(OTf)(η^6–(Mes)–κ^1–*C*–C(H)N(CH$_3$)Ar^{Mes})(CNAr^{Mes2})$_2$](OTf), and [Mo(η^6–(Mes)–η^3–(CH$_2$CHN)–Ar^{Mes})(CNAr^{Mes2})$_2$](OTf)$_2$

	[Mo(THF)(η^6–(Mes)–κ^1–*C*–C(H)N(H)Ar^{Mes})(CNAr^{Mes2})$_2$](OTf)$_2$ (**46**)	[Mo(OTf)(η^6–(Mes)–κ^1–*C*–C(H)N(CH$_3$)Ar^{Mes})(CNAr^{Mes2})$_2$](OTf) (**47**)	[Mo(η^6–(Mes)–η^3–(CH$_2$CHN)–Ar^{Mes})(CNAr^{Mes2})$_2$](OTf)$_2$ (**48**)
Formula	$MoC_{81}H_{85}N_3O_7F_6S_2$	$MoC_{78}H_{79}N_3O_6F_6S_2$	$MoC_{98}H_{118}F_6N_3O_{11}S_2$
Crystal System	Triclinic	Triclinic	Monoclinic
Space Group	*P*–1	*P*–1	$P2_1/n$
a, Å	14.6764(15)	19.405(2)	18.3428(12)
b, Å	16.4987(16)	20.466(3)	15.0960(10)
c, Å	18.9786(17)	24.036(3)	32.525(2)
α, deg	64.894(6)	92.216(7)	90
β, deg	73.988(7)	96.899(5)	94.127(4)
γ, deg	80.254(7)	110.449(5)	90
V, Å^3	3992.7(7)	8762.8(19)	8988.5(10)
Z	2	4	4
Radiation (λ, Å)	Cu–K$_\alpha$, 1.54178	Cu–K$_\alpha$, 1.54178	Mo–K$_\alpha$, 0.71073
ρ (calcd.), g/cm^3	1.237	1.083	1.321
μ, mm^{-1}	2.380	0.254	0.267
Temp, K	100(2)	100(2)	100(2)
θ max, deg	68.71	18.85	25.76
data/parameters	13397 / 4 / 927	13510 / 20 / 1820	16625 / 0 / 1048
R_1	0.1117	0.1362	.0986
wR_2	0.1339	0.1678	0.1395
GOF	1.328	1.026	1.051

Table 5.6. Crystallographic Data Collection and Refinement Information for Mo(η^6–(Mes)–κ^1–*C*–C(H)N(H)Ar^{Mes})(CNAr^{Mes2})$_2$

	Mo(η^6–(Mes)–κ^1–*C*–C(H)N(H)Ar^{Mes})(CNAr^{Mes2})$_2$ (**49**)
Formula	$MoC_{75}H_{75}N_3$
Crystal System	Triclinic
Space Group	*P*–1
a, Å	11.6434(3)
b, Å	15.6398(4)
c, Å	19.0465(5)
α, deg	66.1380(10)
β, deg	72.2500(10)
γ, deg	73.4500(10)
V, Å^3	2968.51(13)
Z	2
Radiation (λ, Å)	Cu–K$_\alpha$, 1.54178
ρ (calcd.), g/cm^3	1.249
μ, mm^{-1}	0.267
Temp, K	100(2)
θ max, deg	25.30
data/parameters	10090 / 0 738
R_1	0.0312
wR_2	0.0379
GOF	1.024

5.9 Acknowledgements

Chapter 5 is currently being prepared for publication by Ditri, T. B.; Ripatti, D. S.; Moore, C. E.; Rheingold, A. L.; Figueroa, J. S. The dissertation aurthor is the primary author of this paper.

5.10 References

(1) Li, X. W.; Pennington, W. T.; Robinson, G. H. *J. Am. Chem. Soc.* **1995**, *117*, 7578–7579.

(2) Phillips, A. D.; Wright, R. J.; Olmstead, M. M.; Power, P. P. *J. Am. Chem. Soc.* **2002**, *124*, 5930–5931.

(3) Power, P. P. *Chem. Commun.* **2003**, 2091.

(4) Shah, S.; Simpson, M. C.; Smith, R. C.; Protasiewicz, J. D. *J. Am. Chem. Soc.* **2001**, *123*, 6925.

(5) Waterman, R.; Hillhouse, G. L. *Organometallics* **2003**, *22*, 5182.

(6) Carson, E. C.; Lippard, S. J. *Inorg. Chem.* **2006**, *45*, 828–836.

(7) Gavenonis, J.; Tilley, T. D. *Organometallics* **2004**, *23*, 31–43.

(8) Klein, D. P.; Young, V. G.; Tolman, W. B.; Que, L. *Inorg. Chem.* **2006**, *45*, 8006.

(9) Wolf, R.; Brynda, M.; Ni, C.; Long, G. J.; Power, P. P. *J. Am. Chem. Soc.* **2007**, *129*, 6076–6077.

(10) Bryan, A. M.; Merrill, W. A.; Reiff, W. M.; Fettinger, J. C.; Power, P. P. *Inorg. Chem.* **2012**, *51*, 3366–3373.

(11) Ellison, J. J.; Ruhlandt–Senge, K.; Power, P. P. *Angew. Chem., Int. Ed. Engl.* **1994**, *33*, 1178–1180.

(12) Rekken, B. D.; Brown, T. M.; Fettinger, J. C.; Lips, F.; Tuononen, H. M.; Herber, R. H.; Power, P. P. *J. Am. Chem. Soc.* **2013**, *135*, 10134–10148.

(13) Rekken, B. D.; Brown, T. M.; Olmstead, M. M.; Fettinger, J. C.; Power, P. P. *Inorg. Chem.* **2013**, *52*, 3054–3062.

(14) S. Buyuktas, B.; P. Power, P. *Chem. Commun.* **1998**, 1689–1690.

(15) Alexander Merrill, W.; Stich, T. A.; Brynda, M.; Yeagle, G. J.; Fettinger, J. C.; Hont, R. D.; Reiff, W. M.; Schulz, C. E.; Britt, R. D.; Power, P. P. *J. Am. Chem. Soc.* **2009**, *131*, 12693–12702.

(16) Boynton, J. N.; Guo, J.–D.; Fettinger, J. C.; Melton, C. E.; Nagase, S.; Power, P. P. *J. Am. Chem. Soc.* **2013**, *135*, 10720–10728.

(17) Boynton, J. N.; Merrill, W. A.; Reiff, W. M.; Fettinger, J. C.; Power, P. P. *Inorg. Chem.* **2012**, *51*, 3212–3219.

(18) Li, J.; Song, H.; Cui, C.; Cheng, J.–P. *Inorg. Chem.* **2008**, *47*, 3468–3470.

(19) Merrill, W. A.; Steiner, J.; Betzer, A.; Nowik, I.; Herber, R.; Power, P. P. *Dalton Trans.* **2008**, 5905–5910.

(20) Merrill, W. A.; Wright, R. J.; Stanciu, C. S.; Olmstead, M. M.; Fettinger, J. C.; Power, P. P. *Inorg. Chem.* **2010**, *49*, 7097–7105.

(21) Ni, C.; Fettinger, J. C.; Long, G. J.; Power, P. P. *Inorg. Chem.* **2009**, *48*, 2443–2448.

(22) Ni, C.; Rekken, B.; Fettinger, J. C.; Long, G. J.; Power, P. P. *Dalton Trans.* **2009**, 8349–8355.

(23) Gavenonis, J.; Tilley, T. D. *Organometallics* **2002**, *21*, 5549–5563.

(24) Gavenonis, J.; Tilley, T. D. *J. Am. Chem. Soc.* **2002**, *124*, 8536–8537.

(25) Hill, J. E.; Balaich, G. J.; Fanwick, P. E.; Rothwell, I. P. *Organometallics* **1991**, *10*, 3428–3430.

(26) Hill, J. E.; Fanwick, P. E.; Rothwell, I. P. *Organometallics* **1990**, *9*, 2211–2213.

(27) Hill, J. E.; Fanwick, P. E.; Rothwell, I. P. *Organometallics* **1991**, *10*, 15–16.

(28) Ni, C.; Power, P. P. *Chem. Commun.* **2009**, 5543–5545.

(29) Stanciu, C.; Olmstead, Marilyn M.; Phillips, Andrew D.; Stender, M.; Power, Philip P. *Eur. J. Inorg. Chem.* **2003**, *2003*, 3495–3500.

(30) Carson, E. C.; Lippard, S. J. *J. Am. Chem. Soc.* **2004**, *126*, 3412–3413.

(31) Carson, E. C.; Lippard, S. J. *Inorg. Chem.* **2005**, *45*, 828–836.

(32) Carson, E. C.; Lippard, S. J. *Inorg. Chem.* **2005**, *45*, 837–848.

(33) Hagadorn, J. R.; Que, L.; Tolman, W. B. *Inorg. Chem.* **2000**, *39*, 6086–6090.

(34) Hagadorn, J. R.; Que, L.; Tolman, W. B.; Prisecaru, I.; Münck, E. *J. Am. Chem. Soc.* **1999**, *121*, 9760–9761.

(35) Klein, D. P.; Young, V. G.; Tolman, W. B.; Que, L. *Inorg. Chem.* **2006**, *45*, 8006–8008.

(36) Yoon, S.; Lippard, S. J. *J. Am. Chem. Soc.* **2005**, *127*, 8386–8397.

(37) Burdett, J. K. *Inorg. Chem.* **1975**, *14*, 375–382.

(38) Perutz, R. N.; Turner, J. J. *Inorg. Chem.* **1975**, *14*, 262–270.

(39) Perutz, R. N.; Turner, J. J. *J. Am. Chem. Soc.* **1975**, *97*, 4800–4804.

(40) Ditri, T. B.; Carpenter, A. E.; Ripatti, D. S.; Moore, C. E.; Rheingold, A. L.; Figueroa, J. S. *Inorg. Chem.* **2013**, *52*, 13216–13229.

(41) Ditri, T. B.; Fox, B. J.; Moore, C. E.; Rheingold, A. L.; Figueroa, J. S. *Inorg. Chem.* **2009**, *48*, 8362–8375.

(42) Fox, B. J.; Sun, Q. Y.; DiPasquale, A. G.; Fox, A. R.; Rheingold, A. L.; Figueroa, J. S. *Inorg. Chem.* **2008**, *47*, 9010–9020.

(43) Guy, M. P.; Coffer, J. L.; Rommel, J. S.; Bennett, D. W. *Inorg. Chem.* **1988**, *27*, 2942–2945.

(44) Fox, B. J.; Millard, M. D.; DiPasquale, A. G.; Rheingold, A. L.; Figueroa, J. S. *Angew. Chem., Int. Ed.* **2009**, *48*, 3473–3477.

(45) Stewart, M. A.; Moore, C. E.; Ditri, T. B.; Labios, L. A.; Rheingold, A. L.; Figueroa, J. S. *Chem. Commun.* **2011**, *47*, 406–408.

(46) Emerich, B. M.; Moore, C. E.; Fox, B. J.; Rheingold, A. L.; Figueroa, J. S. *Organometallics* **2011**, *30*, 2598–2608.

(47) Margulieux, G. W.; Weidemann, N.; Lacy, D. C.; Moore, C. E.; Rheingold, A. L.; Figueroa, J. S. *J. Am. Chem. Soc.* **2010**, *132*, 5033–5035.

(48) Fox, B. J.; Millard, M. D.; DiPasquale, A. G.; Rheingold, A. L.; Figueroa, J. S. *Angewandte Chemie, International Edition* **2009**, *48*, 3372–3372.

(49) Labios, L. A.; Millard, M. D.; Rheingold, A. L.; Figueroa, J. S. *J. Am. Chem. Soc.* **2009**, *131*, 11318–11319.

(50) Lyapkalo, I. M.; Ioffe, S. L.; Strelenko, Y. A.; Tartakovsky, V. A. *Russ. Chem. Bull.* **1996**, *45*, 2245–2247.

(51) Ditri, T. B.; Moore, C. E.; Rheingold, A. L.; Figueroa, J. S. *Inorg. Chem.* **2011**, *50*, 10448–10459.

(52) Morse, D. B.; Rauchfuss, T. B.; Wilson, S. R. *J. Am. Chem. Soc.* **1990**, *112*, 1860–1864.

(53) Herrmann, W. A.; Thiel, W. R.; Herdtweck, E. *J. Organomet. Chem.* **1988**, *353*, 323–336.

(54) Connor, J. A.; Jones, E. M.; McEwen, G. K.; Lloyd, M. K.; McCleverty, J. A. *J. Chem. Soc., Dalton Trans.* **1972**, 1246–1253.

(55) Lyons, L. J.; Pitz, S. L.; Boyd, D. C. *Inorg. Chem.* **1995**, *34*, 316–322.

(56) Rommel, J. S.; Weinrach, J. B.; Grubisha, D. S.; Bennett, D. W. *Inorg. Chem.* **1988**, *27*, 2945–2949.

(57) Minelli, M.; Maley, W. J. *Inorg. Chem.* **1989**, *28*, 2954–2958.

(58) Allen, F. *Acta Crystallographica Section B* **2002**, *58*, 380–388.

(59) Chiu, K. W.; Howard, C. G.; Wilkinson, G.; Galas, A. M. R.; Hursthouse, M. B. *Polyhedron* **1982**, *1*, 803–808.

(60) Luck, R. L.; Morris, R. H.; Sawyer, J. F. *Organometallics* **1984**, *3*, 247–255.

(61) Adams, H.; Bailey, N. A.; Bannister, C.; Faers, M. A.; Fedorko, P.; Osborn, V. A.; Winter, M. J. *J. Chem. Soc., Dalton Trans.* **1987**, 341–348.

(62) Filippou, A. C.; Völkl, C.; Grünleitner, W.; Kiprof, P. *Angew. Chem., Int. Ed. Engl.* **1990**, *29*, 207–209.

(63) Lentz, D. *J. Organomet. Chem.* **1990**, *381*, 205–212.

(64) Martins, A. M.; Calhorda, M. J.; Romão, C. C.; Völkl, C.; Kiprof, P.; Filippou, A. C. *J. Organomet. Chem.* **1992**, *423*, 367–390.

(65) Burkey, D. J.; Debad, J. D.; Legzdins, P. *J. Am. Chem. Soc.* **1997**, *119*, 1139–1140.

(66) Calvo, M.; Galakhov, M. V.; Gómez–García, R.; Gómez–Sal, P.; Martin, A.; Royo, P.; Vázquez de Miguel, A. *J. Organomet. Chem.* **1997**, *548*, 157–175.

(67) Shapiro, P. J.; Zehnder, R.; Foo, D. M.; Perrotin, P.; Budzelaar, P. H. M.; Leitch, S.; Twamley, B. *Organometallics* **2006**, *25*, 719–732.

(68) Braunschweig, H.; Dörfler, R.; Gruss, K.; Köhler, J.; Radacki, K. *Organometallics* **2010**, *30*, 305–312.

(69) Alvarez, M. A.; Garcia, M. E.; Ruiz, M. A.; Vega, M. F. *Dalton Trans.* **2011**, *40*, 8294–8297.

(70) Bassett, J.–M.; Berry, D. E.; Barker, G. K.; Green, M.; Howard, J. A. K.; Stone, F. G. A. *J. Chem. Soc., Dalton Trans.* **1979**, 1003–1011.

(71) Kool, L. B.; Rausch, M. D.; Herberhold, M.; Alt, H. G.; Thewalt, U.; Honold, B. *Organometallics* **1986**, *5*, 2465–2468.

(72) Alcalde, M. I.; de la Mata, J.; Gomez, M.; Royo, P.; Pellinghelli, M. A.; Tiripicchio, A. *Organometallics* **1994**, *13*, 462–467.

(73) Green, M. L. H.; Haggitt, J.; Mehnert, C. P. *J. Chem. Soc., Chem. Commun.* **1995**, 1853–1854.

(74) Liu, C.–Y.; Chen, D.–Y.; Cheng, M.–C.; Peng, S.–M.; Liu, S.–T. *Organometallics* **1995**, *14*, 1983–1991.

(75) Buschmann, J.; Bartolmäs, T.; Lentz, D.; Luger, P.; Neubert, I.; Röttger, M. *Angew. Chem., Int. Ed. Engl.* **1997**, *36*, 2372–2374.

(76) Barybin, M. V.; Young, V. G.; Ellis, J. E. *J. Am. Chem. Soc.* **1999**, *121*, 9237–9238.

(77) J. Mathieson, T.; G. Langdon, A.; B. Milestone, N.; K. Nicholson, B. *J. Chem. Soc., Dalton Trans.* **1999**, 201–208.

(78) Meiere, S. H.; Brooks, B. C.; Gunnoe, T. B.; Carrig, E. H.; Sabat, M.; Harman, W. D. *Organometallics* **2001**, *20*, 3661–3671.

(79) Moigno, D.; Callejas–Gaspar, B.; Gil–Rubio, J.; Brandt, C. D.; Werner, H.; Kiefer, W. *Inorg. Chim. Acta* **2002**, *334*, 355–364.

(80) Walther, M.; Jung, C. M.; Bergmann, R.; Pietzsch, J.; Rode, K.; Fahmy, K.; Mirtschink, P.; Stehr, S.; Heintz, A.; Wunderlich, G.; Kraus, W.; Pietzsch, H.–J.; Kropp, J.; Deussen, A.; Spies, H. *Bioconjugate Chem.* **2006**, *18*, 216–230.

(81) Brennessel, W. W.; Ellis, J. E. *Angew. Chem., Int. Ed.* **2007**, *46*, 598–600.

(82) Galan, B. R.; Pitak, M.; Keister, J. B.; Diver, S. T. *Organometallics* **2008**, *27*, 3630–3632.

(83) Ohki, Y.; Hatanaka, T.; Tatsumi, K. *J. Am. Chem. Soc.* **2008**, *130*, 17174–17186.

(84) Whited, M. T.; Grubbs, R. H. *Organometallics* **2008**, *28*, 161–166.

(85) Galan, B. R.; Pitak, M.; Gembicky, M.; Keister, J. B.; Diver, S. T. *J. Am. Chem. Soc.* **2009**, *131*, 6822–6832.

(86) Takao, T.; Obayashi, N.; Zhao, B.; Akiyoshi, K.; Omori, H.; Suzuki, H. *Organometallics* **2011**, *30*, 5057–5067.

(87) Knorr, M.; Jourdain, I.; Lentz, D.; Willemsen, S.; Strohmann, C. *J. Organomet. Chem.* **2003**, *684*, 216–229.

(88) Wagner, N. L.; Laib, F. E.; Bennett, D. W. *J. Am. Chem. Soc.* **2000**, *122*, 10856–10867.

(89) Lentz, D. *Angew. Chem., Int. Ed. Engl.* **1994**, *33*, 1315–1331.

(90) Facchin, G.; Mozzon, M.; Michelin, R. A.; Ribeiro, M. T. A.; Pombeiro, A. J. L. *J. Chem. Soc., Dalton Trans.* **1992**, 2827–2835.

(91) Essenmacher, G. J.; Treichel, P. M. *Inorg. Chem.* **1977**, *16*, 800–806.

(92) Michelin, R. A.; Pombeiro, A. J. L.; Guedes da Silva, M. F. C. *Coord. Chem. Rev.* **2001**, *218*, 75–112.

(93) Pombeiro, A. J. L.; da Silva, M.; Michelin, R. A. *Coord. Chem. Rev.* **2001**, *218*, 43–74.

(94) Yamamoto, Y.; Yamazaki, H. *Coord. Chem. Rev.* **1972**, *8*, 225–239.

(95) Luzyanin, K. V.; Pombeiro, A. J. L. In *Isocyanide Chemistry*; Wiley–VCH Verlag GmbH & Co. KGaA: 2012, p 531–550.

(96) Qiu, G.; Ding, Q.; Wu, J. *Chem. Soc. Rev.* **2013**, *42*, 5257–5269.

(97) Cotton, F. A.; Zingales, F. *J. Am. Chem. Soc.* **1961**, *83*, 351.

(98) Malatesta, L.; Bonati, F. *Isocyanide complexes of metals*; Wiley, 1969.

(99) Bonati, F.; Minghetti, G. *Inorg. Chim. Acta* **1974**, *9*, 95–112.

(100) Chatt, J.; Pombeiro, A. J. L.; Richards, R. L.; Royston, G. H. D.; Muir, K. W.; Walker, R. *J. Chem. Soc., Chem. Commun.* **1975**, *0*, 708–709.

(101) Lam, C. T.; Corfield, P. W. R.; Lippard, S. J. *J. Am. Chem. Soc.* **1977**, *99*, 617–618.

(102) Chatt, J.; Pombeiro, A. J. L.; Richards, R. L. *J. Chem. Soc., Dalton Trans.* **1979**, 1585–1590.

(103) Chatt, J.; Pombeiro, A. J. L.; Richards, R. L. *J. Organomet. Chem.* **1980**, *184*, 357–364.

(104) Chatt, J.; Pombeiro, A. J. L.; Richards, R. L. *J. Chem. Soc., Dalton Trans.* **1980**, 492–498.

(105) Pombeiro, A. J. L.; Richards, R. L. *Transition Met. Chem. (London)* **1980**, *5*, 55–59.

(106) Dewan, J. C.; Giandomenico, C. M.; Lippard, S. J. *Inorg. Chem.* **1981**, *20*, 4069–4074.

(107) Pombeiro, A. J. L.; Carvalho, M. F. N. N.; Hitchcock, P. B.; Richards, R. L. *J. Chem. Soc., Dalton Trans.* **1981**, 1629–1634.

(108) Giandomenico, C. M.; Lam, C. T.; Lippard, S. J. *J. Am. Chem. Soc.* **1982**, *104*, 1263–1271.

(109) Pombeiro, A. J. L.; Hughes, D. L.; Pickett, C. J.; Richards, R. L. *J. Chem. Soc., Chem. Commun.* **1986**, 246–247.

(110) Warner, S.; Lippard, S. J. *Organometallics* **1986**, *5*, 1716–1725.

(111) Vrtis, R. N.; Rao, C. P.; Warner, S.; Lippard, S. J. *J. Am. Chem. Soc.* **1988**, *110*, 2669–2670.

(112) Warner, S.; Lippard, S. J. *Organometallics* **1989**, *8*, 228–236.

(113) Dasilva, J.; Pellinghelli, M. A.; Pombeiro, A. J. L.; Richards, R. L.; Tiripicchio, A.; Wang, Y. *J. Organomet. Chem.* **1993**, *454*, C8–C10.

(114) Acho, J. A.; Lippard, S. J. *Organometallics* **1994**, *13*, 1294–1299.

(115) Wang, Y.; Da Silva, J. J. R. F.; Pombeiro, A. J. L.; Pellinghelli, M. A.; Tiripicchio, A.; Henderson, R. A.; Richards, R. L. *J. Chem. Soc., Dalton Trans.* **1995**, 1183–1191.

(116) Seino, H.; Nonokawa, D.; Nakamura, G.; Mizobe, Y.; Hidai, M. *Organometallics* **2000**, *19*, 2002–2011.

(117) Guy, M. P.; Guy Jr, J. T.; Bennett, D. W. *J. Mol. Struct. Theochem* **1985**, *122*, 95–99.

(118) Fischer, E. O.; Schneider, J.; Neugebauer, D. *Angew. Chem., Int. Ed. Engl.* **1984**, *23*, 820–821.

(119) Riera, V.; Ruiz, J.; Jeannin, Y.; Philoche–Levisalles, M. *J. Chem. Soc., Dalton Trans.* **1988**, 1591–1597.

(120) Deeming, A. J.; Donovan–Mtunzi, S. *Organometallics* **1985**, *4*, 693–696.

(121) Fischer, H.; Motsch, A.; Maerkl, R.; Ackermann, K. *Organometallics* **1985**, *4*, 726–735.

(122) Carnahan, E. M.; Lippard, S. J. *J. Chem. Soc., Dalton Trans.* **1991**, 699–706.

(123) Henderson, R. A.; Pombeiro, A. J. L.; Richards, R. L.; da Silva, J. J. R. F.; Wang, Y. *J. Chem. Soc., Dalton Trans.* **1995**, 1193–1199.

(124) Hou, H. Y.; Gantzel, P. K.; Kubiak, C. P. *Organometallics* **2003**, *22*, 2817–2819.

(125) Filippou, A. C.; Wössner, D.; Lungwitz, B.; Kociok–Köhn, G. *Angew. Chem., Int. Ed.* **1996**, *35*, 876–878.

(126) Filippou, A. C.; Lungwitz, B.; Kociok–Köhn, G. *Eur. J. Inorg. Chem.* **1999**, *1999*, 1905–1910.

(127) Kreissl, F. R.; Sieber, W. J.; Wolfgruber, M. *J. Organomet. Chem.* **1984**, *270*, C45–C47.

(128) Lungwitz, B.; Filippou, A. C. In *Transition Metal Carbyne Complexes*; Kreissl, F. R., Ed.; Kluwer Academic Publ: Dordrecht, 1993; Vol. 392, p 249–254.

(129) Lemos, M. A. N. D. A.; da Silva, M. F. C. G.; Pombeiro, A. J. L. *Inorg. Chim. Acta* **1994**, *226*, 9–16.

(130) Amélia, A.; Lemos, N. D. A.; Pombeiro, A. J. L. *J. Organomet. Chem.* **1988**, *356*, C79–C82.

(131) Stumpf, R.; Burzlaff, N.; Weibert, B.; Fischer, H. *J. Organomet. Chem.* **2002**, *651*, 66–71.

(132) Stumpf, R.; Jaeger, M.; Fischer, H. *Organometallics* **2001**, *20*, 4040–4048.

(133) Pangborn, A. B.; Giardello, M. A.; Grubbs, R. H.; Rosen, R. K.; Timmers, F. J. *Organometallics* **1996**, *15*, 1518–1520.

(134) Arnarego, W. L. F.; Chai, C. L. L. *Purification of Laboratory Chemicals*; 5th ed.; Elsevier, 2003.

(135) Peng, Y.; Fischer, R. C.; Merrill, W. A.; Fischer, J.; Pu, L.; Ellis, B. D.; Fettinger, J. C.; Herber, R. H.; Power, P. P. *Chem. Sci.* **2010**, *1*, 461–468.

(136) McElwee–White, L.; Dougherty, D. A. *J. Am. Chem. Soc.* **1984**, *106*, 3466–3474.

(137) Burla, M. C.; Caliandro, R.; Camalli, M.; Carrozzini, B.; Cascarano, G. L.; De Caro, L.; Giacovazzo, C.; Polidori, G.; Spagna, R. *J. Appl. Crystallogr.* **2005**, *38*, 381–388.

(138) Sheldrick, G. M. *Acta. Crystallogr.* **2008**, *64*, 112–122.

Chapter 6

Synthesis and Reactivity of Tetrakisisocyanide Complexes of Molybdenum

6.1 Introduction

The unsaturated group 6 metal carbonyls $M(CO)_{6-n}$ (n = 1 – 4) have a long enduring role as prototypical molecules for the study of the photo–generated metal carbonyls.[1–19] This attention is garnered from their distinct coordination behavior which is attributed to the interplay of the low–coordination numbers, unencumbering ligands, strongly π–acidic ligand fields, and electron rich metal centers characteristic of these species. However, the same properties that make the group 6 unsaturated metal carbonyls appealing targets render them inherently reactive species. Consequently, their study has been limited to gas phase and matrix isolation techniques with, little information regarding their condensed phase structure and reactivity patterns.

Over the past 40 years, IR studies have revealed that the photo generated group 6 unsaturated metal carbonyls species $M(CO)_4$, $M(CO)_3$ and $M(CO)_2$ are unique in that they retain their residual $M(CO)_6$ parent skeleton and therefore possess *cis*–divacant octahedron (D_{4h}), trigonal pyramidal (C_{3v}) and bent (C_{2v}) geometries, respectively.[2,3,5,7–11,16,17]

Nevertheless, despite these efforts, there still remains some ambiguity in structural assignments. For example, in Turner's early matrix isolation experiments, two IR bands were observed for the $Cr(CO)_3$ and $Mo(CO)_3$ carbonyls consistent with the A_1 and E modes of C_{3v}–symmetric molecules.[3] Interestingly, the A_1 band was detected in methane but not argon matrices, with its absence in the latter attributed to the low intensity expected for this frequency. However, ensuing gas–phase IR studies by others consistently report only one band for $M(CO)_3$ complexes, suggestive of a trigonal planar, D_{3h}–symmetric geometry.[9–11,16,17] Similarly, the A_1 band for the *cis*–divacant octahedral (C_{4v}) $M(CO)_4$ carbonyl is rarely detected in gas–phase IR studies[10,11,16,17] in contrast to calculations that suggest it should be of moderate intensity.[18] The few inconsistences in these reports can largely be attributed to the convolution of the IR spectra that occurs when several photodecomposition products are observed simultaneously, a feature especially problematic with the group 6 carbonyls. If corroborating spectroscopic data could be obtained, the discrepancy between the various IR investigations could largely be ignored. Seeking further elucidation of the chemical reactivity, and molecular structure of the group 6 unsaturated metal carbonyls, our group has targeted low coordinate isocyanides as potential models for this elusive class of molecules.

In an effort to stabilize coordinatively unsaturated metal isocyanides our group has introduced a series of encumbering *m*–terphenyl isocyanide ligands.[20–22] At present, the alkyl–substituted *m*–terphenyl isocyanide ligands $CNAr^{Mes2}$ and $CNAr^{Dipp2}$ (Ar^{Mes2} = 2,6–(2,4,6–$Me_3C_6H_2$)C_6H_3; Ar^{Dipp2} = 2,6–(2,6–(*i*–Pr)$_2C_6H_3$)$_2C_6H_3$) have been successfully employed for the stabilization of isocyanide analogues of the unsaturated binary carbonyls $Pd(CO)_2$, $Ni(CO)_3$, and $Co(CO)_4$.[23–26] However, in our attempts to expand these studies to include the group 6 isocyanide species $[Mo(CNAr^{R2})_2]$ and $[Mo(CNAr^{R2})_3]$, undesirable η^6–binding to the zerovalent molybdenum center by either arene solvent or by the flanking aryl ring of the *m*–terphenyl ligand precluded the isolation of coordinatively unsaturated

molybdenum isocyanides.[22,27] Speculation that a zerovalent molybdenum center supported by four *m*–terphenyl ligands may show resistance towards η^6–bond formation lead us to target [Mo(CNAr^{R2})$_4$] complexes. Initially, our efforts focused on the addition of a forth CNAr^{R2} ligand to the arene–tethered, trisisocyanide complexes Mo(η^6–(R)–κ^1–*C*–CNAr^{R})(CNAr^{R2})$_2$(Ar^{R2} = Ar^{Dipp2} and Ar^{Mes2}). Disappointingly, both Mo(η^6–(R)–κ^1–*C*–CNAr^{R})(CNAr^{R2})$_2$ isocyanides were resistant to further CNAr^{R2} ligand incorporation under both thermolytic and photolytic conditions. The propensity for zerovalent molybdenum centers to form η^6–interactions with arenes, coupled with the persistence of these interactions indicated that a straight–forward preparation of tetrakisisocyanide complexes was unlikely. Therefore, we reasoned that synthesis of tetrakisisocyanide complexes would likely require either mid–valent molybdenum synthons incapable of forming appreciable η^6–bonds, or low–valent molybdenum precursors protected from η^6–binding interactions by non–labile supporting ligands. Accordingly, the synthesis and reactivity of molybdenum tetrakis–CNAr^{Mes2} *m*–terphenyl isocyanide complexes is reported herein.

6.2 Synthesis and Oxidation Chemistry of Mo(CO)$_2$(CNAr^{Mes2})$_4$

In an earlier report, we outlined the oxidative decarbonylation of the tricarbonyl trisisocyanide *fac*–Mo(CO)$_3$(CNAr^{Mes2})$_3$ (**5**) by addition of 3.55 equiv of molecular iodide, affording the diiodo–triiodide complex *mer*–MoI$_2$(I$_3$)(CNAr^{Mes2})$_3$ (**25**).[28] Interestingly, more careful study of the above reaction revealed that the oxidation proceeds through the divalent dicarbonyl trisisocyanide intermediate MoI$_2$(CO)$_2$(CNAr^{Mes2})$_3$ (**50**), and conditions were optimized to isolate this species exclusively (Figure 6.1, Scheme 6.1). As revealed by the molecular structure of MoI$_2$(CO)$_2$(CNAr^{Mes2})$_3$ (**50**), the pentagonal bipyramidal geometry creates two distinct ligands environments, however, only a single set of CNAr^{Mes2} resonances is detected by ^{1}H NMR spectroscopy ($CDCl_3$). Studies of idealized coordination geometries

have revealed that there are small potential energy differences between the three most common seven–coordinate geometries: 1:5:1 D_{5h} pentagonal bipyramid, 1:4:2 C_{2v} capped trigonal prism, and 1:3:3 C_{3v} capped octahedron.[29,30]. Solution FTIR experiments support these claims and reveal that the isomerization of $MoI_2(CO)_2(CNAr^{Mes2})_3$ (**50**) occurs in solution at room temperature. Although the maximal number of ν_{CO} and ν_{CN} stretches for any single isomer of $MoI_2(CO)_2(CNAr^{Mes2})_3$ (**50**) is 2 and 3, respectively, FTIR studies revealed 4 ν_{CO} and 4 ν_{CN} stretching modes (Table 6.1). Therefore, at least two isomeric forms of $MoI_2(CO)_2(CNAr^{Mes2})_3$ (**50**) are present in solution and their interconversion is observable on the FTIR time scale. Notably, our spectroscopic observations are consistent with X–ray crystallographic studies of other $MX_2(CO)_2L_3$ (M = Mo or W, X = Br or I, L = CNR or PR_3) complexes in which more than one geometric isomer of the seven–coordinate complex was structurally characterized.[31,32]

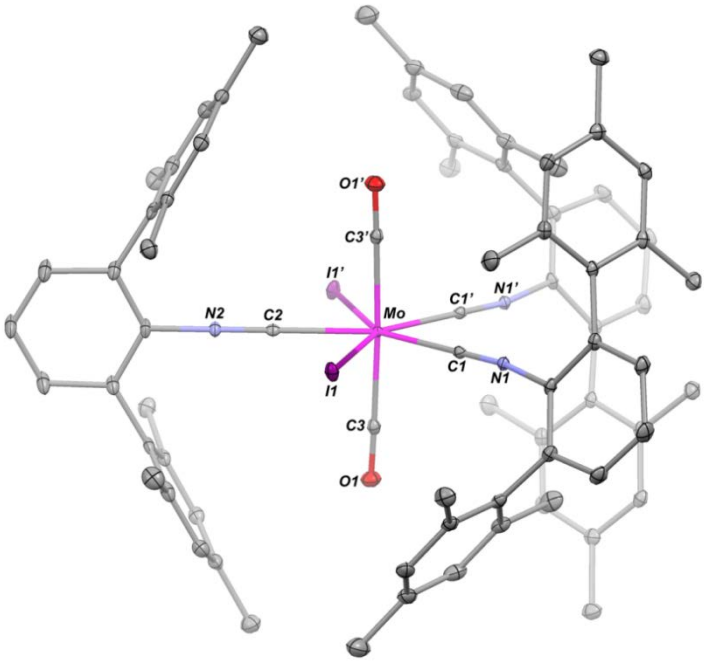

Figure 6.1. Molecular Structure of $MoI_2(CO)_2(CNAr^{Mes2})_3$ (**50**). Selected bond distances (Å) and angles (Deg): Mo1–C1 = 2.111(3); Mo1–C2 = 2.121(4); Mo1–C3 = 2.041(3); Mo1–I1 = 2.8767(2); C1–Mo1–C1' = 76.11(13); C1–Mo1–I1 = 70.46(16); C2–Mo1–I1 = 71.488(6); C2–Mo1–C3 = 88.68(7).

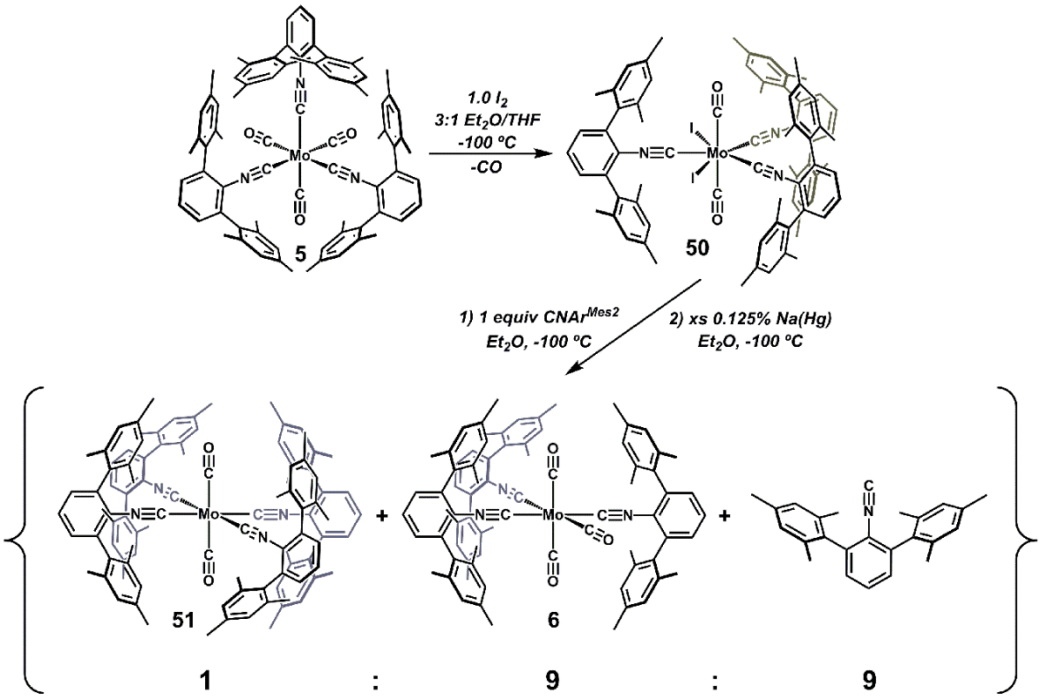

Scheme 6.1. Synthesis of $MoI_2(CO)_2(CNAr^{Mes2})_3$ (**50**) and *trans*–$Mo(CO)_2(CNAr^{Mes2})_4$ (**51**).

Table 6.1. Solution ν_{CN} and ν_{CO} Stretching Frequencies

Complex	ν_{CN} (cm^{-1})	ν_{CO} (cm^{-1})
$MoI_2(CO)_2(CNAr^{Mes2})_3$ (**50**)	2157 (w sh)	2018 (w)
	2125 (vs)	1984 (vs)
	2114 (w sh)	1962 (vs)
	2080 (s)	1949 (w sh)
trans–$Mo(CO)_2(CNAr^{Mes2})_4$ (**51**)	2078 (w)	1910 (s)
	2014 (w sh)	
	1972 (vs)	
[*trans*–$Mo(CO)_2(CNAr^{Mes2})_4$](I_3) (**52**)	2077 (vs)	1960 (vs)
[*trans*–$MoI_2(CNAr^{Mes2})_4$](I_3) (**54**)	2121 (vs)	
[*trans*–$MoI_2(CNAr^{Mes2})_4$](OTf) (**55**)	2121 (vs)	

[a] Data from reference 42.

The diiodo–dicarbonyl bisisocyanide species $MoI_2(CO)_2(CNAr^{Mes2})_3$ (**50**) was a particularly enticing synthon because it: i) can be reduced to a coordinatively unsaturated mixed isocyanide/carbonyl species, and ii) provides a route to tetrakisisocyanide complexes.

In a previous study, reduction of a similar Mo(II) mixed halide/carbonyl/isocyanide complex featuring the more sterically encumbering *m*–terphenyl isocyanide $CNAr^{Dipp2}$ was investigated as a means to generate a mixed carbonyl/isocyanide analogue of $[Mo(CO)_4]$. However, treatment of the bisisocyanide complex $MoI_2(CO)_2(CNAr^{Dipp2})_2$ (**14**) with a range of reducing agents resulted in the formation of the tetracarbonyl bisisocyanide complex *trans*–$Mo(CO)_4(CNAr^{Dipp2})_2$, (**7**) and a multitude of other unidentified products.[27] Disappointingly, similar lability of the Mo–CO linkage was observed in the reduction of $MoI_2(CO)_2(CNAr^{Mes2})_3$ (**50**), and primarily *mer*–$Mo(CO)_3(CNAr^{Mes2})_3$ (**6**) was obtained. However, as outlined in Scheme 1, when reductions are executed in the presence of an additional equivalent of $CNAr^{Mes2}$, limited quantities of the dicarbonyl tetraisocyanide species *trans*–$Mo(CO)_2(CNAr^{Mes2})_4$ (**51**) were isolated. The limited solubility of *trans*–$Mo(CO)_2(CNAr^{Mes2})_4$ precluded its structural characterization and also the detection of its ^{13}C NMR *C*≡N and *C*≡O resonances. Nevertheless, both a single set of $CNAr^{Mes2}$ ^1H NMR resonances and a single ν_{CO} stretch in the FTIR spectrum are consistent with $Mo(CO)_2(CNAr^{Mes2})_4$ (**51**) possessing *trans*–oriented carbonyl ligands (Table 6.1). Given that the generation of *trans*–$Mo(CO)_2(CNAr^{Mes2})_4$ (**51**) by reduction of $MoI_2(CO)_2(CNAr^{Dipp2})_2$ (**14**) was low yielding and required its separation from considerable amounts of *mer*–$Mo(CO)_3(CNAr^{Mes2})_3$ (**6**), alternative synthetic strategies were explored. Accordingly, photolysis of a 1:1 mixture of *fac*–$Mo(CO)_3(CNAr^{Mes2})_3$ (**5**) and $CNAr^{Mes2}$ in THF solution with a low–pressure Hg lamp (254 nm) provides *trans*–$Mo(CO)_2(CNAr^{Mes2})_4$ (**51**) with a 65 % overall yield (Scheme 6.2).

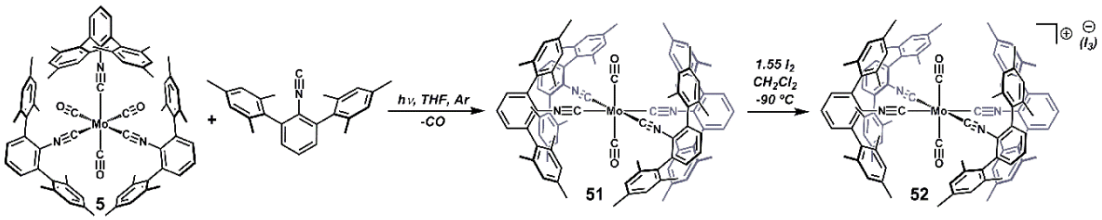

Scheme 6.2. Synthesis of *trans*–$Mo(CO)_2(CNAr^{Mes2})_4$ (**51**) and [*trans*–$Mo(CO)_2(CNAr^{Mes2})_4](I_3)$ (**52**).

In order to convert mixed carbonyl/isocyanide metal species to carbonyl free zerovalent isocyanides our group has employed a two–step synthetic approach that utilizes an oxidative decarbonylation step reminiscent of Colton's seminal works[33–39] to form mixed halogen/isocyanide complexes which are subsequently reduced to low–valent isocyanides.[27,28] To date, the zerovalent isocyanides (η^6–C_6H_6)$Mo(N_2)(CNAr^{Dipp2})_2$ (**21**), Mo(η^6–(Mes)–κ^1–*C*–$CNAr^{Mes}$)$(CNAr^{Mes2})_2$ (**24**), and Cr(η^6–(Mes)–κ^1–*C*–$CNAr^{Mes}$)$(CNAr^{Mes2})_2$ (**42**) have been obtained via this methodology. However, nn previous studies we have encountered isocyanide/carbonyl species that were either resistant to decarbonylation following their oxidation, or resistant to chemical oxidation altogether. Unfortunately, *trans*–$Mo(CO)_2(CNAr^{Mes2})_4$ (**51**) belongs to the former category.[27] Accordingly, treatment of *trans*–$Mo(CO)_2(CNAr^{Mes2})_4$ (**51**) with 1.55 equivalents of molecular iodine in CH_2Cl_2 solution results in the formation of the dicarbonyl bisisocyanide salt [*trans*–$Mo(CO)_2(CNAr^{Mes2})_4](I_3)$ (**52**, Scheme 6.2, Figure 6.2, Table 6.1). Heating of [*trans*–$Mo(CO)_2(CNAr^{Mes2})_4](I_3)$ (**52**) in CH_2Cl_2 solution at 100 °C for several days, both with and without additional equivalents of I_2 resulted in no observable signs of decarbonylation as determined by ^{1}H NMR spectroscopy ($CDCl_3$). Furthermore, [*trans*–$Mo(CO)_2(CNAr^{Mes2})_4](I_3)$ (**52**) was unreactive towards a range of chemical oxidants and the decarbonylation reagents trimethylamine and pyridine N–oxide. It's likely that despite possessing 1^+ oxidation state, the presence of four Lewis–acidic $CNAr^{Mes2}$ ligands renders the metal center in $[Mo(CO)_2(CNAr^{Mes2})_4](I_3)$ (**52**) appreciably π–

acidic, and therefore, the loss of CO unlikely. Nevertheless, given the observed stability of $[Mo(CO)_2(CNAr^{Mes2})_4](I_3)$ (**52**), alternative synthetic routes for the generation of tetrakisisocyanides were explored.

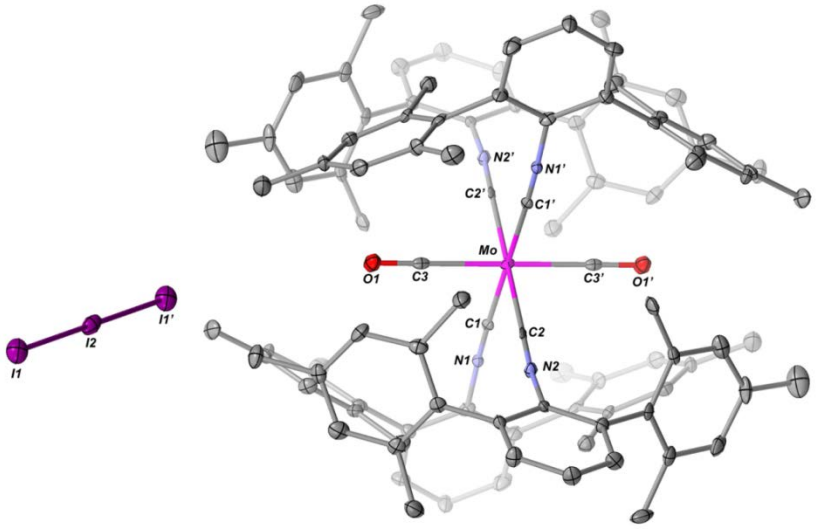

Figure 6.2. Molecular Structure of [*trans*–$Mo(CO)_2(CNAr^{Mes2})_4](I_3)$ (**52**). Selected bond distances (Å) and angles (Deg): Mo1–C1 = 2.130(10); Mo1–C2 = 2.128(10); Mo1–C3 = 2.033(12); I2–I1 = 2.9107(10); C1–Mo1–C2 = 90.8(3); C1–Mo1–C2' = 89.2(3); C2–Mo1–C3 = 89.5(3).

6.3 Synthesis and Reactivity of Trivalent Tetrakisisocyanides

In 2002, Leigh and co–workers reported that the reaction between excess trimethylsilyl iodide (TMSI) and $MoCl_4(NCMe)_2$ proceeds via a metathetical/reductive mechanism to afford the Mo(III) complex $[MoI_2(NCMe)_4](I_3)$.[40] For our goals, $[MoI_2(NCMe)_4](I_3)$ was an appealing synthon because it hosts 4 labile NCMe ligands and its 3^+ oxidation state would inhibit the formation of metal–arene interactions. However, in our hands, the use of $[MoI_2(NCMe)_4](I_3)$ was problematic due to its limited solubility in most organic solvents. In his studies pertaining to the synthesis and reactivity of the tricarbonyl trisnitriles $M(CO)_3(NCR)_3$ (M = Cr, Mo, or W, R = CH_3, CH_2CH_3, or $CH_2CH_2CH_3$), Kubas reported improved solubility and more facile of nitrile displacement for complexes containing

larger nitrile ligands.[41,42] Inspired by these reports and employing similar methods to those outlined by Leigh, we isolated and characterized the Mo(III) diiodo–tetrakisnitrile salt $[MoI_2(NCEt)_4](I_3)$ (**53**). Importantly, $[MoI_2(NCEt)_4](I_3)$ (**53**) has marked solubility in CH_2Cl_2. Thus treatment of $[MoI_2(NCEt)_4](I_3)$ (**53**) with 4.0 equiv of $CNAr^{Mes2}$ results in the formation of diiodide–tetrakisisocyanide [*trans*–$MoI_2(CNAr^{Mes2})_4](I_3)$ as determined by X–ray diffraction (**54**, Figure 6.3, Scheme 6.3, Table 6.1). As expected, [*trans*–$MoI_2(CNAr^{Mes2})_4](I_3)$ (**54**) is paramagnetic and gives rise to a solution magnetic moment of μ_{eff} = 1.83(1) μ_B, consistent with an S = 1/2, d^3 metal center. The IR spectrum of [*trans*–$MoI_2(CNAr^{Mes2})_4](I_3)$ (**54**) in $CDCl_3$ solution is also consistent with its formulation, exhibiting a single high–energy ν_{CN} band at 2121 cm^{-1}. The solubility of [*trans*–$MoI_2(CNAr^{Mes2})_4](I_3)$ (**54**) was limited to the CH_2Cl_2 and $CHCl_3$, therefore, in the interest of more facile reactivity studies, the diiodide–tetrakisisocyanide salt [*trans*–$MoI_2(CNAr^{Mes2})_4](OTf)$ (**55**) was isolated and characterized (Figure 6.4, Scheme 6.3). As expected, the structural and spectroscopic properties of [*trans*–$MoI_2(CNAr^{Mes2})_4](OTf)$ (**55**) are nearly identical to those of [*trans*–$MoI_2(CNAr^{Mes2})_4](I_3)$ (**54**) (Table 6.1). Notably, exchange of the $[I_3]^-$ counterion with $[OTf]^-$ resulted in [*trans*–$MoI_2(CNAr^{Mes2})_4](OTf)$ (**55**) being soluble in both fluorobenzene and THF.

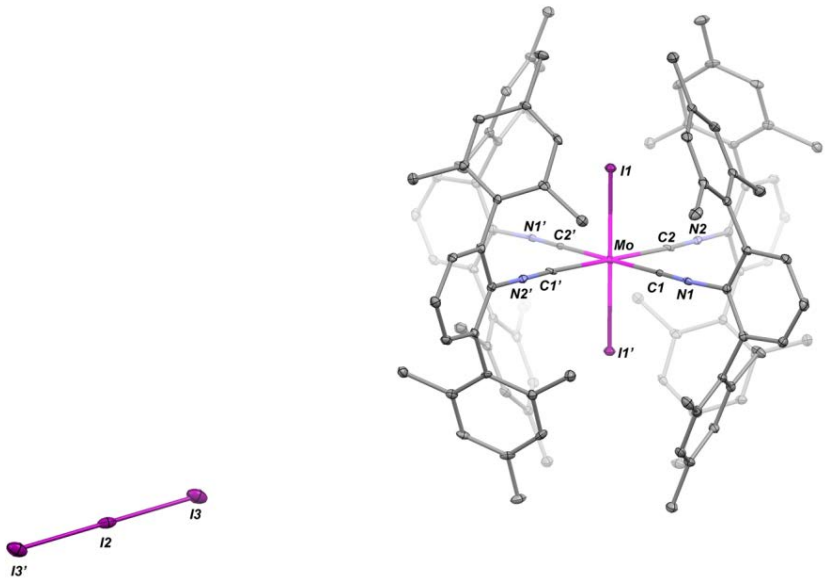

Figure 6.3. Molecular Structure of [*trans*–$MoI_2(CNAr^{Mes2})_4](I_3)$ (**54**). Selected bond distances (Å) and angles (Deg): Mo1–C1 = 2.152(6); Mo1–C2 = 2.168(7); Mo1–I1 = 2.6293(5); I2–I3 = 2.9049(8); C1–Mo1–C2 = 90.4(2); C1–Mo1–C2' = 89.6 (2); C2–Mo1–I1 = 91.48(16).

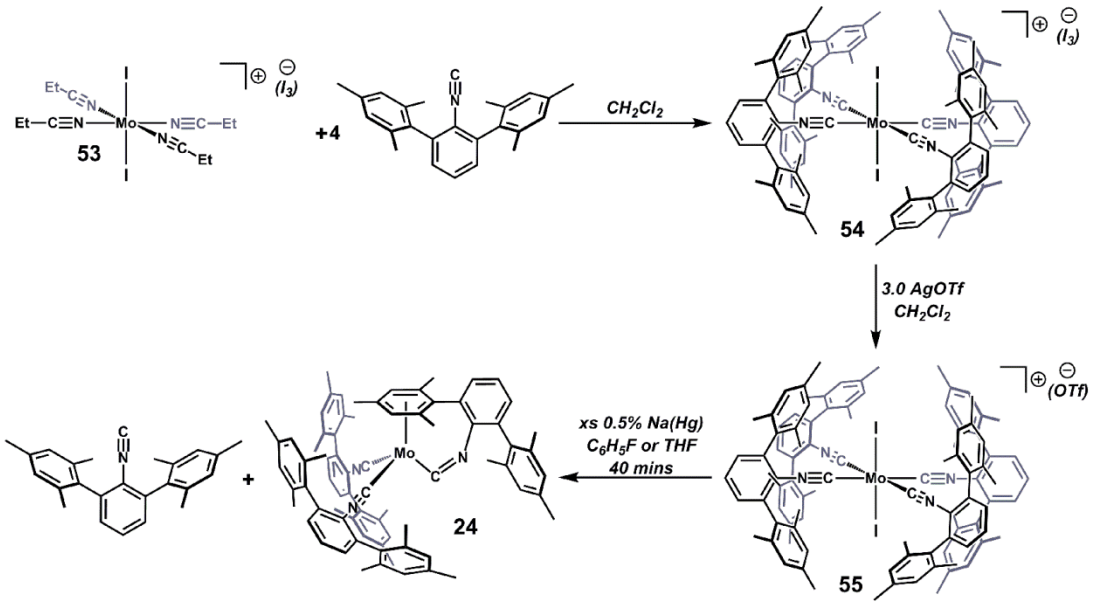

Scheme 6.3. Synthesis and reactivity of trivalent tetrakis isocyanides.

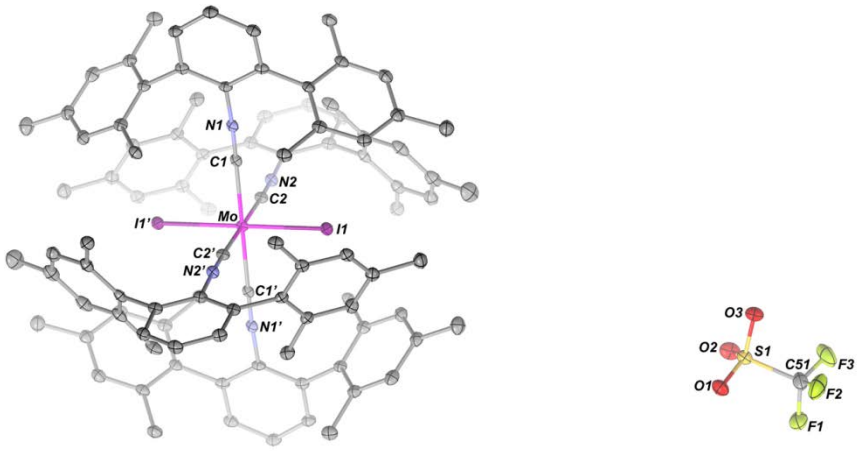

Figure 6.4. Molecular Structure of [$MoI_2(CNAr^{Mes2})_4$](OTf) (**55**). Selected bond distances (Å) and angles (Deg): Mo1–C1 = 2.131(4); Mo1–C2 = 2.137(4); Mo1–I1 = 2.6318(3); C1–Mo1–C2 = 89.88(15); C1–Mo1–C2' = 90.12(15); C2–Mo1–I1 = 89.70(12).

Isolation of the Mo(III) isocyanide [*trans*–$MoI_2(CNAr^{Mes2})_4$](OTf) (**55**) allowed us to assess its ability to serve as a precursor to low–valent, low–coordinate isocyanides, and we envisioned that its reduction would provide an isolable isocyanide analogue of $Mo(CO)_4$. Indeed, the generation of coordinatively unsaturated group six species by reduction of mixed ML_mX_n type–complexes (L = neutral ligand, X = halogen, m = 2–4, n = 2–4) is promising, as evidenced by the many examples of zerovalent dinitrogen complexes obtained by this methodology.[21,43–48] However, reduction of [*trans*–$MoI_2(CNAr^{Mes2})_4$](OTf) (**55**) by 0.5 % Na(Hg) in either THF of fluorobenzene solution resulted in the generation of the trisisocyanide complex Mo(η^6–(Mes)–κ^1–*C*–$CNAr^{Mes}$)$(CNAr^{Mes2})_2$ (**24**) and an equivalent of free $CNAr^{Mes2}$ (Scheme 6.3). Unfortunately, we were unable to determine at which oxidation state in the Mo(III) → Mo (0) reduction sequence the metal center ejects an equivalent of $CNAr^{Mes2}$ or forms a η^6–Mes bond. ^{1}H NMR spectra of aliquots of the reactions mixture taken 20 mins after the addition of [*trans*–$MoI_2(CNAr^{Mes2})_4$](OTf) (**55**) to a mixture 0.5 % Na(Hg) and fluorobenzene revealed the formation of a new paramagnetic product with no evidence of unbound $CNAr^{Mes2}$ ligand. However, attempts to isolate and characterize this intermediate

were unsuccessful. Considering these observations, we tentatively suggest that the [Mo($CNAr^{Mes2}$)$_4$] fragment remains intact through at least the Mo(III) → Mo(II) reduction.

The retention of neutral donor ligands in the reduction of mid–valent, halo–substituted group six complexes has been observed for metal centers supported by phosphines,[43,45] PNP–type pincers,[47,48], ANA–type pincers,[44] and thioethers.[46] Interestingly, although many of these ligands foster aryl substituents, maximum saturation of the metal centers they support is most often achieved through the binding of dinitrogen rather than the η^6–binding of ligand aryl groups. This discrepancy may be attributed to how readily the ligand architecture assists in the formation of η^6–interactions. For example, the aforementioned ligands host arenes bound directly to the atoms coordinating the metal center. Therefore, in order for the metal–arene interaction to occur, the metal–ligand bond has to first be broken. The same is not true for the *m*–terphenyl isocyanide ligand. The flexibility of the 4–atom linkage between the flanking aryl group and the metal center facilitates the formation of metal–η^6–arene bonds, circumventing the need to break metal–ligand bonds. Another possibility is that the stabilization of multiple dinitrogen molecules by the metal center requires supporting ligands with substantial Lewis–acidity (i.e. phosphines, PNP–pincers, etc.). It's worth noting that Peterson and Nguyen recently reported that the Mo(0) phosphine complex *trans*–Mo(N_2)$_2$(triphos I)($PMePh_2$) (triphos I = bis(diphenylphosphinoethyl)–phenylphosphine) decomposes after 12 h of heating at 60 °C to form the η^6–arene complex (η^6–C_6H_5PMePh)Mo(triphos I) revealing that zerovalent group 6 phosphine complexes are also susceptible to the η^6–binding of ligand.[49]

6.4 Concluding Remarks

In conclusion, $[MoI_2(NCEt)_4](I_3)$ (**53**) was proven to be a useful synthon for the generation of mid–valent molybdenum isocyanide complexes, as demonstrated by its application in the synthesis of $[MoI_2(CNAr^{Mes2})_4](I_3)$ (**54**). Chemical reduction of $[MoI_2(CNAr^{Mes2})_4](OTf)$ (**55**) revealed that although mid–valent *m*–terphenyl isocyanide complexes are stable and resistant to forming η^6–arene interactions, once reduced to lower–valent species, an isocyanide ligand is ejected at the expense of η^6–"capping" interactions with the metal. Clearly, the loss of an isocyanide ligand results as an effort to maximize saturation of the low–valent molybdenum center. Efforts to isolate coordinatively unsaturated $[Mo(CNR)_4]$ isocyanide complexes are ongoing.

6.5 Synthetic Procedures

General Considerations. All manipulations were carried out under an atmosphere of dry dinitrogen using standard Schlenk and glovebox techniques. Solvents were dried and deoxygenated according to standard procedures.[50] Unless otherwise stated, reagent–grade starting materials were purchased from commercial sources and either used as received or purified by standard procedures.[51] The *m*–terphenyl isocyanide $CNAr^{Mes2}$, $MoCl_4(EtCN)_2$, and *fac*–$Mo(CO)_3(CNAr^{Mes2})_3$ were prepared according to literature procedures.[20,21,52] Methylenechloride–d_2 and chloroform–*d* (Cambridge Isotope Laboratories) were vacuum distilled from NaH and then stored over 3 and 4 Å molecular sieves under N_2 for 2 d prior to use. Celite 405 (Fisher Scientific) was dried under vacuum (24 h) at a temperature above 250 ˚C and stored in the glovebox prior to use. Solution ^1H and $^{13}C\{^1H\}$ spectra were recorded on Varian Mercury 300 and 400 spectrometers, a Varian X–Sens500 spectrometer, or a JEOL ECA–500 spectrometer. ^1H and $^{13}C\{^1H\}$ chemical shifts are reported in ppm relative to $SiMe_4$

(^{1}H and ^{13}C δ = 0.0 ppm) with reference to residual solvent resonances of 5.32 ppm (^{1}H) and 53.84 ppm (^{13}C) for methylenechloride–d_2, and 7.24 ppm (^{1}H) and 77.23 ppm (^{13}C) for chloroform–*d*. FTIR spectra were recorded on a Thermo–Nicolet iS10 FTIR spectrometer. Samples were prepared as CD_2Cl_2 and $CDCl_3$ solutions and injected into a ThermoFisher solution cell equipped with KBr windows. For solution FTIR spectra, solvent peaks were digitally subtracted from all spectra by comparison with an authentic spectrum obtained immediately prior to that of the sample. The following abbreviations were used for the intensities and characteristics of important IR absorption bands: vs = very strong, s = strong, m = medium, w = weak, vw = very weak; b = broad, vb = very broad, sh = shoulder. Combustion analyses were performed by Robertson Microlit Laboratories of Madison, NJ (USA).

Synthesis of $MoI_2(CO)_2(CNAr^{Mes2})_3$ (50). To a thawing 3:1 Et_2O/THF solution of *fac*–$Mo(CO)_3(CNAr^{Mes2})_3$ (**5**, 1.766 g, 1.474 mmol, 1 equiv, 100 mL) was added a thawing Et_2O solution of I_2 (0.374 g, 1.474 mmol, 1 equiv, 40 mL). The reaction mixture stirred until it reached room temperature, after which all volatiles were removed under reduced pressure. The remaining green/brown solid was dissolved in toluene (30 mL), filtered, layered with *n*–pentane (70 mL) and stored at –35 °C for 1 d, whereupon green crystals of $MoI_2(CO)_2(CNAr^{Mes2})_3$ were obtained. Yield: 1.500 g, 1.053 mmol, 71%. ^{1}H NMR (400.1 MHz, $CDCl_3$, 20 ˚C): δ = 7.42 (t, 3H, *J* = 8 Hz, *p*–Ph), 7.18 (d, 6H, *J* = 8 Hz, *m*–Ph), 6.85 (s, 12H, *m*–Mes), 2.35 (s, 18H, *p*–C*H*$_3$), 1.99 (s, 36H, *o*–C*H*$_3$) ppm. ^{13}C{^{1}H} NMR (100.6 MHz, $CDCl_3$, 20 °C): δ = 214.4, (*C*≡O), 162.5 (*C*≡N), 139.0, 137.7, 135.7, 133.4, 129.9, 129.2, 128.9, 126.9, 21.5, 21.0 ppm. FTIR ($CDCl_3$, KBr windows): (ν_{CN}) 2157 (wsh) cm^{-1}, 2125 (vs) cm^{-1} 2114 (wsh) cm^{-1}, 2080 (s) cm^{-1}, (ν_{CO}) 2018 (w) cm^{-1}, 1984 (vs) cm^{-1}, 1962 (vs) cm^{-1}, 1949 (wsh) cm^{-1}, also 2977, 2951, 2920, 2863, 1613, 1456, 1415, 1275, 1244, 1189, 1063,

and 1032 cm^{-1}. Anal. Calcd for $C_{77}H_{75}N_3O_2I_2Mo$: C, 64.94; H, 5.31; N, 2.95. Found: C, 64.69; H, 5.55; N, 2.95.

Synthesis of *trans*–Mo(CO)$_2$(CNAr^{Mes2})$_4$ (51). Method A. A mixture of *fac*–Mo(CO)$_3$(NCMe)$_3$ (**5**, 3.000 g, 2.503 mmol, 1 equiv) and CNAr^{Mes2} (0.850 g, 2.503 mmol, 1 equiv) was loaded in a Pyrex ampule, dissolved in THF (150 mL), and irradiated with a 254 nm Hg lamp under an Ar purge for 12 h. The reaction mixture was then concentrated to ca. 1/5 its original volume under reduced pressure and filtered. The resulting orange solid was washed with THF (4 x 20 mL), *n*–pentane (20 mL), and then dried *in vacuo* affording *trans*–Mo(CO)$_2$(CNAr^{Mes2})$_4$ as an orange powder. Yield: 0.065 g, 0.054 mmol, 65%. ^{1}H NMR (400.1 MHz, $CDCl_3$, 20 °C): δ = 7.42 (s, 4H, *p*–Ph), 6.86 (s, 16H, *m*–Ph), 5.78 (b s, 4H, *m*–Mes), 2.54 (s, 24H, *p*–CH_3), 1.77 (s, 24H, *p*–CH_3) ppm. ^{13}C{^{1}H} NMR (100.6 MHz, $CDCl_3$, 20 °C): 140.4, 137.1, 136.5, 135.7, 130.2, 129.4, 128.9, 128.5, 21.9, 20.1 ppm (the *C*≡N and *C*≡O resonances were not conclusively identified after prolonged scanning). FTIR ($CDCl_3$, NaCl windows): (ν_{CN}) 2078 (w), 2014 (w sh), and 1972 (vs) cm^{-1}, (ν_{CO}) 1910 (vs) cm^{-1} also 2922, 2859, 1613, 1579, 1458, 1415, 1379, 850, 800, 581, and 514 cm^{-1}. Anal. Calcd for $C_{102}H_{100}N_4O_2Mo$: C, 81.14; H, 6.68; N, 3.71. Found: C, 76.17; H, 6.04; N, 3.34.

Method B. To a stirred mixture of sodium amalgam (Na/Hg) (Na: 0.016 g, 0.702 mmol; Hg: 16.0 g; 0.125% w/w; 20 equiv Na/Mo) in thawing Et_2O (50 mL) was added a thawing Et_2O solution of $MoI_2(CO)_2(CNAr^{Mes2})_3$ (**50**, 0.050 g, 0.035 mmol, 1.0 equiv) and CNAr^{Mes2} (0.012 g, 0.035 mmol, 1.0 equiv, 50 mL). The reaction was stirred for 2 h, after which the solution was decanted from the residual amalgam, filtered, and all volatile materials were removed under reduced pressure. The resulting orange solids were washed with washed with THF (4 x 2 mL) and then then dried *in vacuo*. Yield: 0.005 g, 0.003 mmol, 9%.

Synthesis of [*trans*–Mo(CO)$_2$(CNAr^{Mes2})$_4$](I$_3$) (52). To a thawing CH_2Cl_2 solution of *trans*–Mo(CO)$_2$(CNAr^{Mes2})$_4$ (**51**, 0.200 g, 0.132 mmol, 1.0 equiv, 10 mL) was added a thawing CH_2Cl_2 solution of I_2 (0.052 g, 0.205 mmol, 1.55 equiv, 5 mL). The reaction mixture was stirred for 2 h, after which all volatiles were removed under reduced pressure. The resulting purple solids were washed with C_6H_6 (4 x 10 mL) and then then dried under vacuum pressure. Dissolution of the resulting purple residue in 5:1 fluorobenzene/$CHCl_3$ (5 mL total) solution followed by filtration and storage at –35 ˚C for 24 h resulted in purple crystals, which were collected and dried *in vacuo*. Yield: .110 g, 0.058 mmol, 44%. ^{1}H NMR (400.1 MHz, $CDCl_3$, 20 ˚C): δ = 19.09 (b s, 8H, *p*–Ph), 8.35 (b s, 18H, *m*–Ph), 2.66 (b s, 48H, *m*–C*H*$_3$), 2.53 (b s, 24H, *p*–C*H*$_3$), –29.67 (vb s, 4H, *m*–Mes) ppm. μ_{eff} (Evans Method, $CDCl_3$ with O(SiMe$_3$)$_2$, 400.1 MHz, 20 ˚C) = 1.62(±0.06) μ_B (average of 4 independent measurements). FTIR ($CDCl_3$, KBr windows): (ν_{CN}) 2077 (vs) cm^{-1}, and (ν_{CO}) 1960 (vs) cm^{-1} also 2976, 2951, 2923, 2860, 1614, 1458, 1380, 1278, 1245, 1189, 1039, 855, and 805 cm^{-1}. Anal. Calcd for $C_{102}H_{100}N_4O_2I_3Mo$: C, 64.80; H, 5.33; N, 2.96. Found: C, 62.72; H, 5.01; N, 2.86.

Synthesis of [*trans*–MoI$_2$(NCEt)$_4$](I$_3$) (53). To a propionitrile solution of $MoCl_4(NCEt)_2$ (6.00 g, 17.24 mmol, 1.0 equiv, 150 mL) was added trimethylsilyl iodide (TMSI) (19.323 g, 96.58 mmol, 5.6 equiv). Following the addition, the resulting red brown/red solution was refluxed for 2 h. After this period, the reaction mixtures was concentrated to ca. 1/3 its original volume under reduced pressure, filtered and stored at –35 ˚C for 1 d, whereupon orange/red crystals of [$MoI_2(NCEt)_4$](I_3) were obtained. Yield: 5.45 g, 5.732 mmol, 33%. FTIR (CD_2Cl_2, KBr windows): (ν_{NC}) 2276 (vs) cm^{-1} also 3000, 2954, 2929, 1460, 1413, 1302, 1069, and 780 cm^{-1}. Anal. Calcd for $C_{12}H_{20}N_4I_5Mo$: C, 15.16; H, 2.12; N, 5.89. Found: C, 15.07; H, 2.06; N, 5.89.

Synthesis of [*trans*–$MoI_2(CNAr^{Mes2})_4$](I_3) (54). A mixture of [$MoI_2(NCEt)_4$](I_3) (1.500 g, 1.577 mmol, 1.0 equiv) and $CNAr^{Mes2}$ (2.142 g, 6.311 mmol, 4.0 equiv) was dissolved in CH_2Cl_2 (150 mL) and stirred for 48 h. The resulting purple solution was filtered and all volatiles were removed under reduced pressure. The remaining purple residue was washed with Tol (6 x 20 mL), MeCN (2 x 10 mL), *n*–pentane (20 mL), and then dried *in vacuo* affording [*trans*–$MoI_2(CO)_2(CNAr^{Mes2})_4$]($I_3$) as a purple powder. Yield: 2.560 g, 1.226 mmol, 78%. X–ray diffraction quality crystals were grown from saturated $CHCl_3$ solution. ^{1}H NMR (400.1 MHz, $CDCl_3$, 20 ˚C): δ = 8.23 (d, 8H, *J* = 8 Hz, *m*–Ph), 7.51 (t, 4H, *J* = 8 Hz, *p*–Ph), 6.66 (s, 4H, *m*–Mes), 2.54 (s, 48H, *m*–C*H*$_3$), 1.58 (s, 24H, *o*–C*H*$_3$) ppm. μ_{eff} (Evans Method, $CDCl_3$ with $O(SiMe_3)_2$, 400.1 MHz, 20 ˚C) = 1.83(±0.01) μ_B (average of 3 independent measurements). FTIR ($CDCl_3$, KBr windows): (ν_{CN}) 2121 (vs) cm^{-1}, 2946, 2919, 2858, 1612, 1455, 1410, 1377, 1277, 1027, 1027, 853, and 805 cm^{-1}. Anal. Calcd for $C_{100}H_{100}N_4I_5Mo$: C, 57.51; H, 4.83; N, 2.68. Found: C, 57.40; H, 4.76; N, 2.19.

Synthesis of [*trans*–$MoI_2(CNAr^{Mes2})_4$](OTf) (55). To a CH_2Cl_2 solution of [*trans*–$MoI_2(CO)_2(CNAr^{Mes2})_4$]($I_3$) (**54**, 1.0 g, 0.479 mmol, 100 mL) was added CH_2Cl_2 solution of AgOTf (0.369 g, 1.437 mmol, 3.0 equiv, 20 mL). The reaction mixture was allowed to stir for 12 h, after which all volatile materials were removed under reduced pressure. Dissolution of the resulting red residue in fluorobenzene (30 mL) followed by filtration and storage at –35 ˚C for 24 h resulted in purple crystals, which were collected and dried *in vacuo*. Yield: 0.650 g, 0.350 mmol, 73%. ^{1}H NMR (400.1 MHz, $CDCl_3$, 20 ˚C): δ = 8.22 (d, 8H, *J* = 8 Hz, *m*–Ph), 7.50 (t, 4H, *J* = 8 Hz, *p*–Ph), 6.66 (s, 4H, *m*–Mes), 2.54 (s, 48H, *m*–C*H*$_3$), 1.58 (s, 24H, *o*–C*H*$_3$) ppm. μ_{eff} (Evans Method, $CDCl_3$ with $O(SiMe_3)_2$, 400.1 MHz, 20 ˚C) = 1.65(±0.02) μ_B (average of 4 independent measurements). FTIR ($CDCl_3$, KBr windows): (ν_{CN}) 2121 (vs) cm^{-1}, 2974, 2953, 2922, 2860, 1613, 1495, 1459, 1442, 1275, 1262, 1225, 1164, 1074 and

1032 cm^{-1}. Anal. Calcd for $C_{101}H_{100}N_4I_2SO_3F_3Mo$: C, 65.33; H, 5.43; N, 3.02. Found: C, 59.74; H, 475; N, 2.61.

6.6 Crystallographic Structure Determinations.

General Considerations. Single crystal X–ray structure determinations were carried out at low temperature on a Bruker Platform or Kappa Diffractometers equipped with a Bruker APEX, APEX II, and Photon 100 area detectors. All structures were solved via direct methods with SIR 2004[53] and refined by full–matrix least–squares procedures utilizing SHELXL–2013.[54] Crystallographic data collection and refinement information are listed in Tables 6.2 and 6.3.

Table 6.2. Crystallographic Data Collection and Refinement Information for $MoI_2(CO)_2(CNAr^{Mes2})_3 \cdot THF$, [*trans*–$Mo(CO)_2(CNAr^{Mes2})_4](I_3) \cdot CHCl_3 \cdot C_6H_5F$, and [*trans*–$MoI_2(CNAr^{Mes2})_4](I_3)$

	$MoI_2(CO)_2(CNAr^{Mes2})_3 \cdot THF$ (**50**·THF)	[*trans*–$Mo(CO)_2(CNAr^{Mes2})_4](I_3) \cdot CHCl_3 \cdot C_6H_5F$ (**52**·$CHCl_3 \cdot C_6H_5F$)	[*trans*–$MoI_2(CNAr^{Mes2})_4](I_3)$ (**54**)
Formula	$MoC_{85}H_{91}I_2N_3O_4$	$MoC_{116}H_{114}Cl_6F_2I_3N_4O_2$	$MoC_{100}H_{100}N_4I_5$
Crystal System	Monoclinic	Triclinic	Triclinic
Space Group	*C*2/*c*	*P*–1	*P*–1
a, Å	21.5509(11)	14.5725(6)	13.2754(18)
b, Å	16.8052(9)	15.1181(7)	14.345(2)
c, Å	21.6335(12)	15.4941(7)	14.425(2)
α, deg	90	84.100(3)	70.210(2)
β, deg	101.5930(10)	71.063(3)	63.203(2)
γ, deg	90	63.458(3)	70.250(2)
V, $Å^3$	7675.1(7)	2884.8(3)	2250.3(5)
Z	4	1	1
Radiation (λ, Å)	Mo–Kα, 0.71073	Cu–Kα, 1.54178	Mo–Kα, 0.71073
ρ (calcd.), g/cm^3	1.357	1.337	1.541
μ, mm^{-1}	1.026	8.907	1.908
Temp, K	100(2)	100(2)	100(2)
θ max, deg	25.44	54.23	25.55
data/parameters	7075 / 0 / 440	6758 / 51 / 610	8152 / 0 / 511
R_1	0.0284	0.0712	0.0610
wR_2	0.0353	1.045	0.0750
GOF	1.134	0.999	1.028

Table 6.3. Crystallographic Data Collection and Refinement Information for [*trans*–$MoI_2(CNAr^{Mes2})_4$](OTf)·3(C_6H_5F)

	[*trans*–$MoI_2(CNAr^{Mes2})_4$](OTf)·3(C_6H_5F) (**55**·3(C_6H_5F))
Formula	$Mo_{0.5}C_{69}H_{65}F_6IN_2O_3S$
Crystal System	Monoclinic
Space Group	*C*2/*c*
a, Å	34.4441(5)
b, Å	20.7547(3)
c, Å	21.0475(6)
α, deg	90
β, deg	125.92
γ, deg	90
V, Å^3	12184.5(4)
Z	8
Radiation (λ, Å)	Cu–Kα, 1.54178
ρ (calcd.), g/cm^3	1.408
μ, mm^{-1}	5.808
Temp, K	100(2)
θ max, deg	67.40
data/parameters	10571 / 0 / 757
R_1	0.0499
wR_2	0.0691
GOF	1.061

6.7 Acknowledgements

Chapter 6 is currently being prepared for publication by Ditri, T. B.; Moore, C. E.; Rheingold, A. L.; Figueroa, J. S. The dissertation author is the primary author of this paper.

6.8 References

(1) Graham, M. A.; Poliakoff, M.; Turner, J. J. *J. Chem. Soc. A* **1971**, 2939–2948.

(2) Burdett, J. K.; Graham, M. A.; Perutz, R. N.; Poliakoff, M.; Rest, A. J.; Turner, J. J.; Turner, R. F. *J. Am. Chem. Soc.* **1975**, *97*, 4805–4808.

(3) Perutz, R. N.; Turner, J. J. *J. Am. Chem. Soc.* **1975**, *97*, 4800–4804.

(4) Perutz, R. N.; Turner, J. J. *Inorg. Chem.* **1975**, *14*, 262–270.

(5) Perutz, R. N.; Turner, J. J. *J. Am. Chem. Soc.* **1975**, *97*, 4791–4800.

(6) Fletcher, T. R.; Rosenfeld, R. N. *J. Am. Chem. Soc.* **1985**, *107*, 2203–2212.

(7) Seder, T. A.; Church, S. P.; Weitz, E. *J. Am. Chem. Soc.* **1986**, *108*, 4721–4728.

(8) Ishikawa, Y.; Hackett, P. A.; Rayner, D. M. *J. Phys. Chem.* **1988**, *92*, 3863–3869.

(9) Ishikawa, Y.; Hackett, P. A.; Rayner, D. M. *J. Mol. Struct.* **1988**, *174*, 113–116.

(10) Ganske, J. A.; Rosenfeld, R. N. *J. Phys. Chem.* **1989**, *93*, 1959–1963.

(11) Ishikawa, Y.; Brown, C. E.; Hackett, P. A.; Rayner, D. M. *J. Phys. Chem.* **1990**, *94*, 2404–2413.

(12) Buntin, S. A.; Cavanagh, R. R.; Richter, L. J.; King, D. S. *J. Chem. Phys.* **1991**, *94*, 7937–7950.

(13) Dougherty, T. P.; Heilweil, E. J. *Chem. Phys. Lett.* **1994**, *227*, 19–25.

(14) Ehlers, A. W.; Frenking, G. *J. Am. Chem. Soc.* **1994**, *116*, 1514–1520.

(15) Pollak, C.; Rosa, A.; Baerends, E. J. *J. Am. Chem. Soc.* **1997**, *119*, 7324–7329.

(16) Andrews, L.; Zhou, M.; Gutsev, G. L. *J. Phys. Chem. A* **2003**, *107*, 990–999.

(17) Andrews, L.; Zhou, M.; Gutsev, G. L.; Wang, X. *J. Phys. Chem. A* **2003**, *107*, 561–569.

(18) Ishikawa, Y.; Kawakami, K. *J. Phys. Chem. A* **2007**, *111*, 9940–9944.

(19) Kim, J.; Kim, T. K.; Kim, J.; Lee, Y. S.; Ihee, H. *J. Phys. Chem. A* **2007**, *111*, 4697–4710.

(20) Fox, B. J.; Sun, Q. Y.; DiPasquale, A. G.; Fox, A. R.; Rheingold, A. L.; Figueroa, J. S. *Inorg. Chem.* **2008**, *47*, 9010–9020.

(21) Ditri, T. B.; Fox, B. J.; Moore, C. E.; Rheingold, A. L.; Figueroa, J. S. *Inorg. Chem.* **2009**, *48*, 8362–8375.

(22) Ditri, T. B.; Carpenter, A. E.; Ripatti, D. S.; Moore, C. E.; Rheingold, A. L.; Figueroa, J. S. *Inorg. Chem.* **2013**, *52*, 13216–13229.

(23) Fox, B. J.; Millard, M. D.; DiPasquale, A. G.; Rheingold, A. L.; Figueroa, J. S. *Angew. Chem., Int. Ed.* **2009**, *48*, 3473–3477.

(24) Labios, L. A.; Millard, M. D.; Rheingold, A. L.; Figueroa, J. S. *J. Am. Chem. Soc.* **2009**, *131*, 11318–11319.

(25) Margulieux, G. W.; Weidemann, N.; Lacy, D. C.; Moore, C. E.; Rheingold, A. L.; Figueroa, J. S. *J. Am. Chem. Soc.* **2010**, *132*, 5033–5035.

(26) Emerich, B. M.; Moore, C. E.; Fox, B. J.; Rheingold, A. L.; Figueroa, J. S. *Organometallics* **2011**, *30*, 2598–2608.

(27) Ditri, T. B.; Moore, C. E.; Rheingold, A. L.; Figueroa, J. S. *Inorg. Chem.* **2011**, *50*, 10448–10459.

(28) Ditri, T. B.; Ripatti, D. S.; Moore, C. E.; Rheingold, A. L.; Figueroa, J. S.; Synthesis of η^6–Arene–Tethered m–Terphenyl Isocyanide Complexes of Chromium and Molybdenum: Activation of Isocyanides towards Electrophilic Addition. *Inorg.*, In Preperation.

(29) Muetterties, E. L.; Guggenberger, L. J. *J. Am. Chem. Soc.* **1974**, *96*, 1748–1756.

(30) Brocas, J. *J. Math. Chem.* **1993**, *14*, 153–174.

(31) Dewan, J. C.; Roberts, M. M.; Lippard, S. J. *Inorg. Chem.* **1983**, *22*, 1529–1533.

(32) Drew, M. G. B.; Wilkins, J. D. *J. Chem. Soc., Dalton Trans.* **1977**, 557–560.

(33) Anker, M.; Colton, R.; Tomkins, I. *Aust. J. Chem.* **1967**, *20*, 9–12.

(34) Bowden, J.; Colton, R. *Aust. J. Chem.* **1968**, *21*, 2657–2661.

(35) Colton, R.; Rix, C. *Aust. J. Chem.* **1968**, *21*, 1155–1158.

(36) Colton, R.; Rix, C. *Aust. J. Chem.* **1969**, *22*, 305–310.

(37) Colton, R.; Tomkins, I. *Aust. J. Chem.* **1966**, *19*, 1143–1146.

(38) Colton, R.; Tomkins, I. *Aust. J. Chem.* **1966**, *19*, 1519–1521.

(39) Drew, M.; Tomkins, I.; Colton, R. *Aust. J. Chem.* **1970**, *23*, 2517–2520.

(40) Leigh, G. J.; Sanders, J. R.; Hitchcock, P. B.; Fernandes, J. S.; Togrou, M. *Inorg. Chim. Acta* **2002**, *330*, 197–212.

(41) Kubas, G. J. *Inorg. Chem.* **1983**, *22*, 692–694.

(42) Kubas, G. J.; Van der Sluis, L. S. *Inorg. Synth.* **1990**, *28*, 29–33.

(43) Mock, M. T.; Chen, S.; Rousseau, R.; O'Hagan, M. J.; Dougherty, W. G.; Kassel, W. S.; DuBois, D. L.; Bullock, R. M. *Chem. Commun.* **2011**, *47*, 12212–12214.

(44) Tanabe, Y.; Kuriyama, S.; Arashiba, K.; Miyake, Y.; Nakajima, K.; Nishibayashi, Y. *Chem. Commun.* **2013**, *49*, 9290–9292.

(45) Weiss, C. J.; Groves, A. N.; Mock, M. T.; Dougherty, W. G.; Kassel, W. S.; Helm, M. L.; DuBois, D. L.; Bullock, R. M. *Dalton Trans.* **2012**, *41*, 4517–4529.

(46) Yoshida, T.; Adachi, T.; Kaminaka, M.; Ueda, T.; Higuchi, T. *J. Am. Chem. Soc.* **1988**, *110*, 4872–4873.

(47) Arashiba, K.; Miyake, Y.; Nishibayashi, Y. *Nat Chem* **2011**, *3*, 120–125.

(48) Arashiba, K.; Sasaki, K.; Kuriyama, S.; Miyake, Y.; Nakanishi, H.; Nishibayashi, Y. *Organometallics* **2012**, *31*, 2035–2041.

(49) Ning, Y.; Sarjeant, A. A.; Stern, C. L.; Peterson, T. H.; Nguyen, S. T. *Inorg. Chem.* **2012**, *51*, 3051–3058.

(50) Pangborn, A. B.; Giardello, M. A.; Grubbs, R. H.; Rosen, R. K.; Timmers, F. J. *Organometallics* **1996**, *15*, 1518–1520.

(51) Arnarego, W. L. F.; Chai, C. L. L. *Purification of Laboratory Chemicals*; 5th ed.; Elsevier, 2003.

(52) Allen, E. A.; Bridson, B. J.; Fowles, G. W. A. *J.Chem. Soc. (Resumed)* **1964**, 4531–4534.

(53) Burla, M. C.; Caliandro, R.; Camalli, M.; Carrozzini, B.; Cascarano, G. L.; De Caro, L.; Giacovazzo, C.; Polidori, G.; Spagna, R. *J. Appl. Crystallogr.* **2005**, *38*, 381–388.

(54) Sheldrick, G. M. *Acta. Crystallogr.* **2008**, *64*, 112–122.